CLOSED QUANTUM MANY-BODY SYSTEMS OUT OF EQUILIBRIUM

A quantum information perspective

MATHIS FRIESDORF

Berlin, 2015

Dissertation zur Erlangung des Grades eines Doktors der Physik,
eingereicht am Fachbereich Physik der Freien Universität Berlin

Dahlem Center for Complex Quantum Systems
Freie Universität Berlin
14195 Berlin, Germany

Erstgutachter: Prof. Dr. Jens Eisert, *Freie Universität Berlin*

Zweitgutachter: Prof. Dr. Felix von Oppen, *Freie Universität Berlin*

Datum der Verteidigung: 08.02.2016

CONTENTS

1 INTRODUCTION: QUANTUM MANY-BODY SYSTEMS OUT OF EQUILIBRIUM 1

2 PUBLICATIONS OF THE AUTHOR OF THIS THESIS 5

I Equilibration & Localisation 7

3 EQUILIBRATION 9
- 3.1 Basic principle 10
- 3.2 Local systems 12
- 3.3 Static ensembles 16
- 3.4 Equilibration in free systems 17
- 3.5 Equilibration on average 25
- 3.6 Summary: Equilibration 34

4 THERMALISATION 35
- 4.1 Eigenstate thermalisation hypothesis 35
- 4.2 Alternative routes to thermalisation 37
- 4.3 Failure of thermalisation 38
- 4.4 Summary: Thermalisation 39

5 LOCALISATION WITHOUT INTERACTIONS 41
- 5.1 Anderson localisation 41
- 5.2 Eigenmode localisation 44
- 5.3 Summary: Non-interacting localisation 51

6 MANY-BODY LOCALISATION 53
- 6.1 Localised Operators 55
- 6.2 Local constants of motion imply information propagation 58
- 6.3 Many-body localised states 63
- 6.4 Eigenvectors and suppression of transport 65
- 6.5 Defining many-body localisation 70
- 6.6 Summary: Many-body localisation 73

7 SUMMARY: EQUILIBRATION & LOCALISATION 75

II Dynamical quantum simulations 77

8 ULTRA-COLD BOSONS AS A DYNAMICAL QUANTUM SIMULATOR 79
- 8.1 Concept of a quantum simulation 80
- 8.2 Ultra-cold atoms 82
- 8.3 Available measurements 85
- 8.4 Summary: Ultra-cold bosons as a dynamical quantum simulator 87

9 DYNAMICS OF QUANTUM PHASE TRANSITIONS 89
9.1 Defining quantum phase transitions 90
9.2 Paradigmatic Models 91
9.3 Critical exponents 95
9.4 Adiabatic theorem 96
9.5 Kibble-Zurek mechanism 97
9.6 Summary: Dynamics of quantum phase transitions 100

10 DYNAMICALLY PROBING THE MOTT-SUPERFLUID TRANSITION 101
10.1 Crossing the phase transition 102
10.2 1D Results 103
10.3 Higher dimensions 107
10.4 Summary: Dynamically probing the Mott-superfluid transition 109

11 QUANTUM FIELD TOMOGRAPHY 111
11.1 Ultra-cold bosons in a continuous optical setup 112
11.2 Reconstructing phase correlations 113
11.3 Investigating thermalisation 115
11.4 Summary: Quantum field tomography 116

12 SUMMARY & OUTLOOK 117

BIBLIOGRAPHY 121

A MATRIX-PRODUCT STATES 135

B LIEB-ROBINSON BOUNDS 137

C FERMIONIC GAUSSIFICATION 143

D CONSTANTS OF MOTION IMPLY INFORMATION PROPAGATION 153

E ENERGY FILTERING 157

F EIGENSTATE LOCALISATION 161

G EXPERIMENTALLY CROSSING THE MOTT-SUPERFLUID TRANSITION 167

ACKNOWLEDGEMENTS 171

SUMMARY OF RESULTS 173

GERMAN SUMMARY OF RESULTS 175

DECLARATION OF ORIGINALITY 177

CURRICULUM VITAE 179

FOREWORD

Understanding the out of equilibrium behaviour of interacting quantum many-body systems has motivated physicists from various fields for over a century. These systems lie at the cross-section of quantum mechanics, solid-state physics, material sciences and thermodynamics and are connected to some of the most intriguing open problems in these fields. Naturally, they have been studied extensively and trying to even list the achieved, often ground-breaking results, both of theoretical and experimental nature, would prod a lifetime of academic research.

Given this vast amount of interesting research, this thesis necessarily has to be narrow in scope. We will restrict the discussion to few, yet paradigmatic phenomena that we believe to be physically relevant. In the process, we will investigate equilibration, thermalisation and its limits, break-down of propagation due to disorder, the dynamics of quantum phase transitions, continuous quantum field tomography, as well as various aspects of modern experiments with ultra-cold atoms in a mindset of analogue quantum simulations.

Rather than giving justice to the traditional approaches of condensed matter, thermodynamics or material sciences, we will fully focus on the perspective of quantum information theory. Motivated by the unprecedented experimental control of ultra-cold atoms in optical lattices, we focus on the behaviour of small systems where individual atoms or spins can be tracked. We aim at establishing rigorous mathematical statements and concise interpretations of experimental results. Using new mathematical tools and relying on information theoretic interpretations, we hope that this thesis will provide a useful contribution to the study of the intriguing behaviour of quantum many-body systems out of equilibrium.

LEGEND

L	number of spins in a lattice
$\mathcal{L}$	lattice
$d_{\mathcal{L}}$	lattice dimension
d_{spin}	local spin dimension
d_H	total Hilbert space dimension
γ	spectral gap
N	particle number
X, Y, Z, S	local region on a lattice
$d(X, Y)$	distance on the lattice
$\sigma^x, \sigma^y, \sigma^z$	Pauli-Matrices
$\sigma^{s\,\dagger}, \sigma^s$	spin creation / annihilation operator
$f^\dagger, f$	fermionic creation / annihilation operator
$b^\dagger, b$	bosonic creation / annihilation operator
n_j	number operator on site j
σ_j^k	operator basis
$\mathcal{D}$	space of density matrices
A, B, W, H	hermitian operators
A_t	time evolved operator
M	general operator
U, V	unitary operators
S_α	Renyi entropies
S_1	von-Neumann entropy
$\|\cdot\|$	operator norm
$\|\cdot\|_1$	1-norm

1

INTRODUCTION: QUANTUM MANY-BODY SYSTEMS OUT OF EQUILIBRIUM

The study of interacting quantum many-body systems began more than a century ago and still remains one of the most active fields in modern physics. In condensed matter physics, these systems provide the basis for investigating transport properties and give rise to intriguing phenomena such as quantum phase transitions or superconductivity. Often their study requires extensive perturbation analysis or numerical simulations using super-computers. This complexity, which often makes them exceedingly hard to describe, is also one of their most intriguing features.

More recently, such systems have also been the focus for an investigation in the light of quantum information theory. While the motivating questions, such as the study of electronic transport, are often akin to those of more traditional approaches, the used tools and general mindset differ significantly. These tools are often taken from classical information theory, such as the Shannon entropy, but also computational complexity theory and other concepts from computer science are applied. Particular focus is often put on establishing rigorous mathematical results. While this necessarily means that the attention is focussed on simplified paradigmatic models, in its rigor and due to its fresh viewpoint, quantum information significantly contributed to the way we currently view the physics of interacting atoms.

In this thesis, we explore this point of view and employ it to investigate many intriguing physical properties from *thermalisation*, over the *break-down of conductance* due to randomness, to the *dynamics of quantum phase transitions* [1–6]. While free systems, capturing non-interacting particles, will be used as guidelines, the focus is clearly placed on interacting models and it is precisely the effect of such interactions that this thesis is investigating. We specifically focus on understanding out of equilibrium behaviour of interacting quantum many-body systems. This area poses many notoriously hard questions and we need to employ diverse mathematical tools, numerical simulations and experimental investigations to approach them. A crucial theme for the whole thesis will be, how this dynamical behaviour can be connected to static properties of the model, such as local structure in eigenstates. In general these connections are hard to establish for the interacting case, which clearly highlights the complexity associated with such models. Whenever successful, however, such connections between static spectral features and dynamical behaviour provide substantial insight into the true nature of those systems and help to provide a comprehensive picture of their physical behaviour, be it for *many-body localisation* or *quantum phase transitions*.

This thesis consists of two main parts. In the first, we present analytical ways of rigorously capturing the out of equilibrium evolution of interacting quantum many-body systems. We put great emphasis on following experimentally realistic settings and are guided by the capabilities of modern experiments probing interacting atoms. The achieved results are based on involved mathematical tools. In order to keep the presentation accessible and connect it to physical intuition, most technical steps are discussed separately in appendices.

The second part of this thesis also revolves around dynamical behaviour of interacting quantum systems, but is more experimentally minded. We present the exciting possibility to probe long-standing physical questions in the laboratory. Specifically, we focus on ultra-cold atoms in optical lattices, explore their capabilities in detail and employ them to study the dynamics of quantum phase transitions. We now discuss the structure and findings of this thesis in more detail, beginning with the first main part.

In chapter 3, we describe how measurements on quantum systems pushed out of equilibrium, for example by a sudden change of the Hamiltonian, after some time can again be described in terms of static

ensembles, i.e. they *equilibrate*. We describe how this is compatible with the unitary nature of quantum mechanical evolution and investigate the role of the allowed observables and initial states. Following the experimental setting of ultra-cold atoms in lattice systems and similar platforms, we focus on locally interacting models on a lattice structure, which is carefully introduced.

Based on free systems describing non-interacting particles, we show that such equilibration can be connected to transport properties of the model. Specifically, we investigate free fermionic Hamiltonians with an evolution that allows for particle propagation. In this setting, we are able to prove that dynamically states become locally indistinguishable from Gaussian states, i.e. after some time, results of local measurements are completely captured in terms of a single correlation matrix [6]. Afterwards, we turn to interacting models and present a very general way of proving equilibration. We approach the time evolution in these interacting systems both on a rigorous mathematical as well as intuitive level and connect it to notions of information propagation and entanglement growth.

Having described how local expectation values of out of equilibrium states can be captured with static ensembles, we turn to an investigation of the nature of those ensembles in chapter 4. We present sufficient conditions to ensure that they look like thermal Gibbs states, that is, they *thermalise*. This provides at least a partial quantum mechanical explanation for the immense success of thermodynamics in describing large quantum mechanical models and resolves the apparent contradiction between unitary quantum evolution and the monotonic increase of entropy expected in thermodynamics.

Following the presentation of systems that thermalise, we turn to the counterpart, where transport is strongly suppressed due to random local potentials, i.e. *localisation*, in chapter 5. Aside from giving a large class of models that fail to thermalise, this phenomenon is of independent physical interest, as it provides the basic mechanism how random impurities can lead to a complete absence of conductance in solid states. To approach such behaviour, we first review static and dynamic localisation of single electrons in such a random field, based on seminal work by Anderson. We formulate these finding in a many-body language relying on entanglement entropies, tensor network states and dynamical evolution of local operators. Starting from this preparatory discussion, we consider electronic interactions and investigate their influence on localised systems in so-called many-body localisation.

Many-body localisation is being extensively studied in recent years. Despite great efforts, a full characterisation of the phenomenon is still outstanding and its discussion in the literature is multifaceted. In chapter 6, we present different aspects of many-body localisation, ranging from a dynamical suppression of transport properties, over the existence of local constants of motion, to localising behaviour in the eigenstates of the model. Given this inchoate picture of many-body localisation, both its true nature as well as experimental probes of the phenomenon are controversially debated. We therefore follow the goal of establishing a unified definition that is experimentally testable and provides useful theoretical insight.

Motivated by this goal, we link different facets of many-body localisation relying on an in-depth mathematical analysis. Specifically, we prove that the existence of local constants of motion in interacting models, quite surprisingly, is sufficient to show that these models allow for information propagation [5], that is, two parties can use a many-body localised model to communicate. Moreover, we show how a dynamical suppression of information propagation on the low-energy sector can be used to obtain a simple, localised structure of the low-energy eigenstates, thus partially generalising the exponential clustering theorem [4]. In this way, we provide two intriguing connections of static and dynamic properties in the context of interacting localising systems. Based on those efforts, we summarise different features of many-body localisation and propose a possible definition of the phenomenon. This will conclude the first main part of the thesis.

In the second part, we discuss the exciting prospect of *quantum simulators*, which are experimental devices that potentially outperform classical computers. We focus on ultra-cold atoms, as they provide one of the most promising platforms for performing such simulations and already allow to prepare and control

ensembles with several thousand atoms. For these systems, we carefully introduce their capabilities in a language of quantum simulators and demonstrate how they can be employed to solve out of equilibrium problems in many-body quantum physics.

We begin with a general overview of quantum simulators in chapter 8 and discuss similarities and differences to the idea of a quantum computer. For simulators based on ultra-cold atoms, we review the experimental basics and discuss the available measurements and Hamiltonians of such experiments. We argue that in optical lattices, nearest neighbour interactions, in particular the Bose-Hubbard model, directly emerge, thus connecting this experimental discussion to earlier chapters of this thesis.

Our main application of a quantum simulator will be the dynamical study of quantum phase transitions. In order to introduce the setting, we present the basic definitions and mechanisms of such transitions in chapter 9. We focus our attention on the Bose-Hubbard model, partly because it is a realistic model for solid-state physics, but also because it provides rich physical behaviour due to its interacting nature. We show how general static properties of quantum phase transitions can be captured in terms of critical exponents. From this, we move towards the dynamic crossing of critical points and present the Kibble-Zurek mechanism, which gives basic intuition for the underlying physical processes.

In order to approach the dynamics of those transitions in more depth, we rely on a joint numerical, analytical and experimental effort, in an instance of a partially certified analogue quantum simulation presented in chapter 10. This work constitutes the first experimental study of the dynamics of an essentially homogeneous quantum system entering a critical phase in such a setting [1]. We show that the experimental results agree extremely well with numerical investigations in one dimension, thus partially certifying the analogue quantum simulation. We proceed to apply this quantum simulator to two and three dimensions, a regime that cannot be accessed using currently known numerical or analytical schemes. With this simulation, we study realistic experimental time scales of dynamically crossing a quantum phase transition and uncover complex behaviour outside the scope of the Kibble-Zurek mechanism or any other known theory.

Finally, in chapter 11, we focus once more on the idea of a quantum simulator, but now look at the last step of the simulation, namely how to extract the results of the experiment. We argue that this often implies that *quantum many-body tomography* has to be performed, which is a reconstruction of the experimental quantum state. We show how this can conceptually be achieved in the context of continuous quantum fields, which constitute one of the hardest instances for tomography. Moreover, we perform a proof-of-principle application for ultra-cold atoms in a continuous optical trap [2]; a platform that has very successfully been used in the past to study issues of equilibration and thermalisation.

In this way, this thesis presents various aspects of out of equilibrium behaviour of quantum many-body systems, both from a theoretical as well as experimental side. Moreover, by employing advanced mathematical tools, we link dynamic and static properties of interacting Hamiltonians and thus provide important intuition for their often exceedingly complicated behaviour.

2

PUBLICATIONS OF THE AUTHOR OF THIS THESIS

[1] S. Braun, M. Friesdorf, S. S. Hodgman, M. Schreiber, J. P. Ronzheimer, A. Riera, M. del Rey, I. Bloch, J. Eisert, and U. Schneider. "Emergence of coherence and the dynamics of quantum phase transitions". *Proc. Natl. Acad. Sci.* 112 (2015), p. 3641.

[2] A. Steffens, M. Friesdorf, T. Langen, B. Rauer, T. Schweigler, R. Hübener, J. Schmiedmayer, C. A. Riofrio, and J. Eisert. "Towards experimental quantum field tomography with ultracold atoms". *Nat. Comm.* 6 (2015), p. 7663.

[3] J. Eisert, M. Friesdorf, and C. Gogolin. "Quantum many-body systems out of equilibrium". *Nature Phys.* 11 (2015), p. 124.

[4] M. Friesdorf, A. H. Werner, W. Brown, V. B. Scholz, and J. Eisert. "Many-body localisation implies that eigenvectors are matrix-product states". *Phys. Rev. Lett.* 114 (2015), p. 170505.

[5] M. Friesdorf, A. H. Werner, M. Goihl, J. Eisert, and W. Brown. "Local constants of motion imply transport" (2014). arXiv: 1412.5605.

[6] M. Gluza, C. Krumnow, M. Friesdorf, C. Gogolin, and J. Eisert. *Gaussification and equilibration in free Hamiltonian systems*. In preparation.

Part I

Equilibration & Localisation

3

EQUILIBRATION

A theory is the more impressive the greater the simplicity of its premises, the more different kinds of things it relates, and the more extended its area of applicability. Therefore the deep impression that classical thermodynamics made upon me. It is the only physical theory of universal content which I am convinced will never be overthrown, within the framework of applicability of its basic concepts.

Albert Einstein

The above quote is maybe the most concise way to summarise the immense success thermodynamics had in past centuries. Based on statistical physics, a framework was established within which the theory is consistent, and despite ongoing debates on various different aspects, is one of the soundest physical theories we have. Surely thermodynamics is an impressive way to capture the collective behaviour of large ensembles of atoms. Despite the great underlying complexity of describing 10^{23} interacting atoms, for many practical purposes it is somehow sufficient to describe the collection of atoms with a few macroscopic parameters, such as pressure and temperature.

For someone with a background in quantum mechanics, this seems almost magical. Surely a full description of this physical setup ought to include a solution of the Schrödinger equation, should crucially depend on the precise initial condition and feature truly quantum mechanical effects, ranging from the uncertainty relation to entanglement. So, how can it be that for an overwhelming majority of practical purposes, all this complexity is hidden from the macroscopic observer. In other words: Why does nature look so thermal?

This question is almost as old as quantum mechanics itself, beginning with the work of von-Neumann [25], which is an impressive demonstration of his knowledge and already poses and answers many important questions relating to the apparent contradiction of quantum mechanics and thermodynamics. Based on this seminal work, the question emerged how to consolidate the unitary dynamics of quantum mechanics and the necessary growth of entropy in thermodynamics. In recent years, the topic moved into the focus of attention again. Based on the breath-taking progress in the experimental control over several thousands of atoms, for example in optical lattices, the emergence of thermodynamics can finally be probed in the laboratory [1, 3, 26–37]. What is more, the immense progress in numerical codes and increase in computational power has enabled large scale computer simulations to investigate those questions [32, 38–41]. Finally, many essential mathematical and theoretical concepts were established in recent years and both the applicability and limitations of thermodynamical descriptions of quantum mechanical systems are becoming significantly clearer [3, 4, 42–47].

In this thesis, we review the basic ideas and concepts how quantum mechanics can lead to an evolution that is, in many contexts, indistinguishable from thermodynamical descriptions. Based on locally interacting many-body models, we look both at rigorous mathematical results as well as experimental probes for this question. Afterwards, we specifically focus on the break-down of thermodynamic descriptions, due to the presence of disorder. Based on the seminal work of Anderson [48], we look at interacting electrons in a random lattice, the breakdown of electronic flux and the corresponding failure of the system to even out initial imbalances in particle number or energy. We start by describing the basic principle behind thermalising behaviour of complex quantum many-body systems.

3.1 BASIC PRINCIPLE

In classical mechanics, the evolution of a generic system is only constrained by its energy and in ergodic systems explores the full phase space of fixed energy evenly, in a suitable sense [7]. Thus, the time average can be replaced by an average over the micro-canonical ensemble, which in turn approaches the canonical ensemble in the thermodynamic limit [8]. In contrast, integrable systems have constants of motion, thus only explore a small section of phase space and can be captured in terms of these constants of motion and action-angle variables [7].

In quantum mechanics, the Schrödinger equation is linear and thus any system is integrable in the sense that with growing system size there always exist an exponentially large number of constants of motion. In the case of arbitrarily large but finite systems, which will be investigated in this thesis, one can simply diagonalise the Hamiltonian and the evolution is then given by

$$|\psi(t)\rangle = \sum_k \langle k|\psi\rangle e^{-itE_k} |k\rangle \ ,$$

where $|k\rangle$ denotes the eigenstates of the Hamiltonian, assuming for simplicity that they are non-degenerate. Obviously, any projector onto eigenstates of a Hamiltonian or functions thereof are constants of motion, as they commute with the Hamiltonian

$$\left[H, |k\rangle\langle k|\right] = 0$$

and the evolution explores only a vanishing fraction of the full Hilbert space. In this way, on a finite system, all states show recurrence behaviour and return arbitrarily close to their starting point. For some states, such as the superposition of few eigenstates, this will even take place after short times. This recurrence behaviour poses a fundamental challenge to one of the main pillars of thermodynamics, namely the second law. After all, how could entropy grow consequently, if it has to return to its original value after some time? Moreover, looking at the above time evolution, it seems entirely unclear how the microcanonical ensemble should appear and any description in terms of a Gibbs state seems, a priori, completely out of reach.

Thus, it is clear that thermodynamic descriptions of quantum mechanical systems can never be able to capture arbitrary settings, meaning that it is easy to construct large classes of initial states and Hamiltonians that do not allow for a description in terms of Gibbs states. Therefore, the obvious task is to precisely identify the settings and mechanisms that lead to a thermodynamic description. After all, experimentally prepared states will surely not be individual eigenstates, at least for large energy corresponding to the bulk of the spectrum. There spectral gaps are so small and the density of states so large that any realistic state is a superposition of many different eigenstates. Thus, natural states are not arbitrary points in Hilbert space, but rather have rich underlying structure. Most importantly, typical measurements only obtain some rough information of the state and are far from fully specifying the exact state.

In the following, we dive deeper into the underlying mechanism of thermalisation. The first requirement in order to describe experimental observations in terms of statistical ensembles is that they become time independent. Usually, one starts with a system that was pushed out of equilibrium [3]. This can be done in many ways. Since experimentally it is typically hard to directly alter states, it is common to alter the Hamiltonian. For this one prepares a thermal state of the original Hamiltonian, often one that is close to the ground state. Then the Hamiltonian is altered either suddenly, a process known as a quench, or slowly along some path in Hamiltonian space, which is known as a ramp [49]. For quenches, one moreover distinguishes so-called local quenches [50], where only few Hamiltonian terms are altered and global quenches [26, 51], where Hamiltonian terms are altered everywhere on the lattice, for example by changing a global magnetic field. Geometric quenches correspond to the sudden alteration of the

geometry of the lattice [52, 53]. Finally, periodic driving, in which the Hamiltonian is altered along some periodic curve, is also a very interesting possibility [54, 55]. In this section, we focus on the effects of sudden quenches, either local or global.

After the quench, we investigate the measurement outcomes of observables and want to understand to what extent they equilibrate. To approach those measurement outcomes, we introduce some mathematical notation for measuring and distinguishing quantum states.

Operators and state distinguishability

For capturing distinguishability of states, we employ the usual norms induced by the scalar product of the Hilbert space. For hermitian operators, they take the following form

$$\begin{aligned} \|A\| &= \sup_{\psi:\|\psi\|=1} |\langle\psi|A|\psi\rangle| = \sup_{\rho\in\mathcal{D}} |\mathrm{Tr}(A\rho)| , \\ \|A\|_1 &= \mathrm{Tr}(|A|) , \end{aligned}$$

where $\mathcal{D}$ denotes the set of density matrices. They are referred to as operator norm and 1-norm, respectively. These norms can be directly connected to the operational distinguishability of states which is carried out below. In the case of finite lattices with bounded Hilbert spaces, such as spins, the norms can be calculated using the spectrum of the operator

$$\begin{aligned} \|A\| &= \max_{E\in\mathrm{spec}(A)} |E| , \\ \|A\|_1 &= \sum_{E\in\mathrm{spec}(A)} |E| . \end{aligned}$$

For convenience, we work with normalised operators, whenever possible; in particular for spin systems. Observables will be normalised in the operator norm

$$\|A\| = 1 .$$

Since all bounds and statements can trivially be rescaled by the corresponding operator norm, this is without loss of generality and moving to the general case is straightforward.

In order to accurately describe non-equilibrium settings and capture them in form of static ensembles, we need ways to quantify the distinguishability of states. The most direct way to achieve this is given by the 1-norm distance. Let us imagine that we have two states ρ and σ that are close in 1-norm $\|\rho-\sigma\|_1 = \epsilon$. We are now promised that the system is either in the state ρ or in σ with equal probability and are given the task to find out which it is. For this, we perform a projection measurement that has two outcomes corresponding to some projector P and $Q = 1 - P$. The probabilities for the two measurement outcomes between the two states can now only differ by ϵ

$$\mathrm{Tr}\left(P(\rho-\sigma)\right) \leqslant \|P\|\|\rho-\sigma\|_1 = \epsilon .$$

The best possible strategy to guess the state after such a single measurement is to separate $\rho-\sigma$ into a positive and negative part. Then P is taken as the projector onto the positive eigenspaces and $Q = 1 - P$ is the orthogonal projector. Then, if the measurement outcome P appears, one assumes that the system was in state ρ and if Q appears, one would guess that the state was σ. This gives an error probability

$$\frac{1}{2} - |\mathrm{Tr}(P\rho) - \mathrm{Tr}(P\sigma)| - |\mathrm{Tr}(Q\rho) - \mathrm{Tr}(Q\sigma)| = \frac{1}{2} - \|\rho-\sigma\|_1 = \frac{1}{2} - \epsilon ,$$

where we used that P and Q separate positive and negative part of $\rho-\sigma$ and therefore the 1-norm can be expressed in terms of them. Thus, the error in guessing the state is at least $\frac{1}{2} - \epsilon$ for any possible measurement [56, 57].

We now express equilibration using the norms introduced above. As we argued before, the full state is always distinguishable from a static ensemble. This makes it crucial to consider realistic experimental distinguishability. In any experiment, there is typically some set of observables $\mathcal{A}$ whose expectation value can be efficiently measured. This set is typically rather small and in particular grows at most polynomially with the system size. This restriction to extracting only partial information of the state is crucial and ultimately the reason why equilibration happens under very generic conditions [42–44]. Such a reduced set $\mathcal{A}$ of observables naturally induces a norm

$$\|\rho\|_{1,\mathcal{A}} := \sup_{A\in\mathcal{A}} |\mathrm{Tr}\,(A\rho)|\,,$$

which is bounded by the usual 1-norm, but could potentially be smaller.

The above distinguishability in terms of expectation values can also be reformulated using POVM measurements. Given a set of measurement projectors $M = \{P_1, \cdots, P_n\}$, we can define the corresponding distinguishability as [58]

$$D_M(\rho,\omega) := \frac{1}{2}\sum_j \left|\mathrm{Tr}\left(P_j\,(\rho-\sigma)\right)\right|\,.$$

For the purpose of this thesis, the typical set of restricted observables are local measurements on a large but finite lattice system. This setting is in the focus of many investigations of equilibration [3, 32, 42, 59], as it corresponds to a large class of realistic experimental observables, such as the measurement of the orientation of local spins [39, 60, 61] or distribution of ultra-cold atoms in an optical lattice [32, 62, 63]. Naturally, one could also think of experimental settings where non-local observables can be accessed, such as a measurement of momentum [57, 62]. Most of our discussion also applies to such non-local sets of observables $\mathcal{A}$ as long as they only provide a small amount of information on the prepared quantum state. For local measurements, this discussion is simplified as necessarily only limited information on the global state can locally be measured, which is additional motivation to restrict to this setting. To discuss this case of local systems and measurements on them, we introduce the basic setting and notation in the following section.

3.2 LOCAL SYSTEMS

In this thesis, we focus our efforts on *lattice models* with *local interactions*. These models play a crucial role in our understanding of quantum many-body systems and in the study of condensed matter theory. While physical forces, like the Coulomb interaction, are usually long range, one is often capable of employing effective local models, for example due to screening effects which shield the electronic repulsion [9]. A paradigmatic class of examples is given by tight-binding models, which are derived by looking at the overlap of electronic orbitals and which are often capable of accurately capturing electrons in atomic lattice structures [9]. Notable instances are Fermi- and Bose-Hubbard models, which accurately describe the interplay of interactions and conductivity in electronic systems [10]. Other local systems often considered are spin systems describing the magnetization behaviour of solid states, such as Heisenberg models [9]. These and similar systems clearly provide motivation to study locally interacting atoms on lattice structures. Additional incentive comes from recently emerging experiments which allow to implement such models on a large scale, while still allowing for control on the level of single constituents. For the purpose of this thesis, ultra-cold atoms in optical lattices will take the center stage [62], but also ion chains [37] or photonic platforms [64] are capable of experimentally probing locally interacting lattice models.

Motivated by these models, throughout this thesis we assume that the physical system at hand can be captured by a regular structure. For this, we stick to the simplest setting of a cubic lattice in $d_{\mathcal{L}}$-dimensions.

The results presented in this thesis can easily be extended to more general systems, such as interacting atoms on a Kagome or hexagonal lattice [62] as long as the lattice has a finite dimension. In order to keep the notation and setting accessible and to provide physical intuition, we nevertheless refrain from describing our results in a general graph theoretical language incorporating general lattices.

Each site of the $d_{\mathcal{L}}$-dimensional lattice $\mathcal{L}$ is equipped with a local degree of freedom, which could be a spin or a bosonic or fermionic orbital. For many physical settings, we think of a family of systems with varying size and look at statements that are independent of this size. On the lattice, we assume that there is some natural distance defined, which for simplicity is defined as the largest distance over all lattice axes, which results in the sets of equi-distant points being rectangles. On the lattice, we use $X, Y, S \subset \mathcal{L}$ to denote local regions. We further need enlarged versions of these regions, denoted by X_l that contains X as well as all sites within distance l. The distance of two sets X, Y is taken to be the smallest distance between all sites within the region. For a set, $|X|$ denotes the number of sites in the set and $\mathrm{diam}(X)$ the largest possible distance of sites within the set. Its boundary is denoted by ∂X. For any set X, we also need the complement X^c consisting of all sites of the lattices that are not in X.

The local constituents can be summarised in one global Hilbert space $\mathcal{H}$, which is given by the tensor product of the local systems in the case of spins or by the usual Fock space in case of fermions or bosons. A general spin quantum state on L sites with a local spin-system with dimension d_{spin} is naturally captured by the tensor of its coefficients in the computational basis

$$|\psi\rangle = \sum_{j_1,\cdots,j_L=1}^{d_{\mathrm{spin}}} c_{j_1,\cdots,j_L} |j_1,\cdots,j_L\rangle \ .$$

For fermions or bosons, a similar expression in second quantisation can be used.

We assume that the local constituents of the lattice are coupled by a Hamiltonian that is local, in a sense to be made precise now. For this, we first define a complete operator basis σ_j^r, where j labels the physical site and r the element of the local operator basis. For fermions or bosons, the local operator basis can be constructed using the canonical creation and annihilation operators. For site j, we denote them by $f_j^\dagger$ and f_j for fermions and $b_j^\dagger$ and b_j for bosons. While the antisymmetry of the fermionic wavefunctions only allows for $f_j, f_j^\dagger, f_j^\dagger f_j, f_j f_j^\dagger$ as possible combinations, for bosons one needs to consider an infinite number of strings of bosonic creation and annihilation operators on each site. For spin systems, one always has a finite local operator basis and for convenience we set

$$\sigma_j^0 = \frac{1}{\sqrt{d_{\mathrm{spin}}}} \mathbb{1} \ ,$$

where $\frac{1}{\sqrt{d_{\mathrm{spin}}}}$ is a normalisation constant and work with a hermitian basis ortho-normalised with respect to the Hilbert Schmidt scalar product

$$\mathrm{Tr}\left(\sigma_{j_1}^{r_1} \sigma_{j_2}^{r_2}\right) = \delta_{j_1,j_2} \delta_{r_1,r_2} \ ,$$

where j_1, j_2 denote the lattice site and r_1, r_2 labels the operators on the sites. Note that this implies that all basis operators except for the identity are traceless. As a simple example, the local operator basis for a spin-1/2-system in this gauge is, for example, given by the normalised Pauli-matrices $\frac{1}{\sqrt{2}}\mathbb{1}$, $\frac{1}{\sqrt{2}}\sigma^x$, $\frac{1}{\sqrt{2}}\sigma^y$, $\frac{1}{\sqrt{2}}\sigma^z$. With this construction, we are ready to define the support of an operator.

Definition 1 (Support)**.** *The support of an operator is the smallest set, such that the operator acts trivially outside of this set. For spin systems, this can be defined as*

$$\mathrm{supp}(A) := \arg\min_X \{|X| : A = A_X \otimes \mathbb{1}_{X^c}\} \ .$$

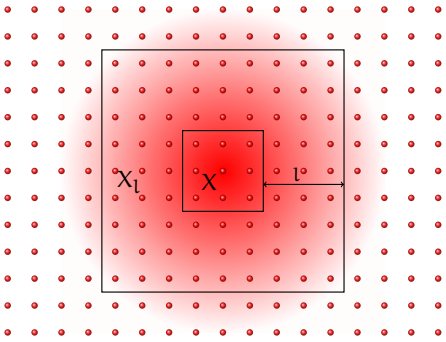

Figure 3.1: *Taken from Ref. [5].* Graphical depiction of a cubic lattice system with distances given by the maximum over the distances of each axis direction. Therefore the enlarged sets X_l of squares are also squares. The support of an approximately local operator is indicated using red color, with its localisation center marked by X.

The support of an operator can be determined from its unique decomposition into the local operator basis, which, for spin systems, can be constructed using

$$A = \sum_{r_1,\cdots,r_L=1}^{d_{\text{spin}}} \operatorname{Tr}\left(A\sigma_1^{r_1}\cdots\sigma_L^{r_2}\right)\sigma_1^{r_1}\cdots\sigma_L^{r_2} .$$

We call an operator *strictly local*, iff it has a finite support that is independent of the lattice size. When we want to stress the support of a local observable, we use it is a subscript, meaning that A_X is supported on X. The algebra of all operators local to some region X is denoted by $\mathcal{A}_X$. In a slight abuse of notation, the distance between strictly local observables $d(A, B)$ is defined as the distance of their supports.

Aside from strictly local operators, we also need *approximately local operators*, which can be defined using a reduction map. For any finite region S, we define a reduction map Γ_S that takes out the part of the operator on this region. In the picture using the local operator algebra, this corresponds to dropping all terms that have non-identity contributions outside the region S. For spin systems, this can be achieved by performing a trace over S^c, as all operators other than the identity have zero trace. Thus, for spin systems, we can write the *reduction map* as

$$\Gamma_S(A) = \mathbb{1}\otimes \operatorname{Tr}_{S^c}(A)\,\frac{1}{d_{\text{spin}}^{|S^c|}} ,$$

where d_{spin} is the local spin dimension. Alternatively, it can also be shown that such a local reduction can be achieved by a random twirl over the unitary Haar measure [65]

$$\Gamma_S(A) = \int_{S^c} dU\; UAU^\dagger .$$

Using this reduction map, approximate locality of an operator is a statement how well it can be approximated by these reductions.

Definition 2 (Local operator)**.** *An operator is called strictly local, iff it has finite support independent of the system size. Correspondingly, an operator is called approximately local iff there exists a set* X *and its enlarged sets* X_l*, such that*

$$\|A - \Gamma_{X_l}(A)\| \leqslant f(l) ,$$

for some function f *with suitable decay independent of the system size. Typically* f *is chosen to decay exponentially.*

A prime example to be considered later is the time evolution of an initially local observable in the Heisenberg picture. This is also a clear example, why it is often crucial to think of the operator as a family of operators depending on the system size and make statements that are independent of this size.

In contrast to local operators that, at least approximately, only act on a small part of the system, a Hamiltonian is called local if it only couples objects over a small length scale, meaning that it is a sum of local operators. Typically it is defined in the following way. We first express the Hamiltonian in the local operator basis above and order this decomposition with respect to the supporting sets Z

$$H = \sum_Z h_Z \ .$$

Note that, as follows from the above operator basis construction, this decomposition is unique up to an overall energy shift. In particular, this means that h_Z only contains those operators in the Hamiltonian that are not already contained in subsets of Z. For this thesis, we are interested in families of Hamiltonians for different system sizes. Locality of the Hamiltonian is then a statement how the Hamiltonian terms h_Z can be bounded by the size of the sets Z independent of the system size.

Definition 3 (Local Hamiltonian)**.** *Let $H = \sum_Z h_Z$ be the operator basis decomposition of some Hamiltonian. Then H is called quasi-local, iff the local Hamiltonian terms can be bounded*

$$\|h_Z\| \leqslant Ce^{-\mu \operatorname{diam}(Z)} \ ,$$

for some constant μ independent of the system size. It is called local or finite range, iff there exists a length scale l_0 independent of the system size, such that

$$\|h_Z\| = 0 \ \forall \operatorname{diam}(Z) > l_0 \ .$$

A different way of phrasing this definition is that a finite range Hamiltonian is the sum of strictly local operators and a quasi-local Hamiltonian is the sum of approximately local operators. Most results that can be obtained for quasi-local Hamiltonians can still be obtained in the case where the Hamiltonian terms do not decay exponentially, but only algebraically, as long as the decay is suitably strong compared to the lattice dimension $d_{\mathcal{L}}$ [66, 67], if the decay in the results is changed accordingly. We forego this generalisation in order not to complicate the results.

Turning back to the issue of equilibration and thermalisation, we take the local operators introduced above as our set of available measurements. More precisely, we restrict to some local subset of the lattice $S \subset \mathcal{L}$ that will be chosen independent of the global system size and use operators A_S supported on it. For those local operators, we will use the following notation for the distinguishability

$$\|\rho\|_{1,S} := \|\rho\|_{1,\mathcal{A}_S} = \sup_{A_S \in \mathcal{A}_S} |\operatorname{Tr}(A\rho)| \ ,$$

where $\mathcal{A}_S$ denotes the algebra of operators supported on S. Allowing for arbitrary measurements on subregions allows to fully reconstruct the local density matrix. Therefore, the difference between a time evolved state $\rho(t)$ and a static ensemble ρ_{stat} that can be accessed on the local region S is given by

$$\|\rho(t) - \rho_{\text{stat}}\|_{1,S} = \|\operatorname{Tr}_{S^c}(\rho(t) - \rho_{\text{stat}})\|_1 \ .$$

As motivated above, this local distinguishability will be used as our measure for how distinguishable quantum states are. For this quantity, we will find that time-evolved states will often equilibrate, in the sense that they locally become indistinguishable from a static ensemble

$$\|\operatorname{Tr}_{S^c}(\rho(t) - \rho_{\text{stat}})\|_1 < \epsilon \ ,$$

for some small error ϵ for the overwhelming majority of times. Before we present the details of such equilibration, let us briefly comment on the static ensembles that appear in this way.

3.3 STATIC ENSEMBLES

If equilibration takes place, it immediately follows that the state ρ_{stat} needs to be given by the infinite time average [42]

$$\rho_{\text{stat}} = \omega := \lim_{T\to\infty} \frac{1}{T}\int_0^T dt\ \rho(t) = \sum_k P_k \rho P_k \ ,$$

where P_k are the possible degenerate eigenprojectors of the Hamiltonian. This state corresponds to the maximum entropy state, keeping all constants of motion, namely the eigenprojectors of the Hamiltonian, fixed [68]. This behaviour can thus be seen as a dynamical Jaynes principle [42], which corresponds to the maximisation of the entropy keeping a set of expectation values fixed.

While equilibration as such can easily be proven for most times [69], it is very hard to get time scales on when this equilibration sets in. While very promising results for free systems exist [6, 70], the best known bounds that hold for generic systems are exponentially large in the system size [58, 71]. We comment on this in detail later and find that there are indeed systems where the equilibration time scales are diverging for a natural class of states.

Once one knows that the system can be described by a static ensemble on a realistic experimental time scale, the obvious question is how this ensemble can be characterised. As described above, it can be seen as the maximum entropy state keeping all constants of motion fixed. When only looking at a small set of measurements, it is, however, often not necessary to include all eigenprojectors as constants of motion. In fact, it is heavily debated which constants of motion are needed. The corresponding ensemble relating to the maximum entropy keeping the expectation value of some constants of motion $\mathcal{Z}_m$ fixed is called the *generalised Gibbs ensemble* (GGE) [3, 72–74]

$$\begin{aligned}\rho_{\text{GGE}} = &\underset{\substack{\sigma\in\mathcal{D},\\ \forall m:\,\mathrm{Tr}\,\mathcal{Z}_m\sigma=\mathrm{Tr}\,\mathcal{Z}_m\rho}}{\arg\max} S_1(\sigma)\\ =&\frac{1}{\mathcal{Z}_0} e^{-\sum_m \mu_m \mathcal{Z}_m} \ ,\end{aligned}$$

where $\mathcal{D}$ is the space of density matrices, $S_1(\rho) = -\mathrm{Tr}(\rho\log(\rho))$ denotes the *von-Neumann entropy*, $\mathcal{Z}_0 = \mathrm{Tr}(e^{-\sum_m \mu_m \mathcal{Z}_m})$ and the Lagrange multipliers μ_m are fixed by the expectation values of the constants of motion. Finally, if the only constant of motion that needs to be included is the expectation value of the energy, then the system thermalises, in the sense that the expectation value of selected observables can, for most times, be described by a Gibbs state,

$$\rho_{\text{Gibbs}} = \frac{1}{\mathcal{Z}_0} e^{-\beta H} \ ,$$

where $\mathcal{Z}_0 = \mathrm{Tr}(e^{-\beta H})$. This is the maximum entropy state, keeping the expectation value of the energy fixed. The energy, or correspondingly the temperature, is of course fixed by the initial state and does not change over time.

A notable class of systems that does not show this behaviour are localising systems. These show a strong suppression of transport, which leads to particle or energy imbalances being preserved for all times. Thus, they can never be captured in terms of thermal ensembles, but rather possess detailed memory of their precise initial conditions. The origin of this memory is precisely that these models have local constants of motion. As those constants of motion could be used as local measurements, yet their value can never change, it is clear that such constants of motion need to be included in any static description in terms of a generalised Gibbs ensemble.

In the following, we lay the ground-work for describing physical systems in terms of static ensembles, by describing the essential mechanisms behind equilibration. We investigate these questions from two complementary viewpoints that are very common in the study of quantum many-body systems. The first is an algebraic viewpoint, where the locality of the lattice explicitly enters. In combining Lieb-Robinson bounds with transport properties of the system, one finds that mixing takes place and central-limit type arguments can be applied. This formulation has the nice feature of immediately being connected to our physical intuition. What is more, it provides meaningful equilibration time scales. Its downside is that it so far only applies to rather special Hamiltonians and generalisation to more complex systems seem hard.

In contrast to this description in terms of local algebras and commutators, the other viewpoint is that of working with eigenvalues and eigenvectors of the Hamiltonian. Here, the Hamiltonian is simply seen as some matrix and assumptions on its eigendecomposition are made. It has the strong advantage of very broad applicability. In particular, equilibration can be shown under very mild conditions on the spacing of the energy levels. Its downside is that physical intuition is usually lost. For example, it does, a priori, not seem to have any intuitive connection to the spreading of quasi-particles in a lattice and any signature of locality is well hidden in the complicated structure of the eigenstates. Due to the generic nature of those bounds, they do not incorporate our physical intuition like ballistic spreading and thus include settings where equilibration indeed takes a long time. More precisely, the best known bounds are exponentially long in the system size.

We start with the first of these two approaches. Based on known results for bosons, we mostly focus on the fermionic case, where the underlying principles are clearer, since unbounded operators are avoided.

3.4 EQUILIBRATION IN FREE SYSTEMS

In the following, we present equilibration results in a paradigmatic setting which can still be easily accessed, namely bosonic or fermionic systems that are free in the sense that they capture non-interacting particles. Due to their simple algebraic structure, these models can often be solved exactly and provide valuable intuition for the study of more general models. Importantly, they provide a physically realistic setting for which realistic equilibration time scales can rigorously be derived.

We present such equilibration results in free fermionic systems [6]. Based on a related line of argument in the bosonic case [45, 73, 75], we show that, for rather general initial states, explicit time scales can be derived, which are very short and of the same order as those experimentally observed in more generic Hamiltonian models [32, 76]. The main advantage of the fermionic setting compared to bosons is that it is more directly accessible, due to the finite Hilbert spaces involved. This makes the presentation intuitive to understand and allows to focus on the underlying physics. To begin, we first introduce free systems, which can be captured in terms of quadratic Hamiltonians.

3.4.1 *Free systems*

For general bosonic or fermionic systems, we work with the collections of mode operators of the form

$$r = \left(c_0, c_0^\dagger, \cdots, c_L, c_L^\dagger\right)^T ,$$

where c and $c^\dagger$ denote either bosonic or fermionic annihilation and creation operators. For simplicity, we assume that the fermions are spinless and thus work with just one fermionic species. For the above operators r_j, we introduce a function $d(j,k)$ that captures the distance between the corresponding operators on the lattice. As each lattice site has two indices associated to it, corresponding to creation and annihilation operator, $d(k,j)$ is not a metric, as $d(k,j) = 0$ does not imply $k = j$.

Naturally, any bosonic or fermionic Hamiltonian can be expressed in terms of these operators. Such a Hamiltonian is called free or quadratic, iff it is a quadratic polynomial in these operators

$$H = \sum_{j,k=1}^{2L} r_j^\dagger h_{j,k} r_k \ ,$$

where h is an arbitrary hermitian matrix. Such operators can be solved in a particularly easy way by diagonalising the interaction matrix h using mode transformations that leave the commutation or anti-commutation relations invariant. In particular, for bosons the matrix can be diagonalised in a symplectic way. The corresponding commutation relations are then preserved and diagonalising h corresponds to moving to a new set of bosonic modes. For fermions, the same is true using orthogonal transformations. Sometimes this rotation into the eigenmodes of the problem is named Bogoliubov transformation in the literature [11]. In both cases, the transformed Hamiltonian takes the following easy form

$$H = \sum \lambda_k \tilde{c}_k^\dagger \tilde{c}_k \ .$$

Given a fixed number of particles, the ground state of those systems is simply given by filling these eigenmodes according to their energies and all other eigenstates can be obtained by populating the eigenmodes in different configurations, as their population is completely decoupled. In this sense, quadratic Hamiltonians correspond to non-interacting particles. We now turn to the thermal states of such Hamiltonians, which can be described in a conceptually simple way.

3.4.2 *Gaussian states*

The thermal states of free Hamiltonians are called *Gaussian states* [77, 78]. They are uniquely defined by only specifying their expectation values with respect to quadratic combinations of creation and annihilation operators. These matrices are called correlation matrices

$$\gamma_{j,k} = \mathrm{Tr}\left(\rho r_j r_k\right)$$

and capture the expectation value of arbitrary combinations of two fermionic basis operators. There is an enormous literature focussing solely on Gaussian states and many interesting properties of these matrices can be derived. Most importantly, for fermionic systems, they can always be diagonalised by an orthogonal transformation which conserves the fermionic anti-commutation relations [79]. For bosons, the same can be achieved using a symplectic transformation that in turn preserves the bosonic commutation relations [77]. In both cases, this allows to decompose the correlation matrix into its eigenvalues n_k, in the same way as for free Hamiltonians, which are the particle numbers in the corresponding eigenmodes $\tilde{c}_k$. Gaussian states are then the states of the form

$$\rho = \frac{1}{\mathcal{Z}_0} \exp\left(-\sum_k n_k \tilde{c}_k^\dagger \tilde{c}_k\right) \ ,$$

where $\mathcal{Z}_0 = \mathrm{Tr}\left(-\exp\left(\sum_k n_k \tilde{c}_k^\dagger \tilde{c}_k\right)\right)$ is a normalisation factor. In this way, a Gaussian state is the generalised Gibbs ensemble corresponding to the maximum entropy state keeping the correlation matrix, or alternatively its eigenmode occupations, fixed.

Another interesting feature of those Gaussian states is that it is straightforward to calculate their n-point correlation functions

$$\mathrm{Tr}\left(\rho\, r_{j_1} \cdots r_{j_n}\right) \ .$$

In particular, they can be decomposed according to *Wick's theorem*, which states that any n-point function of a Gaussian state can be decomposed in terms of products of 2-point functions [12]. For fermions, this can be written in terms of a determinant, which is easy to calculate, whereas it takes the form of a permanent in the bosonic case [80–82]. Such Gaussian states allow to investigate large scale systems, thus giving rise to an extensive literature focusing on this paradigmatic setting.

3.4.3 *Equilibration in the Gaussian setting*

We begin by looking at equilibration in the setting of Gaussian states and free Hamiltonians. There, the full evolution of the state can be captured by keeping track of the correlation matrix, as it uniquely defines the Gaussian state. Thus, many essential concepts in the study of the dynamics of quantum many-body systems can be easily defined and are conceptually lucid. For simplicity, we will focus on the fermionic case, in order to avoid the mathematical difficulties connected to the unbounded bosonic operators. In this case, evolution under a free Hamiltonian is a mode transformation and preserves the fermionic anti-commutation structure, in the sense that creation or annihilation operators are mapped to a sum of those operators in an orthogonal way

$$r_k(t) = \sum_j V_{k,j}(t)\, r_j \ .$$

For the correlation matrix, this yields the evolution

$$\gamma_{r_1,r_2}(t) = \sum_{j_1,j_2} V_{r_1,j_1}(t) V_{r_2,j_2}(t) \gamma_{j_1,j_2}(0) \ .$$

The evolution $V_{k,j}(t)$ shows a rich structure that contains many important features, which we also encounter in a more general way in later parts of this thesis. Firstly, the particles do not move arbitrarily fast over the lattice, but rather the spreading happens, at most, in a ballistic fashion. This result, which also can be generalised to interacting systems, is called a Lieb-Robinson bound (see appendix B).

Definition 4 (Free Lieb-Robinson bounds)**.** *The evolution V of a free systems is said to fulfil Lieb-Robinson bounds, iff*

$$\|V_{k,j}(t)\| \leqslant C_{LR}\, e^{\mu(\nu|t|-d(j,k))} \ ,$$

where C_{LR}, μ, ν are constants independent of the system size and $d(j,k)$ denotes the spatial distance between the positions j and k.

Theorem 1 (Free Lieb-Robinson bounds from locality)**.** *Given a free Hamiltonian $H = \sum_{j,k} r_j^\dagger h_{j,k} r_k$ with finite range interactions*

$$\exists\, l_0 : \quad h_{j,k} = 0 \quad \forall\, d(j,k) > l_0 \ ,$$

and uniformly bounded matrix elements $\exists \kappa : |h_j, k| \leqslant \kappa$, then it fulfils Lieb-Robinson bounds with suitable constants C_{LR}, μ, ν.

These bounds put an upper limit on the speed of any propagation in the lattice, be it information, particles or energy. This is discussed in more detail, when we treat those bounds in the general context of interacting systems. The main interest in Lieb-Robinson bounds stems from the fact that they are extremely universal and, as stated above, can be derived from nothing but locality of the Hamiltonian [73] (see appendix B for the general formulation in interacting models).

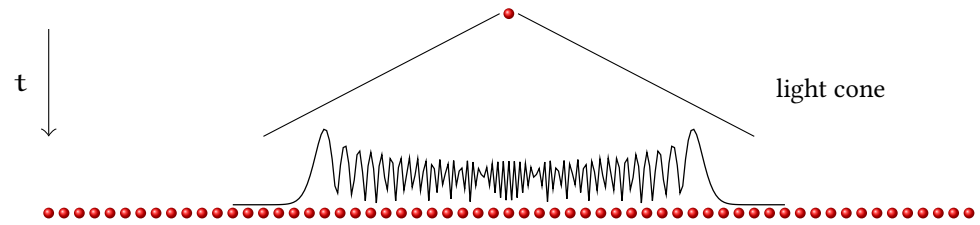

Figure 3.2: The figure schematically shows the spreading of a single fermionic operator in time over the lattice. The evolution is contained inside a light cone given by Lieb-Robinson bounds. The black curve shows a numerical simulation of a free fermionic hopping Hamiltonian on 201 lattice sites with the fermionic operator starting at the middle. Schematically plotted is the absolute value of the matrix elements $|V_{j,k}|$ after time $t = 35$ in natural units, which clearly shows that this Hamiltonian spreads the matrix elements over the lattice, thus leading to a homogeneous suppression of them.

The second important feature in the evolution of free systems relates to the question whether these bounds are actually saturated. After all, it could also be that particles in the system cannot move at all. As we discuss in chapter 5, this is the case when random potentials are introduced to the free system. For translationally invariant models, however, one typically expects particles to indeed spread over arbitrary distances. We capture such behaviour with the following definition.

Definition 5 (Transport for free Hamiltonians)**.** *We will say that a free Hamiltonian on a system with* L *sites on a* $d_{\mathcal{L}}$ *dimensional lattice with evolution matrix* V *has transport iff*

$$|V_{k,j}| \leqslant C_{\text{trans}} \min\{t^{-d_{\mathcal{L}}/3}, L^{-d_{\mathcal{L}}/3}\} \quad \forall\, k, j\ ,$$

for some suitable constant C_{trans} *and for all times* $t \in [0, t_{\text{rec}}]$*, where* t_{rec} *denotes a recurrence time.*

The intuition behind this definition is that an initially localised annihilation or creation operator spreads over a large area, such that its component on an single localised annihilation operator is dynamically suppressed. The choice of the exponent $1/3$ is justified by the fact that it can be shown that, for example, the free hopping Hamiltonian with constant on-site potential shows this behaviour [73] (see Fig. 3.2). Naturally, this suppression cannot continue indefinitely. At some point in time, lower bounded by Lieb-Robinson bounds, the evolution hits the boundary of the system. From this moment on, the matrix elements will roughly be uniformly distributed over the lattice, until eventually the recurrence of the system takes place.

It should be noted that the above definition of transport is very much tailored to free systems. As we discuss in detail later, describing transport in interacting models is far less clear cut. For example, we encounter settings where particles are localised, while operators still become non-local in the Heisenberg picture over time. In these models, we can thus send information through the chain, despite energy and particles being localised even for infinite times (see chapter 6). This can never happen for free fermions, as an annihilation operator always remains a linear superposition of local creation and annihilation operators and thus particles themselves have to propagate.

The above transport assumption is already sufficient to derive fast equilibration for the simplest case of having particles only on a certain small region X of a 1D chain. Then, only operators supported on this region X can contribute to the expectation value, which gives

$$|\mathrm{Tr}\,(r_k r_l \rho)\,| \leqslant (2|X|)^2\, C_{\text{trans}}^2\, t^{-2d_{\mathcal{L}}/3}\ ,$$

for fermionic operators on arbitrary positions k, l. Here we used that there are only $2|X|$ possibilities, corresponding to creation and annihilation operators on $|X|$ many sites, that can contribute to the expectation

value, but each of these is homogeneously suppressed due to the transport in the system. Thus any local expectation value has to equilibrate to zero on a very short time scale in this setting.

Naturally, the above case is of limited interest as such relaxation has to move towards the vacuum. Still, it already shows how well controlled equilibration in free systems often is. An important result that goes beyond this simple setting is provided in Ref. [73], where the evolution of occupation numbers of initial states that are periodic product states under free hopping Hamiltonians is considered. In this case, the equilibration time scale is given by the periodicity of the initial state, determining the length scale in the problem, divided by the hopping strength. This time scale is independent of the system size and equilibration thus happens quickly.

More generally, equilibration in free models can be obtained by tracking the evolution of the correlation matrix, which lead to notable results [45, 75, 83–85]. As they are often specific to the models considered, we will not present the details here. There is, however, one important aspect that all these free equilibration results have in common. The corresponding Hamiltonians have eigenmode energies that are non-degenerate. Thus, the correlation matrix dephases over time and its infinite time average is diagonal in the Hamiltonian eigenmode basis. This is a special instance of using that equilibration provably moves towards the infinite time average, which will be used and explained in detail in section 3.5. In this way, if those systems equilibrate, they equilibrate to the generalised Gibbs ensemble (GGE) keeping the expectation values of the linearly many number operators of the Hamiltonian eigenmodes fixed [75]

$$\rho \to \rho_{\mathrm{GGE}} = \frac{1}{\mathcal{Z}_0} e^{-\sum_k n_k \tilde{c}_k^\dagger \tilde{c}} ,$$

where $\mathcal{Z}_0 = \mathrm{Tr} e^{-\sum_k \mu_k \tilde{c}_k^\dagger \tilde{c}}$ and $\tilde{c}_k$ is the annihilation operator for eigenmode k.

While Gaussian states are a paradigmatic setting, they are necessarily connected to non-interacting particles. In order to understand equilibration in more generic systems, two generalisations are needed, namely to derive results for strongly correlated initial states and to move to interacting Hamiltonians. In the next section, we show how the first step can be performed.

3.4.4 *Equilibration through Gaussification*

The following section is based on Ref. [6]. We sincerely thank Marek Gluza, Christian Krumnow, Christian Gogolin and Jens Eisert for collaborating on this successful project.

In this section, we show how the Gaussian equilibration results presented above can be extended to settings where the initial state is far from Gaussian. In order to achieve this, we show that under the evolution of a free system with transport, many initial states end up locally looking Gaussian on short time scales. While this result immediately allows to extend equilibration results to correlated initial states, it is also of independent interest, as it in general captures the emergence of local Gaussianity, even in settings that do not equilibrate quickly.

We begin in some initial state ρ, that is assumed to have exponential clustering correlations

$$|\mathrm{Tr}(\rho AB) - \mathrm{Tr}(A\rho)\mathrm{Tr}(B\rho)| \leqslant C_{\mathrm{clust}} e^{-d(A,B)/\xi} ,$$

where ξ is a correlation length, A, B are normalised local operators and C_{clust} is a constant independent of those operators. We further assume that the state has a fixed particle parity, in the sense that the expectation value of any odd polynomial of fermionic operators vanishes. In contrast to the initial state, which is allowed to be quite generic, the conditions on the Hamiltonian are more restrictive. Firstly, we assume that the Hamiltonian is free, in the sense that it is quadratic in the creation and annihilation

operators (see section 3.4.1). The physical condition placed on it are Lieb-Robinson bounds and transport, as introduced above. In the above setting, we arrive at the following result, which allows to extend the Gaussian results to the setting of correlated initial states.

Theorem 2 (Gaussification)**.** *Let H be a free fermionic Hamiltonian that has transport and admits Lieb-Robinson bounds. Further, let ρ be an initial state with exponential clustering correlations and fixed particle parity and S be some finite region of consecutive sites. Then for any $\epsilon > 0$, there exists a time interval $[t_{\text{relax}}, t_{\text{rec}}]$, such that*

$$\|\text{Tr}_{S^c}\left[\rho(t) - \rho_G(t)\right]\|_1 \leqslant (2|S|)^{(4+4d_{\mathcal{L}})|S|+1}\epsilon \;\forall t \in [t_{\text{relax}}, t_{\text{rec}}]\,,$$

where ρ_G is the Gaussian state fixed by the correlation matrix of ρ and t_{relax} is constant in the system size.

This result shows that under the evolution of a free Hamiltonian that has transport, initial states with exponentially decaying correlations dynamically Gaussify, in the sense that they will locally resemble Gaussian states after a short relaxation time. In the following, we provide the proof in the simplified setting of having a subsystem S that contains only two sites. This greatly simplifies the proof and still shows the basic mechanisms behind it. We thus focus on an intuitive presentation of the underlying principle. The mathematical details as well as the extension of the proof to larger subsystems S are contained in appendix C.

Proof. We begin by formulating the problem in the Heisenberg picture, which relies on expressing the local 1-norm as an expectation value with fermionic annihilation and creation operators. At this point, we use the simplifications that come with dealing with fermions rather than bosons. Then, the transport properties of the Hamiltonian are used. Firstly, the fermionic operators will be restricted to the causal Lieb-Robinson cone, as in the bosonic case [73]. In a second step, a careful local grouping of the fermionic operators is performed. Using exponential clustering, one can then show that the expectation value decouples into patches. In case they consist of more than two operators, we will be able to use transport to show that they contribute very little to the expectation value. This gives only clusters with two operators, also referred to as pairs, which can never resolve the difference between the state ρ and its Gaussian version ρ_G, which is taken to have the same second moments.

Heisenberg picture: We begin by reformulating 1-norm closeness in terms of expectation values of operators

$$\|\text{Tr}_{S^c}\left(\rho(t) - \rho_G(t)\right)\|_1 = \sup_{\substack{A \in \mathcal{A}_S \\ \|A\|=1}} \left|\text{Tr}\left(A\rho(t) - A\rho_G(t)\right)\right| \,.$$

In the next step, we expand the operator A in a fermionic operator basis for the subsystem S

$$A = \sum_{m_1,\cdots,m_{2|S|}} a_{m_1,\cdots,m_{2|S|}} \left(r_1(t)\right)^{m_1} \cdots \left(r_{2|S|}(t)\right)^{m_{2|S|}} \,,$$

where r_1 to $r_{2|S|}$ are the fermionic operators on the subsystem. Normalisation of the operator $\|A\| = 1$ implies that all of the $2^{2|S|}$ possible coefficients satisfy $|a_{j_1,\cdots,j_{2|S|}}| \leqslant 1$. Thus, the proof of the theorem can be reduced to showing that

$$\left|\text{Tr}\left(r_{s_1} \cdots r_{s_q}(t)(\rho - \rho_G)\right)\right| \leqslant \epsilon' \,,$$

for some collection of $q \leqslant 2|S|$ operators labelled with the indices s_1 to s_q. For this, we expand the time evolution of the fermionic word

$$\left| \sum_{j_1,\cdots,j_q} V_{s_1,j_1}(t) \cdots V_{s_r,j_q}(t) \operatorname{Tr}\left(r_{j_1} \cdots r_{j_q} (\rho - \rho_G)\right) \right| ,$$

which will be analysed and restricted to the Lieb-Robinson cone in the next step.

Causal cone: Based on Lieb-Robinson bounds introduced above, we will separate the lattice $\mathcal{L}$ in two sets: An effective light-cone $\mathcal{C} = \{i \in \mathcal{L} \,|\, \exists j \in S : d(i,j) < (v + 2v_\epsilon)|t|\}$ and its complement $\mathcal{L}\backslash\mathcal{C}$, where v_ϵ will be picked such that the final bound is optimal. In the next step, we will use the bounds to restrict the full dynamics of all fermionic operators to the inside of the effective light cone. Using the exponential suppression provided by Lieb-Robinson bounds, this can be done with an error (see appendix C)

$$\epsilon' \mathrel{+}= 2C'_{LR}(d_{\mathcal{L}}) e^{-\mu v_\epsilon |t|} ,$$

where $C'_{LR}(d_{\mathcal{L}})$ is a constant resulting from summing up the exponential series and $+=$ here and later on denotes that this error is acquired in addition to the other error sources. With this, we can assume that all indices are inside the Lieb-Robinson cone, up to an error that decays exponentially with time, since we enlarged the light cone by $2v_\epsilon|t|$. In the next step, a careful book-keeping of the index positions will be performed.

Tracking index positions: At this point, we will use that the subsystem consists of two sites, such that at most four fermionic operators corresponding to indices j_1, j_2, j_3, j_4 can contribute. The goal is to perform a careful separation of the different configurations of those four indices over the light cone into parts that look Gaussian and a rest that is dynamically suppressed. For this, we introduce a length scale Δ and will say that a set of indices are Δ-close-by, if they can be ordered in a way such that consecutive indices are within distance Δ of each other. The notion of Δ-closeness is then used to effectively separate the indices into patches of indices sitting within distance Δ of each other (see appendix C for a formal definition). For each of those patches C_r, we introduce the operators

$$\hat{C}_r := \prod_{s \in C_r} V_{s,j_s}(t) r_{j_s} ,$$

which contain all fermionic operators supported on it. We proceed by using the fact that these patches are separated from each other by a length scale Δ and separate them using the exponential clustering correlations of the initial state. Ignoring a sign resulting from reordering the fermionic operators into the patches gives expressions of the form

$$\langle \hat{C}_1 \rangle_\rho \cdots \langle \hat{C}_l \rangle_\rho ,$$

where $\langle \cdot \rangle_\rho$ denotes the expectation value with respect to the initial state ρ. The analogous argument for the case of larger subsystems, creates an error term (see appendix C)

$$\epsilon' \mathrel{+}= (2|S|)^{2|S|+1} |\mathcal{C}|^{2|S|} C_{\text{clust}} e^{-\Delta/\xi} .$$

For the Gaussian state, a similar procedure can be carried out using Wick's theorem, which gives an error term (see appendix C)

$$\epsilon' \mathrel{+}= (2|S|)^{4|S|} |\mathcal{C}|^{2|S|} C_{\text{clust}} e^{-\Delta/\xi} .$$

Both contributions have an exponential suppression in the length scale Δ. By letting it grow algebraically with time $\Delta \propto t^\alpha$ both these contributions are exponentially suppressed in time.

Using transport: Having decoupled the patches, we now separate the terms according to their index configuration as follows.

A) The case of all four indices being close-by.

B) Two pairs of indices being respectively close-by, but separated from each other.

C) All other partitions, which therefore have a single index separated by a distance larger Δ from the rest.

The terms in contribution C) are zero, as the expectation value of a single fermionic operator vanishes due to a fixed particle parity in the initial state. The quadratic terms in contribution B) are identical for the actual state ρ and its Gaussian counterpart ρ_G, which is fixed by demanding that is has the same second moments. Thus, they do not contribute to the deviation from Gaussianity. The full non-Gaussianity of the initial state is thus contained in contribution A). We now use the transport property of the Hamiltonian (see Def. 5) to show that it is dynamically suppressed.

Here, we use that all the four indices are Δ-close to each other in contribution A). For this cluster, the number of positions and thus of index configurations scales like the size of the light cone $|\mathcal{C}| \propto t^{d_\mathcal{L}}$. Yet, due to transport, we have a homogeneous suppression of four fermionic operators and thus get a total scaling

$$\epsilon' \propto t^{d_\mathcal{L}} t^{-\frac{4}{3} d_\mathcal{L}} ,$$

which is algebraically suppressed in time. In case the subsystem is larger than two sites, significant difficulties appear. While the above characterisation into three contributions can directly be generalised, it is not directly clear how to bound the contributions of clusters of fermionic indices, as combinatorial prefactors quickly destroy the argument. Employing an elaborate counting scheme and using unitarity of the evolution, this can nevertheless be performed. The full technical proof of this suppression is contained in appendix C and yields

$$\epsilon' \mathrel{+}= (2|S|)^{(4+4d_\mathcal{L})|S|+1} 2\, C_{\text{trans}}^4 \Delta^{4d_\mathcal{L}} |\mathcal{C}|\, t^{-\frac{4d_\mathcal{L}}{3}} \left(1 + |\mathcal{C}|^2 C_{\text{clust}} e^{-\Delta/\xi}\right) .$$

Collecting all error terms and choosing a suitable scaling of the separation length Δ in total gives the scaling (see appendix C)

$$\epsilon \propto t^{-\frac{d_\mathcal{L}}{6}} ,$$

which concludes the proof. Thus the non-Gaussianity that can locally be observed is suppressed algebraically in time. For any fixed error ϵ, we can therefore find a relaxation time t_{relax}, such that the difference to a Gaussian state is bounded by ϵ for all times $t \in [t_{\text{relax}}, t_{\text{rec}}]$. Here, the recurrence time is set by the point where the homogeneous suppression breaks down. □

With the above argument, we are able to derive equilibration for a number of free systems, even in settings where the initial state is far from Gaussian. For this, we use the fact that they evolve to a state that is locally indistinguishable from a Gaussian state, together with the equilibration of correlation matrices. In the greater programme of describing dynamical quantum processes with static ensembles, this is a crucial step, which gives explicit realistic time scales for which the system locally can be described in terms of a static ensemble.

Our next goal is to obtain similar results for interacting models. Due to the complex nature of these systems, the obtained results are somewhat limited in comparison, especially concerning the equilibration time scales. Despite these difficulties, we find that generic interacting quantum many-body systems show equilibration behaviour.

3.5 EQUILIBRATION ON AVERAGE

Complementary to the above setting, which so far can only be applied to free Hamiltonian systems, are approaches that work directly with the eigendecomposition of the Hamiltonian [69]. The quantity that is typically investigated here is the squared distinguishability

$$|\mathrm{Tr}\left(A(t)\left(\rho-\omega\right)\right)|^2 .$$

The main difference to the previous approach is that this quantity is not evaluated for a specific instance in time, but rather time averages are being considered

$$\frac{1}{T}\int_0^T \mathrm{d}t\ |\mathrm{Tr}\left(A(t)\left(\rho-\omega\right)\right)|^2 .$$

This can be seen as an infinite time average weighted with the normalised indicator function of the interval $[1, T]$. For large enough times, this finite time average will be indistinguishable from the infinite time average. Without prior assumptions, however, the required time T can be doubly exponentially large in the system size, while under realistic physical conditions, it is usually much smaller [71]. These finite time averages are discussed in the next section, where they are used to capture equilibration time scales. More generally speaking, also different time averages can be considered

$$\int \mathrm{d}t\ f(t)\ |\mathrm{Tr}\left(A(t)\left(\rho-\omega\right)\right)|^2 \ ,$$

which are also known as energy filters (see appendix E). We will mostly stick to the simple time average with equal weight for all times and denote the infinite time average as

$$\overline{f} := \lim_{T\to\infty}\frac{1}{T}\int_0^T \mathrm{d}t\ f(t) .$$

Due to the fact that the squared distinguishability in the integral is strictly positive, we can directly deduce that, if the integral is small, the difference in expectation value has to be small for most times. It is, however, always possible that for some rare times, the states are perfectly distinguishable. This is in sharp contrast to equilibration in free systems presented above, where for a whole interval in time, equilibration was proven.

Following Refs. [69, 86], we focus on spin systems and explicitly expand the above integral. For simplicity, we assume a Hamiltonian spectrum that is fully non-degenerate. This makes the infinite time average state completely diagonal

$$\omega = \overline{\rho(t)} = \sum_k |k\rangle\langle k|\,\rho\,|k\rangle\langle k| \ ,$$

where $|k\rangle$ denotes the eigenstates of the Hamiltonian. Thus the integral above takes the following form

$$\overline{|\mathrm{Tr}\left(A(t)\left(\rho-\omega\right)\right)|^2} = \overline{\left|\sum_{j,k:j\neq k}\langle j|A|k\rangle\langle k|\rho|j\rangle\, e^{-it(E_k-E_j)}\right|^2} .$$

The square can, in a next step, be expanded explicitly

$$\overline{|\mathrm{Tr}\left(A(t)\left(\rho-\omega\right)\right)|^2} = \sum_{j,k:j\neq k}\langle j|A|k\rangle\langle k|\rho|j\rangle \sum_{r,s:r\neq s}\langle s|A|r\rangle\langle r|\rho|s\rangle\, \overline{e^{-it\left((E_k-E_j)-(E_s-E_r)\right)}} .$$

At this point, it is clear that the distinguishability over time is immediately connected to the difference of energy gaps. Let us therefore briefly look into the structure of spectrum of local Hamiltonians.

For local Hamiltonians, it can be shown that the distributions of the eigenvalues is Gaussian, in the sense that the integrated density of states approaches a cumulative normal distribution when the system size grows [87]. In essence the argument relies on using that most Hamiltonian terms commute and are thus independent. Therefore, a form of a central limit theorem can be used [87]. From this, we can also deduce that the distribution of arbitrary energy differences is, to a good approximation, distributed according to a Gaussian, as differences of Gaussian distributions are again Gaussian. In contrast, when one only looks at the differences between energy levels that are next to each other, important structure appears. The literature roughly divides the behaviour of these consecutive gaps into two classes. The first is, when their likelihood approaches a Poissonian distribution with index zero, when the system size is increased, meaning that they are distributed according to

$$P(\Delta) = \frac{1}{\Delta} e^{-E/\Delta} .$$

The other assumes a Wigner-Dyson distribution

$$P(\Delta) = \frac{E}{\Delta} e^{-\alpha E^2/\Delta^2} ,$$

associated to the behaviour of random matrices drawn from the Gaussian orthogonal ensemble (GOE) [88]. A Poissonian distribution is typically associated to so-called integrable models [89], which can be decomposed into non-interacting subspaces, whereas a Wigner-Dyson distribution, in a suitable sense, tells us that the model is interacting. The above statement takes different forms in the current literature [42, 88, 89] and seems like a folklore theorem, while a strict statement of the consequences of the spacing of the consecutive gaps remains elusive so far. These distributions refer to the limiting behaviour of consecutive gaps when the system size approaches infinite.

For finite systems, it is also crucial whether exactly the same value for an energy gap can appear twice when looking at all possible energy differences, rather than just consecutive ones. If this is not the case, then the gaps are called non-degenerate.

Definition 6. *(Non-degenerate energy gaps) A Hamiltonian is said to have non-degenerate energy gaps, iff for the spacing of its energy levels* $E_{k,j,r,s}$*, the following uniqueness result holds*

$$\forall\, k \neq j, r \neq s : E_k - E_j = E_r - E_s \Rightarrow k = r \wedge j = s .$$

This assumption guarantees that the time averages considered above dephase in the infinite time average. The condition is very generic, in the sense that it is fulfilled, as soon as arbitrarily small random nearest neighbour interactions are added to the system [69]. In order to understand its physical meaning, it is useful to first look at a commuting Hamiltonian $H = H_A + H_B$ with $[H_A, H_B] = 0$. Here the excitations of H_A and H_B are independent and the corresponding excitation energies appear as gaps many times in the spectrum. A particular example of such commuting Hamiltonians are the free systems we encountered earlier. Here the occupation of the eigenmodes was completely independent and the corresponding eigenmode energy appears as an energy gap all over the spectrum. In this way, the condition above guarantees that the corresponding Hamiltonian is fully interacting. In other words, there is no tensor product decomposition of the full Hilbert space, such that the Hamiltonian does not couple these two subsystems. Following from this assumption, one can rigorously derive a very general equilibration result for the infinite time average. This is very much complementary to the equilibration in free models.

Theorem 3. *(Equilibration on average) Given a Hamiltonian on a spin system with local dimension* d_{spin} *with non-degenerate energy gaps, then the infinite time average distinguishability on a subsystem* S *can be bounded by [69]*

$$\overline{\|\mathrm{Tr}_{S^c}(\rho_t - \omega)\|_1} \leqslant \frac{d_{spin}^{|S|}}{2 {d_{eff}}^{1/2}} .$$

Here ω *is the dephased state introduced above,* N *is the total number of spins and the effective dimension counts how many eigenstates of the Hamiltonian are part of the state*

$$d_{eff} = \frac{1}{\mathrm{Tr}(\omega^2)} .$$

The above theorem states that the average distinguishability between the time evolved state and the static ensemble ω is small, if the effective dimension is large. Due to the fact that the theorem is formulated for the infinite time average, it does not contain any information on time scales, but rather just means that the states are barely distinguishable for most times. The effective dimension plays a crucial role and it is at this point that the initial state enters. In particular, a large effective dimension excludes the case where only a few eigenstates are superimposed and the evolution would thus be quickly recurrent. In local systems, a large effective dimension can be motivated by looking at the entanglement structure of the eigenstates. For this reason and as a preparatory discussion for many later part of this thesis, we now introduce entanglement measures and discuss the properties of local states.

3.5.1 *Local states*

In this section, we explore local descriptions of states. We begin by reviewing the essentials of entanglement. A bipartite quantum state between two regions X and Y is called *separable*, iff it can be written as

$$\rho = \sum_j \lambda_j \rho_X^j \otimes \rho_Y^j ,$$

where $\lambda_j > 0$ and ρ_X^j, ρ_Y^j are density matrices. All states that are not of this form are called entangled. For mixed states, deciding whether an arbitrary given state is entangled or not is is a NP-hard problem in the language of complexity theory [90], meaning that it most likely cannot be solved in a time polynomial in the size of the system on which the state is defined [91, 92]. For pure states, the calculation of entanglement is greatly simplified. In fact, all the different ways to capture entanglement for mixed states collapse to the same measure, which captures how mixed local reductions of the states are [91]. For a bipartite setting between regions X and X^c, a state is entangled exactly iff

$$S_1(\mathrm{Tr}_{X^c}(\rho)) > 0 ,$$

where $S_1(\rho) = -\mathrm{Tr}(\rho \log(\rho))$ denotes the *von-Neumann entropy*. We call this entanglement measure the entanglement entropy. A more fine-grained measure of how mixed a states is, is given by the *Renyi entropies*.

Definition 7 (Renyi entropies)**.** *The family of quantities*

$$S_\alpha(\rho) := \frac{1}{1-\alpha} \mathrm{Tr}\left(\rho^\alpha\right) ,$$

with $\alpha > 0$ are called the Renyi entropies. For $\lim_{\alpha\to 1}$, they approach the standard von-Neumann entropy.

Naturally, each Renyi entropy directly also gives a way to quantify entanglement for pure states. Two special abbreviations are common in the literature, namely $H_{max} := S_0$, which captures the rank of ρ and $H_{min} := \lim_{\alpha\to\infty} S_\alpha$, which is the largest eigenvalue of ρ. As the names suggest, they fulfil

$$H_{min} \leqslant S_\alpha \leqslant H_{max} \quad \forall\alpha \,.$$

One of the key insights in the research of local systems is that the local interaction structure of a Hamiltonian also reflects itself in the properties of its eigenstates, at least for low energies. The state with the lowest energy is called the *ground state*. In case there is a uniform lower bound for the excitation energy to the first excited state, independent of the system size, the model is called gapped and the largest possible lower bound is called the *spectral gap* γ. Using such a gap, one can infer a lot of structure of the ground state. Even though the results can often be generalised to degenerate subspaces, we restrict to the conceptually simpler case of a unique ground state. On a mathematically rigorous level, a key result is the *exponential clustering theorem* [66, 93, 94].

Theorem 4 (Exponential clustering theorem)**.** *Let H be a quasi-local Hamiltonian with spectral gap $\gamma > 0$ and unique ground state $|E_0\rangle$. Then this ground state has exponentially decaying correlations, in the sense that*

$$|\langle E_0|AB|E_0\rangle - \langle E_0|A|E_0\rangle\langle E_0|B|E_0\rangle| \leqslant Ce^{-\mu d(A,B)} \,,$$

where A, B are local operators and C, μ are constants that strongly depend on the gap γ, but are independent of the system size.

We will later demonstrate that such a statement can be generalised also to higher excited states in the context of localising systems (see section 6.4) and provide a proof reminiscent to that of the exponential clustering theorem. Another important feature of ground states of gapped models is that their entanglement entropy can be bounded in one dimension (1D) [95–97].

Theorem 5 (1D area law)**.** *Let H be a quasi-local Hamiltonian in 1D with spectral gap $\gamma > 0$ and unique ground state $|E_0\rangle$. Then the entanglement entropy of this ground state across any bi-partite cut is bounded by a constant, independent of the system size.*

Here the assumption that the system is one-dimensional is absolutely crucial. A similar result also holds for the more general Renyi entropies [95]. This result is a particular case of a so-called area law [98]. While entanglement entropies generically scale like the volume of the considered region, and thus fulfil a *volume-law*, an *area-law* implies that the entropy only grows like the boundary of that region.

Definition 8 (Area law)**.** *A state ρ is said to satisfy an area-law for some entanglement measure $\mathcal{E}_X$ between region X and its complement, iff its entanglement between that region and its complement is bounded by the size of boundary $|\partial X|$ of that set*

$$\mathcal{E}_X(\rho) \leqslant C|\partial X| \,,$$

for some constant C that is independent of the system size and the region X.

It is often suspected that the ground state of gapped local Hamiltonians also fulfil an area-law for the entanglement entropy in higher dimensions than 1D, but the proof remains elusive despite considerable efforts [98]. However, there are important instances, where it has already been successfully proven [99–101]. Interestingly, the exponential clustering theorem is in no way restricted to 1D. Intuitively, one might assume that if a pure state has decaying correlations, this might be enough to achieve a bound for the

entanglement. In 1D, this indeed turned out to be true [102, 103]. In higher dimension, it is unclear whether a similar result can hold [102, 103]. As it would immediately imply an area-law for the ground states of gapped local Hamiltonians, it is likely that the proof will be hard.

Finally, especially in one dimension, it is often useful to approximate states with tensor networks. There is a whole zoo of such tensor-network states and one could easily fill this whole thesis with a review of such states. Here we focus on the setting of 1D pure states that can be captured as matrix-product states (MPS) [104], which are defined as follows (see also appendix A).

Matrix-product states

A state $|\psi\rangle$ is called a matrix-product state with bond dimension D, if we can write it as

$$|\psi\rangle = \sum_{j_1,\cdots,j_L=1}^{d_{\text{spin}}} c_{j_1,\cdots,j_L} |j_1,\cdots,j_L\rangle \ ,$$
$$c_{j_1,\cdots,j_L} = \langle A_1[j_1]| A_2[j_2] \cdots A_{L-1}[j_{L-1}] |A_L[j_L]\rangle \ ,$$

where $\langle A_1[j_1]|$ and $|A_L[j_L]\rangle$ are boundary vectors of size D and $A_k[j]$ for each position k are complex $D \times D$ matrices. For sufficiently large D any state can be captured in this form. One speaks of a state being an MPS if the bond dimension for an approximation with fixed 1-norm error grows only linearly with the system size. If the state is translational invariant, then one can choose the matrices A to be the same at all sites and drop the subscript.

The success in approximating a state with a low bond dimension MPS is directly connected to the entanglement entropy for spatial cuts. For example, given an area-law for a Renyi-entropy S_α with $0 \leqslant \alpha < 1$, one can prove that the state can efficiently be approximated in one-norm with an MPS that has a bond dimension growing linearly with the system size (see appendix A for details).

Let us now discuss these results in the context of equilibration and the effective dimension in local quantum systems. A natural assumption on the initial state is that it is to some extent locally described, for example in the form of exponential clustering correlations characteristic of ground states of gapped models. Since most eigenstates of generic local Hamiltonians are expected to be very entangled [87], it seems intuitive that many eigenstates are needed to write down the initial state, thus giving a large effective dimension of the initial state. This assumption can be tested numerically, at least on small systems, which often shows that the effective dimension increases exponentially with the system size, in particular when looking at states with an energy in the bulk of the spectrum [3, 26, 42]. A usual setting where this is the case are global quenches, where all local Hamiltonian terms are changed [3, 26].

Rigorous results come from the study of random Hamiltonians. In this setting, it is assumed that the eigenstates are distributed according to some random ensemble, for example the Haar measure [13]. In this setting, one can show that eigenstates are strongly entangled and correspondingly many initial states that are, for example, described with a low bond dimension MPS have a large effective dimension [13]. The effective dimension in Thm. 3 can also be replaced by some other measure of how spread out the initial state is as a distribution over the eigenstates. As a single eigenstate does not evolve at all, a common measure is also the second largest populated eigenstate, which can be used instead of the effective dimension [105].

Theorem 3 discussed above is an equilibration result very much complementary to the equilibration in free systems that we described in the previous section. Its clear strength is that it can be applied to very

general settings. In particular, the only assumption on the Hamiltonian are the non-degenerate energy gaps. More recently, it was pointed out that fully non-degenerate energy gaps are by no means necessary [71]. Doing a careful counting, some degenerate energy gaps can be accounted for, without significantly altering the results [70, 71]. In the following, we look at the time scale, on which equilibration on average takes place. As mentioned before, the corresponding bounds are very large and far from the short time scales encountered in free models in section 3.4.3.

3.5.2 *Time scales*

The above result merely says something about the infinite time average, but it is unclear how long it will take for the effect to set in. In particular, it could well be that the state remains distinguishable from its infinite time average for a very long time, which is greater than any experimentally accessible time scale. In order to make these results applicable to experimental setting, the questions of time scales is thus of utmost importance.

Unfortunately, while there were important efforts to obtain bounds on the equilibration time [58, 59, 71, 86, 106], the best known bounds are still very long. In order to get some handle on finite time averages, one first separates the full energy scale into small parts ϵ. For each of these sections, the number of energy gaps contained in it are counted and referred to as $\mathcal{N}(\epsilon)$ [71]. For a POVM measurment with M possible outcomes, one can then derive the following bound [58]

$$\frac{1}{T}\int_0^T \mathrm{d}t\; D_M(\rho,\omega) \leqslant \frac{M}{4}\sqrt{\frac{5\pi\mathcal{N}(\epsilon)}{2d_{\mathrm{eff}}}\left(\frac{3}{2}+\frac{1}{\epsilon T}\right)},$$

which gives an estimate for the average distinguishability over a time interval T. Let us have a look at how this equilibration time scales with the system size.

The crucial point in this estimate is the linear coupling between ϵ and T. The number of gaps $\mathcal{N}(\epsilon)$ in a certain energy interval ϵ increases exponentially with the square of the system size, at least for energy differences close to zero. Thus, to keep the number of gaps of the order of the effective dimension, which increases only exponentially with the system size, ϵ in turn has to be made exponentially smaller. Thus, this decrease in ϵ has to be compensated by an exponential growth of the equilibration time T. Therefore the bound above still falls short of providing a reasonable experimental time scale.

This is, however, a consequence of the general applicability of the result. In fact, settings can be constructed where the above bounds are saturated [58], even though they are somewhat contrived. More recently, even translationally invariant models were found where equilibration time scales are very long [86, 107, 108]. There, particles travel extremely slowly, for example only in a logarithmic fashion and it takes a long time for them to explore the full system (see chapter 6).

The above discussion clearly shows that more structure is needed to arrive at physically realistic time scales. These assumptions will likely be similar to the ones encountered in the context of equilibration in free systems. Explicitly, we expect Lieb-Robinson bounds, transport and special local structure in the initial state to play a crucial role and ultimately be the reason why many models in nature equilibrate quickly, often even on a time scale independent of the system size [32]. While no proofs of fast equilibration in generic interacting models were achieved, we still think that it is worthwhile to explore this topic further, before we move towards the investigation of the static ensembles in the chapters on thermalisation (see chapter 4) and localisation (see chapter 6). For this, we give a more detailed picture of how the evolution of local systems takes place.

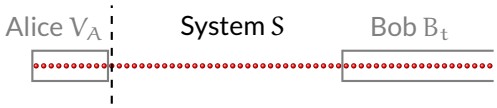

Figure 3.3: Shown is a sketch of the information propagation in an Alice-Bob type setting. Alice encodes a bit by either applying a unitary V_A on her part of the chain or doing nothing. After an evolution time t, Bob makes a measurement on his part of the chain. Whether the two parties can communicate this way depends on whether the support of Bob's measurement B_t over time leaves the region S.

3.5.3 *Local dynamics*

In this section, we look at the implications of locality for the dynamical evolution of the Hamiltonian. This can most conveniently be investigated in the Heisenberg picture, where observables rather than states are evolved in time. Naturally, the locality of the evolution can also be formulated in the Schrödinger picture, where operator locality can be translated to entanglement of the state. We establish this connection explicitly for some important results later on.

In order to capture the spreading of operators in the Heisenberg picture, we introduce some mathematical definitions in this direction. The spreading of operator support can conveniently be captured by comparing the time evolved observable with its truncated versions

$$\|B_t - \Gamma_S(B_t)\| ,$$

where Γ_S denotes the truncation map introduced in section 3.2.

This quantity directly relates to information propagation in the system. For this, let us introduce a common Alice-Bob type setting (see Fig. 3.3). Here different parts of a spin system, for simplicity a 1D chain, are given to two parties [109]. Let us use a setting where a small region X is initially handed to Bob, on which he can measure some local observable B. Alice's task is to either do nothing or apply a local unitary V_A on her part of the chain, which is denoted by S^c. This way, the two parties are trying to communicate a classical bit between them. Using the Γ map, one can capture the signal strength, meaning how well Bob can detect Alice's action. Let us start with the lower bound

$$\begin{aligned}
&\|B_t - \Gamma_S(B_t)\| \geqslant \kappa \\
\Rightarrow &\|B_t - \Gamma_S(B_t)\| = \left| \int_{S^c} dU \operatorname{Tr}\left(V_A \left[B_t, V_A^\dagger \right] \rho \right) \right| \geqslant \kappa \\
\Rightarrow &\exists V_A : \left| \operatorname{Tr}\left(V_A \left[B_t, V_A^\dagger \right] \rho \right) \right| \geqslant \kappa \\
\Rightarrow &\exists V_A : \left| \operatorname{Tr}\left(B_t V_A^\dagger \rho V_A \right) - \operatorname{Tr}(B_t \rho) \right| \geqslant \kappa ,
\end{aligned}$$

where we used that the Haar measure is normalised. Thus, from the lower bound, we can deduce that the action of a unitary on the region S^c can be detected by an observable initially localised on X. Thus in the above Alice-Bob protocol, the two parties can provably communicate, if a lower bound to the error of the Γ map is known. Similarly, an upper bound directly allows to conclude that this observable cannot be used to send signals through the chain

$$\begin{aligned}
&\|B_t - \Gamma_S(B_t)\| \leqslant \kappa \\
\Rightarrow \left| \operatorname{Tr}\left(B_t V_A^\dagger \rho V_A \right) - \operatorname{Tr}(B_t \rho) \right| &= \left| \operatorname{Tr}\left(V_A \left[B_t, V_A^\dagger \right] \rho \right) \right| \\
&= \left| \operatorname{Tr}\left(V_A \left[B_t - \Gamma_S(B_t), V_A^\dagger \right] \rho \right) \right| \\
&\leqslant \|B_t - \Gamma_S(B_t)\| \leqslant \kappa .
\end{aligned}$$

We now present a way to obtain very general upper bounds using only locality of the Hamiltonian in the form of Lieb-Robinson bounds [110]. In section 3.4.3, we already encountered their simplified version for free systems, there a single fermionic creation operator dynamically was mapped to a superposition of such operators, which were distributed over a region that spread ballistically. In a more abstract language, it could be seen as a statement how quickly the support of the fermionic observable spreads over the lattice. For interacting spin systems, such a bound takes the following form.

Definition 9 (Lieb-Robinson bound)**.** *Let* B_X *be an initially local operator and* $B_X(t)$ *its dynamical evolution. A system is said to fulfil Lieb-Robinson bounds, iff*

$$\|B_X(t) - \Gamma_{X_l}(B_X(t))\| \leqslant C_{LR}\,|X|\,e^{-\mu(l-\nu|t|)}\,,$$

with constants C_{LR}, μ, ν *independent of the system size and* X_l *the enlarged regions around* X *(see chapter 3.2). Here* ν *plays the role of a velocity linearly connecting space and time.*

This can be seen as an effective light cone, with which the support of an operator increases. Outside of the cone, the support of the operator is exponentially suppressed. Thus, these bounds provide a direct way to upper bound the speed of information in any local spin model. As in the case of free systems, the main feature of Lieb-Robinson bounds is that they can be derived in very general systems, relying on nothing but locality of the Hamiltonian [66, 93, 110–112].

Theorem 6 (Lieb-Robinson bound from locality)**.** *Let* H *be a family of quasi-local spin Hamiltonians for different system sizes with terms that are uniformly bounded independent of the system size. Then there exists constants* C_{LR}, μ, ν *independent of the system size, such that for all local operators* B_X*, we have*

$$\|B_X(t) - \Gamma_{X_l}(B_X(t))\| \leqslant C_{LR}\,|X|\,e^{-\mu(l-\nu|t|)}\,.$$

In other words, the system fulfils a Lieb-Robinson bound.

In this way, the evolution of any local Hamiltonian can be captured in terms of an effective light cone. Interestingly, this result can be used to establish a connection between the speed of sound in quantum systems and the speed of light in relativistic theories. In fact, one can show that in the continuum limit of letting the lattice spacing go to zero, an exact light cone emerges and the exponential tails vanish [113].

In recent years, Lieb-Robinson bounds have played a crucial role in our understanding of local Hamiltonian models. Fundamental insights into the ground states of local models, such as the exponential clustering theorem and the 1D area-law proof (see section 3.5.1), both rely on Lieb-Robinson bounds [66, 95]. In a similar spirit, we will later see an application of the bounds to connect dynamical localisation to the structure of individual eigenstates (see section 6.4). Moreover, the classification of quantum phases heavily benefited from this tool [114, 115]. In fact, the only known instance where such a quantum phase, in this case one with topological order, is provably stable to a physically realistic perturbation also relies on Lieb-Robinson bounds [116, 117].

Such bounds were derived in many important settings. For spin systems, one can generalise them to more general graphs as well as interactions that only decay algebraically [36, 66, 67], as long as their decay is strong enough [67]. The result can also be directly carried over to fermionic systems. For bosons, the discussion is more complex, due to the locally unbounded Hilbert spaces. This leads to the situation that Lieb-Robinson bounds are often experimentally observed [31], while a proof for such situations is still outstanding. Interestingly, even special bosonic settings can be constructed, where arbitrarily fast

spreading of information is provably possible [118], highlighting the incompatibility between quantum mechanics and special relativity. The details of these generalisations, as well as an attempt to provide an intuitive proof for Lieb-Robinson bounds in spin systems, are contained in appendix B.

As described above, Lieb-Robinson bounds can be seen as a direct way to bound the speed with which information can travel through the system. As information can always be encoded in sending particles or energy, this naturally also bounds the speed of any form of transport in the system. It is, however, crucial to note that these concepts are no longer as clearly linked in interacting models, as they were in free systems. In interacting models, the operator can explore an exponentially large algebra. From a physical point of view, this means that models can be created that show a complete absence of particle or energy transport, but still allow to send information through them. We explicitly construct this in section 6.2 in the context of localising models. This discussion highlights the importance of exploring all facets of transport in a quantum information language in interacting models, which is an area that would certainly be an interesting research topic in the near future.

The above described Lieb-Robinson bounds provide a clear intuition for the dynamics of local models. Starting with a local observable, it expands its support at most in a linear fashion. As states can be constructed that have strong inhomogeneities, it is clear that the observable first needs to explore the full lattice, before equilibration for arbitrary states is possible. Therefore, as long as no information of the initial state is used other than a large effective dimension, equilibration needs to take at least linearly long in the system size. Still, there is a huge gap between those linear lower bounds and the exponentially long bounds that can be derived for generic models.

Recently, it was speculated that tighter bounds on equilibration could be derived using transport [119]. Similar to the free system, such a transport assumption would guarantee that the Lieb-Robinson bound is not only an upper bound, but rather accurately describes the behaviour of the system. Outside of the realm of localising systems (see chapter 6), this seems to indeed be the case, as is impressively demonstrated in experimental probes of such light-cone behaviour [34, 36, 120]. While we share the underlying intuition, there still seems to be a long way to go to turn it into rigorous mathematics. Not only is the precise notion of transport unclear, but also special features of the initial state are needed. Aside from having to some spatial homogeneity, such as translational invariance, we expect that they have to be local to some extent.

Let us now look at equilibration from the point of view of numerical simulations and state dynamics. As described in the beginning, the usual way how to explore the out of equilibrium dynamics is to start with some equilibrium state, for example the ground state of a local Hamiltonian. Thus, the initial state can often efficiently be captured as a tensor network state with low bond dimension, at least in 1D (see section 3.5.1). Then the system is pushed out of equilibrium. This can either happen by a sudden change, which is known as a quench, or by continuously tuning a Hamiltonian parameter, which is known as a ramp. During these out of equilibrium dynamics the time evolution can be simulated in a tensor network language. For this, the unitary evolution is broken into small time steps, using a so-called Trotter decomposition [121] and is sequentially applied to the MPS [122].

This application of unitary gates increases the bond dimension, which is truncated again after every step. How well this truncation can work is ultimately determined by the growth of entanglement over time [41]. Assuming that the Hamiltonian is local, Lieb-Robinson bounds give an upper bound on how fast this can happen. As it turns out, in local models, the entanglement over any cut can at most grow linearly, which means that a state initially fulfilling an area law, will also fulfil an area law for later times, albeit with a linearly growing prefactor [65, 123, 124]. For the simulation of quenches with MPS [41], this means that a linear growth of the bond dimension is sufficient. Thus, short time evolution can provably efficiently be captured.

Again, as explained when presenting Lieb-Robinson bounds, equilibration is likely to take at least linearly long in the system size, at least for spatially inhomogeneous states. Often, we expect the equili-

bration to move towards strongly mixed states, for example thermal states. Naturally, the global state always remains pure under the Hamiltonian evolution and the only way to locally look strongly mixed is by building up entanglement. In settings where entanglement growth is very slow, such as localising systems (see chapter 6), equilibration therefore also takes a long time. This concludes our discussion of equilibration of local expectation values. Before we move towards the description of the static ensembles, let us quickly summarise our insights into equilibration of quantum many-body systems.

3.6 SUMMARY: EQUILIBRATION

In the preceding chapter, we investigated out of equilibrium settings, for example created by a sudden change of of the Hamiltonian. We described two crucial results that capture the equilibration behaviour of quantum many-body systems. They were formulated in two complementary pictures. The first looked at free systems described by Gaussian states, where the evolution of creation and annihilation operators has a particularly easy structure. This allowed us to investigate equilibration directly and gave rise to realistic physical settings where equilibration provably happens on a short time scale. We further demonstrated that this Gaussian description can still be applied for non-Gaussian initial states, as long as the evolution obeys Lieb-Robinson bounds, bounding the speed of particle propagation and has transport. This was achieved by showing that the evolution of a free fermionic systems with transport provably moves towards states that locally look Gaussian [6].

The complementary approach looked at equilibration on average, where time averaged distinguishability from a static ensemble is considered. There, extremely general states and Hamiltonians are investigated. This came at the price of only being able to derive results on average that only hold for very long time scales. As captured by Lieb-Robinson bounds for interacting models, we saw that spreading of information in local models happens at most ballistically. Based on this, we speculated that, similar to the setting of free systems, fast equilibration might rely on the actual evolution of the Hamiltonian leading to ballistic spreading of particles. Defining such transport seems, however, to be a difficult task, most importantly as information and particle propagation are very distinct processes in generic quantum systems (see section 6.2). By looking at equilibration in a picture of local states, we captured it in terms of entanglement growth. This gave rise to descriptions in terms of tensor networks, a tool that plays a prominent role in many sections of this thesis.

To summarise, despite the sketched difficulties, especially concerning realistic equilibration time scales, for many practical purposes, local expectation values of time-dependent states can often be captured in terms of static ensembles. For completeness, let it be noted that there are also other possible routes to equilibration. For measurements that are low-rank projectors, for example, equilibration can be proven to happen very quickly [58]. Another approach is to carefully consider the nature of macroscopic observables and ask how well one would reasonably be able to measure fluctuations of macroscopic systems [70, 105, 125]. While this approach does not apply to mesoscopic quantum systems usually considered in optical lattices or ion traps and is thus somewhat neglected in this thesis, it is certainly an interesting avenue to understand equilibration for large scale physical models. Finally, many insights also come from models where eigenstates are drawn randomly. As pointed out above, a large effective dimension of many initial states can be derived [42]. What is more, one even can show that in such models, typical observables quickly equilibrate with very mild assumptions on the spectrum [126, 127].

In the next chapter, we investigate the nature of the static ensembles. In particular, we are interested in the question to what extent they can be captured in terms of Gibbs states. Afterwards, we show that such a description breaks down in models with randomness and investigate how this randomness effects the equilibration and the corresponding static ensembles in the model (see chapter 5).

4

THERMALISATION

In the previous chapter, we explored conditions under which measurement outcomes of the system can be described in terms of static ensembles. We further argued that the emerging equilibrium state necessarily is equal to the infinite time average, which takes the following form for the case of non-degenerate energies

$$\omega = \lim_{T\to\infty} \frac{1}{T}\int_0^T dt\ \rho(t) = \sum_k |k\rangle\langle k|\,\rho\,|k\rangle\langle k| \ .$$

This can be seen as the maximum entropy state, keeping all constants of motion, namely the eigenprojectors of the Hamiltonian $|k\rangle\langle k|$, fixed [3, 42]. From a practical point of view, this still does not help when trying to capture the equilibrium state, as full diagonalisation of the Hamiltonian is required to obtain the constants of motion. Moreover, the equilibrium state still has 2^n free parameters, corresponding to the overlap with the eigenprojectors.

Fortunately, it is often by no means necessary to specify the values of all those constants of motion. In the previous chapter, we already encountered the example of free systems, whose infinite time average is provably captured in terms of a generalised Gibbs ensemble with only the linearly many eigenmode number operators as constants of motion. This emerging description in terms of a small set of parameters seems to be common behaviour of quantum many-body systems. Thus, the full information provided by the overlaps with the different eigenvectors is hidden from the macroscopic observer for many realistic settings.

For interacting models, one often even finds that a single parameter is sufficient for accurately capturing equilibrated expectation values. This parameter is the Lagrange multiplier which describes the energy constraint present in any closed quantum system and is the inverse temperature $\beta = \frac{1}{k_B T}$. As before, we restrict the available measurements to some small region, thus directly ensuring that only a small amount of information of the state can be extracted. In this setting, thermalisation means that local expectation values look thermal, in the sense that

$$\left\| \mathrm{Tr}_{S^c}\left(\omega - \frac{1}{Z_0} e^{-\beta H}\right)\right\|_1 \leqslant \epsilon \ ,$$

where $Z_0 = \mathrm{Tr}(e^{-\beta H})$ denotes the partition sum. In this case, it is sufficient to locally describe the equilibrium state in terms of a single parameter, namely β, instead of 2^n degrees of freedom corresponding to the eigenvector occupations.

In this chapter, we review different approaches to thermalisation. First, we look at the *eigenstate thermalisation hypothesis* (ETH), which resolves the issue at the level of individual eigenstates. Afterwards, other approaches are investigated, where less structure of the eigenstates is assumed at the price of less generic initial states.

4.1 EIGENSTATE THERMALISATION HYPOTHESIS

For thermalisation, the different eigenstates involved in the infinite time average ω need to combine to a thermal ensemble. The ETH is an extreme form to solve this problem, by demanding that each eigenstate

itself already has a thermal form. While there are many version of it, we restrict to the most direct approach [128–131].

Statement 1. *(Eigenstate thermalisation hypothesis) A Hamiltonian* H *is said to fulfil the ETH, if its eigenstates* $|E_k\rangle$ *in the bulk of the spectrum are locally indistinguishable from the Gibbs state*

$$\left\| \mathrm{Tr}_{S^c} \left(|E_k\rangle\langle E_K| - \frac{1}{Z_0} e^{-\beta_k H} \right) \right\|_1 \leqslant \epsilon \, ,$$

where β_k *is chosen such that the thermal state has energy* E_k *and* ϵ *is sufficiently small.*

In order to turn this statement of the ETH into a definition, some things would still need to be clarified. Firstly, demanding the ETH only for the bulk of the spectrum is necessary, as ground states often have little entanglement and thus do not look thermal. That being said, the precise cross-over to behaviour in the bulk of the spectrum would need to be specified. Secondly, the role of ϵ is unclear. Intuitively, it should be a function of the system size that decays sufficiently quickly with it. So far, there seems to be no consensus on such a rigorous version of the ETH [42].

The ETH assumes that each eigenstate locally looks thermal with a temperature fixed by its energy. Assuming this hypothesis, it is quite clear how thermalisation would take place. If a state has a high effective dimension, meaning large overlap with many eigenvectors, then it equilibrates according to the results of the previous chapter. The ensemble is then captured in terms of the dephased state ω. If this distribution is narrow in energy, which is well possible as any fixed energy window in the bulk of the spectrum still contains exponentially many eigenstates, then the infinite time average would simply be a mixture of many states that all locally look thermal with roughly the same temperature. Thus, the full state would be locally indistinguishable from a Gibbs state of that temperature [42]. While intuitively this line of argument it quite clear, a further investigation of the precise mathematical assumptions and the resulting scaling would surely be needed.

Note that the ETH in itself does by no means guarantee thermalisation for all initial states. In particular, merely assuming a large effective dimension is not sufficient. After all, the involved eigenstates in ω could be far from each other in energy and thus lead to a classical mixture of local expectation values of Gibbs states with very different temperatures. As the mixture of Gibbs states with different temperatures is not again a Gibbs state, it seems likely that such a state could not be captured in terms of a thermal ensemble. Thus, even if one is willing to assume the ETH, thermalisation still requires some promise of having a narrow energy distribution in the initial state, or at least only large weight in a small energy region that would thus dominate the expectation value.

The ETH was extensively tested numerically in various contexts, with sometimes striking success [38, 131–133]. One direct, but nevertheless important consequence of the ETH is the fact that most eigenstates have to be strongly entangled. After all, they are supposed to locally look like a Gibbs state. As the entropy of this thermal state is usually extensive, at least for temperatures away from the ground state, this directly shows that the eigenstates fulfil a volume- rather than an area-law.

While it is unclear to what extent it truly is the defining mechanism behind thermalisation, its investigation clearly has moved the field forward substantially. In particular, it gave rise to a closer investigation of the eigenstates and showed that their entanglement features are closely connected to the physical question of how to capture dynamical time evolution. That being said, it is clear that the ETH is exceedingly hard to test, even numerically. While the original question of thermalisation can be accessed experimentally or using simpler numerical tools, testing the ETH in an experiment is impossible, if only for the fact that individual eigenstates in the middle of the spectrum can never be prepared. Thus, it is clearly still a hypothesis. Interestingly, it was recently argued that as long as thermalisation takes place for states that are narrow in energy [42] or for all product states [134] of an interacting model, then the ETH is not only

sufficient, but in fact necessary in order to achieve thermalisation. This would, in a certain sense, also greatly simplify its numerical and experimental verification.

That being said, the original question we are following, namely why nature looks thermal, could also be related to specific structure in the initial state and demanding that exponentially many product states thermalise is not necessarily connected to the actual behaviour of quantum models. In fact, it seems intuitive to assume that in realistic initial states, the weight of the individual eigenvectors in an energy region will be a rather smooth function. Thus, it might not be necessary that each eigenstate itself looks thermal but rather only that a mixture of them does. In the following, we will explore this approach to thermalisation further.

4.2 ALTERNATIVE ROUTES TO THERMALISATION

The ETH resolves the issue of thermalisation by placing very strong assumptions on the eigenstates, while initial state can be quite general. Ref. [135] proceeds along different lines and obtains thermalisation by a perturbative coupling to a bath. In this context, no promise on the behaviour of individual eigenstates is needed, while the Hamiltonian and the initial state are now restricted. The argument assumes a small subsystem coupled to a large bath, which is assumed to have a Gaussian distribution of energies, which seems reasonable in the context of large locally interacting systems (see chapter 3.2). The whole system is placed in a state that is close to the microcanonical ensemble, in the sense that the eigenstates within one interval are approximately evenly populated. Note that this class of states is still very large and also includes pure states [135]. Coming from a point of view of experimental preparations with realistic uncertainties, this seems very natural.

The coupling between system and bath is assumed to be bounded in operator norm. This allows for a perturbation analysis relying on the change of eigenprojectors of the Hamiltonian [135] (see also Thm. VII.3.1 in Ref. [14]). In this setting, it can then be shown that the subsystem looks like a Gibbs state, which gives a route to thermalisation that is free of assumptions on the level of individual eigenstates.

The main weakness of the above approach is that, due to the fact that it relies on perturbation theory, it is restricted to a coupling between system and bath that is bounded in operator norm. For systems coupled only at the boundary, for example small connected subsystems of a large lattice, this seems reasonable in one spatial dimension, but poses a severe restrictions in two or higher dimensions. Still, it is a crucial result, in that it highlights that the ETH is by no means the only way to guarantee thermalisation in interacting quantum systems. This topic is comprehensively reviewed in Ref. [42].

More generally speaking, this approach solves the issue of thermalisation by assuming a smooth function in the eigenvector occupations within a small energy interval. Such a state is, in essence, a microcanonical ensemble. Recently, the structure of such microcanonical ensembles was investigated in the context of translationally invariant systems and in fact it was shown under rather general conditions that they are locally indistinguishable from a Gibbs state [136, 137]. These results are connected to thermalisation based on a similar reasoning as the work discussed above, where the microcanonical ensemble can be seen as coming from a preparation procedure that populates eigenstates with similar energy equally.

Often, thermalisation is investigated in the context of global quenches (see chapter 3). There, one begins in an eigenstate of one Hamiltonian and abruptly changes some Hamiltonian parameter. The initial state typically has overlap with many different eigenstates of the new Hamiltonian [138–140], which guarantees equilibration on average (see section 3.5), at least in the setting of non-degenerate energy gaps. These states typically roughly uniformly populate eigenstates around a certain energy [138–140]. This highlights that in the setting of quenches, there is some structure of the initial state that could be used, much in the spirit of the above mentioned publications.

Finally, it is worth noting that considerable progress was achieved in the investigation of the structure of thermal states. In particular, it was found that they have exponentially clustering correlations at large enough temperature [141]. This does not only give a universal upper bound to any phase transition temperature, but can also be used to show that temperature can be defined locally [141]. Such a local structure of thermal states is an important insight and could potentially prove very useful in understanding to what extent dynamics of non-equilibrium states can be captured using thermal ensembles.

Having reviewed different aspects of thermalisation behaviour, we now move towards a setting in which the non-equilibrium state does not thermalise. While there are many levels at which thermalisation can fail, we focus on the most interesting scenario, where equilibration takes place, but the equilibrium state has memory of its precise initial condition and can thus not be captured with a single parameter β.

4.3 FAILURE OF THERMALISATION

While thermalisation is expected to be a very generic phenomenon, there are systems and settings in which the description in terms of a simple Gibbs ensemble fails. For example, as we already discussed in section 3.4, free systems require the inclusion of linearly many constants of motion in a generalised Gibbs ensemble.

Generally, it is a hard problem to decide which constants of motion are required to accurately capture local expectation values. There is, however, one clear case where constraints have to be included, namely if the system possesses local constants of motion. After all, these local constants of motion are possible local measurements and, in general, their value cannot be accurately captured in terms of a Gibbs state. This can be seen by the following argument.

By definition, these local operators commute with the Hamiltonian. Thus, the eigenstates of H can be separated into different sectors corresponding to the eigenvalues of the constant of motion. Furthermore, as the operator is supported on a small region, its influence on the global energy scale necessarily is small. More precisely, each eigenvector sector will contain states with arbitrary energy density, at least for large enough systems. Thus only tuning the temperature cannot be sufficient to select any of those sectors.

Now imagine a state that only has initial support in one of those sectors. As there are only a fixed number of such sectors, but exponentially many eigenstates, this is still perfectly compatible with a large effective dimension and provable equilibration. As the local operator is a constant of motion, the dynamics of this sector is decoupled from the others and it is clear that a description in terms of a Gibbs state can never emerge. In this way, any local constant of motion has to be included in a static ensemble in terms of a generalised Gibbs ensemble.

If such a local constant of motion exists, it is also clear that the ETH cannot be fulfilled, as there exists a local operator that can distinguish eigenstates, despite the fact that they can be close in energy density. This clearly hints at a failure of thermalisation being connected to the structure of individual eigenstates. In fact, it turns out that the failure of a system to thermalise can be connected to a lack of a special form of entanglement in the eigenstates [68].

In the following two chapters, we will investigate the paradigmatic setting of *localisation*, where such a lack of entanglement, as well as the existence of local constants of motion is created by random local potentials. This randomness prohibits thermalisation, strongly suppresses transport and is often considered as an explanatory mechanism for a breakdown of conductance in solid-state physics. Before we dive into this, let us briefly summarise our insights into thermalisation.

4.4 SUMMARY: THERMALISATION

To summarise, in this chapter we investigated the precise nature of the equilibrated ensembles. Based on the fact that these ensembles are given by infinite time averages, we argued that its description is closely connected to constants of motion. One class of such constants of motion are the eigenstates of the Hamiltonian. Thus, their specific structure is of crucial importance to capture the static ensemble. Following the eigenstate thermalisation hypothesis (ETH), the eigenstates are strongly entangled and already individually look locally like a thermal Gibbs state. We argued that this hypothesis can be employed to show thermalisation in case the initial state has a sufficiently narrow energy distribution. In the context of global quenches, this seems to indeed be the case and the ETH would be sufficient to rigorously capture thermalisation, meaning that the out of equilibrium state can locally be captured in terms of thermal ensembles.

In some way, however, shifting the issue of thermalisation to the level of individual eigenstates is unsatisfactory. After all, the ETH is only a hypothesis that, so far, cannot be approached analytically, cannot be measured experimentally and can only be checked numerically with large effort. Thus, also approaching thermalisation without assuming the ETH is an important endeavour. For this, we argued that more structure in the initial state is needed.

Given the fact that experimental preparations always have an energy uncertainty, it will commonly be hard to purposely select eigenstates with similar energy. Thus, typical initial states have a distribution of eigenvectors that is relatively smooth. Based on such assumptions, we saw that perturbation theory can also be used to obtain thermalisation, without having to place assumptions on individual eigenstates. More recently, these arguments, which are mostly restricted to 1D, have been embedded in proofs that the microcanonical ensemble locally looks like a Gibbs state. Such approaches could also be suitable candidates to explain thermalisation and could provide a proof of the phenomena without having to rely on heavy assumptions such as the ETH.

In contrast to this investigation of thermalisation, first models were presented where this description in terms of Gibbs states fails. There, the systems shows some memory of its precise initial configuration, for example due to the presence of a local constant of motion. In such cases, only accounting for the energy constraint is not sufficient, but rather other constants of motion have to be included in a generalised Gibbs construction. In the following, we explore a large class of systems where this memory of the initial conditions is created by the presence of random local potentials.

5

LOCALISATION WITHOUT INTERACTIONS

In the following two chapters, we explore the dynamical behaviour of many-body systems with strong local random potentials. These models provide an intriguing class of systems to explore the notions of equilibration and thermalisation presented so far. In particular, as is argued in the following chapters, these models show very slow equilibration behaviour, if they equilibrate at all and a failure to thermalise. Rather the existence of local constants of motion leads to the model having a local memory and these constants of motion need to be included in the description of the static ensemble.

The results of this chapter, are, however, also interesting outside of the realm of equilibration and thermalisation. Firstly, because these models are, to a certain extent, easy to solve. This allows to establish links between dynamic and static features and to extend prominent results, like the exponential clustering theorem, to other eigenstates. Thus, they provide an ideal arena to understand Hamiltonian properties and their physical implications in more depth.

Secondly, these systems are extremely important from a condensed matter point of view, as they provide an explanation how impurities can lead to a complete break-down of conductance. This is largely based on Anderson's work back in 1958, capturing free electrons in a random potential. One of the key questions, namely to what extent these results are stable in the presence of electron-electron interactions, is, however, still open and has recently been investigated with considerable effort. The discussion of interacting electrons is postponed to an upcoming chapter and heavily builds on the tools and intuition provided in the following discussion of non-interacting electrons in a random potential.

This chapter should be seen mostly as a review of known results for non-interacting electrons, but already formulated in a many-body language. We start our discussion by a review of Anderson's results for single electrons. From this, we move towards the case of many non-interacting electrons. Similar to our take on equilibration, such free models provide an ideal arena to first understand the basic concepts. We argue that the random local potential leads to a localisation of the eigenmodes of the system, which in turn results in a breakdown of transport and thermalisation, thus connecting back to our investigations of equilibration and thermalisation. Using these insights, we proceed to establish possible definitions of localisation that are meaningful in the context of many particle quantum mechanics. This will guide our way towards comprehensively capturing the localisation of many interacting particles.

5.1 ANDERSON LOCALISATION

Following an advanced Drude model, electrons can be considered as classical particles, which travel freely through regular lattices, but are scattered at random impurities. This leads to a increased resistivity due to quantum interferences and resulting weak localisation [142], but could never explain why impurities can lead to a complete absence of transport. In a seminal work in 1958 [48], Anderson studied the conductivity properties of a tight-binding model with random on-site potential. In this simplified model of a dirty crystal, he was able to give strong arguments that allow to conclude that randomness can indeed lead to a complete breakdown of the propagation of single electrons. This result sparked large interest, both in the physical as well as in the mathematical community [46, 47, 76, 142, 143] and has lead to several intriguing experimental explorations of the phenomenon [144–146]. In the last 50 years the results were put on a very rigorous mathematical footing, which we will summarise in the following.

The tight-binding model studied by Anderson is based on single electron cubic lattices described in terms of a $l^2(\mathbb{Z}^d)$ sequence. Using $|l\rangle$ as the characteristic vector of lattice site l, the Hamiltonian is given as [143, 147, 148]

$$H = -J \sum_{\langle j,k\rangle} |j\rangle\langle k| + \sum_j w_j \, |j\rangle\langle j| \ , \tag{5.1.1}$$

where $\langle j, k\rangle$ denotes nearest neighbours on the lattice and J is the hopping strength. For simplicity, we assume that w_j is independent and identically distributed, for example drawn uniformly from some interval $[-h, h]$, even tough also some correlated random distributions can be considered, as long as the correlations decay rapidly enough [143]. The first term is the well-known hopping term that allows the electron to move to neighbouring lattice sites and, together with a constant potential, is the discrete lattice Laplacian. In more recent work [143], the model was extended to also allow for long-range hopping, as long as the corresponding weight decays sufficiently fast.

In order to describe the mathematics of Anderson localisation, it is crucial to state the problem on an infinite dimensional lattice. For this, let us first define the resolvent set of an hermitian operator H

$$R(H) = \{z : (H - z\mathbb{1})^{-1} \text{ exists}\} \ .$$

The spectrum of an operator is then the complement of this resolvent set $\sigma(H) = \mathbb{R} \setminus R(H)$ [15]. It can be divided into two parts

$$\textbf{Pure point } \sigma_{pp} = \{z : (H - z\mathbb{1}) \text{ is not injective}\} \ ,$$
$$\textbf{Continuous } \sigma_{cont} = \{z : (H - z\mathbb{1}) \text{ is not surjective}\} \ .$$

The pure point spectrum corresponds to the operator having proper eigenvalues and eigenvectors, as in the finite-dimensional case. The new feature in infinite dimensions is that the spectrum also has other contributions and for example the momentum operator has only continuous spectrum. Thus, part of the spectrum is not connected to eigenvectors. In the case of the momentum operator, the common way to approach this in the physics literature is to still talk of "eigenvectors" in form of plain waves. These, however, do not lie inside the Hilbert space of $\mathbb{L}^2$ functions.

The distinction into pure point and continuous spectrum also directly gives a decomposition of the Hilbert space [143]

$$\mathcal{H} = \mathcal{H}_{pp} \oplus \mathcal{H}_{cont} \ .$$

These Hilbert spaces are characterised in the RAGE theorem, due to Ruelle, Amrein, Georcescu, and Enss [143]. Abstractly speaking, it tells us that the pure point spectrum corresponds to localised wave vectors that dynamically stay confined to certain regions, while the wave functions from the continuous Hilbert space leave any finite region over time. In this sense, the pure point spectrum corresponds to localisation, whereas the continuous spectrum leads to transport.

In order to state the result, we first introduce a reduction map for the l^2 sequence, by just setting all elements outside a certain region to zero

$$\langle j| \, \Omega_X(|\psi\rangle) = \begin{cases} \langle j|\psi\rangle & j \in X \ , \\ 0 & \text{else} \ . \end{cases}$$

The RAGE theorem then takes the following form [143].

Theorem 7 (RAGE). *Let X be a finite subset of the lattice, X_l its enlargements (see chapter 3.2) and Ω_X the reduction map introduced above. Then, for any Hamiltonian H, we have the following characterisations of the Hilbert spaces*

$$|\psi\rangle \in \mathcal{H}_{\mathtt{cont}} \Leftrightarrow \lim_{l\to\infty} \lim_{T\to\infty} \frac{1}{2T} \int_{-T}^{T} dt \, \|\Omega_{X_l}(e^{-itH}|\psi\rangle)\| = 0 \,,$$
$$|\psi\rangle \in \mathcal{H}_{\mathtt{pp}} \Leftrightarrow \lim_{l\to\infty} \sup_{t} \|\Omega_{X_l^c}(e^{-itH}|\psi\rangle)\| = 0 \,,$$

where $\mathcal{H}_{\mathtt{pp}}$ corresponds to the pure point spectrum space of H and $\mathcal{H}_{\mathtt{cont}}$ to the continuous spectrum space.

Thus, the evolution of states supported on the Hilbert space of the continuous spectrum is outside any finite region for almost all times. In contrast, the pure point part of the Hilbert space consists of states that are initially localised and, even for arbitrarily long times, travel long distances only with a small probability that vanishes as the distance approaches infinity. For the localised part, naturally also superpositions can be considered, which implies that the initial set is not necessarily connected, but does not change the transport properties. With this, we are ready to return to Anderson localisation.

In the following, we will restrict to 1D systems, where localisation takes place for all energies. The possibility of a mobility edge will be discussed afterwards. The first result concerns the spectrum of the Hamiltonian presented in Eq. (5.1.1). Anderson found that it consists only of eigenvalues and there is no continuous part [48, 143]. Using the RAGE theorem, this directly gives us a form of localisation. The Hamiltonian, however, fulfils even stronger localisation, which can be stated in a dynamical as well as a static version. We begin with the static or spectral reading.

Anderson localisation: Spectral reading

The Anderson Hamiltonian shows spectral localisation in the following sense [143, 147, 148].

Theorem 8. *(Single particle: Spectral localisation) For any energy interval $[E_0, E_1]$, the corresponding eigenvectors $|\phi_k\rangle$ of the Anderson Hamiltonian in Eq. (5.1.1) are exponentially localised with probability one, in the sense that*

$$\exists l_0 \; \forall |\phi_k\rangle : \; \exists x_0 \; \forall j \; |\langle j|\phi_k\rangle| \leqslant e^{-|j-x_0|/l_0} \,,$$

where l_0 is a uniform localisation length for all eigenvectors in the interval and x_0 is a localisation center .

Here it is important to stress the probabilistic nature of the Anderson model. Naturally, not all disorder realisations lead to a localised model. After all, a possible realisation is the translationally invariant case. Thus, statements about Anderson localisation are usually formulated in terms of expectation values, meaning that with probability one, a drawn realisation has a certain property. Aside from this static statement about the eigenvectors of the model, there is also a dynamical result which states that wave-packets initially localised on one site remain exponentially localised even for infinite times [143, 147, 148]. This can be seen as a bound for the transitions amplitudes in the system.

Anderson localisation: Dynamic reading

Theorem 9. *(Single particle: Dynamical localisation) With probability one, the time evolution of the Anderson Hamiltonian (Eq. (5.1.1)) is exponentially localised, in the sense that*

$$\exists \mu \; \forall |j\rangle, |k\rangle \; \sup_t |\langle j| e^{-itH} |k\rangle| \leqslant e^{-\mu|j-k|} ,$$

where μ is a uniform decay parameter.

Summarising these two results, on-site disorder drawn, for example, uniformly from an interval $[-h, h]$ with probability one leads to both spectral as well as dynamical localisation as stated above in the case of single electrons in 1D. Here, it should be noted that these result are not equivalent and models on special lattices can be constructed that have spectral, but not dynamic localisation [143]. Such single-particle localisation has also been experimentally investigated on various platforms [144–146] and the phenomenon is by now well understood.

In two dimensions, Anderson localisation of all eigenvectors is commonly expected to still hold, even though a rigorous proof has so far been elusive [142]. In 3D, localisation becomes connected with the available energy in the system. This gives rise to the exciting perspective of having a mobility edge, meaning that the model has fully suppressed propagation at low energies, while transport becomes activated when enough energy is available. Such behaviour has not been fully captured mathematically, but successfully observed experimentally [142, 145, 149, 150]

These single particle results are now the basis for our discussion of localisation for many electrons. We first show that they can be translated to an eigenmode localisation for non-interacting particles in the next section. This eigenmode localisation has numerous physical implications and directly yields insights into equilibration and leads to a break-down of thermalisation. Based on this, true many-body localisation then will move into our focus. Building on the results for non-interacting particles, we look at possible definitions of the phenomenon and explore its physical nature in all of its facets.

5.2 EIGENMODE LOCALISATION

Using single-particle Anderson localisation, one can directly investigate localisation for free systems consisting of non-interacting particles. By exploring this in detail and recasting it in a many-body language, we lay the ground-work for capturing localisation in the context of interacting particles. The starting point is to use Anderson localisation to deduce that the eigenmodes of non-interacting models localise. For simplicity and in order to better fit to the later chapter on interacting models, we perform this in a nearest neighbour spin or fermionic model, but it can equally well be done for bosonic systems.

In contrast to the previous section, here we work with finite systems, in order to avoid the complications concomitant with having to describe the system in terms of a quasi-local algebra [16]. Strictly speaking, Anderson localisation does not give localisation of electrons on finite lattices. That being said, in practice the results are expected to hold as long as the system is large enough and the realisations will be localised with an overwhelmingly large probability. After all, any numerical [151–153] or experimental investigation [144–146] of the phenomenon necessarily takes place on a finite system and still localisation can be observed. In this way, the restriction of the theorems to infinite systems should not be seen as a physical requirement. In practice localisation will take place even on rather small models.

The many-body models investigated in this section involve physical particles, such as electrons. Thus, they will preserve the total particle number. As this constraint is highly important for later purposes, let us properly define it.

Definition 10 (Particle number conservation)**.** *Let* $N = \sum_j n_j$ *be the number operator of a fermionic or bosonic system and* $M = \sum_j \sigma_j^z$ *be the magnetic field operator of a spin system. A bosonic / fermionic system is called particle number conserving iff its Hamiltonian commutes with the number operator*

$$[H, N] = 0 \, .$$

Correspondingly a spin system is called particle number conserving, iff its Hamiltonian preserves the magnetic field

$$[H, M] = 0 \, .$$

This is motivated by considering spin flips as quasi-particles and the Hamiltonian conserving their number.

The definition for spin systems already alludes to a mapping between spins and fermionic particles, called the Jordan-Wigner transformation, which we encounter later on. Under this map, particle conservation is mapped to a conservation of the magnetic field. In order to capture the localisation of non-interacting particles, we will look at a simple spin model. At this point, we mostly focus on spin models, as they are conceptually simple to describe and more importantly provide the main basis for the investigation of many-body localisation in chapter 6. The system is described by a Hamiltonian acting on a spin-1/2-chain. We look at the so-called XX model with randomly drawn magnetic fields

$$H_{XX} = -J \sum_j \left(\sigma_j^x \sigma_{j+1}^x + \sigma_j^y \sigma_{j+1}^y \right) + \sum_j w_j \sigma_j^z \, ,$$

where w_j is randomly chosen as before. This Hamiltonian has a particularly simple structure, which is not directly visible in this spin representation. It can, however, be mapped to a fermionic system using a Jordan-Wigner transformation, which results in a free Hamiltonian. This transformation is introduced in the following.

5.2.1 *Jordan-Wigner transformation*

As discussed earlier, quadratic fermionic or bosonic systems have a simple structure and can be solved by rotating them to their eigenmodes (see section 3.4.1). This solution of free Hamiltonians can be extended to spin systems by mapping them to fermions. To prepare for this transformation, for each site j, we introduce spins creation and annihilation operators of the form

$$\sigma^{s\,\dagger}_j = \frac{1}{\sqrt{2}} (\sigma_j^x + i\sigma_j^y) \, ,$$
$$\sigma^s_j = \frac{1}{\sqrt{2}} (\sigma_j^x - i\sigma_j^y) \, ,$$

where σ_j^x, σ_j^y are the usual Pauli-matrices. Interestingly, however, these operators are neither fully commuting, nor fully anti-commuting. In particular, they fulfil

$$[\sigma^s_j, \sigma^{s\,\dagger}_k] = 0 \quad \forall j \neq k \, ,$$
$$\{\sigma^s_j, \sigma^{s\,\dagger}_j\} = \mathbb{1} \, ,$$

where $[\cdot, \cdot]$ denotes the commutator and $\{\cdot, \cdot\}$ denotes the anti-commutator. This special structure makes these operators hard to deal with and ultimately is the reason for the success of mapping them to anti-commuting fermions. The key point in this mapping is that the isometry between spin and fermion system

needs to translate between commuting and anti-commuting operators. This is achieved in the so called Jordan-Wigner transformation [154], which provides a presentation of spins as fermions and vice versa.

Jordan-Wigner

The Jordan-Wigner transformation consists of the following mapping between commuting spin-1/2 operators and anti-commuting fermionic operators

$$\begin{aligned}\sigma_j^z &= f_j f_j^\dagger - f_j^\dagger f_j = 1 - 2n_j \,, \\ \sigma_j^s &= \prod_{l<j} (1-2n_l) f_j \,, \\ {\sigma^s}_j^\dagger &= \prod_{l<j} (1-2n_l) f_j^\dagger \,.\end{aligned}$$

Here an ordering of the lattice sites is assumed, which is arbitrary but fixed for all operators.

The Jordan-Wigner transformation maps nearest-neighbour spin operators to nearest-neighbour fermionic operators. In particular, in 1D we have

$$\begin{aligned}\sigma_j^s{}^\dagger \sigma_{j+1}^s &= f_j^\dagger f_{j+1} \,, \\ \sigma_{j+1}^s{}^\dagger \sigma_j^s &= f_{j+1}^\dagger f_j \,, \\ \sigma_j^z \sigma_{j+1}^z &= 4 n_j n_{j+1} - 2n_j - 2n_{j+1} + 1 \,.\end{aligned}$$

This mapping crucially relies on the systems being confined to 1D, while in higher dimensions any ordering of the lattice size necessarily leads to very non-local fermionic strings, thus destroying the locality of the model.

Finally, let us comment that Jordan-Wigner is far from being an optimal mapping between spins and fermions. While it establishes the connection at a very intuitive level and is invaluable as an analytic tool, in numerical simulations this mapping is often replaced by the Bravyi-Kitaev transformation, which uses particle number conservation [155]. In the following, we will use the Jordan-Wigner transformation to investigate the behaviour of localised spin systems and establish a connection to Anderson localisation.

5.2.2 *Non-interacting spin Hamiltonians*

In this section, we carry out the Jordan-Wigner transformation of the XX-model and connect this spin system to Anderson localisation of fermionic particles. As a first step, we rewrite the model in terms of spin creation and annihilation operators

$$H_{XX} = -J \sum_{j=1}^{L-1} \left({\sigma^s}_j^\dagger \sigma_{j+1}^s + {\sigma^s}_{j+1}^\dagger \sigma_j^s \right) + \sum_{j=1}^{L} w_j \left(1 - 2 {\sigma^s}_j^\dagger \sigma_j^s \right) \,,$$

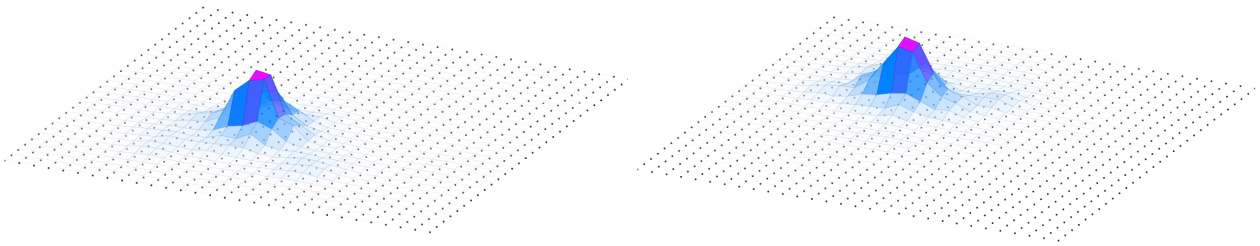

Figure 5.1: Two randomly chosen examples of eigenmodes for a free fermionic system on a 2D 30x30 lattice with a local potential drawn uniformly randomly from the interval $[-2, 2]$. Plotted is the absolute value of the eigenvector. Remarkably, even on this rather small system, the eigenmodes are already very localised.

where L as usual denotes the system size. Here, for simplicity, we work with open boundary conditions, as the periodic case requires a careful analysis of the boundary terms [154]. Now carrying out the Jordan-Wigner transformation yields the following fermionic representation in 1D

$$H = \sum_{j,k=1}^{L} f_j^\dagger h_{j,k} f_k \,,$$

$$h = \begin{bmatrix} -2w_1 & -J & 0 & 0 & \dots \\ -J & -2w_2 & -J & 0 & \dots \\ 0 & -J & -2w_3 & -J & \dots \\ \vdots & & \ddots & \ddots & \ddots \end{bmatrix} ,$$

where we omitted the global energy shift by $\sum_j w_j$. This interaction matrix is the same as the Anderson lattice Hamiltonian in Eq. 5.1.1, which stems from the fact that the interaction matrix of a free Hamiltonian captures the system's behaviour for single particles.

With this, we know that the eigenvectors of the interaction matrix h, which are the eigenmodes, are exponentially localised. As mentioned earlier, there are so far no mathematically rigorous finite size estimates for Anderson localisation. Nevertheless, when investigating these free fermionic models numerically, the eigenmodes are strongly localised with overwhelming probability (see Fig. 5.1).

Using the fact that the Hamiltonian is quadratic, we can solve it by diagonalising the interaction matrix h and define new fermionic creation operators

$$\tilde{f}_k^\dagger = \sum_j \langle j|\phi_k\rangle \, f_j^\dagger \,,$$

where $|\phi_k\rangle$ are the eigenvectors of h. Given that the eigenmodes of the system are localised, the same holds for these rotated operators, as captured in the following lemma.

Lemma 1 (Eigenmode-operator localisation)**.** *Assuming that all eigenvectors of a 1D free system are localised*

$$\exists l_0 \; \forall |\phi_k\rangle \;\; \exists x_0 \; \forall j \; |\langle j|\phi_k\rangle| \leqslant e^{-|j-x_0|/l_0} \,,$$

then the fermionic creation and annihilation operators for those eigenmodes are also approximately local in the operator sense (see chapter 3.2)

$$\forall k : \exists \{X_l\} : \left\| \tilde{f}_k - \Gamma_{X_l}(\tilde{f}_k) \right\| \leqslant 2e^{-l/l_0} \frac{1}{1-e^{-1/l_0}} \,,$$

$$\left\| \tilde{f}_k^\dagger - \Gamma_{X_l}(\tilde{f}_k^\dagger) \right\| \leqslant 2e^{-l/l_0} \frac{1}{1-e^{-1/l_0}} \,,$$

where $\{X_l\}$ are the sets containing all sites within distance l to the respective localisation center x_0.

Proof. For the proof, we pick an eigenmode $|\phi_k\rangle$ with localisation length l_0 and center x_0 and build sets X_l that include all sites within distance l to x_0. Then, we get the following bound on the rotated fermionic annihilation operators

$$\begin{aligned}\left\|\tilde{f}_k - \Gamma_{X_l}(\tilde{f}_k)\right\| &\leqslant \sum_{j\notin X_l} |\langle j|\phi_k\rangle| \, \|\tilde{f}_k\| \leqslant \sum_{r>l} \sum_{\substack{j \\ |j-x_0|=r}} e^{-|j-x_0|/l_0} \\ &\leqslant \sum_{r>l} 2e^{-r/l_0} \qquad \leqslant 2e^{-l/l_0} \frac{1}{1-e^{-1/l_0}} \, .\end{aligned}$$

Here we used that in 1D, there are only two points with fixed distance to the center x_0. The proof for the creation operator is identical, as the complex conjugate of the eigenvector does not change its locality properties. □

Thus, Anderson localisation implies that the fermionic eigenmode operators can be truncated to local regions with an error that decays exponentially with the size of the truncation. A similar estimate would also hold in higher dimensions, where the sum over all points with a fixed distance would lead to a polynomial prefactor that is dominated by the exponential decay at large distances. Using the above derivation, we obtain the following expression for the Hamiltonian

$$H = \sum_k \lambda_k \tilde{f}_k^\dagger \tilde{f}_k = \sum_k \lambda_k \tilde{n}_k \, . \tag{5.2.1}$$

Here all number operators $\tilde{n}_k = \tilde{f}_k^\dagger \tilde{f}_k$ commute with each other and are approximately local following lemma 1. In this sense, finite system size localisation of a single electron directly gives localisation for non-interacting spin systems and naturally also for free fermionic systems.

While the localisation of eigenmodes is a natural language for non-interacting systems, the very notion of eigenmodes relies on the Hamiltonian being quadratic. This will greatly complicate our investigation of many-body localisation, as the language employed in the results of Anderson is no longer suitable. Rather, we have to switch to a true many-body picture of the phenomenon and look at locality of the dynamical evolution, the Hamiltonian spectra, the entanglement properties of eigenvectors and the existence of local constants of motion.

It is thus instructive to present the above eigenmode localisation in a way that can be carried over to the setting of many-body localisation, capturing interacting fermions or spins. We therefore look at different aspects of locality and relate them to the derived Hamiltonian decomposition in Eq. (5.2.1), thus laying ground-work for later chapters. Moreover, we explore the physical implications of localised eigenmodes, in particular with respect to equilibration and thermalisation. We begin by looking at the time evolution of local operators in these systems.

5.2.3 *Localised operators*

In this section, we investigate the dynamical evolution of local operators in free spin or fermionic systems with random local potentials. For those models, we have the decomposition from Eq. (5.2.1)

$$\begin{aligned} H &= \sum_k \tilde{n}_k \, , \\ [H, \tilde{n}_k] = 0 \;\&\; [\tilde{n}_j, \tilde{n}_k] &= 0 \quad \forall j, k \, . \end{aligned}$$

As argued earlier, given a sample of the randomly chosen local potentials, we strongly expect that this random sample will lead to fully localised eigenmodes, even for finite systems. From this, we know that

the Hamiltonian can be decomposed into commuting, approximately local operators. Thus, the model has an extensive number of approximately local constants of motion. This is immediately true for the fermionic picture, but also carries over to the 1D spins systems above, as there the fermionic strings involved in the Jordan-Wigner transformation of f and $f^\dagger$ cancel. In 2D, this is no longer the case and it seems entirely unclear whether a XX-type Hamiltonian with local disorder allows such a decomposition in dimensions larger than one.

Thus, in 1D, many approximately local operators exist that do not move at all. Concerning the evolution of other local operators, one can use the localisation of the fermionic eigenmodes to directly infer a strong suppression of propagation [156, 157]. In order to approach this, we can expand the initially local fermionic operator in terms of the rotated operators $\tilde{f}$ and $\tilde{f}^\dagger$. In this expansion only terms with support nearby contribute significantly. The eigenmode operators are invariant in time, up to a global phase, so that their absolute weight in this decomposition does not change. Thus, the weight is trapped in eigenmode operators that are supported close-by. In this way, a localisation of all fermionic eigenmodes implies a localisation of the evolution of any local operator.

Mathematically speaking, this is best captured in terms of a zero-velocity Lieb-Robinson bound (see appendix B). The strongest form of such a statement is given by the truncated Hamiltonian formulation of Lieb-Robinson bounds [4]. We take this as a basic definition, for later purposes.

Definition 11 (Strong dynamical localisation)**.** *A Hamiltonian H exhibits strong dynamical localisation iff its time evolution satisfies*

$$\|A(t) - e^{itH_A^l} A e^{-itH_A^l}\| \leqslant C_{loc}\, e^{-\mu l} \quad \forall\, t\,,$$

for a suitable $\mu > 0$, where A is an arbitrary local observable, $C_{loc} > 0$ a constant independent of the system size and H_A^l denotes a Hamiltonian which includes all interactions contained in a region of distance no more than l from the support of A.

This definition rigorously captures the behaviour of a localised Anderson system in a true many-body language. Due to this suppression of propagation, we can directly establish some connections to the equilibration and thermalisation results discussed in chapters 3 and 4. Interestingly, both presented equilibration results cannot be applied to the case of non-interacting localised particles. While the Hamiltonian is free, it does not have transport, thus making it impossible to apply the equilibration result shown in section 3.4. Moreover, due to the free structure, the model has hugely degenerate energy gaps, which does not allow to derive equilibration on average (see section 3.5). Both is compatible with the expected physical behaviour of such systems. Since excitations are trapped locally, one is capable of producing local oscillations that are never damped away. Thus, equilibration simply does not happen and it is no wonder that the known bounds cannot be applied.

The above argument, however, does not address the issue of equilibration completely. After all, it might well be possible that the localisation length of the system is extremely large. Then, while it might be true that the evolution only sees a local section of the system, the effective size might still be large enough to practically talk about equilibration up to an error that decreases with the localisation length. One could, for example, think of applying the equilibration results in free systems (see section 3.4) up to a time scale for which the localisation length has not yet been reached. This would give a form of equilibration for the model. Moreover, since the evolution of a local observable only takes place on a finite region, it would trivially be independent of the system size.

In such a setting, one could therefore still ask whether thermalisation takes place. As discussed earlier, if free systems equilibrate, they provably equilibrate towards a generalised Gibbs ensemble using the linearly many number-operators as constants of motion (see section 3.4), thus showing that just using a Gibbs state can never work. Using a many-body language, this absence of thermalisation can also be

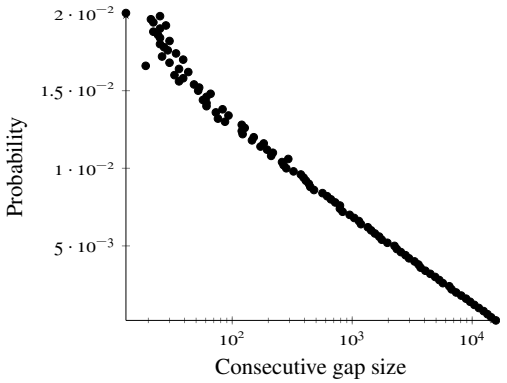

Figure 5.2: Poissonian level spacing for the non-interacting Anderson model of many particles. The system size is $L = 4000$ averaged over 50 realisations. Plotted is the probability of a spacing between consecutive energies over its size. The decay is exponential, as is expected from a Poissonian distribution.

seen as follows. The absence of particle transport implies that particle number or energy imbalances can never even out. Therefore, such initial conditions are always remembered and the state looks, at all times, locally very different from a thermal state, with a homogeneous particle number and energy distribution. More generally, one could think of locally measuring the constants of motion of the Hamiltonian. As their value can never change over time, it is clear that they would have to be included in a generalised Gibbs construction for the static ensemble.

This concludes our discussion of the evolution of local operators under non-interacting localised Hamiltonians. We saw that they can only equilibrate on a region given by the localisation length and can never thermalise. As we described in chapter 4, this absence of thermalisation is often connected to a lack of entanglement in the eigenvectors of the system. This will be investigated in the following section.

5.2.4 *Spectral properties of free localised systems*

In this section, we use Anderson localisation to investigate the behaviour of eigenstates and eigenenergies of models with many non-interacting particles in a random local potential. Let us first comment on the spectrum of these Hamiltonians. Due to the randomness, the eigenvalues will be non-degenerate with probability one. The spectral gaps, however, necessarily are hugely degenerate due to the commuting structure of the free system. Moreover, the consecutive energy gaps are distributed according to a Poissonian distribution (see Fig. 5.2).

We now turn to the eigenvectors of the system. We begin by noting that specifying all occupation numbers of the eigenmodes uniquely determines the eigenstate. Thus, we can directly obtain the eigenstates of the model by occupying the single-particle orbitals

$$|k_1, k_2, \cdots, k_L\rangle = \left(\tilde{f}_1^\dagger\right)^{k_1} \left(\tilde{f}_2^\dagger\right)^{k_2} \cdots \left(\tilde{f}_L^\dagger\right)^{k_L} |\emptyset\rangle \ ,$$

where $|\emptyset\rangle$ denotes the vacuum state. Due to this particularly simple structure, for any spatial cut, only the fermionic modes around the cut can contribute significantly to the eigenvector entanglement. Thus, intuitively it is clear that localisation of all eigenmodes implies an area-law for all eigenvectors for arbitrary energies and particles numbers. This area-law behaviour can also be rigorously proven directly starting from the Anderson model and working on sufficiently large systems [158, 159]. In fact, in 1D the above construction also gives rise to an efficient approximation in terms of a matrix product state (see appendix

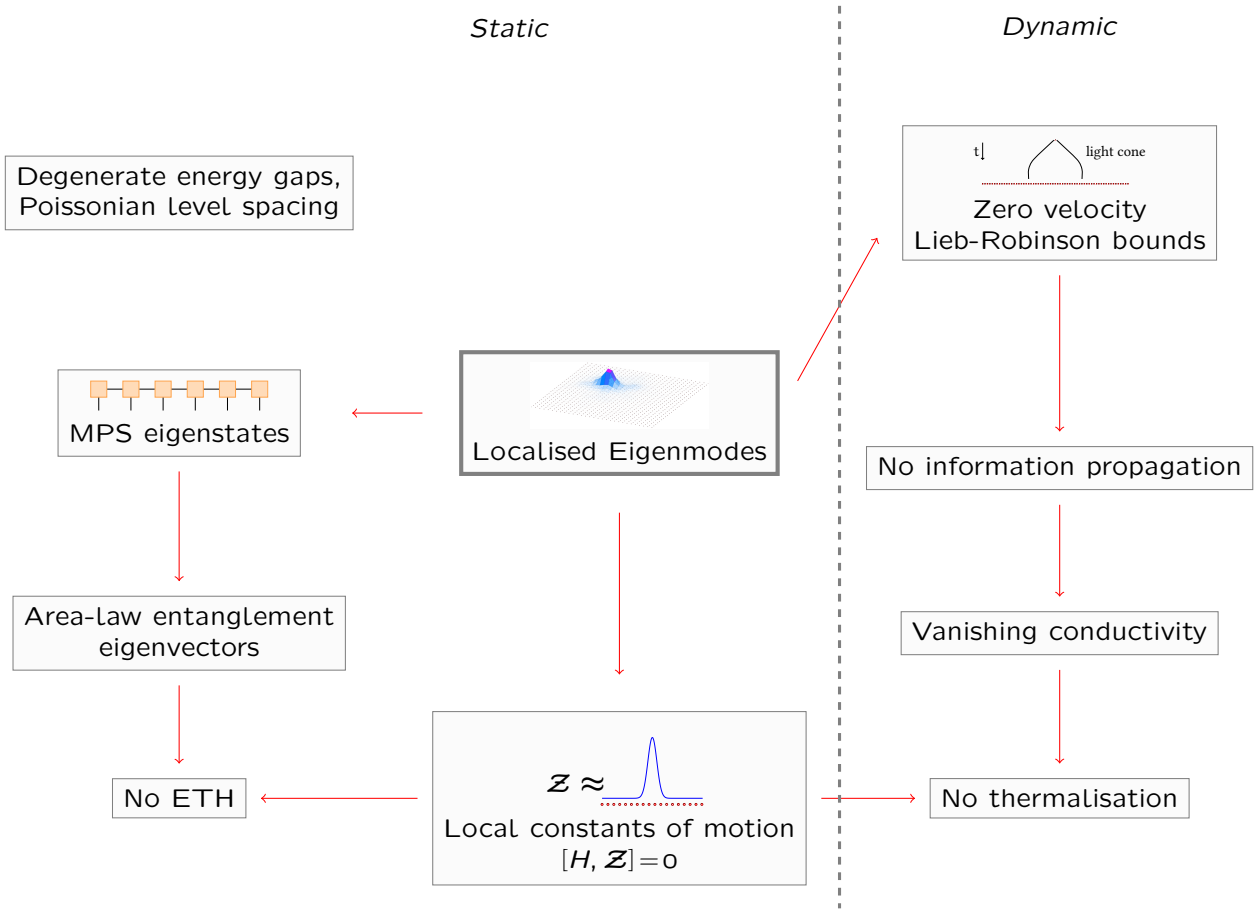

Figure 5.3: This figure gives an overview over important aspects of 1D Anderson localisation in a many-body language. Central to the characterisation is the localisation of the eigenmodes of the model. From there, a zero-velocity Lieb-Robinson bound, MPS eigenstates and the existence of local constants of motion follow. These in turn can be connected to various other localisation properties. Somewhat complementary are spectral characterisations, which state that the model has degenerate energy gaps, since it is free, and a Poissonian level spacing.

A). Further, due to the fact that local constants of motion exist, the ETH has to be violated, as argued in section 4.1.

This concludes our discussion of the properties of non-interacting particles in a random potential. We briefly summarise our insights before we proceed towards understanding those models in the presence of interactions.

5.3 SUMMARY: NON-INTERACTING LOCALISATION

In this chapter, we introduced one-dimensional Anderson localisation, which is characterised by local random potentials, causing single electrons to be completely localised, both in a static and dynamic sense. Great care was taken to present those results on a mathematically rigorous level, while still keeping the connection to physical experiments and numerical simulations.

Building on those single particle results, we turned to the case of many non-interacting particles. Here, Anderson localisation implies the localisation of the fermionic eigenmodes and results in a Hamiltonian that can be written in terms of commuting and approximately local number operators. While, mathemati-

cally speaking, the application of Anderson localisation to finite systems is not directly possible, numerical evidence suggests that this eigenmode localisation takes place even on finite samples with large probability. Using the Jordan-Wigner transformation, we further saw how this result can be carried over to spin models.

Based on this eigenmode localisation, we were able to obtain diverse localisation properties in a language of quantum many-body systems (see Fig. 5.3). Aside from the existence of approximately local constants of motion, we saw that full eigenmode localisation implies a complete absence of any kind of transport, resulting in initially local operators that will remain approximately local for arbitrary times. Moreover, we saw that this eigenmode localisation also reflects itself in the structure of the eigenstates, which show a uniform area-law for the entanglement entropy. Finally, we used the eigenmode localisation to argue that equilibration can only take place on sizes up to the localisation length and that thermalisation necessarily has to break down. In this way, we saw many different aspects of localisation, ranging from the evolution of local operators, over eigenvector properties, to signatures in the out of equilibrium behaviour of these systems.

In the following, we move to the case of interacting systems. There, the insights from this discussion are crucial for capturing localisation in all of its facets, in particular because the notion of eigenmodes can no longer be employed. We continue to investigate issues of equilibration and thermalisation, in such models. Interestingly, we will see that propagation is no longer fully suppressed, but rather that entanglement can grow without limits at a very slow rate. In contrast, the system still has local constants of motion, thus demonstrating that the localisation properties discussed above do not imply each other. This highlights the importance of establishing a clear and unified definition of what many-body localisation should be.

6

MANY-BODY LOCALISATION

After having studied the localisation of non-interacting particles in the previous section, it is crucial to ask what happens in the presence of interactions. In fact, the very applicability of Anderson's results to any realistic disordered solid-state system depends on its robustness to the presence of electronic repulsion. This question is already included in Anderson's original work [48]. Nevertheless, even today, it is far from being comprehensively answered.

The arising complications are largely due to the fact that, as soon as interactions are present, the free structure in the Hamiltonian naturally disappears. Therefore, the previous way of capturing localisation in terms of eigenmodes can no longer be employed, but the preparations using a true many-body language in the previous chapter will prove useful. Based on those different formulations and facets of localisation, we explore the interacting case.

The original question in the study of many-body localisation was to what extent interactions could enable transport. In a seminal work by Basko, Aleiner and Altshuler [46, 47], a careful perturbation argument is carried out that strongly suggests that Anderson localisation should be robust under the inclusion of interactions. Based on those results, there is a commonly held believe that the interacting model should still have a vanishing dc-conductance [160], meaning that particles are localised even for infinite times. More precisely, they find a dependence on temperature, suggesting that there should be a mobility edge, such that transport is fully suppressed for low temperature, while it becomes activated for high temperature. This mobility edge is shifted with the strength of the randomness. For the spin or fermionic systems considered here, with a finite-dimensional local Hilbert space, this implies that for strong randomness, there should be no transport even for infinite temperature. In our discussion, we restrict to this case of strong randomness, where localisation happens for arbitrary energy. Moreover, we will also limit our discussion to 1D models, as they have been studied in much more detail and the basis of MBL, given by Anderson localisation, is best understood there. This follows the general spirit of this thesis to comprehensively lay groundwork for the investigation of interacting quantum many-body systems. In a similar spirit, we will avoid the discussion of disorder realisations and averages and rather work with single realisations and investigate the connection of localisation properties on this level.

Curiously, even in this simplified 1D MBL setting, the absence of conductance does not mean that the model has a full suppression of propagation in the sense of a zero-velocity Lieb-Robinson bound. In particular, in the Schroedinger picture, it is numerically found that entanglement of states can grow without bounds [151, 152, 161, 162]. This means that the different aspects of Anderson localisation are no longer equivalent in the presence of interactions and many different possible definitions of the phenomenon of many-body localisation (MBL) have thus been put forward. In essence, any of the different aspects of single-particle localisation were, at some point in time, considered as a reasonable definition.

In the following, we review the analytical, numerical and experimental efforts to explore static and dynamic features of MBL. Our approach is largely model independent and is based on establishing fundamental connections between different localisation properties of operators and states. That being said, for most people in the community many-body localisation is connected to a model that describes many electrons that are coupled with a nearest neighbour interaction. In the 1D case, the Hamiltonian in its

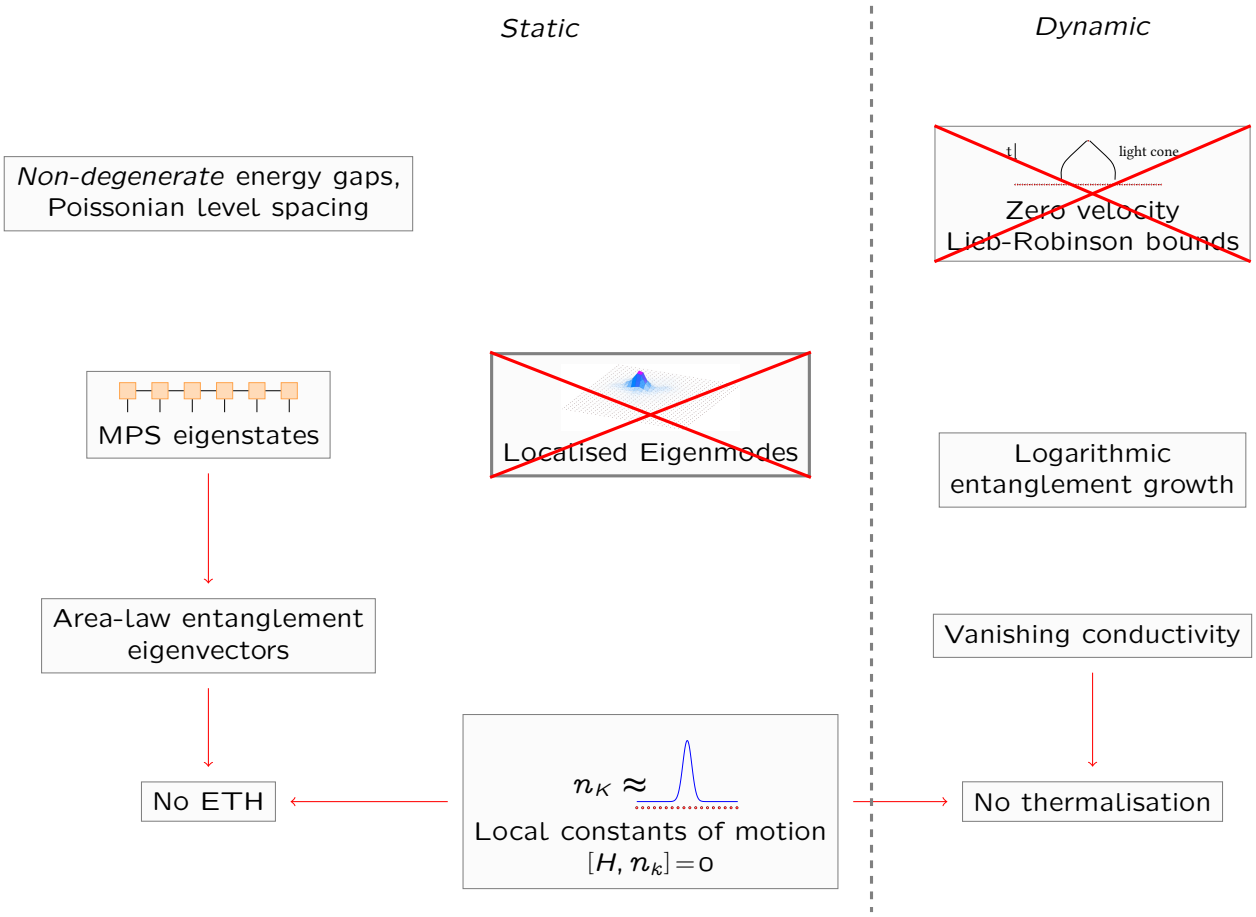

Figure 6.1: This figure presents the different facets of many-body localisation, which are divided into static and dynamic features. In sharp contrast to the case of an Anderson insulator, we can no longer meaningfully talk about eigenmodes. Moreover, the system does not have a zero-velocity Lieb-Robinson bound, but rather entanglement entropies can grow without bounds. This leaves the characterisation of MBL in an inchoate state and makes it hard to characterise the phenomenon in a comprehensive way. In this chapter, we go through each of different facets of MBL in detail. Moreover, in an attempt to unify those decoupled approaches, we explore links between static and dynamic properties, thus paving the way for a unified definition of MBL.

fermionic version, or using the Jordan-Wigner transformation (see section 5.2.1) in its spin formulation, takes the following form

$$\begin{aligned} H &= -J \sum_j \left(f_j^\dagger f_{j+1} + f_{j+1}^\dagger f_j \right) + \sum_j w_j \left(1 - 2 n_j \right) + U \sum_j n_j n_{j+1} \,, \\ &= -J \sum_j \left(\sigma^x{}_j \sigma^x_{j+1} + \sigma^y{}_j \sigma^y_{j+1} \right) + \sum_j w'_j \sigma^z_j + U' \sum_j \sigma^z_j \sigma^z_{j+1} \,, \end{aligned}$$

where the interaction strength U and the random field w_j are shifted in the transformation (see section 5.2.1). In the literature, this model has been investigated extensively, both numerically and analytically and many of its dynamic and static features have been taken as fundamental aspects of MBL.

During our review of those results, a multi-faceted picture of MBL emerges, which is displayed in Fig. 6.1 and will be explained step by step in the proceeding sections. Despite great efforts, many questions in this newly developing field cannot yet be fully answered. In an endeavour to nevertheless give structure to those results, we present recent efforts to unify the different approaches and to interrelate their characteristic features. In particular, we present two mathematically rigorous links between static

and dynamic features of localisation, which tie together different lines of thought in the study of MBL. We connect them to insights into equilibration and thermalisation and thus provide a detailed picture of MBL. This brings us closer to a single unified definition of the phenomenon and hopefully presents a significant contribution to the long-term goal of capturing MBL in a rigorous mathematical language and making it experimentally accessible. We begin by exploring the evolution of local operators in MBL systems.

6.1 LOCALISED OPERATORS

As argued in earlier sections of this thesis, the evolution of local operators contains important structure, from causal cones in the language of Lieb-Robinson bounds to transport properties of particles and information. In the Anderson model, we saw a full suppression of propagation in the sense of a zero-velocity Lieb-Robinson bound. For the interacting systems considered in many-body localisation, this is no longer the case. Rather one finds that entanglement grows until it reaches a volume law in finite systems [151, 152] and thus is unbounded for infinite systems. This distinct difference to an Anderson insulator came as a surprise and to date no complete classification of the transport behaviour of MBL systems has been achieved. Based on the current literature and our own research, we expect the following behaviour connected to the time evolution of local operators.

- A full suppression of energy and particle transport [46, 47]
- Complete suppression of propagation for very low energies [4, 157]
- The existence of local constants of motion [163–166]
- Unbounded propagation of information [5]

Here the first three are in complete accordance with the behaviour of Anderson insulators. In contrast, the last one is markedly different and shows the interacting nature of those systems. In the following, we discuss those aspects of propagation in more detail, beginning with energy and particle transport.

6.1.1 *A full suppression of energy and particle transport*

One of the key features of free systems is the fact that there is no conceptual difference between the propagation of information, particles or energy as all of them are directly linked together. After all, the only possibility for a creation operator to spread in a free system is by obtaining support on other single creation or annihilation operators far away. For systems with particle number conservation, this means that any form of transport is precisely captured by the movement of single particles.

For interacting systems, this is no longer the case, but rather it is possible to send information through a chain without sending energy or particles [5]. Following the current consensus in the field, this is the expected behaviour of many-body localised systems [5, 167]. In fact, the observed unbounded entanglement growth is a rather special dephasing effect [162] and would fit together well with a complete absense of particle or energy transport. This is also in accordance with the intuition presented in the original work by Anderson [48], as it would imply a vanishing dc conductivity. A rigorous proof of such a behaviour starting from a concrete model is however still open, at least on a mathematically rigorous level, which does not rely on the perturbative methods used in Refs. [46, 47].

Looking back to our discussion on thermalisation, such a suppression of energy transport would directly imply a break-down of thermalisation. After all, the energy profile of a thermal state is always evenly distributed, whereas MBL systems are not capable of reducing such energy imbalances on length scales larger than the localisation length, even if one waits for infinite times.

6.1.2 *Complete suppression of propagation for very low energies*

When looking at the unbounded entanglement growth, one realises that a superposition of many eigenstates is necessary to achieve it [5, 152, 162]. This suggests to assume that such growth is not possible, when only the first couple of excited states are used in the model. This would provide intuition for an *information mobility edge*, below which any form of transport is completely suppressed [157, 168]. Denoting by $|k\rangle, |l\rangle$ eigenstates of the Hamiltonian with energy E_k, E_l respectively, we capture this concept in the following way [4].

Definition 12 (Information mobility edge)**.** *A Hamiltonian H is said to have an information mobility edge at energy E_{mob} iff for all times t, all density matrices $\rho \in \mathrm{span}\{|l\rangle\langle k| : \ E_l, E_k \leqslant E_{mob}\}$ and all normalised local operators A, B, the Hamiltonian time evolution satisfies*

$$|\mathrm{Tr}\left(\rho[A(t), B]\right)| \leqslant \min(t, 1) C_{mob}\, e^{-\mu d(A,B)} ,$$

with constants $C_{mob}, \mu > 0$ independent of t. That is, all propagation is suppressed for states supported only on the low-energy sector below the energy E_{mob}.

Intuition for the presence of such behaviour for interacting models can come from the perturbation arguments performed in Refs. [46, 47]. In particular, if one assumes an Anderson insulator with a strong positive chemical potential and adds interactions, then the low-energy sector should still consist of few electron states, which hardly feel the presence of interactions. Thus, for those states, the propagation should be completely suppressed, as in the case of an Anderson insulator. It should be noted that the above definition refers to fixed energies, in contrast to other notions of mobility edges in terms of an energy density, which relates to an energy that grows with the system size.

6.1.3 *The existence of local constants of motion*

Recently, the existence of local constants of motion has moved into the focus of attention, as it is one of the key features of non-interacting localising systems. These are operators that are approximately local and still completely invariant over time. In the case of non-interacting Anderson insulators, such approximately local constants of motion are given by the rotated number operators $\tilde{n}_k$ or polynomials thereof (see chapter 5).

In a similar way, it is often assumed that MBL is connected to the existence of an extensive number of commuting, approximately local constants of motion. Again, similar to the setting of an Anderson insulator, the Hamiltonian can completely be expressed in terms of products and sums of these local operators [5, 164–166]. In the non-interacting case, this expression is only linear, whereas for the MBL case, one expect higher order interactions in terms of these simple, number-operator type constants of motion [163, 169]. Thus, the Hamiltonian is often assumed to be of the form

$$H = \sum_i h_i \mathcal{Z}_i + \sum_{i,j} J_{i,j} \mathcal{Z}_i \mathcal{Z}_j + \cdots , \tag{6.1.1}$$

where $\mathcal{Z}_i$ are approximately local commuting operators with a simple spectrum similar to that of a number operator. The couplings $J_{i,j}$ are usually assumed to decay exponentially with the distance [163, 169]. This is chosen in accordance with the logarithmically slow growth [163, 169] that is observed numerically [151, 152]. In contrast, other authors have also considered MBL Hamiltonians, which are a simple sum of commuting constants of motion [165]

$$H = \sum_j \tilde{h}_j ,$$

which can for example be obtained by performing an infinite time average of the Hamiltonian with itself. As the Hamiltonian commutes with itself, the full operator is unchanged, but the local terms will be diagonalised in the global basis at the cost of loosing exact locality [97]. Given that the full Hamiltonian has to have non-degenerate energy gaps, such constants of motion cannot have a simple spectrum, as they are commuting. Thus, such constants of motion themselves have a complex spectrum, which makes their locality very hard to exploit, since perturbation methods cannot be employed (see appendix D).

An immediate consequence of the Hamiltonian given by a polynomial of approximately local commuting operators is that these operators are independent of time. Thus, there are certain local operators that remain local for arbitrary times and in fact even stay completely invariant. As in the case of free models, it is immediately clear that these operators have to be included in any description of out of equilibrium situations in terms of static ensembles. Therefore, they necessarily enter into constructions in the form of generalised Gibbs ensembles (see chapter 3).

6.1.4 *Unbounded propagation of information*

The above aspects of the dynamical behaviour of many-body localisation focus on the similarities to the non-interacting settings of an Anderson insulator. Yet, the numerically observed unbounded growth of entanglement entropies clearly implies that not all propagation is suppressed. The usual picture for this is that the interactions cause a slight splitting of the eigenvalues of the Hamiltonian, which in turn enables propagation.

Connected to this is the investigation of entanglement growth over time. The typical setting here is to start with a product state and observe how it evolves under the time evolution of the interacting Hamiltonian. In stark contrast to the non-interacting setting, one observes a growth of entanglement entropies that typically takes place at a logarithmic rate [152, 161]. Thus, for infinite systems it would result in an unbounded entanglement [151, 152, 161, 162, 169].

This hints at the possibility to use MBL systems for sending information. In fact, we show in section 6.2 that such behaviour can be rigorously derived from remarkably few assumptions. Based on the mere existence of local constants of motion and the fact that the model is fully interacting, we construct other operators that spread without bounds in the Heisenberg picture. This directly gives rise to an Alice-Bob type protocol in which the two parties can provably communicate, if enough energy is available in the system to activate states above the information mobility edge.

In this way, the logarithmic entanglement growth is connected to a logarithmic growth of support of operators in the Heisenberg picture. This definitely holds true in case the Hamiltonian is of the form in Eq. (6.1.1) [5]. Such slow growth of operator support implies that expectation values can only equilibrate after a time that scales exponentially with the system size, at least for general initial states. Thus, equilibration in MBL models is commonly expected to be exponentially slow, even for states that have exponentially large effective dimension [5]. Therefore, MBL systems are a prime example of naturally occurring models in which the bounds on equilibration times derived in section 3.5 provide a tight scaling, even for physically realistic initial states.

6.1.5 *Summary: Local operator in MBL systems*

In this section, we summarised the current viewpoint on the evolution of local operators under MBL Hamiltonians. Following the inchoate state of current research, we gave intuition how local operators dynamically behave in such systems. We presented the common intuition that energy and particle propagation are fully suppressed, just like in an Anderson insulator. Similarly, when only looking at low

energies, the interactions should not be sufficient to enable propagation. Moreover, we expect that the Hamiltonian can be decomposed into approximately local and commuting constants of motion. In contrast to the case of an Anderson insulator, the Hamiltonian should also have higher order interactions between those constants of motions, which ultimately cause the unbounded growth of entanglement [163–166].

In the following section, we explore this connection further. In an effort to understand the propagation properties of MBL Hamiltonians, we present a rigorous mathematical proof that those system have an unbounded growth of operator support in the Heisenberg picture and can thus be used to send information through them. Interestingly, the proof uses equilibration results in an unexpected way and relies solely on the existence of a single approximately local constant of motion and a non-degenerate spectrum associated with interacting models.

6.2 LOCAL CONSTANTS OF MOTION IMPLY INFORMATION PROPAGATION

The following section is based on Ref. [5]. We sincerely thank Albert H. Werner, Marcel Goihl, Jens Eisert and Winton Brown for the very fruitful collaboration.

In the following, we review a recent work relating static and dynamic properties of many-body localisation. In particular, we argue that the existence of a constant of motion together with a generic Hamiltonian spectrum implies that the system can be used to send classical information through it [5]. It is interesting to connect this to the equilibration results of free fermionic systems presented in section 3.4. There we saw that transport can lead to equilibration behaviour. The result presented in the following can, to some extent, be seen as the inverse implication. Based on equilibration results, we show that the system provably allows for information propagation, as long as the existence of a local constant of motion is assumed.

6.2.1 *Information propagation*

In order to capture how information can be sent through these models, we briefly review the protocol introduced in section 3.5.3. We imagine that there are two parties, for brevity referred to as Alice and Bob, who control different parts of a spin system [109, 170]. For simplicity, let us restrict to 1D and let Alice control some part at the left end. We further assume a fixed separation between the parties and finally that Bob controls the rest of the chain. Alice now encodes a message by either doing nothing or acting on her part of the spin chain with a local unitary V_A. At a later time, Bob measures some local operator B_t. How well these two parties can communicate with such a protocol is captured by the difference in expectation value for Bob, depending on Alice's action,

$$s := |\langle\psi| V_A B_t V_A^\dagger |\psi\rangle - \langle\psi| B_t |\psi\rangle| ,$$

which can be seen as a signal strength s. At time zero, the support of V_A and B are spatially separated and the above quantity is zero. Over time, the support of B_t might grow and thus eventually lead to a signal. Such a procedure amounts to a positive channel capacity in the language of information theory if $s > 0$. In yet less information theoretic terms: a local modification necessarily leads to a measurable state modification far away in the chain for later times. Thus, whether the two parties can communicate crucially depends on the growth of the support of the operator in the Heisenberg picture. In this way, the following quantity is a meaningful way to capture the capability of a Hamiltonian to propagate information.

Definition 13 (Information propagation on average)**.** *A Hamiltonian allows for information propagation on average, if for any $\epsilon > 0$, there exists a strictly local observable B with $\|B\| = 1$, such that, for each finite region $S \subset \mathcal{L}$,*

$$\overline{\|B_t - \Gamma_S(B_t)\|} \geqslant 1 - \epsilon \, ,$$

where Γ_S is the truncation map and $\overline{f_t} = \lim_{T\to\infty} \frac{1}{T} \int_0^T dt f_t$ denotes the infinite time average of a function f_t.

This definition is very restrictive in the sense that it demands that the lower bound can be chosen arbitrarily close to 1. On the other hand, it does not require any information on the corresponding time, but only refers to the infinite time average, which is connected to the overwhelming majority of times. To calculate this average, very large times might be needed (see chapter 3). Correspondingly, it is well possible for the support of the observable to take exponentially long to grow. From this definition, we can immediately conclude, that we have

$$s = |\langle\psi| V_A B_t V_A^\dagger |\psi\rangle - \langle\psi| B_t |\psi\rangle| > 1 - \epsilon \, ,$$

for some initial state vector $|\psi\rangle$, which follows directly from rewriting the reduction map in terms of a unitary twirl over the Haar measure (see section 3.5.3). Hence we can interpret $1 - \epsilon$ as a signal strength s. Thus, if a Hamiltonian allows for information propagation in the above sense, Alice and Bob can indeed communicate using the described protocol and send information. This result is independent of the distance between them, as long as Bob is allowed to measure on a large enough subsystem. Our main result states that this information propagation can be rigorously deduced from only the existence of a local constants of motion with a suitable spectrum and non-degenerate energies and energy gaps in the Hamiltonian. For this, we state a formal definition of a local constant of motion suited for later purposes.

Definition 14 (Local constant of motion)**.** *Let Z be an operator that commutes with the Hamiltonian and has M disjoint eigenvalues, all separated by a spectral gap lower bounded by $\gamma > 0$, independent of the system size. Z is an exactly local constant of motion, iff it is strictly local and an approximately local constant of motion, iff it is approximately local according to Def. 2.*

The main purpose of this definition is to ensure that the spectrum of the operator is similar to that of a number operator in the sense that it has a fixed number of distinct eigenvalues separated by a spectral gap. Without this, our perturbation analysis could not be carried out and the approximate locality of the operator would be rendered useless (see appendix D). Note that for the exactly local case, the spectral assumptions are automatically fulfilled and our definition thus indeed captures the concept of a local constant of motion (see appendix D). Finally, to recapitulate earlier definitions, the decay of the approximately local operator will be captured by a decay function, where we assume a localisation region X such that

$$\|Z - \Gamma_{X_l}(Z)\| \leqslant g(l) \, ,$$

with X_l denoting the set containing X and all its neighbours up to a distance l, as usual (see chapter 3.2). Using this approximate locality, a direct consequence of the simple spectrum of the constant of motion is that the dimension of the eigenspaces has to grow exponentially in the system size. This can be seen from a perturbation theory point of view, where the exponentially small tails are not sufficient to create transitions between distinct energy values. Thus, the spectrum is approximately given by that of a strictly local operator, which has the feature of exponentially growing eigenspaces since it is extended by tensoring with identity (see appendix D). With this insight, our theorem takes the following form.

Theorem 10 (Information propagation). *Let* H *be a Hamiltonian with non-degenerate energies and gaps and* $\mathcal{Z}$ *be an approximately local constant of motion with decay function* g *with localisation region* X*, spectral gap* $\gamma > 0$ *and eigenspaces with dimension larger than* $\widetilde{d}_{\min}$*. Then* H *necessarily has information propagation on average in the sense that there exists a local operator* B *initially supported on* $X_l \supset X$ *with* $\|B\| = 1$ *such that* B_t*, on average, has support outside any finite region* S

$$\overline{\|B_t - \Gamma_S(B_t)\|} \geqslant 1 - 13\frac{g(l)}{\gamma} - \frac{d_s}{2\widetilde{d}_{\min}^{1/2}} \,. \tag{6.2.1}$$

We remark, that the first non-constant term in Eq. (6.2.1) can be chosen arbitrarily small by picking the initial support X_l large enough, thus making $g(l)$ arbitrarily small and the second non-constant term decays exponentially with system size L, due to the exponential growth of the degeneracy $\widetilde{d}_{\min}$. This result shows that for many-body localising Hamiltonians, a zero velocity Lieb-Robinson bound does not occur and it is always possible to use the system to send information. The results does not rely on any specific form of the Hamiltonian and uses only the existence of a single approximately local constant of motion. Our results do not provide any statement on the influence of the involved energy scale and are perfectly compatible with the existence of an information mobility edge, in the sense of Def. 12. Let it be noted that the results certainly do not apply to an Anderson insulator, which has hugely degenerate energy gaps. This is in accordance with our previous discussion, which argued that an Anderson insulator shows a full suppression of propagation, as all eigenmodes are localised. Let us now turn to a sketch of the proof.

6.2.2 *A sketch of the proof*

Our results only rely on the existence of an approximately local constant of motion and assume no specific structure of the Hamiltonian. In order to first present the argument in its simplest form, however, we here assume that the Hamiltonian is diagonal and the local sites consist of spin-1/2 systems. A good example is the following simple MBL model

$$H = \sum_j h_j \sigma_j^z + \sum_{i,j} J_{i,j} \sigma_i^z \sigma_j^z \,,$$

where σ^z are the Pauli-Z-matrices and $J_{i,j} \in \mathbb{R}$ decays exponentially with the distance between the spins. The proof relies on perturbation arguments and a nifty construction of a local observable B [5], but the main idea is similar to the following proof sketch, which relies on using equilibration results following from non-degenerate energy gaps [69].

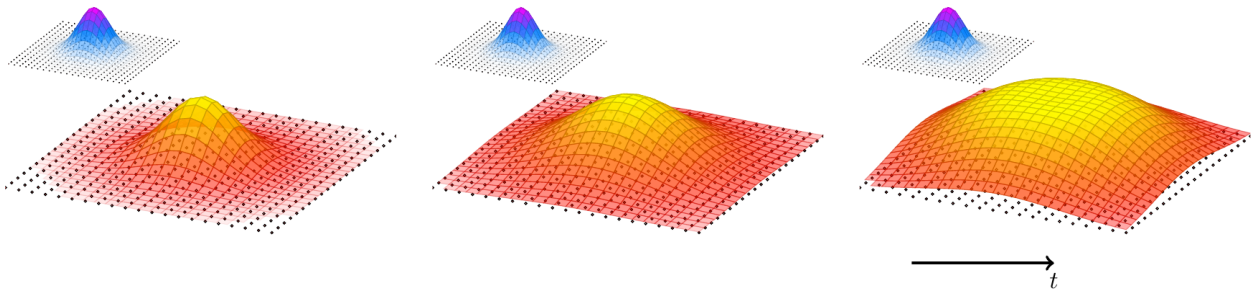

Figure 6.2: A schematic visualisation of the main result presented here. A constant of motion, on a 2D lattice, here drawn in blue, together with non-degenerate energy gaps is sufficient to show that a different operator exists, drawn in red, that has to spread without limits in the Heisenberg picture.

For this, we construct two objects. Firstly, a state that is the equal superposition of all eigenstates and secondly, a local operator B that initially has expectation value one with respect to this state, but at the same time has a zero diagonal in the energy eigenbasis and thus zero expectation value for the equilibrated infinite time average. Since equilibration guarantees that local expectation values are described by the infinite time average, this allows us to conclude that the Heisenberg evolution of the operator B has to be non-local (see Fig. 6.2).

Lemma 2 (Diagonal Hamiltonians)**.** *Let H be a diagonal Hamiltonian with respect to the local σ^z basis on a spin-1/2 lattice with non-degenerate eigenvalues and gaps. Let $B = \sigma_j^x$ be the Pauli-X-matrix supported on spin j. Then H necessarily has transport on average in the sense that the operator B_t has, on average, support outside any finite region S*

$$\overline{\|B_t - \Gamma_S(B_t)\|} \geqslant 1 - d^{|S|-N/2} .$$

Proof. For the argument, we use a state vector $|\psi\rangle$ that is initially a product with $|+\rangle$ on all sites. Let us point out that this $|\psi\rangle$ simply reflects an equal superposition of all eigenstates of the system and is thus an infinite temperature state. Since we assume that the Hamiltonian has non-degenerate energies, we know that the infinite time average of $\rho = |\psi\rangle\langle\psi|$ is diagonal, since all off-diagonal elements correspond to non-zero energy gaps and are thus dephased away. Moreover, as the diagonal is invariant under the time evolution, we know that the time-averaged state ω is the normalised identity matrix. Considering a subsystem S, we can use the non-degenerate energy gaps to employ the equilibration results from section 3.5 for the expected deviation from the infinite time average

$$\overline{\left\|\mathrm{Tr}_{S^c}(\rho_t - d^{-N}\mathbb{1})\right\|_1} \leqslant \frac{d_{\mathrm{sys}}}{2{d_{\mathrm{eff}}}^{1/2}} \leqslant d^{|S|-N/2} . \tag{6.2.2}$$

Here N is the total number of spins and the effective dimension, previously defined using the infinite time average (see section 3.5), counts how many eigenstates of the Hamiltonian are part of the state

$$d_{\mathrm{eff}} = \frac{1}{\sum_k |\langle k|\psi\rangle|^4} .$$

The above result states that, for most times, the reduced state of ρ_t looks like the identity. Due to the time reversal symmetric way in which these equilibration results are proven (see section 3.5), they also directly apply to the inverse evolution ρ_{-t} [69]. To investigate the transport properties of the Hamiltonian, we look at the time evolution of an observable B consisting of a single Pauli-X-operator somewhere in the region S. The key trick is to use the initial expectation value and to insert time evolution operators

$$1 = \mathrm{Tr}(B_0\rho_0) = \mathrm{Tr}(B_t\rho_{-t}) . \tag{6.2.3}$$

Since we know that the equilibrated state is the normalised identity, the expectation value of any local traceless operator A has to vanish on average

$$\overline{\mathrm{Tr}(A\rho_{-t})} = 0 .$$

Since B_0 is traceless and the time evolution leaves the trace invariant, we can conclude that the operator B_t on average cannot be local anymore. More precisely, we have that

$$\begin{aligned}\overline{\|B_t - \Gamma_S(B_t)\|} &= \overline{\left\|B_t - d^{|S|-N}\mathbb{1}_{S^c} \otimes \mathrm{Tr}_{S^c}(B_t)\right\|} \\ &\geqslant \overline{\left|\mathrm{Tr}(B_t\rho_{-t}) - d^{|S|-N}\mathrm{Tr}_S\left(\rho_{-t}^S \mathrm{Tr}_{S^c}(B_t)\right)\right|} ,\end{aligned}$$

where we used that $\|B\| \geqslant |\mathrm{Tr}(B\rho)|$ and defined $\rho^S = \mathrm{Tr}_{S^c}(\rho)$. Next we use the inverse triangle inequality, Eq. (6.2.3) and insert $0 = \mathrm{Tr}(d^{-|S|}\mathbb{1}_S \mathrm{Tr}_{S^c}(B))$ which is using the fact that the reduced observable has zero expectation value with the infinite time average

$$\begin{aligned}\overline{\left|\mathrm{Tr}(B_t\rho_{-t}) - \mathrm{Tr}_S\left(\rho^S_{-t} d^{|S|-N}\mathrm{Tr}_{S^c}(B_t)\right)\right|} &\geqslant 1 - \overline{\left|\mathrm{Tr}_S\left(\rho^S_{-t} d^{|S|-N}\mathrm{Tr}_{S^c}(B_t)\right)\right|} \\ &\geqslant 1 - \overline{\left|\mathrm{Tr}_S\left((\rho^S_{-t} - d^{-|S|}\mathbb{1}_S) d^{|S|-N}\mathrm{Tr}_{S^c}(B_t)\right)\right|}\,.\end{aligned}$$

Another application of $|\mathrm{Tr}(B\rho)| \leqslant \|B\|\|\rho\|_1$ allows us to use the equilibration results in Eq. (6.2.2). Using $\|d^{|S|-N}\mathrm{Tr}_{S^c}(B_t)\| \leqslant 1$ yields the estimate

$$\begin{aligned}\overline{\|B_t - \Gamma_S(B_t)\|} &\geqslant 1 - \left\|\rho^S_{-t} - d^{-|S|}\mathbb{1}_S\right\|_1 \left\|d^{|S|-N}\mathrm{Tr}_{S^c}(B_t)\right\| \\ &\geqslant 1 - d^{|S|-N/2}\,.\end{aligned}$$

This concludes the proof in the simplest setting. □

The main idea for the proof still can be carried out in the setting where the Hamiltonian is no longer assumed to be diagonal, but where only the existence of an approximately local constant of motion is guaranteed. For this, it is first assumed that the constant of motion is exactly local. This implies that it is possible to distinguish different sets of eigenvectors locally and thus allows to construct local observables that have zero diagonal in the eigenbasis of the Hamiltonian. Moreover, a state with large expectation value with respect to this observable can be constructed. This again allows to use the equilibration results for this state, together with the off-diagonality of the observable in order to prove transport. Finally, the argument is concluded by performing a perturbation analysis, which makes room for the decaying tails of the approximately local constant of motion. This argument requires a detailed mathematical analysis and is contained in appendix D.

6.2.3 *Summary: Information propagation in MBL*

In this section, we saw that systems with suitably non-degenerate spectrum and an approximately local constant of motion, provably allows for information propagation. We explicitly constructed local excitation operators whose effect spreads over arbitrary distances, thus giving rise to a protocol to use MBL systems for signalling. Our results are nicely complemented by recent work showing that if the Hamiltonian can be written in terms of approximately local constants of motion, logarithmic Lieb-Robinson bounds can be derived [166]. Our result can be seen as a rigorous proof that this logarithmic cone can never be tightened to a zero-velocity Lieb-Robinson bound, at least if one allows for infinite energy in the system. Let it be noted that, in contrast to the setting in Ref. [166], we do not require any special decomposition of the Hamiltonian, but rather the existence of a single approximately local constant of motion is sufficient. What is more, this work constitutes an important step towards proving a lower Lieb-Robinson bounds in generic spin models. While upper bounds on information propagation can easily be obtained (see appendix B), proving that propagation actually takes place is an exceedingly hard task, at least outside of the regime of free models (see section 3.4). In this context, our work can be seen as the first proof of propagation in an interacting physical model, albeit we are not yet able to provide the corresponding time scale. It is interesting to note that this time scale is directly linked to equilibration time scales and any progress on finding useful bounds on those (see section 3.5) would immediately yield a time scale for the information propagation proven in this section.

This concludes our discussion of the propagation of operators in MBL systems. In the following, we turn to the behaviour of states and in particular look at eigenstates of MBL systems. Here local descriptions, for example in the form of tensor networks, play a crucial role.

6.3 MANY-BODY LOCALISED STATES

As we saw in the previous sections, structure of eigenvalues and eigenvectors can often be directly connected to physical behaviour. For example, we saw that non-degenerate energy gaps give rise to equilibration behaviour and eigenstates fulfilling the ETH guarantee thermalisation. In this section, we investigate these spectral properties of MBL systems. We argue that eigenstates of such models are expected to have a particularly easy structure, at least if the randomness is sufficiently strong. We present different formulations of this statement and compare the interacting eigenstates to the case of an Anderson insulator. In the entanglement behaviour, we see a sharp distinction between eigenstates of generic models, which usually fulfil a volume law for the entanglement entropy, while MBL eigenstates are expected to fulfil an area-law. In this way, the randomness leads to a distinctly different eigenstate behaviour, at least if the randomness is sufficiently strong [171]. While entanglement entropies are an important aspect, also the violation of the ETH as well as tensor network tool approximations are considered as static localisation properties. We begin by looking at the eigenvalues of those models.

6.3.1 *Spectral transition*

In the condensed matter community, one prominent feature of systems is to look at the gaps between consecutive eigenvalues. A distinction is made between the Poissonian case which occurs for non-interacting models (see Fig. 5.2) and the Wigner-Dyson surmise expected for interacting models [172]. For MBL systems, it is found that they have Poissonian level spacing [173]. Interestingly, this transition does not seem to occur for arbitrary randomness, but rather there is a sort of phase transition for suitable strong random potentials [171].

Furthermore, it was uncovered that the level spacing can behave differently depending on the investigated energy. In particular, it is possible to have a disorder strength such that the low-energy sector already has Poissonian statistics, while the high-energy eigenvalues follow the Wigner-Dyson surmise [171]. This is a very exciting development, since it shows that for interacting models, there can be a mobility edge even in 1D; a behaviour impossible for the normal Anderson model. Note that this distribution of gaps is independent of the question whether the energy gaps are non-degenerate. In fact, as argued earlier, such non-degeneracy is expected independent of the localising nature of the system and solely relying on the fact that it is interacting. We now turn to the eigenstates of the system.

6.3.2 *Fock space localisation*

One possible approach is to investigate how the many-body eigenstates look in the original localised orbitals of the single-particle setting. In the non-interacting case all eigenstates naturally can be specified by giving the occupation numbers of the individual orbitals resulting in Fock states in those localised orbitals. Once interactions are turned on, it is natural to ask how many of these original Fock configurations significantly contribute to the new eigenstates. For generic models, one would expect that this number grows exponentially with the system size, while for localised systems, it should grow at most linearly. Moreover, for states with fixed particle number, one would expect no growth at all for localised systems, while generic models should need more and more Fock configurations to construct the many-body eigenvectors. This intuition was confirmed by perturbation arguments [46, 47] and was an early characterisation of MBL.

6.3.3 *Eigenvector entanglement*

A different characteristic feature of localisation is the entanglement property of individual eigenstates. In the non-interacting case all of them fulfil an area-law, meaning that their entanglement scales like the size of the boundary of the cut. Thus, in 1D all eigenstates have a constant half-chain entanglement entropy independent of the system size. This has also been considered as a possible characterisation of MBL [174]. Numerically, strong disorder indeed seems to imply an area-law behaviour, while again settings are possible that show a mobility edge, now in the sense that low-energy states have little entanglement, while eigenstates in the middle of the spectrum show a volume law [171].

Aside from entanglement, also other probes for the behaviour of localising eigenstates were proposed. In particular, the correlation matrix $\langle f_k^\dagger f_j \rangle$ evaluated on individual eigenstates has proven to be a useful probe [175]. Moreover, also the total correlations of eigenstates were proposed as an investigative tool and show a similar drastic change of behaviour between localising and thermalising regime [176].

6.3.4 *Tensor-network approximations*

Concomitant with the above indications that eigenstates of MBL systems have little entanglement, it is often argued that they should allow for an efficient approximation in terms of tensor networks [174]. In one dimension, these two statements are equivalent, at least when the entanglement is captured in terms of Renyi entropies (see chapter 3.2). In higher dimensions, however, this is no longer the case. While a tensor-network description directly implies an area-law, the converse is no longer true [103]. Therefore, demanding that the eigenstates of MBL systems are efficiently captured in terms of tensor-networks is a strictly stronger statement then only bounding their entanglement.

6.3.5 *Breakdown of ETH*

Immediately connected to the entanglement behaviour of individual eigenstates is the validity of the eigenstate thermalisation hypothesis (see chapter 4). It was proposed as a possible mechanism for thermalisation and, in its most intuitive form, states that already individual eigenvectors should locally be indistinguishable from the global Gibbs state, where the temperature is fixed by the corresponding energy of the eigenstate [26, 131]. This implies that eigenstates should locally be very mixed and is thus incompatible with an area-law for the entanglement entropy. In this way, the break-down of the ETH is a similar approach to MBL [153, 161], but is strictly stronger than only demanding an area-law behaviour of the entanglement of all eigenstates.

6.3.6 *Summary: Spectral features of MBL*

In this section, in addition to the different discussed aspects of dynamical localisation of local operators, we now saw a plethora of static characterisations that capture local eigenstates or the spectrum. We encountered various ways in which eigenstates of MBL systems are localised, in contrast to the dynamical behaviour of MBL. While product states obtain arbitrarily large entanglement over time, all eigenstates of the system have little entanglement, at least in the case of strong disorder considered here. As dephasing of a superposition of many product eigenstates can still lead to a large entanglement, these two pictures are perfectly compatible [5].

Based on the above eigenstate localisation, many people think of MBL as a quantum phase transition for all eigenstates or equivalently at "infinite temperature". We will encounter such transitions for the usual ground state case in chapters 9 and 10. There again, the juxtaposition of static and dynamic properties will pose intriguing physical questions that require extensive numerical, analytical and experimental efforts.

In summary, we encountered a very tangled landscape of localisation properties, both in static and dynamic formulations. Within the scope of this thesis, we are not able to fully clarify all aspects, but provide further significant steps in this direction. In particular, we now present an insightful link that connects the dynamic features discussed earlier with the eigenvector localisation described in this section.

6.4 EIGENVECTORS AND SUPPRESSION OF TRANSPORT

The following section is based on Ref. [4]. We sincerely thank Albert H. Werner, Winton Brown, Volkher B. Scholz and Jens Eisert for the very insightful collaboration.

In this chapter, we present a link between dynamic and static properties of MBL [4], in the spirit of the well-known exponential clustering theorem (see Thm. 4 and Refs. [66, 94]). The general idea is to use a dynamical suppression of propagation and from that derive that correlators in eigenstates have to decay exponentially. In contrast to the exponential clustering theorem, our result is not limited to the ground state. Rather, the strong suppression of propagation on the low-energy sector of MBL allows to show such exponential clustering for many excited states of the model.

We begin with some generic assumptions on the spectrum of the Hamiltonian [4], which seem natural in the context of MBL systems or Anderson insulators with local random potentials.

- *Non-degenerate energies (**AI**):* The energies of the full Hamiltonian are assumed to be non-degenerate. The smallest gap between these energies is called γ.
- *Locally independent gaps (**AII**):* The energies of reduced Hamiltonians H_A and H_B which include all interactions inside rectangular regions A and B respectively (see Fig. 6.3), are assumed to be non-degenerate when viewing them as operators on their respective truncated Hilbert spaces $\mathcal{H}_A$ and $\mathcal{H}_B$. The smallest gap is called $\tilde{\gamma}$. Moreover, the gaps of these Hamiltonians need to be locally independent with respect to each other, in the sense that

  $$E_a - E_{a'} = E_b - E_{b'} \Rightarrow a = a', b = b' ,$$

  where a, a' and b, b' label the eigenvalues of H_A and H_B respectively. Thus, the only possible way in which the spectral gaps can be the same is if they both are zero. The smallest difference of these gaps is called η.
- *Non-symmetric gaps (**AIII**):* For all eigenvalues E_k of the full Hamiltonian the spectrum is no-where symmetric, in the sense that

  $$\min_{r \neq s} \big| |E_r - E_k| - |E_s - E_k| \big| \geqslant \zeta > 0 \quad \forall\, k .$$

Note that the above conditions allow for degenerate energy gaps and are, with high probability, fulfilled by Anderson insulating models. Assumption **AII** can also be reformulated, by demanding that the joint Hamiltonian $H = H_A + H_B$ supported on two disjoint rectangular regions has non-degenerate energies, since these energies are all possible sums of the local energies $E_a + E_b$. We now turn to describing our dynamical assumptions, which are the basis for our proof of exponential clustering of eigenstates.

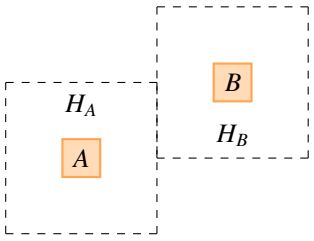

Figure 6.3: *Taken from Ref. [4].* This figure shows the Hamiltonian decomposition used in the proof of theorem 11. For the two considered observables A, B truncated Hamiltonians H_A, H_B are used that include all terms around the support of those operators and have a square support that is chosen as large as possible without overlapping.

6.4.1 *Strong dynamical localisation*

We first present the main result in the easiest possible setting. Here, we assume a full suppression of propagation in the sense that the systems has strong dynamical localisation (see Def. 11). This assumption is certainly rather strong and probably only fulfilled in the case of non-interacting particles. We move towards MBL systems in the next step, but for now restrict ourselves to this easiest case.

The goal is to exponentially bound the correlator $\langle k| AB |k\rangle - \langle k| A |k\rangle\langle k| B |k\rangle$, where $|k\rangle$ is an eigenstate of the Hamiltonian and thus show that eigenstates have exponentially clustering correlations. For this, we rely on energy filtering with a Gaussian filter function (see appendix E)

$$I_\alpha^H(A) := \sqrt{\frac{\alpha}{\pi}} \int_{-\infty}^{\infty} dt\, e^{-\alpha t^2} e^{itH} A e^{-itH} ,$$

which partly diagonalises the observable in the Hamiltonian basis up to an error that is distributed according to a Gaussian with width α. By tuning this parameter α, one can interpolate between keeping some locality of the original observable and the error in the diagonalisation. The first key step in showing exponential clustering of eigenstates is to show that the energy filter for two disjoint observables with their respective local Hamiltonians decouple [4].

Lemma 3 (Decoupled energy filtering)**.** *Under the assumption of locally independent gaps (**AII**), energy-filtering of two observables can be factorised into local energy filters*

$$\|I_\alpha^{H_A+H_B}(AB) - I_\alpha^{H_A}(A) I_\alpha^{H_B}(B)\| \leqslant 2^{4L+1} e^{-\xi^2/(4\alpha)} ,$$

with $\xi = \min\{\eta, \sqrt{2}\tilde{\gamma}\}$ and L the system size as usual. Here H_A and H_B are chosen to include all Hamiltonian terms within distance $d(A,B)/2$ of the support of A and B respectively (see Fig. 6.3).

The crucial ingredient used here is the fact that H_A and H_B have independent gaps in the sense of Def. **AII**, which means that their difference is uniformly bounded from below by ξ. Using that the energy filter diagonalises the local observables and labelling the spectrum of H_A and H_B with a and b respectively is the basis for analysing the following term

$$\Big\| I_\alpha^{H_A+H_B}(AB) - \sum_{a,b} |a,b\rangle\langle a,b| AB |a,b\rangle\langle a,b| + \sum_{a,b} |a,b\rangle\langle a,b| AB |a,b\rangle\langle a,b| - I_\alpha^{H_A}(A) I_\alpha^{H_B}(B) \Big\| .$$

What is left to do is to show that both the decoupled as well as the joint filter achieve the diagonalisation in the eigenbasis of H_A and H_B. This analysis is straightforward, but slightly tedious and can be found in

appendix F. Based on this lemma, we can now move to the main result of this section in its simplest form [4], which relies on the strong dynamical localisation as discussed in the chapter on Anderson localisation (see Def. 11).

Theorem 11 (Clustering of correlations of eigenvectors)**.** *If the Hamiltonian shows strong dynamical localisation and its spectrum has non-degenerate energies (**AI**) and locally independent gaps (**AII**), then all its eigenvectors have exponentially clustering correlations*

$$|\langle k|AB|k\rangle - \langle k|A|k\rangle\langle k|B|k\rangle| \leqslant 4C_{loc}\, e^{-\mu d(A,B)/2}\,,$$

where μ and C_{loc} are the constants from the definition of strong dynamical localisation.

Proof. The proof uses the local Hamiltonians H_A and H_B (see Fig. 6.3) and the following estimates

$$\begin{aligned}
\langle k|AB|k\rangle &= \langle k|I_\alpha^H(AB)|k\rangle \\
&\overset{=}{I} \langle k|I_\alpha^{H_A+H_B}(AB)|k\rangle + \Omega(e^{-\mu l}) \\
&\overset{=}{II} \langle k|I_\alpha^{H_A}(A)I_\alpha^{H_B}(B)|k\rangle + \Omega(e^{-\mu l}) \\
&\overset{=}{III} \langle k|I_\alpha^{H}(A)I_\alpha^{H}(B)|k\rangle + \Omega(e^{-\mu l}) \\
&\overset{=}{IV} \langle k|A|k\rangle\langle k|B|k\rangle + \Omega(e^{-\mu l})\,,
\end{aligned}$$

where $\Omega(x)$ denotes a linear scaling in the quantity x. In each step, an error term of the form $C_I e^{-\mu l}$ with C_I to C_{IV} is introduced. The constant C appearing in the main theorem is the sum of them. Constants C_I, C_{III}, C_{IV} directly follow from the properties of the applied Gaussian filter (see Def. 10) and constant C_{II} is derived in lemma 3

$$\begin{aligned}
C_I &= 2C_{loc}\,, \\
C_{II} &= 2^{4L+1} e^{-\xi^2/(4\alpha)} e^{\mu l}\,, \\
C_{III} &= C_{loc}\,, \\
C_{IV} &= e^{-\gamma^2/(4\alpha)} e^{\mu l}\,, \\
C &:= C_I + C_{II} + C_{III} + C_{IV}\,.
\end{aligned}$$

The constants C_{II} and C_{IV} can be chosen arbitrarily small, by picking a sharp enough filter function, meaning a sufficiently small α. In particular, we can choose $C_{II}, C_{IV} \leqslant C_{loc}/2$, which yields

$$C = 4C_{loc}\,.$$

Choosing $l = d(A,B)/2$ concludes the proof. □

As presented above, if a Hamiltonian has strong dynamical localisation, then all its eigenvectors provably have exponentially clustering correlations. In the following section, we move towards a setting that includes the expected behaviour of MBL systems and relies on a considerably weaker assumption.

6.4.2 *Information mobility edge*

In the following, we look at the low-energy sector of an MBL Hamiltonian. While allowing for arbitrary energy scales in an MBL system gives rise to an unbounded growth of entanglement and makes information propagation possible (see section 6.2), this propagation is expected to be no longer possible on the

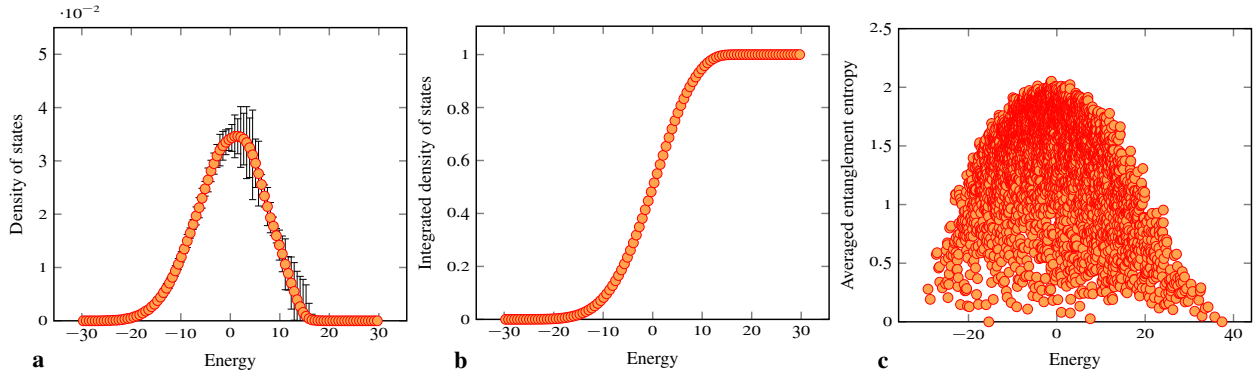

Figure 6.4: *Taken from Ref. [4].* We perform exact diagonalisation of the one-dimensional Heisenberg model with random on-site magnetic field of the form $H = \sum_i (\sigma_i^x \sigma_{i+1}^x + \sigma_i^y \sigma_{i+1}^y + \sigma_i^z \sigma_{i+1}^z + w_i \sigma_i^z)$, where w_i is drawn uniformly from the interval $[-h, h]$. **a** The left plots shows the number of eigenstates for 14 sites as a function of the discretised energy for $h = 1$ averaged over 100 realisations and the variance of this averaging is indicated by vertical error bars. The resulting function is close to a Gaussian. **b** In the middle, the integrated density of states of this model with the same parameters is shown. The corresponding error bars are too small to appear. This quantity is related to the number of states Θ by an exponential factor 2^L. This plot indicates that indeed the number of states has small tails and thus few states at low energies. **c** The right plot depicts the (von Neumann) entanglement entropy of the eigenvectors as a function of the energy. The results were obtained for the disorder strength $h = 4$ on a system of 12 sites and for each individual state an average over the different cuts through the 1D chain was taken. This plot corroborates the intuition that the entanglement entropy and thus the associated bond dimension of the corresponding MPS increase with the energy.

low-energy sector. In particular, we assume an information mobility edge in the sense of no information propagation below a certain energy, as described in Def. 12. Based on this, we are able to show that all states below this information mobility edge provably have exponentially clustering correlations.

Theorem 12 (Clustering of correlations of eigenvectors)**.** *If the Hamiltonian has an information mobility edge at energy* E_{mob} *and it has non-degenerate energies (**AI**) and non-symmetric gaps (**AIII**), then all eigenvectors* $|k\rangle$ *up to that energy* E_{mob} *cluster exponentially, in the sense that for all* $\kappa > 0$

$$\begin{aligned} &|\langle k| AB |k\rangle - \langle k| A |k\rangle\langle k| B |k\rangle| \\ &\leqslant \left(12\pi\Theta(E_k + \kappa) C_{\text{mob}} + \ln \frac{\pi \mu\, d(A,B)\, e^{4+2\pi}}{\kappa^2} \right) \frac{e^{-\mu d(A,B)}}{2\pi} , \end{aligned}$$

where $\Theta(E)$ *is the number of eigenstates up to energy* E *and* κ *can be chosen arbitrarily to optimise the bound.*

The proof of this statement is rather technical and contained in appendix F. Let us highlight some important features of this bound. Firstly, one is able to freely choose an energy cutoff κ that allows to optimise the bound. For those familiar with the proof of the exponential clustering theorem, κ serves as an artificial gap. For typical local models, we expect the density of states to behave like a Gaussian, an intuition that can be numerically tested for small systems (see Fig. 6.4), and rigorously proved in a weak sense [87]. In this case the number of states behaves like a low-order polynomial in the system size at energies close to the ground state energy $E_k + \kappa$. Thus fixing a $\kappa > 0$ independent of the system size leads to a prefactor that scales like a low-order polynomial in the system size where the order of the polynomial increases as one moves to higher energies. In the bulk of the spectrum, the number of

states grows exponentially with the system size, thus rendering our bounds useless as one moves to high energies. Interestingly, this feature of stronger correlations, associated with a larger entanglement in the state, at higher energies seems to be shared by the Heisenberg chain with random on-site magnetic field (see Fig. 6.4).

Our result can also be applied to the ground state of models, where it provides an extension of the previous results [157] and for example for the case of an almost degenerate ground state is a substantial improvement. More importantly, however, the above theorem also applies to excited states and for the first couple of excitations certainly provides highly non-trivial statements.

6.4.3 *Implications on area laws and matrix-product states*

In one dimension, the conclusions of our main theorem about the correlation behaviour of eigenvectors can be turned into a statement about their entanglement structure. It was noted before that many-body localisation should be connected to eigenvectors fulfilling an area law (see Conjecture 1 in Ref. [174]), and eigenvectors being well approximated by matrix-product state vectors of the form (see appendix A)

$$|\mathrm{MPS}_D\rangle = \sum_{j_1,\cdots,j_L=1}^{d_{\mathrm{spin}}} \langle A_1[j_1]|\, A_2[j_2]\cdots A_{L-1}[j_{L-1}]\,|A_L[j_L]\rangle\,|j_1,\cdots,j_L\rangle \ ,$$

where $\langle A_1[j_1]|$ and $|A_L[j_L]\rangle$ are boundary vectors of size D and $A_k[j]$ for each position k are complex $D\times D$ matrices, with D being the bond dimension. Our main theorem allows to rigorously prove this connection.

Corollary 13 (Area laws and matrix-product states)**.** *An eigenvector $|k\rangle$ of a localising Hamiltonian can be approximated by an MPS with fidelity $|\langle k|\mathrm{MPS}_D\rangle| \geqslant 1-\epsilon$, where the bond dimension D for a sufficiently large system is given as follows.*

a *If the Hamiltonian shows strong dynamical localisation and has non-degenerate energies (**AI**) and locally independent gaps (**AII**), then the statement holds for all eigenvectors $|k\rangle$ and, for some constant $C>0$, the approximation has a bond dimension*

$$D = C\,(L/\epsilon)^{\frac{16}{\mu \log_2 e}} \ .$$

b *If the Hamiltonian has an information mobility edge at energy E_{mob}, and has non-degenerate energies (**AI**) and non-symmetric gaps (**AIII**), then the statement holds for all eigenvectors below this energy E_{mob} and the bond dimension is given by*

$$D = \mathrm{poly}\,(\Theta(E_k+\kappa), L) \ ,$$

for any fixed κ which enters in the precise form of the polynomial.

The proof is a direct consequence of our main theorem together with the fact that exponential clustering in one dimension implies an entropy bound for any bipartite cut of the chain [102]. Using techniques from [177] this leads to an efficient MPS approximation with the above bounds on the bond dimension (see appendix F for details).

6.4.4 *Summary: Eigenvectors and suppression of transport*

This concludes the connection between dynamical suppression of propagation and the correlation structure of individual eigenstates. We saw how an information mobility edge can be used to show that the full low-energy sector provably has exponentially clustering correlations and can thus, in 1D, be efficiently approximated by matrix-product states. The result discussed above is one of the few instances where one is able to achieve a direct link between static and dynamic properties of local Hamiltonian models, much in the spirit of the exponential clustering theorem [66, 94]. It highlights the fact that MBL models are not only interesting in their own right as physical models of impurities in solid-state physics, but also are useful for investigating long-standing questions in quantum information, such as the precise connection between eigenvector behaviour and dynamical properties.

In the following, we summarise the different MBL features encountered, order them and propose a possible definition of the phenomenon.

6.5 DEFINING MANY-BODY LOCALISATION

When it comes to a possible definitions of MBL, there are presumably as many opinions as physicists working on MBL, maybe more. In fact, currently it is not even clear to what extent there is only a single MBL phase, or whether it should be further separated into different MBL phases as recently proposed [178, 179]. So far, the different characterisations are very much a question of taste and little consensus has been achieved on the paramount questions which features should be taken as the defining property of MBL. At the current stage, it is therefore also unclear which experimental probes should really be measured in order to ensure that a system is in the MBL phase and how this is connected to other classifications commonly considered.

In the following, we first sort the previously encountered aspects of MBL in a systematic way. We proceed to recapitulate the links presented in this thesis or performed in other publications over the last years. Based on this, we propose a possible unifying definition of MBL and speculate how it is related to other features usually considered. We begin by reevaluating the graphical representation of the different features of MBL (see Fig. 6.5).

The individual boxes should be quite clear at this point. We argued that local operators behave in special way in MBL systems. In general, they slowly spread over the full lattice, corresponding to the possibility to propagate information. Yet, this propagation vanishes when restricting to the low-energy sector. Following our intuition, it should also be absent when only looking at how particles or energy propagates. Finally, there exist certain local operators that do not propagate at all and are even local constants of motion.

When looking at the evolution of states, we encountered a log-growth of entanglement that eventually saturates in a volume-law. Despite this volume-law like behaviour, the infinite time average is not captured by a thermal ensemble, which is not surprising when assuming that local constants of motion exist. Therefore a generalised Gibbs ensemble description is needed.

Finally, we investigated spectral properties, namely non-degenerate energy gaps and consecutive gaps that are distributed according to a Poissonian distribution. The eigenstates of MBL systems are expected to be local, where many possible statements of this locality can be considered.

We now focus our attention on establishing links between these, a priori, disconnected features. Let us begin with the gray arrows, which are straightforward conclusion or are based on results that were known outside of the MBL context. First, let us look at the different features of eigenstates of MBL systems. Surely, a lack of entanglement in the eigenstates implies that the ETH is violated, as does Fockspace localisation.

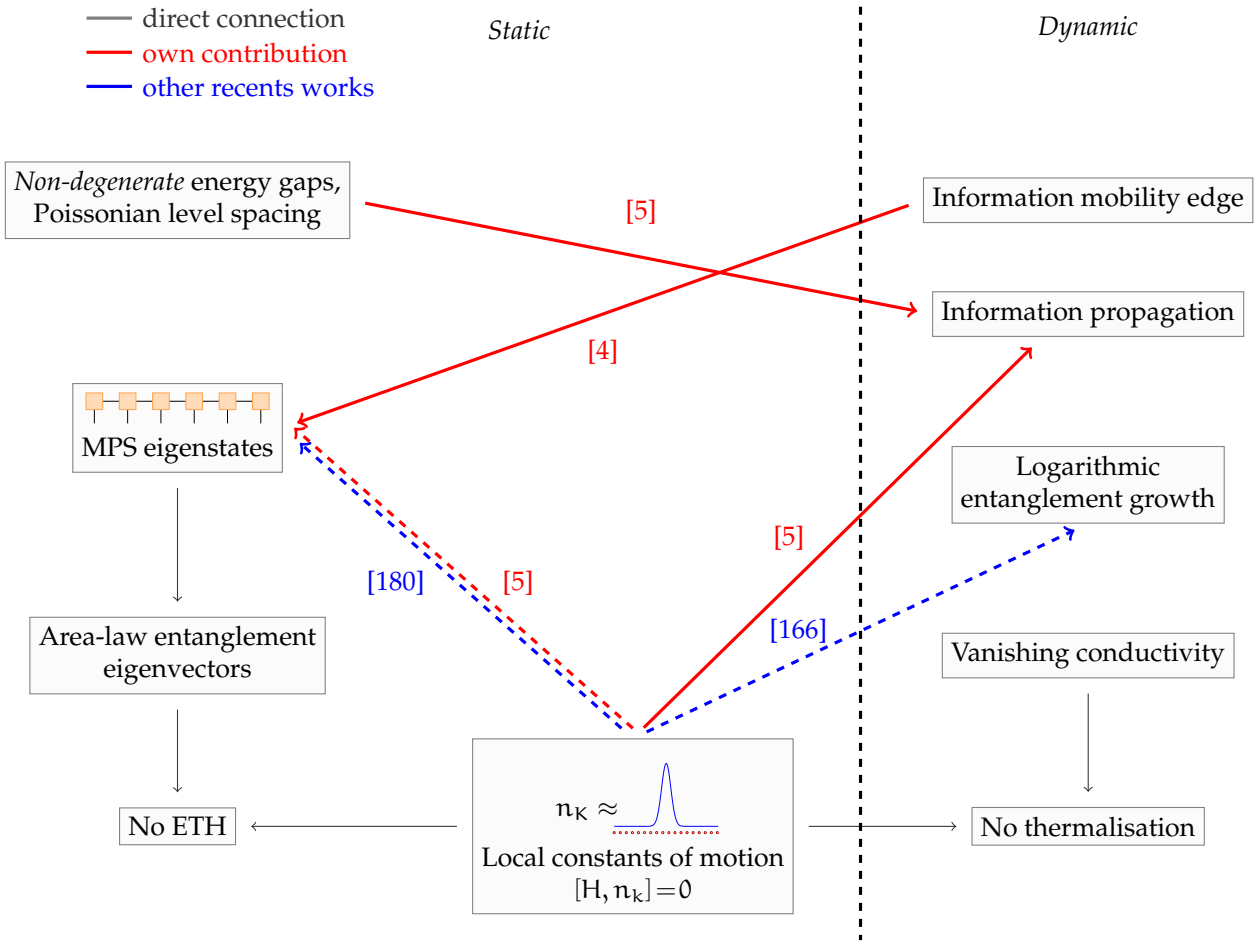

Figure 6.5: A characterisation of MBL and the connections achieved within the scope of this thesis as well as in other publications. Links achieved with the involvement of the author of this thesis are marked in red, while other contributions are drawn in blue. Te arrows are label with the appropriate citation. The established links bring together different aspects of MBL and show that currently much structure is provided by the existence of local constants of motion.

Based on a tensor network representation of a state, we can deduce an area-law behaviour. Moreover if a model does not dynamically thermalise due to memory of the initial conditions, which is implied in this context, then the ETH also has to be violated. Also, if a model does not have particle transport, then initial imbalances will always be remembered and thermalisation cannot take place. The same holds if the system has local constants of motion.

Let us now move to connections that were developed specifically in the MBL context. Recently, local constants of motion have moved into the focus of attention. Ref. [180] provides a proof that a sufficient amount of exactly local constants of motion allows to proof an area-law for all eigenstates. In fact the reference proves that a spectral tensor network can be obtained that captures all eigenstates, which is a strictly stronger statement. Using a perturbation analysis [5] based on our bounds in appendix F , this result can be generalised to the setting of approximately local constants of motion. Further, one can deduce the failure of the system to thermalise [72, 74] from the existence of local constants of motion. Ref. [166] provides a link that local constants of motion are sufficient to show that information propagates only slowly through the system. It, however, leaves open the crucial question whether information propagation is possible at all, meaning whether the logarithmic bounds are tight. In our work [5], we answer this

questions in a very general context. Surprisingly, the existence of a single constant of motion, together with a non-degenerate spectrum, which reflects the fact that the Hamiltonian is interacting, is sufficient to proof that information has to eventually spread through the whole system. This rather intricate insight into the dynamics of interacting systems provides a clear link between equilibration behaviour and local constants of motion.

This rich structure provided by local constants of motion and the Hamiltonian being a polynomial of them would suggest to define MBL via this structure. The clear downside of such a definition is that constructing the local constants of motion is typically very hard and analytically has so far only been performed for the Ising model [181]. Even numerically it is far from clear how this could be performed outside of the regime where the model can be solved completely using exact diagonalisation [164, 165, 182], with first approaches just being conceptually developed [183]. While some have suggested to use time-averaging [165], this has the downside that the emerging constants of motion do not have a simple spectrum and are thus not suited for deriving the eigenstate structure [5].

A further downside of considering local constants of motion as the defining feature of MBL is that they are not directly experimentally accessible. From this point of view, transport properties are much more suited for a definition of MBL, as they could be easily measured. Motivated by this, in Ref. [4], we linked a strict mobility edge for the propagation of information with local structure of the eigenstates. In particular, such a full suppression of information on the low-energy sector is sufficient to obtain exponential clustering of all eigenstates in the low-energy sector. This can be seen as an extension of the exponential clustering theorem to excited states in localising models. Such a full suppression is, however, not sufficient, for a characterisation of MBL for two reasons. Firstly, it does not allow to distinguish an Anderson insulator from an interacting localising model. For this, one would have to complement it with a dephasing measurement, for example as proposed in Ref. [184]. Secondly, it only refers to the low-energy sector and thus leaves out the possibility of a *mobility edge*. In fact, it was numerically observed that, even if the low-energy sector is localising, the eigenstates of the model can still be strongly entangled in the middle of the spectrum [171].

Such a mobility edge is currently being explored intensively, but most questions are still open. In particular, does this actually imply that particle transport is possible at high energies? Will the model thermalise at those energies? Or is there some signature of localisation left, despite the volume-law entanglement in the eigenstates? As we cannot address these issue at the moment, we go back to the simpler setting where localisation takes place for arbitrary energies.

Before we move towards an attempt of a definition, let us further stress the importance of establishing a consensus on the true nature of the phenomenon by exploring a recent debate on MBL in translationally invariant models. Clearly, the original mindset of localisation following the work of Anderson [48] related to impurities in models and relies on randomness in the system. That being said, many features commonly associated with MBL can also be observed in models without such random potentials. For example, the slow growth of entanglement entropies is very much reminiscent of a classical glass, which is also characterised by extremely slow equilibration processes [185]. Recently such classical glasses have served as candidates to derive quantum version thereof [185]. Such and similar approaches indeed give models which equilibrate exponentially slowly and where transport processes only have a logarithmic speed [107, 108, 185–187]. This lead to an ongoing debate to what extent such systems should count as having MBL [188]. It is, however, unclear whether the models in Refs. [107, 108, 185] can truly be characterised in terms of a vanishing conductivity or, much more likely, will allow for transport when they are coupled to an external battery. This debate of the existence of MBL in translationally invariant models stresses further the strong need for some clarification in the field.

Abstractly speaking, a many-body insulator should be a model that has no transport for physical properties such as particle number and energy, like an Anderson insulator, but is interacting, as for example

manifested in non-degenerate energy gaps. This would suggest to define MBL using the following two features.

I The model has no particle or energy transport, in the sense that the amount of particles or energy that is transported can be bounded with a function that is exponentially decaying with the distance for all times.

II The model is fully interacting and allows for information propagation.

There are still many issues connected to such a definition of MBL. Firstly, the precise notion of energy and particle transport would have to be developed in a rigorous mathematical language. Here traditional condensed matter type approaches, like the Kubo formula [17], will certainly play an important role, but are not sufficient for capturing the flow of particles in finite and closed systems. Moreover, such a notion of the suppression of transport would have to be translated to an experimental protocol, similar to the failure of thermalisation that was impressively demonstrated using ultra-cold gases [76]. Secondly, one would need an easy protocol that allows to show that a model is interacting, which will most likely be connected to a protocol testing for information propagation, for example by exploring the influence of a local operation in time. An alternative would be a direct measurement of the unbounded entanglement growth, which seems hard given current experimental techniques [189, 190]. Such interest in entanglement properties of ultra-cold atomic systems will also be encountered in chapter 11, where a possibility to approach this issue is outlined using tensor network tomography. Despite these obvious difficulties, the above two features seem substantially easier to access than constants of motion or the special structure of eigenstates. This is especially true from a numerical point of view, where a full diagonalisation of such models usually needs exponentially large resources. Thus, it seems likely that using the above definition of MBL, one could efficiently test a given system for it.

Naturally, this is only half of what a useful definition needs to offer. Surely it is important that one can actually decide whether a system fulfils it, but moreover, one would like to be able to learn something from this classification. This gives rise to the endeavour of connecting the above definition to different MBL properties usually considered, much in the spirit of the efforts presented in this work. Based on the intuition gained in Ref. [4], we would indeed expect that a suppression of energy or particle transport should be enough to derive a form of localisation of eigenvectors. Ideally, one could further show that it can be connected to the existence of local constants of motion and a Hamiltonian that is a simple function of those operators. Thus would allow to use the rich structure provided by these approximately local constants of motion that currently puts them in the center of many characterisations of MBL (see Fig. 6.5). If such a programme is successful, then the above properties **I** and **II** would be a useful definition of MBL. Firstly, because one can numerically or experimentally decide whether it is fulfilled and secondly, because it would imply the rich localisation structure in terms of local operators and local eigenstates usually associated with MBL. There is, however, still a long way to go before these connections are properly established. Yet, such efforts seem to be the only possibility to bring some structure and clarity in the discussion of MBL, which is currently heavily influenced by misunderstandings and incoherent pictures of the phenomenon. In the following, we summarise our discussion of MBL.

6.6 SUMMARY: MANY-BODY LOCALISATION

In this chapter, we discussed one-dimensional many-body localisation (MBL). Based on Anderson's results for non-interacting electrons, we looked at the case when interactions are included in such a localising system. Since electrons naturally are interacting in any realistic solid-state system, the analysis of the effects of the interactions is paramount for the validity of Anderson's results as an explanation for the break-down of conductance due to random impurities.

Despite decades of interest, great progress on this question was only achieved in the last years and it is an immensely active field to date. This leads to a very multifaceted picture of MBL, which we thoroughly reviewed. Moreover, we presented two successful applications of advanced mathematical tools to link different dynamic and static features of MBL. Based on those connections and similar effort performed in the last two years, we made an attempt to present a unified picture of MBL. Given the current state of research, this was necessarily of a speculative nature. Following the intuition gained in this thesis, we nevertheless presented a possible definition of MBL that can experimentally be checked and argued why it could still be connected to various other localisation properties. While time will show whether this is truly the correct way to capture MBL, we are confident that efforts like this will be needed to move forward in this field. This concludes the first part of this thesis, which we summarise in the following.

7

SUMMARY: EQUILIBRATION & LOCALISATION

In the first part of the thesis, we investigated large spin systems and their emerging complex behaviour. Once pushed out of equilibrium, despite this complex nature, the systems have the tendency to locally relax to an equilibrium value. This *equilibration* can be investigated in two important settings. In the first, free systems provide realistic time scales and can be directly connected to physical intuition, such as spreading of particles. By using transport of the free Hamiltonian, as well as Lieb-Robinson bounds, we demonstrated that such equilibration results can also be generalised to correlated initial states, by proving dynamical Gaussification. A complementary approach is provided by directly looking at the eigenstates and energies of the Hamiltonian. Here, based solely on the assumption of non-degenerate energy gaps, equilibration can be derived.

Building on this, we looked at *thermalisation*, i.e. local expectation values that can be rigorously captured in terms of thermal ensembles. We presented different approaches to thermalisation, interpolating between making assumptions on the eigenstates of the Hamiltonian and on the initial state of the system. While these results to some extent explain the immense success of thermodynamics in describing large-scale quantum many-body systems, they surely do not fully cover the characterisation of static ensembles. In fact, many models can be constructed that show a memory of the precise initial conditions, thus requiring a description in terms of generalised Gibbs ensembles.

Localising systems were originally developed to capture the transport behaviour of electrons in the presence of random impurities. They, however, are also a clear class of models where thermalisation has to fail. Naturally, *localisation* is being explored from many different angles and constitutes an important subfield of the study of condensed matter systems, where it predicts a complete breakdown of conductivity, in contrast to the predictions of the Drude model. Such behaviour is rigorously understood in the absence of interactions, where it can be captured using Anderson localisation, characterised by local random potentials leading to localisation of single electrons in both a dynamic and static fashion. As soon as interactions are included, however, the physical model is substantially more complex.

The resulting *many-body localisation* (MBL), has been investigated with great effort in recent years. Still, a complete picture of the phenomenon has not been achieved. This is largely due to the fact that different localisation properties naturally appearing in non-interacting Anderson insulators are no longer all present in the interacting case. The key example in this direction is the unbounded growth of entanglement, despite static features that are still localised. In this thesis, we presented rigorous mathematical efforts that provided links between static and dynamic features of MBL. We provided a mathematical proof that these systems can be used to send information, based only on a non-degenerate spectrum and the existence of an approximately local constant of motion. We further looked at the structure of individual eigenstates and were able to generalise the exponential clustering theorem to excited states in the context of MBL. With such links, we performed significant steps towards unifying the different pictures and presenting a comprehensive definition of MBL, in the hope to also make the phenomenon more accessible in experiments.

In our discussion of MBL, we saw that random local potentials are capable of strongly changing the behaviour of all eigenstates of a model. This can be seen as an "infinite temperature" *quantum phase transition*, characterised by all eigenstates changing due to a parameter change in the Hamiltonian. In the next chapters, we will encounter the paradigmatic case usually considered as a quantum phase transition, namely where the ground state changes dramatically when an external parameter is moved over a critical point.

Interestingly, these transitions are to a certain extent universal, in that the ground state behaviour around the critical point can be characterised with remarkably few parameters, which are the critical exponents of the model. As in the case of MBL, particular focus will be put on understanding the dynamical features of such a transition. For MBL, the eigenstate localisation resulted in strongly suppressed transport and could thus be dynamically probed. For ground state transitions, the key question will be whether the universality in the static properties can also be probed dynamically. As quantum phase transitions are one of the hardest and most interesting problems in the field of quantum many-body systems, a joint analytical, numerical and experimental effort will be needed to capture their behaviour. This will follow the emerging idea and mindset of a dynamical quantum simulation, which will be the essential tool in the second part of this thesis.

Part II

Dynamical quantum simulations

8

ULTRA-COLD BOSONS AS A DYNAMICAL QUANTUM SIMULATOR

Numerically simulating quantum many-body systems out of equilibrium is, in general, a very challenging task. Yet, given the limited settings which can be completely solved analytically, especially in the presence of interactions, such numerical approaches are often invaluable to understand the dynamics of interacting quantum systems. As described earlier, tensor network tools are extremely useful for this task [41, 191]. In 1D, these work well, as long as spatial entanglement entropies are small [98, 103]. For localising systems, this means that often very long time evolution can be efficiently simulated [151, 152]. For generic models, however, time evolution quickly builds up entanglement and dynamical tensor network simulations are thus limited to small times [41]. Moreover, tensor network tools do not nearly work as well in higher dimensions [191]. Thus, there are many important and long-standing problems in the study of out of equilibrium behaviour of quantum many-body systems whose investigation is greatly hindered by insufficient means to describe and explore the corresponding dynamics numerically.

Quantum simulators provide an exciting possibility to overcome these limitations and promise to achieve a comprehensive understanding of the dynamical behaviour of large scale interacting atomic systems. The idea for such devices emerged in a seminal article by Feynman [192], in which he proposes to use an experimental quantum mechanical setup to artificially engineer and control the behaviour of another quantum system. In this way, rather than enforcing quantum mechanical laws onto a classical computer, one directly use one quantum system to simulate another [192, 193]. This innovative idea has since inspired many collaborations between theoretical and experimental physicists with already very promising results [1, 2, 32, 34, 37, 62, 194–197]. Using novel experimental tools, models of solid state systems, for example using optical lattices, can by now be tuned and probed in the laboratory. Interestingly, while the dynamics are qualitatively similar, due to the vastly different lattice spacing, which is in the 100 pm regime in a usual solid state [9, 62], but in the 100 nm regime in an optical lattice, the corresponding time scales are dramatically different. This makes it possible to resolve the expansion of single electrons on experimentally accessible time scales and thus allows to probe solid state behaviour at the level of individual particles [29, 32, 62, 194]. Based on these exciting efforts, important questions raised on the previous pages have already been tackled, such as the issue of equilibration time scales [32].

While this success is certainly promising, quantum simulators as computational devices are by no means fully understood. One of the most exciting questions relates to the certification of quantum simulators. After all, given that the simulator indeed solved a problem that cannot be accessed using classical means, it is unclear what steps can be performed to gain trust in the result of the simulation [194, 195]. Moreover, given the huge dimension of the Hilbert spaces describing many interacting atoms, it is not at all trivial to retrieve the result of the simulation.

In the remainder of this thesis, we investigate quantum simulators and highlight their potential and current limitations. In this chapter, we explore the basic principle and describe the main steps of a dynamical quantum simulation. We then introduce optical lattices as one of the most promising platforms for such simulations. Following an introductory discussion of quantum phase transitions in chapter 9, we present a study of the dynamics of quantum phase transitions using a quantum simulator in chapter 10. With this, we thus further investigate the relation of static and dynamic properties of Hamiltonians that also played a prominent role in earlier parts of this thesis. Afterwards, motivated by the questions how the results of a quantum simulator can be extracted, we present a successful application of quantum field

tomography for ultra-cold atoms in a continuous setup. We begin with the general underlying principle of a quantum simulator.

8.1 CONCEPT OF A QUANTUM SIMULATION

Quantum simulators are devices that are capable of reproducing the behaviour of a specific model Hamiltonian to a high accuracy without noise or loss processes contributing significantly. Moreover, they are built in such a way that certain non-trivial initial states can be prepared, some degree of control over the Hamiltonian parameters is given and at least partial information of the behaviour of this state can be extracted.

Quantum simulators come in two distinct different variants: digital and analogue simulators. *Digital quantum simulators* are conceptually close to the idea of a quantum computer. The desired Hamiltonian evolution or state preparation is broken down into small unitary gates and these gates are then applied consecutively [196]. In contrast to a full quantum computer, the gate set of a digital quantum simulator is not necessarily universal, but still allows for non-trivial calculations. These devices have several important advantages. Since the evolution is discretised, the unitary gates can be tested for their accuracy individually and error correction procedures can be performed [197]. Moreover, using the unitary gates, initial states can be prepared with great control and the results of the simulation are easily accessible. Unfortunately such devices also have a crucial downside: they are exceedingly hard to build experimentally.

While ion-chain architectures already allow for the application of contrived unitary gate sets [37], these systems still have a long way to go before they will be able to truly outperform classical computers. More promising in this respect is the idea of an *analogue quantum simulation*. Such a device does not build on the possibility of applying almost arbitrary unitary gates, but rather accepts that the system itself has a certain interaction structure and evolves according to its own Hamiltonian. Here one fully embraces the quantum system as is and builds on its intrinsic complexity. Using advanced experimental tools, one tries to maximise the control over the system and develop procedures of preparing interesting initial states and measuring as many features of the state as possible. While this approach is of course limited in its capabilities, at least compared to a full quantum computer, such analogue simulations already provided enlightening insights into the physics of many-body systems that could not have been obtained using numerical descriptions on a classical computer [1, 32, 35, 195].

For the scientific field considered in this thesis, the most important kind of such an analogue quantum simulator is one that is capable of simulating out of equilibrium dynamics. Such a dynamical simulation typically consists of four steps. First, a suitable *initial state* is prepared. Since the experimental tools for preparation are typically limited, one often picks ground states or thermal states of a certain model. Following breath-taking progress in recent years, however, this paradigm is slowly shifting as even influencing the initial state at the level of individual lattices sites has become possible [63].

The second step of the simulation is the *tuning of the Hamiltonian* over a certain path in time. Most important are quenches, where the Hamiltonian is changed abruptly, but also slow changes along a ramp are an important setting, for example allowing for the investigation of the dynamics of a *quantum phase transition* that we will perform in chapter 10 [1, 27, 198]. More recently also periodic driving was used extensively, as it allows for the simulation of topological order [54, 55].

The next step is to extract the result of the simulation. This so-called *read-out* is highly non-trivial, since a naive tomographic reconstruction of the state is impossible for the desired system sizes [199]. Instead, one usually focuses on extracting key properties, such as local expectation values or entanglement features, which is the approach we will take in chapter 10. A more advanced way is to use efficient tomographic tools, which are based on certain natural classes of states [18]. For example, assuming that the final

state is close to being pure, in the sense that it has low rank, one can perform *compressed sensing*. In this setting, surprisingly few random measurements are already sufficient to characterise the state to great accuracy [200, 201]. A different way is given by *tensor network tomography*, which assumes that the result of the simulation is a state that can efficiently be represented in terms of a tensor network. Then, the corresponding state can be reconstructed using only linearly many measurement settings [202, 203]. What is more, once the tensor network state is obtained, it can be used to predict other measurements, thus building trust in the correctness of the state [2]. We will discuss this prospect in detail in chapter 11, where we present a generalisation of such schemes to quantum fields and employ them to study interacting ultra-cold atoms in a continuous setup. There, we will also see how such tensor network tomography of dynamical quantum simulations is related to entanglement growth and how it connects to issues of equilibration, thermalisation and Lieb-Robinson bounds.

Finally, the last step of a quantum simulation is the *certification* [204]. To have a concrete example in mind, let us consider the following experimental work, which is widely considered one of the most promising applications of a quantum simulator to date [32], namely the investigation of the equilibration time scale problem described in detail in section 3.4. To review the setting, we start with an initial state of one particle on every second site of 1D chain. The Hamiltonian is such that the atoms are allowed to move freely, which leads to an equilibration of the initial particle number imbalance between even and odd lattice sites. The extracted result of the quantum simulator is a simple number, namely the occupation of odd lattice sites. This is performed for different evolution times, allowing to directly access equilibration time scales experimentally. The result of the simulator thus is a simple one parameter curve, namely $\langle n_{\text{odd}}(t)\rangle$.

Despite the simplicity of the question, its numerical investigation is exceedingly hard. As discussed above, using tensor network methods, which are by far the best way to address the problem, the biggest issue is the growth of entanglement over time, which requires a linear increase of the bond dimension. Thus, the simulation requires larger and larger resources for longer time and even on large scale supercomputers necessarily stops to be reliable at some point [32]. Thus, the dynamical quantum simulator in this instance really answers a question that cannot be addressed classically [32]. This however, brings us back to the issue of certification. Given this concrete and rather simple result of a quantum simulator, which could even be summarised in terms of a single equilibration time, how can we be sure that it is correct? While this is of course a common question in any physical experiment, it becomes absolutely crucial in the context of quantum simulators, since it is no longer possible to compare the outcome to any classical simulation.

In order to approach the issue of certification, typically a very pragmatic approach is taken, meaning one simply certifies the simulation in a certain regime that is still classically accessible. In the example mentioned above [32], this was done by simulating the evolution for short times, which is still traceable using standard tensor network tools. Since the quantum simulator produces correct results for short times, one has gained trust also in the results for longer times. A different approach is taken in the investigation of a dynamical quantum phase transition [1], to be presented in chapter 10. There, the problem can be simulated in 1D, again using tensor network tools or exact diagonalisation. Again, in this case the quantum simulation can be certified, building trust in it functioning correctly. For 2D and 3D settings, the quantum simulator can then be used to obtain results out of reach for classical computation. This certification in easy regimes is a practical way of approaching the problem. Strictly speaking, however, there is of course no promise that the quantum simulator still works correctly when the difficult part of the simulation is carried out. Here, it is also important to keep in mind that usually large amounts of experimental data are needed to provide sufficiently accurate results. This directly relates to the problem of sampling from probability distributions; an issue controversially discussed in so-called boson sampling

[80–82]. There it turns out that suitable quantum mechanical measurement at the end are needed for a certification with a realistic effort [205].

In conclusion, the question of how to certify a dynamical quantum simulator is still to a large extent open. One often cited possibility is that the quantities one is typically interested in are robust. The intuition behind it is that phenomena like equilibration are so generic that slight imperfections in the experiment do not have important influence. Up to now, this and related approaches are very preliminary. Thus, how to certify quantum simulations outside of the classical regime is certainly one of the most exciting research question in the study of these machines and one can surely be curious how this fundamental issue will be addressed in the near future.

There are several promising experimental platforms for the realisation of quantum simulations. All of them have seen breath-taking progress in recent years [1–3, 32, 34, 37, 62, 195–197]. Ion chains give full control on the level of individual constituents, allow for a tuning of the Hamiltonian and its interaction structure and even full tomography is possible for these systems [36, 37, 196, 197]. Their main limitation is the system size currently reached, which is typically limited to ten to twenty ions in a 1D alignment. Also super-conducting qubits, photonic chips and several more have demonstrated great potential. That being said, we will fully restrict our investigation to ultra-cold atoms in optical potentials. While they do not provide the same tunability and measurement capabilities as ions, they already make it possible to simulate large scale quantum systems with several thousand atoms in 1D, 2D or 3D. Thus, these platforms were used to already obtain results that are out of reach for state of the art classical simulations on modern computers [1, 32, 34, 195].

In the following, we look at the experimental principle underlying the capturing and controlling of ultra-cold atomic systems. We stick to a high-level overview guided mostly by the intention to outline the basic principles, capabilities and limitations relevant for theorists dealing with these systems.

8.2 ULTRA-COLD ATOMS

In this section, we look at the basics of the capturing of atoms [62, 206]. We will focus on the case of trapping them in an optical lattice. The case of a continuous setup relies on different trapping procedures and will be discussed from a theory point of view in chapter 11.

The first step is to heat a certain material such that the contained atoms, for example Pottasium, are evaporated and enter a vacuum chamber. After an initial step of standard cooling procedures, the charge neutral atoms are trapped in a harmonic electromagnetic trap. Afterwards, the atoms are cooled down sufficiently close to absolute zero, which usually means into the nano-Kelvin regime. This is done by supplementing standard cooling procedures with laser cooling and finally evaporative cooling as soon as the atoms are trapped. This last step, where only the cold fraction of the atoms is retained, is only possible for bosons, as it would lead to a drastic particle loss for fermions, which cannot have a macroscopic occupation of the ground state. Thus, evaporative cooling for fermions is often done by adding a bosonic species and perform the cooling on them. Still, cooling fermions is substantially harder, which ultimately is the reason that often certain tools are first developed for bosonic systems.

Once the atoms are cold enough, standing laser waves can be used to create an optical lattice with the desired geometry. They range from standard cubic arrangements to more exotic ones, for example honey-comb lattices. Due to energy minimisation, the atoms start to assemble at the knots of the standing laser-waves, thus creating a lattice geometry. In the case of cubic geometries, the lattice spacing is given by half the wave-length of the used lasers. Using two lasers with a wave length that differs by a factor 2, also superlattices can be implemented. This, for example, allows to achieve initial configurations with

atoms only on every second site, which was, for example, used to investigate equilibration time scales as discussed previously [32].

In the following, we look at the emerging Hamiltonian. In order to simplify the presentation, we do not touch upon fermionic systems, which is a vastly interesting research field in its own right [30, 207, 208], but rather only focus on bosons. There, we argue that a Bose-Hubbard model emerges, which captures the behaviour of the atoms in the lattice to excellent accuracy. Finally, available measurements are discussed, which then concludes the necessary preparation of ultra-cold atoms as a quantum simulation platform that we need for the investigation of the dynamics of quantum phase transitions presented in chapter 10.

8.2.1 *Optical lattices*

The optical lattice should be seen as a sinus-shape standing wave created by a reflected laser beam [27, 62, 206]. To excellent approximation, the particles in the optical lattices interact with each other in the form of a delta contact potential with strength g_0. The corresponding Hamiltonian is thus given by

$$H = \int dx\, \Psi^\dagger(x) \left(\frac{p^2}{2m} + \sin(kx) + V_{\text{trap}}(x) \right) \Psi(x) + g_0 \int dx\, \Psi^\dagger(x)\Psi^\dagger(x)\Psi(x)\Psi(x) \,,$$

where $\Psi(x)$ denotes the second quantised field annihilation operator. For the following discussion, we neglect the trapping potential $V_{\text{trap}}(x)$ and discuss its effects separately later on. If the system is large enough, it can be well approximated by a translationally invariant, periodic system and the corresponding eigenstates of this continuous Hilbert space are the Bloch waves. The physics that is experimentally tested is normally contained within the lowest Bloch band. The eigenvectors in this band can be recombined into the most localised orbitals possible, which are known as Wannier functions. These are localised on the knots of the standing laser wave and have strongly decaying tails away from their center. These functions can be well approximated by a Gaussian

$$w(x) = \frac{1}{(\pi a_{ax}^2)^{1/4}} e^{-\frac{x^2}{2a_{ax}^2}} \,,$$

where $a_{ax} = \sqrt{\hbar/(m\omega_{ax})}$ is the confinement in the axial direction, which in turn is given by

$$\omega_{ax} = \frac{2E_R}{\hbar}\sqrt{V_0} \,,$$

with V_0 being the laser intensity along the corresponding axis and E_R the recoil energy [62]. These localised Wannier orbitals can be used as the basis for a second quantisation of the Hamiltonian model in terms of creation and annihilation operators corresponding to those orbitals [9]. Starting from this, one can rewrite the model as the canonical Bose-Hubbard Hamiltonian [206]

$$H = -J \sum_{\langle j,k \rangle} b_j^\dagger b_k + \frac{U}{2} \sum_j b_j^\dagger b_j^\dagger b_j b_j \,,$$

where $\langle j, k\rangle$ denotes the summation over nearest neighbour sites and $b, b^\dagger$ denote bosonic annihilation and creation operators. Here the nearest neighbour structure is an approximation and relies on the fact that the localised Wannier orbitals have tails that decay so quickly that atoms separated more than one lattice spacing do not interact anymore. The parameters U and J are, as usual in second quantisation, given by overlap integrals between the Wannier orbitals

$$J = \int dx\, w(x - x_j) \left(-\frac{d^2}{dx^2} + V_0 E_R \sin^2(kx) \right) w(x - x_{j+1}) \,,$$
$$U = g_0 \int dx\, |w(x)|^4 \,.$$

For calculating the hopping, one has to look at the coupling of the Hamiltonian between nearest neighbour sites. As it turns out, for this the actual Wannier functions should be taken into account, as the Gaussian approximation leads to rather crude results. Numerically fitting the Wannier functions and evaluating the overlap integrals yields [209]

$$J = \alpha V^{\beta} e^{-\gamma\sqrt{V}} E_R \ ,$$

where V is the laser intensity given in energy recoil $E_R = \hbar^2 k^2/2m$ units, and $\alpha = 1.39666$, $\beta = 1.051$ and $\gamma = 2.12104$. Thus, the hopping can be well controlled by modulating the intensity V of the laser that creates the standing wave. Using that the laser beams of different spatial dimensions in a cubic geometry can be controlled individually, the hopping strength in the different directions can be controlled separately. Choosing the laser intensity very strong in one or two spatial dimensions thus allows to make the system, which intrinsically is three-dimensional, effectively two or one dimensional.

In order to approach the interaction term, we have to look closer at the atomic interaction. Its delta potential comes with a prefactor

$$g_0 = \frac{2\hbar^2 a_s}{m a_\perp^2} \ ,$$

where a_s is the three dimensional s-wave scattering length, m is the mass of the atom, and $a_\perp = \sqrt{\hbar/(m\omega_\perp)}$ is the confinement length in the perpendicular dimension. Performing the interaction integral (8.2.1), the strength of the interaction U becomes

$$U = \frac{g_0}{\sqrt{2\pi}} \frac{1}{a_{ax}} = \sqrt{\frac{2}{\pi}} a_s k\hbar\omega_\perp (V_0)^{1/4} \ .$$

Thus the parameter U also depends on the lattice depth V_{lat}, but in a much weaker fashion then the hopping J. In order to control U and to obtain a second degree of freedom in these models, experimentalists use a Feshbach resonance [210]. By tuning a homogeneous external magnetic field, the scattering length a_s of the atoms can be influenced, thus effectively controlling the parameter U. This resonance allows for the tuning of the interaction in a wide range (see Fig. 8.1). By combining the control given by the Feshbach resonance with the tunability of the intensity of the standing laser wave, almost any path in the Hamiltonian parameter space spanned by U and J can be implemented. In particular, sudden quenches of the hopping strength are possible, but also slow ramps that increase the hopping continuously over time.

The speed of most relevant dynamic in the Bose-Hubbard model is given by the hopping strength. For example, it is the hopping that controls the spread of information and the speed of quasi-particles is crucially determined by it. For that reason, many experimentalist prefer to work in a rescaled time, that takes the hopping strength into account. These are called integrated tunneling events and are defined as

$$\tau_{tunnel} = \int_0^t dt \ \frac{J(V(t))}{\hbar} \ .$$

A good example to see that this is indeed a natural language to talk about the Bose-Hubbard dynamics, is the fact that the experimentally observed Lieb-Robinson cone in the setting of initially having one particle per site is simply $v = 6$ in this rescaled time units [31].

In addition to the optical lattice, the experiment needs an electro-magnetic trap to keep the bosons confined in a small spatial region [62]. Typically, this trap is harmonic, with the corresponding Hamiltonian term being

$$H_{trap} = \sum_j w^2 x_j^2 n_j \ .$$

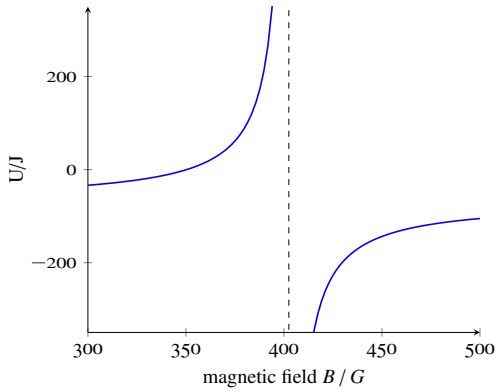

Figure 8.1: *We thank Ulrich Schneider for useful discussions on this.* The plots show the influence of the external magnetic field on the Bose-Hubbard parameter U/J for Potassium-39, for 1D chains with a lattice depth $V = 19E_R$ along the chain and a transversal lattice depth of $V = 30E_R$, where E_R denotes the recoil energy [62]. The Feshbach resonance is located at $B = 402.50$ G.

This trap keeps the atoms confined in its center. Due to ever-increasing control in the manipulation of ultra-cold atoms in optical lattices, by now also other trapping potential such as boxes can be implemented [63], but harmonic traps are still widely used.

Using the above mentioned trap, the shape of the atomic cloud can be altered almost at will. In particular, it is easily possible to create ellipsoidal shapes, where one radius is very small [62]. In this way, the cloud can be made almost 2D. Using newer techniques, the cloud of atoms can also be pressed against a mirror, until it truly consists only of a single 2D layer [63]. As mentioned earlier, however, even 3D clouds can be decoupled by simply tuning up the corresponding laser intensities, until hopping is strongly suppressed. Thus decoupled 2D or 1D arrangements can be implemented [62].

Having reviewed the basics of ultra-cold bosons in an optical lattice, we now move towards different measurement techniques that allow to characterise the experimental state.

8.3 AVAILABLE MEASUREMENTS

Optical lattices allow for the trapping and manipulation of several thousand atoms. On this scale, performing tomography, so actually reconstructing the quantum state, is a more than challenging task. Therefore, the usual approach is to extract few characteristic properties of the experimental states. We will move beyond this paradigm when discussing quantum field tomography in chapter 11. In the following, we present key imaging techniques in optical lattices that measure important properties of the state and thus serve as read-out techniques for the dynamical quantum simulator.

8.3.1 *Time of flight*

A crucially important way of measuring the properties of the atomic state in an optical lattice is given by time of flight (ToF) imaging. [211, 212] The goal is to explore the correlation structure of the atoms and measure the phase correlators

$$\langle b_\mu^\dagger b_\nu \rangle = \mathrm{Tr}\left(\rho b_\mu^\dagger b_\nu\right) \ .$$

For this, the optical lattice and the trap are completely turned off and the particles start to expand freely. In this process, the originally localised Wannier functions begin to overlap and create an interference pattern

akin to a double-slit experiment. After a certain expansion time, a picture of the atomic cloud is taken. Given that the density of the gas reduces quickly, the interactions between atoms are negligible and the expansion process is governed by a free field Hamiltonian. Moving to a Fourier basis, expanding the time evolution of the field operators and employing a stationary phase argument, one can derive the following formula for the final density of atoms [211, 212]

$$\langle \Psi^\dagger(r,t)\Psi(r,t)\rangle = |\hat{w}_0(k)|^2 \sum_{\mu,\nu} e^{ik(r_\mu - r_\nu) - i\frac{m(r_\mu^2 + r_\nu^2)}{2\hbar t}} \langle b_\mu^\dagger b_\nu\rangle \ ,$$

where r denotes the position in the experimentally measured density distribution, $k = \frac{mr}{\hbar t}$ and $\hat{w}$ denotes the Fourier transform of the localised Wannier functions on the lattice [62]. Note that it is usually argued that the second term in the exponential should be small enough to be ignored, but this only works well for long expansion time [212].

Following the above formula, it is clear that the ToF image indeed contains some information on the phase correlators. This allows for the distinction between the two phases of the Bose-Hubbard model to be discussed in detail in chapter 9. The extreme cases for those systems are a product state for the infinitely deep Mott insulator, as well as a perfectly coherent state for the non-interacting superfluid. In the case of long evolution times, where the exponential in the time of flight expression is simplified to a Fourier transform, this gives rise to particularly simple ToF images. For the Mott product state, the correlator is a delta peak, which means that ToF image, which is the Fourier transform, would give a flat profile, modulated by the Gaussian envelope $|\hat{w}_0(k)|^2$. In contrast the perfect superfluid in 2D and 3D has no dependence on distance and the resulting ToF is thus extremely peaked. [27, 62]. Therefore such ToF measurements are ideally suited to distinguish the two different phases of the Bose-Hubbard model. In chapter 10, we demonstrate that this intuition can also be turned into an extraction of the correlation length of the atomic cloud. Note that also first proposal exist that employ the ToF information to access the entanglement in optical lattices [189, 190, 213], taking the particle number conservation into account [214]. These, however, still have a long way to go before allowing for an efficient entanglement measurement under experimentally realistic conditions, which is one of the motivations for the tomographic procedure we present in chapter 11. We now turn to another important measurement, namely an in situ resolution of the atomic positions.

8.3.2 *In situ*

An exciting new prospect is the possibility to resolve the atomic positions on the level of individual sites [63, 215, 216]. Using novel experimental tools, this single-site imaging allows to take a picture of all the lattices sites showing the distribution of atoms. The procedure is as follows. First the lattice is ramped up, such that the Wannier functions become very localised and hopping between sites is strongly suppressed. Then, a laser beam is focused on the atoms and the scattered light collected in a microscope. During this procedure, the atoms are heavily laser-cooled, allowing to scatter many thousand photons of each atom, thus giving a very high resolution. Typically, the used laser light is of similar wave length as the optical lattice, which is still sufficient to clearly distinguish different lattice sites [63, 215, 216]. The scattered light allows for pairs of atoms to form molecules, which leave the optical lattice very quickly. Thus, only the parity of the local atom number can be resolved and an even number of atoms looks like the vacuum. Experimentally, this means that usually settings are considered where the local particle number is small and the distinction of odd and even parity yields important information. Using this technique, particle number fluctuations can be resolved to great accuracy and this tool has already delivered breath-taking images [63, 215, 216].

Importantly, in an optical lattice, all of the above imaging procedures are single-shot images. Averaging over many realisations thus gives the expectation value of the measured operators, but the images contain significantly more information. In particular, fluctuations around the mean value can easily be extracted [217–219]. This technique has, for example, been used successfully to extract density-density fluctuations. For completeness, let it be mentioned that also other tools, like band mapping, which gives certain momentum information of the atoms, have provided important insight [28, 62, 220].

This concludes our discussion of different measurement techniques that are available to extract information from states in optical lattices.

8.4 SUMMARY: ULTRA-COLD BOSONS AS A DYNAMICAL QUANTUM SIMULATOR

In the following, building on and extending the above introduction, we very briefly summarise the capabilities of ultra-cold bosons in optical lattices as a platform for performing analogue dynamical quantum simulations. For this, the key features are the class of initial states that can be prepared, the Hamiltonian time evolutions that can be implemented and finally the information that can be extracted using measurements.

Initial states: The optical lattice gives several techniques to influence the initial state. Naturally thermal states of the Bose-Hubbard Hamiltonian can be prepared. Due to very effective cooling mechanisms, very low temperature states can be realised, which essentially behave like the ground state [27, 62]. In addition, there are two tools that have been used very successfully for the manipulation of the initial state. Firstly, one can superimpose two laser beams with a wavelength that differs by a factor two. Such a superlattice allows for creating an imbalance of particle numbers between odd and even lattice sites. In this way, the initial state with particles only on every second lattice site can be prepared that we already encountered in the context of equilibration earlier (see chapter 3) [76, 221]. Secondly, the newly developed microscopes can be used to influence the states at the level of individual sites [63]. With this, it is in fact possible to create arbitrary binary configurations of particle numbers on a 2D layout. For this, a 2D layout with one particle on every site is constructed. Using a laser focused on individual lattice sites, it is then possible to flip the spin configuration of individual atoms, which can be used to remove them from the optical lattice in a second step.

Hamiltonian: The natural Hamiltonian of bosons in an optical lattice is the Bose-Hubbard Hamiltonian. Tuning the lattice depth and using magnetic fields, the interaction and hopping strength can be tuned at will. In addition, usually harmonic traps are used, even though this is no longer necessary. Superimposing of different lattices gives further control over the Hamiltonian. One of the most exciting applications for this is to use two lattice beams with incommensurate wave length. With this, quasi-periodic lattices can be constructed. This technique has recently been used to observe an instance of particle localisation in optical lattices [76]. The possibility to address single sites of the lattice also greatly increases the ability to tune the Hamiltonian. In particular, almost arbitrary local potentials can be applied to the optical lattice [62]. This also achieves a fully random potential, which would allow to further look at localisation effects and systematically tune the disorder strength. Aside from single site addressing, also tilts of the lattice, created by an inhomogeneous magnetic field have successfully been implemented [60]. Interestingly, this enables to create effective spin models with spinless ultra-cold atoms, where the number of atoms on a site takes the role of the spin.

Read-out: Finally optical lattices provide several important read-out techniques, allowing to extract the result of the analogue quantum simulation. Firstly, the parity of particles on all sites can be measured. Using time of flight techniques also phase correlators can be obtained. By systematically exploiting the fact that all measurements are single-shot, also higher order correlators are directly accessible.

This concludes our discussion of ultra-cold bosons in an optical lattice as an architecture for dynamical analogue quantum simulation. In the next chapter, we introduce quantum phase transitions. Based on this introductory discussion, we present an application of a quantum simulator in the paradigmatic setting of dynamically crossing the Mott-superfluid transition (see chapter 10).

9

DYNAMICS OF QUANTUM PHASE TRANSITIONS

Quantum phase transitions are one of the most intriguing phenomena connecting to quantum many-body physics. Similar to classical phase transitions, they are characterised by a drastic change in the system's behaviour when an external parameter is altered. In classical thermodynamics, the transition is driven by thermal fluctuations and, for example, the system can cross from a low-temperature ferromagnetic phase into a paramagnetic one, when the temperature moves over the Curie point.

In order to observe *classical phases*, large systems necessarily have to be considered. In fact, for a rigorous mathematical definition, infinite systems are needed. Thus, phase transitions are a true many-body phenomenon and a priori, one would expect that their description is highly complex. While this is certainly correct, many aspects of classical phase transitions can be captured exceedingly well with strikingly *simple scaling laws*. Based on renormalisation group theory, critical exponents can be calculated, which separate phase transitions into universality classes. For each of those classes, many important characteristic features of the system around the phase transition can be captured by simple power-law scalings with those critical exponents.

In *quantum phase transitions* the system's behaviour again changes dramatically upon varying an external parameter. In stark contrast to classical phase transitions, this is even possible for zero temperature, as the transition is driven by quantum fluctuations. In this way, one often looks at the ground state of a system and, for example in the case of the transverse field Ising model, also finds a crossing between ferromagnetic and paramagnetic behaviour, but now as a phenomenon of ground states and the low-energy physics connected to it. Similar to the case of classical phase transitions, the static properties of quantum phase transitions is relatively well understood by now, with experiments successfully capturing it in a wide range of settings [27, 37, 195, 208]. Again it turns out that their statics can, with great accuracy, be captured in terms of simple scaling laws, despite their intrinsic complexity [19].

As such, the characterisation of quantum phases, a priori, only refers to the behaviour of the instantaneous ground states and is accompanied by the closing of the spectral gap above it. This usually implies that it is no longer possible to follow the ground state adiabatically and raises the fundamental question how well a quantum phase can be prepared in an experiment. After all, any experimental preparation procedure will take place in finite time and thus certainly will not prepare perfect ground states. This is especially true for critical models, where the ground state is characterised by a diverging correlation length. In order to prepare such a phase, these long-range correlations have to be established, which naturally connects to Lieb-Robinson bounds and poses several intriguing problems in the study of the evolutions of local Hamiltonians.

Still, one would expect that quantum phase transitions can be observed under experimentally realistic conditions. This directly poses the question: What is the dynamical signature of a quantum phase transition? Moreover, it clearly relates to the general theme of this thesis how static and dynamic features of Hamiltonian models are connected. Here, ground states pose a perfect arena to further study this connection, in particular because they can be probed experimentally and have extensively been studied analytically and numerically.

An interesting point is also that, strictly speaking, phase transitions are necessarily connected to infinite systems. Naturally, many signatures of the occurrence of the phase transition should still be present for a finite system and be thus experimentally testable. Here dynamical probes might be ideally suited. After

all, as captured by Lieb-Robinson bounds, any finite time evolution of local observables is necessarily supported on a finite subsystem. Thus, assuming that one succeeds in finding a clear dynamical signature, dynamical experimental probes would constitute an excellent way to demonstrate the onset of the transition in a finite system.

For the connection of static and dynamic features of quantum phase transitions, Kibble and Zurek provided a valuable intuitive explanation, which was originally developed for the case of classical transitions [222–224]. Guided by the adiabatic theorem and the description of the static physics in terms of critical exponents, they provide an argument why and in which form dynamical crossings of quantum phase transitions can also be captured in terms of simple scaling laws. While the Kibble-Zurek mechanism has proven successful in some experimental settings [225–229], its general applicability and even rigorous formulation is a largely open problem. In particular, it is still completely open to what extent it applies to physically testable settings, with experimentally realistic time scales and truly interacting models. It is precisely this fundamental problem of exploring the dynamical signatures of quantum phase transitions in interacting models that will motivate and guide us for the following chapters. We begin by reviewing the essential physics of quantum phase transitions and look at important models with such a transition.

9.1 DEFINING QUANTUM PHASE TRANSITIONS

To define a quantum phase transition, we need to look at the energy difference between the ground state and the first excited state. As discussed in chapter 3.2, a Hamiltonian is called gapped, if this energy difference can be uniformly bounded from below, independent of the system size and the largest possible lower bound is called the spectral gap. The physics of the ground state is closely connected to the spectral gap above it. For example, the exponential clustering theorem (see Thm. 4 in chapter 3.2) states that locality and a spectral gap imply that the ground state correlations are exponentially decaying with a correlation length that is finite and independent of the system size. Usually the converse is also true, namely that models where the spectral gap vanishes as the system size is increased indeed have ground states with a diverging correlation length. These models are called critical.

A quantum phase transition is characterised by the drastic change in the behaviour of the ground state of the model when an external parameter is altered. In order to formulate the phenomenon, it is thus necessary to talk about some family of Hamiltonians $H(g)$, where g is an external parameter , such as a magnetic field, or the laser intensity of an optical lattice. For simplicity, we assume that the dependence on g is linear and taken from an interval $[0, 1]$, which covers most interesting cases

$$H(g) = H_0 + gV \,.$$

Strictly speaking, for each fixed value of g, we will considers Hamiltonians on varying system sizes L. As this system size dependence is always needed, for example to define the spectral gap, we will suppress it in the notation. We further always assume that these Hamiltonians are local, with a locality structure that is independent of the parameter g and the system size L. For example, the Hamiltonian is always nearest-neighbour, for any value of g.

For the Hamiltonian family $H(g)$, we look at the family of ground states $|E_0(g)\rangle$ and a continuous function $\gamma(g)$ describing the spectral gap between the ground state and the first excited state for different values of g. We will use the following definition.

Definition 15. *(Gapped family of Hamiltonians) A family of Hamiltonians* $H(g)$ *is called gapped, if the spectral gap* $\gamma(g)$ *is uniformly lower-bounded independent of* g

$$\exists\, \gamma_0 > 0 : \gamma(g) \geqslant \gamma_0 \quad \forall g \in [0, 1] \,.$$

As long as the spectral gap exists, independent of the system size, then it is clear that the ground state has to be an analytic function of g [15, 20], which excludes the possibility to drastically change at a single parameter value g_0. In particular, as long as the spectral gap remains open, the system cannot change its long-range correlation structure or its scaling for the entanglement entropy (see section 3.5.1). This leads to the following definition of a quantum phase.

Definition 16. *(Quantum phases) Given two states $|\psi_0\rangle$ and $|\psi_1\rangle$ that are ground states of local Hamiltonians H_0 and H_1 respectively, then they are said to be in the same phase, if there exists a path in Hamiltonian space $H(g)$, $g \in [0,1]$ such that $H_0 = H(0)$, $H_1 = H(1)$ and the family of Hamiltonians is gapped.*

Correspondingly, two quantum states are in different phases if no such path in Hamiltonian space can be found. Thus, quantum phase transitions are necessarily connected to a closing of the spectral gap. This can either happen at a single point, which is called a critical point g_0 or for an extended interval, which is known as a critical phase.

The above definition is clearly a static statement about how the ground state changes when an external parameter is varied. As such, it is a priori decoupled from the dynamical behaviour of the system. Yet, following the intuition provided by classical phase transitions, like the melting of ice, it should obviously be possible to probe them in a dynamic fashion. Again, this juxtaposition of dynamical and static features poses an intriguing problem and is the motivation for our study of the dynamics of quantum phase transitions. Before we move to those dynamical aspects, we will first review their static characterisation in more detail. We begin by looking at important models that show such a quantum phase transition.

9.2 PARADIGMATIC MODELS

In the following, we review paradigmatic quantum mechanical models with a quantum phase transitions. We begin with the transverse field Ising model, which has a single critical point separating a ferromagnetic and a paramagnetic phase. It has the clear advantage of being solvable using a Jordan-Wigner transform (see section 5.2.1). The same is true for the XX model, which has a critical phase, instead of just a single critical point. Such models allow for important insights, but at the same time, are not complex enough to uncover the full structure of quantum phase transitions in general.

In contrast, the Bose-Hubbard model, whose phase transition we explore afterwards, is characterised by a full critical phase and shows considerably richer behaviour. This comes at the price of not being exactly solvable, which gave rise to the development of a large collections of effective models describing different aspects of it and ultimately is the reason why a quantum simulator is so useful in exploring the rich physics of its phase transitions, where all the effective models break down.

9.2.1 *Transverse field Ising model*

The first paradigmatic model that we investigate is the transverse field Ising model [19]

$$H_{Is} = -\sum_{\langle j,k\rangle} \sigma_j^x \sigma_k^x - B \sum_j \sigma_j^z \,,$$

where we take $B > 0$ without loss of generality [19] and use periodic boundary conditions. This Hamiltonian can be transformed into a free fermionic Hamiltonian, using a Jordan-Wigner transformation (see section 5.2.1). Applying a mode transformation to this fermionic system, the free Hamiltonian can then be solved. It can be separated into two sectors, corresponding to odd and even parity of fermions, which is

necessary to cope with respectively anti-periodic and periodic boundary conditions [154, 230]. Omitting a global energy shift, the even parity part takes the form [230]

$$H_{Is,even} = \sum_k \lambda_k \left(\tilde{f}_k^\dagger \tilde{f}_k\right) ,$$
$$\lambda_k = 2\sqrt{\left(B - \cos\left(\frac{2\pi}{L}k\right)\right)^2 + \sin^2\left(\frac{2\pi}{L}k\right)} ,$$

where $\tilde{f}$ is some function of B and the usual fermionic operators f. Since it is the only part of the system that is important for the dynamical questions later on, we restrict the discussion to this even particle sector. The above Hamiltonian has only one eigenmode that can become gapless, namely the one corresponding to $k = 0$. Its excitation energy is zero precisely if $B = 1$. Thus, the model has a single critical point at $B = 1$, which separates two phases. For $B > 1$, the external magnetic field is dominant and the spins are aligned with it. For $B < 1$, the spin-spin interaction dominates the physics and the model becomes ferromagnetic.

The transverse field Ising model was extensively study in the context of the dynamics of quantum phase transitions, numerically [225, 231] as well as experimentally [228, 229]. There, one usually focuses on a key property that separates the two phases. In this Ising model, one commonly works with the so-called number of kinks, defined as

$$\frac{1}{2}\sum_j (1 - \sigma_j^z \sigma_{j+1}^z) .$$

This quantity measures how many spins are not parallely aligned and is a useful measure to quantify the number of defects in the paramagnetic phase.

Another exactly solvable model that we already encountered earlier is the XX-model (see chapter 5). It is again exactly solvable and the eigenmode energy with smallest absolute value is the spectral gap of the XX-model. For infinite systems, the eigenmode energies become a continuous cosine function, which leads to a gapless phase for a whole range of parameters g. The same is true for the Bose-Hubbard model. In stark contrast, however, the model is no longer analytically solvable and the origin of the gapless phase is substantially less clear than the presence of gapless modes described above. It thus provides a more realistic model of a quantum phase transition in an complex interacting quantum system.

9.2.2 *Bose-Hubbard*

The Bose-Hubbard model can be thought of as the easiest instance of a model showcasing a conducting-insulating transition due to interactions [9, 10]. It is given by the Hamiltonian

$$H_{BH} = -J \sum_{\langle j,k\rangle} b_j^\dagger b_k + \frac{U}{2}\sum_j b_j^\dagger b_j^\dagger b_j b_j ,$$

where b and $b^\dagger$ are the bosonic annihilation and creation operators. For non-zero hopping, it is convenient to choose a different parametrisation

$$H_{BH} = J\left(-\sum_{\langle j,k\rangle} b_j^\dagger b_k + \frac{U}{2J}\sum_j b_j^\dagger b_j^\dagger b_j b_j\right) ,$$

where J now can be seen as the relevant time scale and U/J captures the phase transition of the model.

We now discuss the different phases of the model. In contrast to the usual approach of statistical thermodynamics, we will not work with a chemical potential, but rather with a fixed particle number

$N = \bar{n}L$, where $\bar{n}$ is the filling fraction. The underlying reason for this decision is that in optical lattice experiments, tuning the chemical potential is not possible, but it is much more natural to think of a fixed number of atoms in the optical trap. In order to observe a phase transition, we will assume that $\bar{n}$ is an integer, meaning that system size and particle number are commensurate. Otherwise, only the superfluid phase would remain.

For very large U, the on-site interaction is the dominant term. The system is then in a *Mott insulator* phase, which carries his name as Mott was the first to characterise the suppressed conductance due to interactions [10]. As creating a particle hole excitation is energetically suppressed by a spectral gap, the phase is insulating with a conductivity that scales like $e^{-\beta\gamma}$, where γ is the energy of the particle-hole excitation and β is the inverse temperature [232]. Therefore, in contrast to localisation where randomness suppresses electronic transport completely often even independent of temperature (see chapter 6), it is thermally activated in this Mott phase. As the phase is gapped, the correlations in the ground state decay exponentially.

The opposite limit is that of zero interactions $U = 0$, which leads to a free bosonic Hamiltonian consisting only of hopping. The corresponding system can be solved with a Fourier transform, with the lowest energy eigenmode corresponding to the Fourier mode with $k = 0$. Since the system is bosonic, all states occupy the ground state which is thus given by

$$|\psi_{SF}\rangle = \left(\frac{1}{\sqrt{L}}\sum_j b_j^\dagger\right)^N |\emptyset\rangle \ ,$$

where $|\emptyset\rangle$ denotes the vacuum and N the number of particles in the system. This phase is usually called the *superfluid phase*. Using a Bogoliubov approximation, which relies on a macroscopic occupation of the ground state, one can in fact show that the model does not have a viscosity for low velocities in this parameter regime and is thus superfluid [233]. It is characterised by strong local particle fluctuations and, for the case of an infinite lattice, the local density approaches that of a coherent state [62]. Its phase correlations are true long-range in the 2D and 3D case and the phase correlator approaches the filling fraction at large distances $\lim_{r\to\infty}\langle b_0^\dagger b_r\rangle = \bar{n}$ [62]. In contrast, in 1D, the phase correlation in the ground state decays algebraically $\langle b_0^\dagger b_r\rangle \propto r^{-K}$ [234]. This can be seen by using a Luttinger liquid theory, which accurately describes the low-energy sector of the Bose-Hubbard model [62, 234]. Thus, one usually says that the model has true long range order in 2D and 3D and quasi long range order in 1D.

The phase transition between the two quantum phases of the ground state strongly depends on the dimension. In 3D it can be reliable found using mean-field techniques [235, 236]. In 2D, usually Monte-Carlo is applied [237], while the 1D case can best be investigated using tensor network tools [234]. The critical values are $(U/J)_c \approx 3.3$ [1D], 16.74 [2D], 29.36 [3D] [62, 237, 238]. In 1D, the error bars are rather large, since the transition happens at a very fine tip, which is hard to locate precisely numerically.

As already touched upon above, the Bose-Hubbard model has two limits which are easy to understand. For $U = 0$, the model becomes a free bosonic Hamiltonian, which can be solved using a Fourier transform. The other limit is the case where $U \gg J$. There, the interactions dominate, which allows to introduce effective fermionic models. Since, in 1D, it is more powerful then the often employed hard-core boson approximation, we present the *doublon-holon model*.

Doublon-Holon

The doublon-holon model provides an effective description of the 1D Bose-Hubbard model in the case of strong interaction $U \gg J$. It assumes a background state of a Fock state with fixed particle number $\bar{n}$ on every site [120]. For simplicity, and since it is the only setting we encounter later in the experiment presented, we restrict to the case of a fixed filling $\bar{n} = 1$. In this case, the Hilbert space is truncated to

allow at most two particles on each site. This effectively turns the bosonic model into a spin system. In this model, two kinds of excitations are introduced: Doublons, which correspond to two particles on a site and holons, which are the lack of a particle. Using a double Jordan-Wigner transformation, which takes both species into account (see section 5.2.1 for basics of Jordan-Wigner), yields fermionic operators d and h fulfilling the usual fermionic anti-commutation relations of a two species fermionic model. In this approximation, the Bose-Hubbard Hamiltonian takes the following form [120]

$$H = -J\sum_{m=0}^{L-1}\left(2d_m^\dagger d_{m+1} + h_m^\dagger h_{m+1} + \text{h. c.}\right) + \sqrt{2}J\sum_{m=0}^{L-1}\left(d_m h_{m+1} + h_m d_{m+1} + \text{h. c.}\right) + U\sum_{m=0}^{L-1}\left(d_m^\dagger d_m\right),$$

where h. c. denotes the hermitian conjugate. In this equation, already a projection term was dropped, which eliminates the possibility of having a doublon and a holon on the same site. Naturally, this should be impossible. Since this is energetically strongly suppressed, it is possible to drop the restriction and work with so-called unconstrained fermions. One should, however, be careful here and check that the condition $\langle d_m^\dagger d_m h_m^\dagger h_m\rangle \simeq 0$ is fulfilled. In practice, this seems to work well for $(U/J) > 8$, below which the doublon-holon model breaks down [31, 120].

Moving to Fourier transformed operators $\tilde{d}$ and $\tilde{h}$ is a first step in solving the model, which yields

$$H = \sum_{k=0}^{L-1} H_k = \sum_{k=0}^{L-1}\left[\epsilon_d(k) d_k^\dagger d_k + \epsilon_h(k) h_k^\dagger h_k \;+ i\sigma(k)(h_{-k}^\dagger d_k^\dagger + d_{-k} h_k)\right],$$

where

$$\epsilon_h(k) = -2J\cos\left(\frac{2\pi}{L}k\right), \quad \epsilon_d(k) = 2\epsilon_h + U, \quad \sigma(k) = 2\sqrt{2}J\sin\left(\frac{2\pi}{L}k\right).$$

The above Hamiltonian, which is simply a free fermionic system, can of course be solved exactly by decoupling it into its eigenmodes using a mode transformation (see section 3.4.1). Here it is important to note that the Hamiltonian above does not conserve the fermionic particle number, which implies that the corresponding vacuum is not an eigenstate of the model.

Further, since the model is fermionic, it is straightforward to calculate the speed of information propagation. Since the correlations can only be established by the travelling of doublons and holons, the relevant speed of the model is given by their relative speed, which is given by [31]

$$v = \max_k \left|v_{\gamma_{h,-k}} - v_{\gamma_{d,k}}\right| = 6J - \frac{32}{3}\frac{J^3}{U^2} + O\left(\frac{J^4}{U^3}\right).$$

It is interesting to see how this compares to the Lieb-Robinson estimate (see appendix B), which is linear in the norm of the local Hamiltonians terms and turns out to be $v_{LR} \approx 44J$. Thus, the Lieb-Robinson estimate is an order of magnitude larger, but reproduces the correct linear scaling in J.

Using the doublon-holon model, also phase correlations functions of the type $\langle b_k^\dagger b_j\rangle$ can be calculated using Wick's theorem, as long as the state is Gaussian in the doublon-holon picture (see section 3.4.2). Due to the fact that two fermionic species are involved, the corresponding matrices become, however, quite involved [1, 120].

Naturally aside from the two approaches presented above, there are many other settings in which the Bose-Hubbard model can be approximately solved and many important techniques have been developed over the years [239]. We forego an introduction of them in order to keep our presentation as simple as possible. This concludes our introduction of paradigmatic models with a quantum phase transition. We now turn to a very general characterisation of such transitions in terms of critical exponents.

9.3 CRITICAL EXPONENTS

One of the most important features of classical phase transitions is that the behaviour close to the phase transitions is to some extent universal. Rather than having to include all microscopic details of a model, many important features around the phase transition scale algebraically with the distance to the transition, where the corresponding exponents are obtained from the universality class the phase transition belongs to [21].

It is one of the most important insights in the study of quantum phase transitions that such a scaling analysis can also be performed [19]. Using renormalisation group theory, again critical exponents can be derived which capture the ground state behaviour close to the transition. For us, two scaling laws are important: that of the spectral gap and of the correlation length in the ground state. We restrict the discussion of such a scaling analysis to the special case of a second order transition, which means that the discontinuity of the ground state energy appears only in the second derivative [21]. For concreteness, we focus on the Bose-Hubbard model, even though the Ising model and the XX chain can be described with a similar scaling analysis. For it, we use the parameter $g = U/J$ for the Bose-Hubbard model. For $g \leqslant g_c$, the system is in superfluid phase, which is gapless. Away from the phase transition, at which the spectral gap has to close, the gap is found to scale algebraically in 2D and 3D

$$\gamma \propto (g - g_c)^{\nu z} .$$

As long as the model is gapped, we know that the correlation length in the ground state has to decay exponentially (see Thm. 4 in chapter 3.2). The corresponding correlation length is also found to scale algebraically, with

$$\xi \propto (g - g_c)^{-\nu} ,$$

the exponent ν is called the correlation length critical exponent and is the same as the ν in the scaling of the gap. The other exponent z in the above scaling is called the dynamical exponent. This originates in the Lagragian renormalisation theory, where space is rescaled with some length scale factor and the exponent z describes the corresponding rescaling of time.

In the case of the Bose-Hubbard model, the above scaling analysis works well in the case of two or three dimensions. The universality class of the Bose-Hubbard model in d dimensions is that of a $d+1$ dimensional XY model [239]. The dynamical exponent is thus $z = 1$ independent of the dimensions [239, 240], while the correlation length critical exponents are [232, 241]

$$\begin{array}{cc} & \nu \\ d = 2 & 0.672 , \\ d = 3 & 1/2 , \end{array}$$

for the $\bar{n} = 1$ Mott lobe. The 1D transition of the Bose-Hubbard model does not obey the usual algebraic scaling, but rather is of Berezinsky–Kosterlitz–Thouless (BKT) type [19, 238]. This means that the gap around the critical point does not close algebraically, but rather in an exponential fashion [239]

$$\gamma \propto e^{-(g-g_c)^{1/2}} .$$

The relation between correlation length and gap is still linear, meaning that

$$\xi \propto 1/\gamma ,$$

as in the 2D and 3D Bose-Hubbard model. It is worth noting that the above scaling behaviour naturally only works in a small region around the critical point. To estimate the size of this region is usually a hard task, as it depends on the microscopic details of the model [19].

Having introduced the bare necessities for the description of the static descriptions of quantum phase transitions, we now move to the investigation of their dynamics. In particular, we investigate what happens when we start in the ground state of the gapped phase and move across the quantum phase transition. The motivation for this is three-fold. Firstly, we believe that the dynamics of quantum phase transitions is an interesting research question in its own right, as it is clearly a fundamental building block in our understanding of these transitions. Secondly, by Lieb-Robinson type arguments, it is clear that dynamical processes are intrinsically local. One could thus hope that dynamical signatures are more easily experimentally accessible then static properties and allow for probing quantum phase transitions in finite systems in the laboratory. Finally, the dynamics of such a transition are directly relating to the speed at which correlations propagate, are a intriguing setting to explore the non-equilibrium dynamics of a quantum many-body system and relate to the fundamental question how well gapless phases can be prepared in finite time. We begin our discussion with the mathematical basis of slow Hamiltonian deformations in the presence of a gap, namely the adiabatic theorem.

9.4 ADIABATIC THEOREM

In this section, we present the *adiabatic theorem*. For this, we assume that the Hamiltonian is slowly varied along some path of gapped Hamiltonians from $g = 0$ to $g = 1$, with the state initially being in a ground state of the Hamiltonian $|\psi(t = 0)\rangle = |E_0(g = 0)\rangle$. In order to simplify the presentation, and since it is the only setting we encounter for the rest of this thesis, we restrict to a unique ground state. Note that due to the fact that the spectral gap remains open, it is sufficient to demand uniqueness of the ground state for any value of g within the interval $[0, 1]$, since perturbation theory excludes the possibility of the ground state degeneracy changing without the closing of a gap [20].

The adiabatic theorem is a statement how well the evolution of the time-evolved state is contained within the ground state manifold. In order to state it, we first introduce a parametrisation of the Hamiltonian path that depends on a total time τ

$$H(t) = H(g = t/\tau),\ t \in [0, \tau] .$$

Here always the same path from $g = 0$ to $g = 1$ is taken, but the total time τ in which this happens is varied. Adiabatic theorems are now a statement how well an evolution starting in the ground state is contained in the ground state manifold as a function of the gap and the time scale τ.

There is a multitude of such theorems, some of which do not even require a spectral gap [22, 242–245]. We present the easiest setting, which still provides an explicit scaling, rather than just an asymptotic statement [243]. As throughout this thesis, we work on a finite system, such that issues connected to unbounded operators are safely avoided.

Theorem 14. *(Adiabatic theorem: Simplest version) Let* $H(g) = H_0 + gV$ *be a gapped family of Hamiltonians with ground states* $|E_g\rangle$ *and uniform gap* γ_0 *and* $H(t/\tau)$ *a time parametrisation of the path* $g = 0$ *to* $g = 1$ *in time* τ*. Then the time evolved state at parameter value* g, $U_\tau(g)\left|E_{g=0}\right\rangle$*, has a fidelity with the instantaneous ground state* $|E_g\rangle$ *that can be bounded as*

$$|\langle E_g| U_\tau(g) \left|E_{g=0}\right\rangle|^2 \geqslant 1 - \left(\frac{2}{\tau}\frac{\|V\|}{\gamma_0^2} + \frac{7g}{\tau}\frac{\|V\|^2}{\gamma_0^3}\right)^2 .$$

As all adiabatic theorems, the above is a statement how well the evolution is contained in the ground state manifold. In leading order in the inverse gap, it scales like $1 - \left(\|V\|/(\tau\gamma_0^2)\right)^2$. The first insight is that, as long as the spectral gap is non-zero, then it is possible to choose τ large enough, meaning the evolution

slow enough, such that the ground state manifold is not left. Another important aspect of the above bound is the scaling in the operator norm $\|V\|$. In the typical setting, V is a globally supported operator, for example a magnetic field on every site. There, the adiabatic theorem needs a time scale τ that grows linearly with the system size to compensate the linear growth of $\|V\|$. This is to be expected, because the fidelity used in the adiabatic theorem is a very fragile error measure. In particular, for product states that are not perfectly aligned on every site, the fidelity decays exponentially in the system size. Presumably, one could formulate less stringent adiabatic theorems, which only look at local distinguishability between the time evolved state and the ground state and correspondingly find a scaling of τ that is independent of the system size.

An important ingredient in such a local adiabatic theorem, but also an investigation that is highly interesting in its own right, is how the ground state $|E_g\rangle$ changes as a function of the parameter g. Since the ground state degeneracy cannot change as long as the spectral gap remains open [20], it is clear that there is some unitary connecting the ground state at different values of g

$$|E_g\rangle = U(g)\,|E_0\rangle \ .$$

Moreover, since there is a spectral gap, the exponential clustering theorem (see Thm. 4 in chapter 3.2) can be applied and the ground states have exponential clustering correlations for all values of g. For 1D, this directly implies an area-law for the entanglement entropy for the family of ground states (see Thm. 8 in chapter 3.2). In higher dimensions, however, the following is, a priori, not clear: If we start in a ground state with an area-law and slowly change the parameter g, will the state at later times, which is close to the instantaneous ground state, also fulfil an area-law? Moreover, if the state can initially efficiently be represented as a tensor network, how will the bond dimension grow?

Motivated by these questions, as well as the investigation of the stability of topological order [116, 117], the above unitary was investigated in recent years, in particular with respect to its locality. It has become known as *quasi-adiabatic continuation* or *spectral flow* [114, 116]. Without going into the details, it turns out that the unitary $U(g)$ has a locality structure, in the sense that Lieb-Robinson bounds in the parameter g can be derived [114]. Thus, if g is only slightly changed, then the ground state changes only locally and its long-range correlations are only slightly changed. From this, one can directly derive that ground states of a gapped family of Hamiltonians fulfil an area-law for all g, if they fulfil it for any value of g within the relevant interval [115]. Note that while an area-law is not sufficient for an efficient tensor network representation in higher dimensions [103], the growth of the bond dimension is still bounded, due to the explicitly local form of the unitary [114, 246]. In the following, we look into the dynamics of quantum phase transitions and encounter the *Kibble Zurek mechanism* that relies on the adiabatic theorem and provides valuable intuition for the crossing of quantum critical points.

9.5 KIBBLE-ZUREK MECHANISM

The Kibble-Zurek mechanism provides a strikingly simple guideline for the behaviour of a dynamical ramp over a quantum phase transition. It was originally developed for thermal transitions, where is was experimentally tested [226–229]. It was later generalised to quantum phase transitions, which is the context in which we encounter it now.

We start in a ground state of a gapped phase and slowly change the Hamiltonian parameter g across a quantum phase transition. The goal is to keep track of the evolution and in particular to understand the behaviour of the ground state at the end of it. As it is our key interest, we will focus the discussion on the Bose-Hubbard model, where we move from the gapped Mott insulator phase into the gapless superfluid. In this case, the relevant parameter separating the two phases is the correlation length, which is the reason why we put particular focus on the behaviour of this correlation length in the state after the ramp.

The basic logic of the Kibble-Zurek mechanism (KZM) is as follows [222, 224, 240, 247]. While we are in the gapped phase, we can use the adiabatic theorem and thus know that the system stays in the ground state manifold (see section 9.4), as long as the parameter g is changed slowly enough. When approaching the phase transition, the spectral gap necessarily closes and the adiabatic theorem is no longer applicable, which usually indeed implies that the ground state manifold is left. The subsequent dynamics is exceedingly complicated, involves excited states and the full complexity of the interacting system emerges. At this point, predicting the dynamics from an analytical point of view seems exceedingly hard.

As a first approximation, one could assume that the dynamics is mostly local, leading to a correlation length that is effectively frozen. Such an assumption, which is usually called the adiabatic-frozen approximation, can then be used to predict the correlation length at the end of the ramp. More precisely, we perform the quench in some time τ and try to predict how the final correlation length ξ scales with this ramp time. For simplicity, we assume that g is a linear function of time

$$g(t) = -\frac{t}{\tau} ,$$

and shift g_c such that the phase transition occurs at $g = 0$. The goal is to find the scaling of the crossover time, between the adiabatic and frozen region, which we denote by t_{crs}. This is done by obtaining an estimate for the breakdown of the adiabatic approximation. Here, the KZM does not rely on the precise scaling in the adiabatic theorem (see Thm. 14), but rather argues as follows. Adiabaticity should be determined by the gap and how it compares to the rate of change measured by $\partial_t g/g$ of the Hamiltonian. The crossing between adiabatic and frozen regime should take place when these two quantities are comparable

$$\gamma(g(t_{crs})) = \frac{\partial_t g|_{t_{crs}}}{g(t_{crs})} .$$

From the critical exponents, we know that the gap, close to the phase transition, scales like $\gamma \propto g^{\nu z}$. Inserting this in the above equation yields

$$t_{crs} \propto \tau^{\frac{\nu z}{1+\nu z}} ,$$

which is the KZM prediction for the crossing point [240, 248]. Following the adiabatic-frozen approximation, this result directly tells us how the correlation length at the critical point should scale depending on the quench rate τ

$$\xi_{final} \propto g^{\nu}(t_{crs}) = \tau^{\frac{\nu}{1+\nu z}} .$$

This is the Kibble-Zurek scaling for the correlation length when moving over the phase transition.

Such a scaling analysis was performed for many different quantum phase transitions. In simple models, such as single qubits [249] and the Ising chain [225, 230] it has worked well and the scaling of the final state was correctly predicted. For us, this is reason enough to look at bit closer at the mechanism. In particular, it seems unclear to what extent the adiabatic-frozen approximation should be taken as an actual description of the dynamics.

A direct investigation of the adiabatic-frozen approximation is, to our knowledge, missing almost completely from the literature. This could be, at least partially, be due to the fact that it is by no means straightforward to turn the above intuition of adiabatic and frozen regimes into a testable prediction that the participating physicists would agree on. In order to gain some intuition, let us look at the evolution of the adiabaticity and the correlation length in the Bose-Hubbard model when moving from the Mott-insulating to the superfluid phase [1]. The numerics follow the experimental study to be presented in chapter 10 and the details of how the Hamiltonian is precisely varied is postponed until then. For now, let

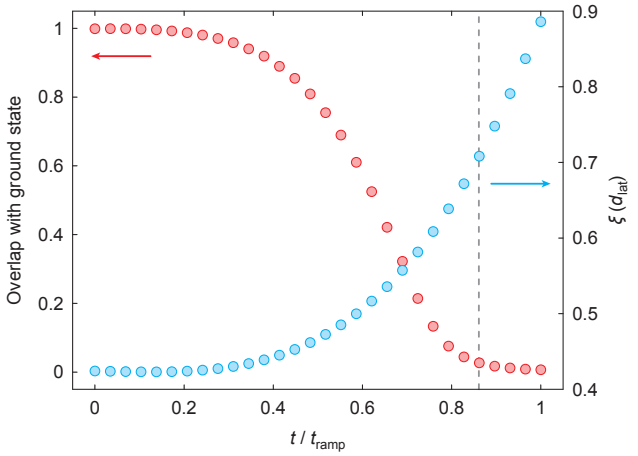

Figure 9.1: *Taken from Ref. [1].* Evolution of adiabaticity and correlation length for a ramp in the Bose-Hubbard model across the quantum phase transition, moving from Mott to superfluid. The precise ramp schedule is discussed in chapter 10. Red dots represent the overlap with the instantaneous ground state. Blue dots display a change of the coherence length ξ. The vertical dashed line indicates the phase transition. We observe that initially the evolution is very adiabatic, while across the phase transition, adiabaticity breaks down and drastic change at the phase transition occurs.

us simply observe that Fig. 9.1 does indeed show an initial regime that is almost adiabatic. This should come as no surprise, as this part of the approximation is backed up by the adiabatic theorem. When, however, looking at the dynamics of the correlation length, no frozen regime seems visible. In particular, the correlation length seems to change most dramatically precisely at the phase transition.

We confirmed that such a behaviour of drastic change at the phase transition takes place for many different ramp schedules and seems to also be fulfilled in the Ising chain (see Fig. 9.2), where the final scaling predicted by KZM is correct [225]. This clearly means that, while the KZM can lead to correct predictions of the final scaling, it should not be taken as an actual approximation of the out of equilibrium dynamics.

For completeness, let it be noted that the above derivation is by no means the only possibility to arrive at the Kibble-Zurek scaling. For example, one approach directly studies the Schroedinger equation and looks at the possibility to do a series of approximations, eventually leading to a direct *scaling collapse* of the dynamics [250–252]. This approach has the advantage of giving a correct description of the approximate dynamics. Its applicability, so far, however seems to be limited to conceptually simple models, like the Ising chain [251] or a mean-field system [250].

A different approach, which in principle can be applied to any system, is *adiabatic perturbation theory* [49, 198, 253]. Here, the ideal evolution is taken to be the adiabatic evolution following the ground state and a perturbation analysis around this is performed. This again can reproduce the KZM scaling. In contrast to the above adiabatic-frozen approximation, it is mathematically rigorous, but relies on extensive knowledge of the behaviour of the low-energy sector. Moreover, since it is a perturbation analysis around the infinitely slow limit, it raises one fundamental question, namely how slow the evolution has to be, for the KZM scaling to occur.

This is just one of many important questions that remain unsolved in the study of the dynamics of quantum phase transitions. In particular, what are the precise conditions for universality to set in? What role do interactions of the model play? How slow does the ramp need to be and does its precise shape matter? What is the role of the system size? Does the complexity of the underlying model matter and is universality maybe only present for integrable systems?

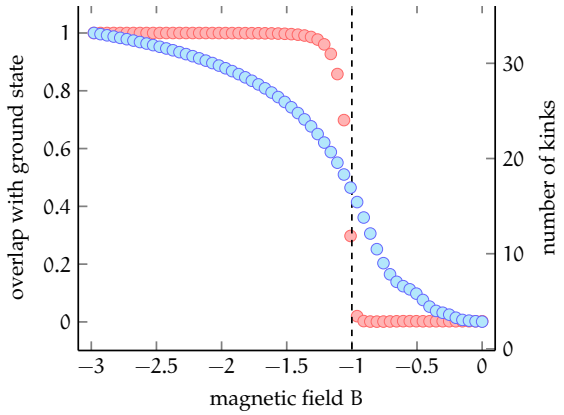

Figure 9.2: We consider a linear ramp from $B = -5$ to $B = 0$ in the Ising model with periodic boundary conditions on $L = 80$ spins on a time scale $\tau = 100$ in the natural units. Displayed is the evolution during this ramp as a function of B. Red dots represent the overlap with the instantaneous ground state. Blue dots display the number of kinks defined as $\frac{1}{2}\sum_j (1 - \sigma_j^z \sigma_{j+1}^z)$, which can be seen as an indicator for the two phases and is the quantity usually considered in KZM scalings in this model [225, 240]. We see that adiabaticity indeed breaks down close to the phase transition at $B = -1$, while the number of kinks show a non-trivial evolution during the full ramp.

While the KZM is certainly an important step and a valuable intuitive tool, it is far from being a complete answer to the above questions. Especially in the setting of realistic experimental systems, that are of limited size and where the dynamics happens on a reasonable time scale, the above questions seem entirely open. Given that analytical tools are limited and their applicability is often questionable, this leaves numerical and experimental studies of the phenomena. Naturally, the dynamics of quantum phase transitions belongs to the most challenging numerical problems in the context of quantum many-body systems. Not only does it refer to time-dependent behaviour, but also the phase transitions needs to be crossed, for which many approximation schemes are known to fail.

9.6 SUMMARY: DYNAMICS OF QUANTUM PHASE TRANSITIONS

In this chapter, we described that ground states of quantum systems are in the same phase, if a gapped path of Hamiltonians can be found that connects them. Thus, a quantum phase transition is necessarily connected to the closing of the spectral gap. By looking at three paradigmatic models, we gained intuition how such transitions can occur. We focussed on the Bose-Hubbard model, which is interacting and thus provides a realistic model of some progresses in solid-state physics. Using critical exponents, the static properties of the model close to the transition can still be well understood and the crucial properties of the ground state can be captured using power-law scaling. Having captured the equilibrium properties of such quantum phase transitions, we looked into their dynamical behaviour. Based on the adiabatic theorem, we encountered the Kibble-Zurek mechanism, which suggests a way to capture the results of dynamical crossing a quantum phase transition in terms of power-laws, similar to the static properties of the systems.

In the following, we aim at understanding those dynamical transitions across quantum phase transitions in more depth. We present a recent study that approaches this issue in the Bose-Hubbard model, which due to its interacting nature, is an exceedingly complicated task. We will therefore rely on the application of a dynamical quantum simulator, which will allow us to uncover complex behaviour that cannot be captured using any known theoretical description.

10

DYNAMICALLY PROBING THE MOTT-SUPERFLUID TRANSITION

The following chapter is based on Ref. [1]. We sincerely thank Simon Braun, Sean S. Hodgman, Michael Schreiber, Jens P. Ronzheimer, Arnau Riera, Marco del Rey, Immanuel Bloch, Jens Eisert, and Ulrich Schneider for the successful collaboration.

Quantum phase transitions are among the most intriguing phenomena connected to the study of interacting quantum many-body systems in and out of equilibrium. Despite their intrinsic complexity, their static properties are often well captured in terms of strikingly simple scaling laws (see chapter 9). While this static description is relatively well understood by now, it is still largely unknown to what extent there also is a dynamical signature of the transition. Exploring this question is surely an interesting endeavour in itself, but also directly relates to the fundamental question how quantum phases can be prepared and measured in experiments.

This issue has so far mostly been approached in free models, which allow for an in-depth investigation and shed light on the complexity of dynamic quantum phase transitions. Following a *sudden quench* in these models, the evolution is well-captured in terms of spreading quasi-particles which move with a ballistic speed, upper bounded by Lieb-Robinson bounds (see appendix B). In contrast, in the context of quantum phase transitions, the Hamiltonian has to be altered slowly. This leads to an ongoing change of the notion of quasi-particles, meaning that they are continuously created and deformed while they spread through the system.

For slow ramps in *interacting models*, the Kibble-Zurek mechanism provides some guideline on what to expect when moving from a gapped phase into criticality (see section 9.5) . Its precise conditions and applicability to experimentally realistic settings is, however, still heavily debated. Given the great difficulty in approaching these questions analytically, numerical studies have proven to be an indispensable tool to simulate the involved processes. Due to the lack of effective models properly capturing the phase transition of interacting systems, these investigations are, however, limited in scope. Thus, despite great effort, it is still largely open how quantum many-body systems dynamically change phases in strongly correlated models.

In this chapter, we present a recent joint effort of theory and experiment to investigate this problem in the paradigmatic setting of the Bose-Hubbard model. These experiments capture, for the first time in such a setting, the dynamics of an essentially homogeneous quantum system entering a critical phase. In contrast, earlier work focussed on the inhomogeneous transition dominated by mass transport [254] or looked at the transition from the gapless into the gapped phase [215]. In the work presented here [1], we find intriguing behaviour outside of the Kibble-Zurek mechanism, thus demonstrating the intricate dynamical behaviour of dynamical quantum phase transitions into a gapless phase.

We begin by reviewing the experimental setting and explain in detail how the relevant parameters are extracted from the experimental data. We show that the experimentally obtained dynamics in 1D exactly fit various numerical simulations, thus certifying the quantum simulation in one spatial dimension. We then proceed to use the quantum simulator in higher dimensions, where numerical tools are absent and the simulator takes the center stage in capturing the relevant physics of the dynamical crossing of a quantum phase transition.

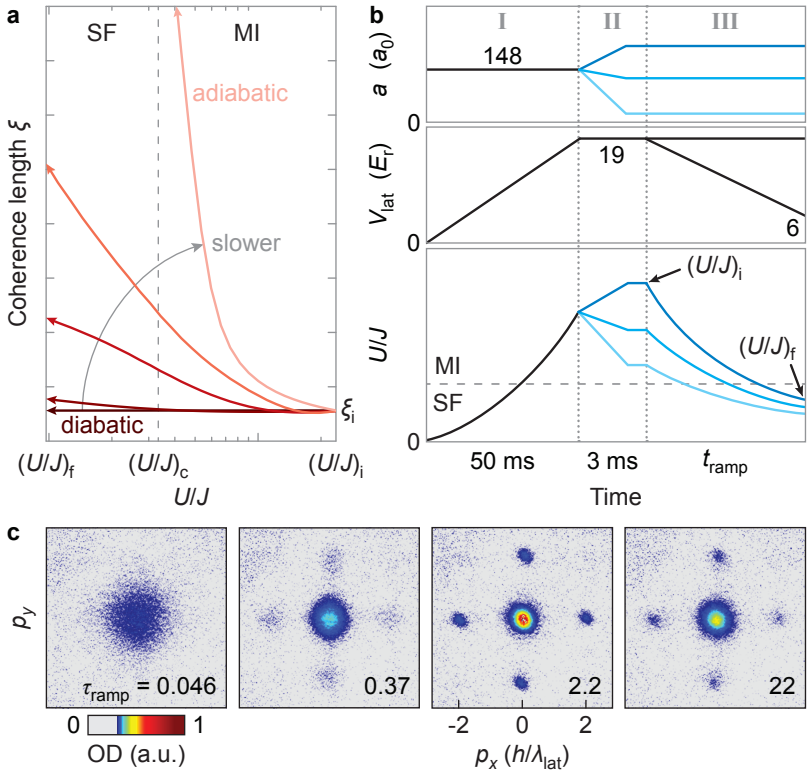

Figure 10.1: *Taken from Ref. [1].* **a** Shown is the evolution of the phase correlation length ξ during the ramp from large U/J (on the right) to small U/J (on the left). For fast ramps, it changes little from its small original value in the Mott phase. For slower evolutions eventually approaching the adiabatic limit, it necessarily has to diverge at the phase transition. **b** This plot shows the experimental ramp protocol in terms of the scattering length a (see section 8.2.1), the lattice depth V_{lat} and the resulting Hamiltonian parameter U/J. In the first part of the ramp (I), the lattice is ramped up to prepare the initial Mott insulator state at fixed scattering length a. During the second step, the initial value $(U/J)_i$ is tuned using a Feshbach resonance which alters the scattering length at fixed lattice depth (see chapter 8). Finally, the lattice is ramped down again, thus crossing the Mott-superfluid transition indicated by the gray line in the U/J plot. **c** These images are the obtained time of flight (ToF) pictures after different evolution times τ_{ramp}. Shown is the optical density in arbitrary units corresponding to the distribution of atoms in a 2D image of positions p_x, p_y measured in inverse units of the laser wave length $\lambda_{lat} = 2d_{lat}$. As is clearly visible, they change from the broad ToF profile of a Mott insulator to the peaked profile expected in the superfluid phase with longer evolution time.

10.1 CROSSING THE PHASE TRANSITION

Our study begins by loading ^{39}K atoms into a 3D optical lattice with lattice depth V_{lat} at $U/J > 250$, which gives a 3D Mott insulator state with almost exactly one atom per site [1]. Starting in this gapped phase, the system is slowly ramped into the superfluid. The two phases of the Bose-Hubbard model are characterised by the behaviour of the phase correlators $\langle b_j^\dagger b_k \rangle$ (see section 9.2.2). Due to the fact that the Mott insulator phase is gapped, all correlations have to decay exponentially, which gives

$$|\langle b_j^\dagger b_k \rangle| = |\langle b_j^\dagger b_k \rangle - \langle b_j^\dagger \rangle \langle b_k \rangle| \leqslant e^{-d(j,k)/\xi} ,$$

where we used that the state has a fixed particle number and thus $\langle b_k^\dagger \rangle, \langle b_j \rangle = 0$ and where $d(\cdot,\cdot)$ denotes the lattice distance between the positions. In contrast, the superfluid phase has long range order. Thus, any correlation length, which is defined in terms of an exponential fit, has to diverge in this phase.

In this way, the correlation length constitutes the ideal quantity to observe the dynamics of crossing the Mott-superfluid phase transition and most important features of the transition are connected to this key quantity. Thus, in the following, we focus on the fundamental question at what rate and by what mechanism the phase correlations are established. For this, it is crucial to make the correlation length experimentally accessible, which constitutes the read-out of our quantum simulation. As described in appendix G, this correlation length can be extracted with a time-of-flight as well as a density measurement. Even for this simple quantity, quite an elaborate analysis is needed, which clearly highlights that the final read-out stage of a quantum simulation has to be taken seriously and should be seen as a direct motivation for our investigation of tomography in chapter 11.

The main goal behind the quantum simulation described here is to explore the dynamical signature of the Mott-superfluid phase transition in the Bose-Hubbard model, in the setting of the Kibble-Zurek mechanism which slowly moves from the gapped phase into criticality. For this, we start in a large Mott insulator and cross the phase transition by linearly ramping down the lattice depth V_{lat} (see Fig. 10.1). In order to study the dynamics, the same dynamical ramp is performed in different time scales. For each total ramp duration τ_{ramp}, the correlation length at the end of the ramp is measured, leading to a correlation length as a function of total ramp time, as discussed when the Kibble-Zurek mechanism was introduced (see section 9.5). For convenience, in this whole chapter, we will measure the ramp time τ_{ramp} in natural units of integrated tunneling events (see section 8.2.1). We now turn to the evaluation of the results in 1D, which can still be numerically checked in order to certify the correct behaviour of the experiment as a dynamical quantum simulator.

10.2 1D RESULTS

In the following, we present the result of Ref. [1] for the dynamical behaviour of the correlation length when moving from Mott to superfluid on different time scales. The discussion is restricted to a high-level overview. We begin by the observations in one spatial dimension, which was achieved by keeping the optical lattice very strong in the other two directions, thus effectively decoupling the 3D cloud into 1D tubes (see section 8.2.1).

The experimentally observed phase correlation length shows several dynamical regimes (see Fig. 10.2). For very short ramps, the system can hardly react at all and the correlation length is dominated by the initial Mott insulator, which has a correlation length significantly below one lattice spacing. In this phase, the dominant Hamiltonian term is the interaction, leading to a state that is close to a product state with exactly one particle per site. Due to the finite initial value of $J > 0$, however, the initial state is slightly entangled and possesses short-range correlations.

For slower evolutions, the full ramp stops being diabatic and the system starts to react to the ramping of the critical parameter over the phase transition. Thus, the correlation length starts to quickly increase up to several lattice spacings. In these two regimes, the experimental data agrees almost perfectly with the numerics performed in a translationally invariant system.

For the numerical analysis, we used three different numerical tools (see Fig. 10.3). The numerically most efficient description relies on the doublon-holon model (see section 9.2.2). As discussed, it is a free fermionic model that is capable of accurately capturing the Bose-Hubbard model on the Mott insulating side away from the phase transition. For that reason, it captures the short evolutions well, which are dominated by the initial state and the evolution in the Mott phase. Since the model is free, very large systems can be simulated. In practice, the explicit numerical calculation of the correlators is involved, as it is a model with two fermionic species and the application of Wick's theorem (see section 3.4.1) becomes non-trivial.

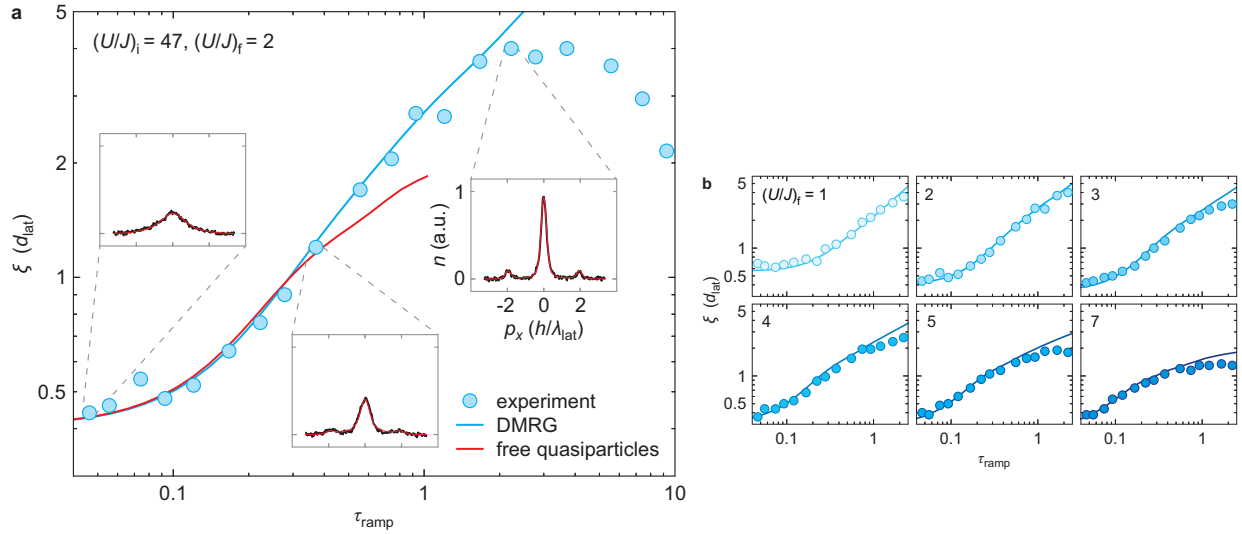

Figure 10.2: *Taken from Ref. [1].* **a** The left plot shows the dynamical behaviour of the correlation length measured in units of the lattice spacing d_{lat} when moving from the Mott insulator into the superfluid phase in different time scales τ_{ramp} in 1D. As the insets show, for longer evolution times, the final ToF image changes from a broad distribution corresponding to a Mott insulator to the peaked image of a superfluid. The experimentally extracted correlation length (blue dots) agrees extremely well with the numerical analysis in terms of a time-dependent DMRG simulation in a homogeneous model of varying size (blue line). While very short evolutions are well-captured in terms of the doublon-holon model (red line), it is not capable of accurately describing the phase transition and breaks down for intermediate ramp times. Finally, for long times, the trap becomes visible leading to a deviation between the experimental data and the numerical analysis in a homogeneous model. **b** The right plot shows the same study, but now for different final ramp positions $(U/J)_f$, showing that all these ramps qualitatively have very similar behaviour.

The doublon-holon model can also be used to connect the experimental results to Lieb-Robinson bounds and the spreading of quasi-particles. While for the Bose-Hubbard model, no exact Lieb-Robinson bound for the correlation length in our context is known (see appendix B), the doublon-holon model is fermionic and thus has such a bound. It captures the speed of spreading of the quasi-particles [120] (see section 9.2.2). In fact, as demonstrated in Fig. 10.4, the qualitative behaviour of the correlation length for short times is reproduced by looking at the maximum correlation length that can be created during the slow ramp, given by [1]

$$\xi(\tau_{ramp}) = \xi_0 + \int_0^{\tau_{ramp}} dt\, v(t)\,,$$

where $v(t)$ is the Lieb-Robinson velocity depending on $H(t)$ (see section 9.2.2).

The second numerical method applied is a full exact diagonalisation of the system, which uses all symmetries of the model, namely translational invariance as well as particle number conservation. Since the initial state is the ground state of the system, we can choose to work in the sector with fixed particle number and states that are invariant under shifts. This greatly reduces the Hilbert space, allowing to describe up to 15 particles on 15 sites. In order to achieve such a description numerically, it is necessary to first construct a complete basis for the corresponding subset. The Hamiltonian is then constructed as a sparse matrix, described by its action on the basis states [255]. This numerical technique is significantly more powerful than the free doublon-holon model for the setup at hand. As it constitutes an approximation-free full solution of the dynamics, it is obviously correct. The only downside of the method is that only relatively small systems can be considered.

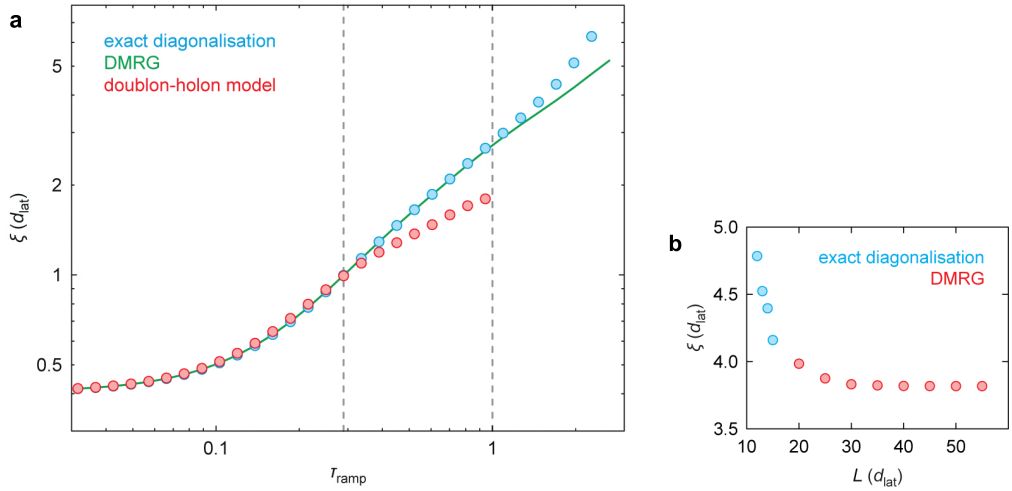

Figure 10.3: *Taken from Ref. [1].* **a** Shown is the numerical analysis of the final correlation length ξ after the ramp, depending on the ramp duration τ_{ramp} using different numerical tools. For short evolutions, the initial state and the Mott phase dominate the dynamics, making a description with the doublon-holon model (red dots) feasible. Exact diagonalisation (blue dots) works for longer times, but eventually breaks down due to the finite system size. Only time-dependent DMRG (green line) can capture the evolution for ramps lasting longer than one tunneling time. The break-down of the doublon-holon model and the exact diagonalisation are indicated by the dashed vertical lines. **b** The plot gives a finite size scaling of exact diagonalisation (blue dots) for small system sizes and t-DMRG data (red dots) for larger systems. As the saturation with the system size L shows, the DMRG result for all times considered here are capable of accurately describing the dynamical behaviour of an infinite system.

For short and intermediate times, the Lieb-Robinson light cone provably restricts the dynamics (see appendix B), thus showing that short time evolution only sees a small subsection of the system. Therefore, the limited system size in exact diagonalisation only becomes relevant for longer times above one tunneling event, as can be seen from a system size scaling (see Fig 10.3).

The third and final method used to described the dynamical evolution at hand is time-dependent DMRG. This crucial numerical tool is of invaluable help in the description of quantum many-body systems [41, 122]. From a modern point of view, its main idea is to always store the state as a matrix-product state (see appendix A). This saves a lot of memory and allows to describe very large system sizes. As long as there is good reason to believe that the desired state has little entanglement and is thus well described in terms of a tensor network, DMRG and related tools are almost exact, sometimes up to machine precision. This is particularly true for ground states of gapped 1D models (see section 3.5.1) and, as it turns out, also applies to our setting of slow quenches.

Using a version of time-dependent DMRG, relying on the open-source code OpenTEBD [122], we are able to describe the slow quenches for substantially longer times [256], with system sizes that are large enough to make them indistinguishable from the behaviour of infinite systems, where the quantum phases are well defined (see Fig. 10.3). In this regime, a substantial deviation between the numerical analysis and the experimental data becomes visible.

For these longer ramp times, the experimentally measured correlation length decreases again, which is a clear signature of the fact that the experiment takes place in a trap, in contrast to the numerical description of an essentially infinite homogeneous system, where the notion of quantum phases are well-defined. A detailed investigation of the influence of the trap is contained in appendix G. Let us stress again that these systems behave indistinguishably for shorter ramp times, thus demonstrating that the experiment reproduces the behaviour of an essentially infinite homogeneous system for short and intermediate times. In this way, the experiment is indeed a dynamical quantum simulator allowing to study the dynamics of

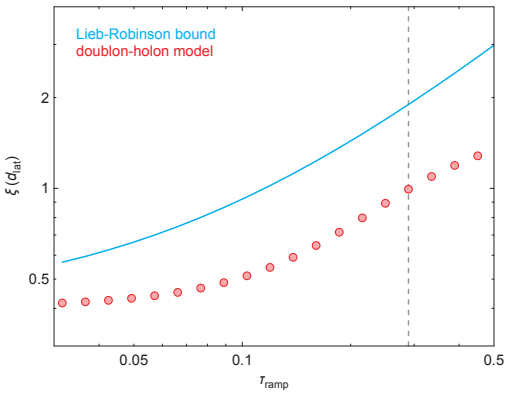

Figure 10.4: *Taken from Ref. [1].* This plot shows the comparison of the growth of the correlation length ξ predicted by the doublon-holon model (red dots) for short total ramp times with an estimate in terms of Lieb-Robinson bounds (blue line). The numerical simulation in terms of the doublon-holon model, which is an excellent approximation up to its breakdown indicated by the gray line, shows similar qualitative behaviour as the maximum correlation length allowed by Lieb-Robinson bounds in this model.

a quantum phase transition. In 1D, we are able to certify it using numerical simulations, which, as we discuss later on, is no longer true in higher dimensions, where the quantum simulator can demonstrate its full power.

To summarise, we demonstrated that the experimentally measured correlation length in 1D shows three distinct dynamical regimes. For short ramps, it hardly changes and is well described with a free fermionic model. For intermediate ramp times, it grows strongly and is in excellent agreement with numerical simulations performed in a homogeneous system. For longer times, the trap causes a decrease of the correlation length, which does not take place in the homogeneous model. In the following, we investigate the intermediate ramp time regime in more detail and relate it to the Kibble-Zurek mechanism discussed earlier (see section 9.5).

10.2.1 *Power-law behaviour*

For intermediate ramp times, we observe a strong growth of the correlation length in the experimental data. Due to the agreement with the numerics performed in a homogeneous model of various sizes, we know that this is indeed the behaviour of an essential infinite homogeneous model which undergoes the Mott-superfluid phase transition. When looking at the growth in detail (see Fig. G.3), we find that there is a central region extending over one order of magnitude that, to good approximation, looks linear in the log-log plots presented. Thus, they are compatible with the power-law growth of the correlation length suggested by the Kibble-Zurek mechanism (KZM). Since the KZM is not an exact theory, it is hard to evaluate to what extent it can be applied it to our setting. Still, in this respect, the intuition provided by it seems to be a useful guideline. In the following, we look into extending this connection and investigate the power-law growth in more detail.

In order to delve deeper into the dynamics of the Mott-superfluid transition of the Bose-Hubbard model, we altered the ramp to end at different positions in the superfluid phase. Following the intuition of the adiabatic-frozen approximation, the final position should have no influence on the observed power-law, as the system is said to be "unable to react" in the gapless phase [240]. This does not seem to be the case, as demonstrated by the experimental and numerical data in Fig. 10.5. We rather observe a strong dependence of the observed power-law on the final position within the superfluid phase that seems to

have a complicated functional form and decreases when going too close to the free case of non-interacting bosons at $U = 0$. In this way, we observe a dynamical signature of the Mott-superfluid phase transition that lies outside the intuition provided by the KZM.

Naturally, we cannot conclude that out experimental findings are in contradiction to the KZM. Given the fact that its formulation is vague from the beginning and its precise assumptions are unclear, one should rather ask to what extent it gives useful intuition. For the setting at hand, this is only partially the case and for predicting the precise behaviour of the power-law, it is not true at all.

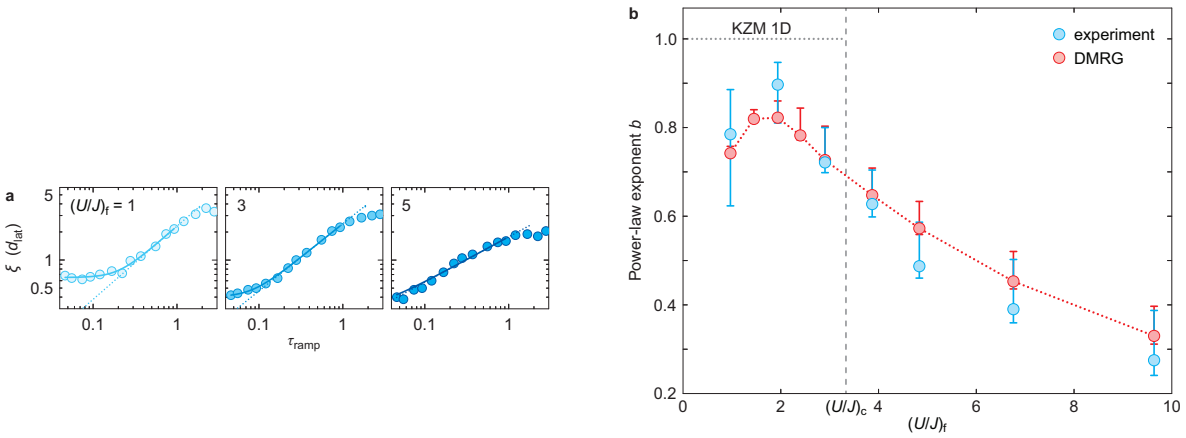

Figure 10.5: *Taken from Ref. [1].* **a** Shown is the dependence of the final correlation length ξ on the ramp time τ_{ramp} and a power-law fit for intermediate ramp times. As this fit shows, for intermediate ramp times, the observed growth of the coherence length is compatible with a power-law fit. **b** Shown is the exponent b of the power-law fit and its dependence on the final lattice depth $(U/J)_f$ for experimental data (blue dot) and numerical simulation using t-DMRG (red dots). The error bars indicate the uncertainty of the exponent b in the power-law fit itself and due to the precise range where the fit is applied. Contrary to an intuition guided by the KZM, the power-law crucially depends on how deep the ramp moves into the superfluid regime.

When plugging in the critical exponents of the Bose-Hubbard model in 1D, the KZM suggests a power-law with exponent one independent of the final position of the ramp [240, 257]. Our results seem to lie significantly below this value. As has recently been pointed out [258], the application of the KZM to the 1D setting might have to be altered due to the special case of a Kosterlitz-Thouless transition. Exploring this special phase transition in more detail would surely be an interesting endeavour, which would necessarily also rely on a deeper understanding of the KZM. We now turn to the case of higher dimensions, where such special cases do not appear.

10.3 HIGHER DIMENSIONS

In the following, we present the investigation of the dynamics of the quantum phase transition of the Bose-Hubbard model in 2D and 3D. Due to the absence of good analytical descriptions of the model at the transition and the extreme difficulty in describing it numerically, quantum simulators are the only feasible tool. As described in section 8.2.1, changing the dimensionality in the experimental architecture is straightforward, as one can ramp down the different spatial lattice dimensions individually. Further, as we numerically checked that in 1D the experimental system accurately describes an essentially infinite homogeneous quantum system for short and intermediate times, we gained confidence that the simulation accurately describes the dynamics of the phase transitions also in 2D and 3D.

The results of the experimental study are presented in Fig. 10.6. The first remarkable feature is a clear similarity between the different dimensions. They behave almost identical for the same final value of U/J. Only the break-down position of the power-law regime seems to vary, with a power-law stretching further in higher dimensions. Given that the critical values and exponents are dramatically different in 1D, 2D and 3D (see section 9.2.2), this similarity is very surprising.

Moreover, when looking at the exponents of the power-law (see Fig. 10.6), we find the same qualitative behaviour as in 1D. The dependence on the final position within in the superfluid phase seems non-trivial and shows the intriguing feature that it decreases again when the final position lies too deep within the superfluid phase. Again, such a behaviour cannot be explained within the scope of the KZM. Further, the general power-law exponents we observe seem to lie significantly above the predicted values.

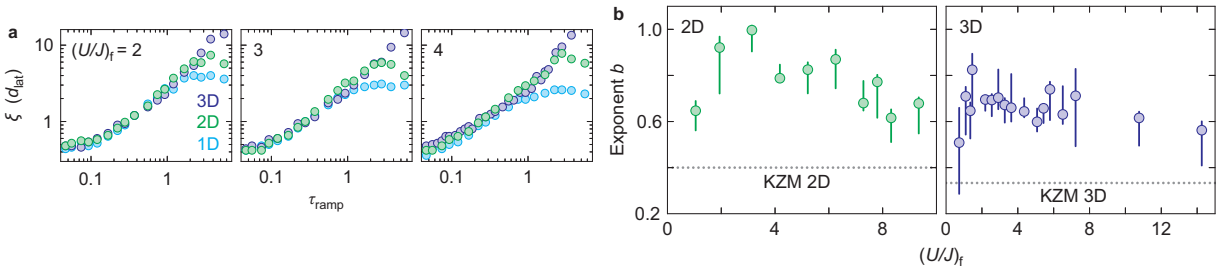

Figure 10.6: *Taken from Ref. [1].* **a** Shown is the experimentally observed behaviour of the correlation length ξ at the end of the ramp for various ramp durations τ_{ramp}. The results are presented for 1D, 2D and 3D for three different final positions $(U/J)_f$ within the superfluid phase, showing a remarkable similarity between the different dimensions. **b** Plotted are the power-law exponents b extracted from the experimental data, depending on the final position $(U/J)_f$ within the superfluid phase for 2D and 3D. As in 1D, the curves show complicated behaviour and share the feature that they start to decrease again when the ramp reaches too deep into the superfluid phase.

In earlier works, some limitations of the KZM have already been pointed out. One often cited intuition, based on classical transitions, is that of coarsening of defects [259]. It suggests that the slow ramp across a critical point cause defects as predicted by the KZM, which after their creation undergo a non-trivial evolution. While this might be well related to the physical processes taking place, its predictive power seems small, as it is by no means clear how this coarsening effect can be captured.

In free models with either a multicritical point [260] or a gapless phase [261, 262], such as the XX model, it was already observed that the KZM had to be altered. In this context, this does not pose a substantial problem, as the models are exactly solvable and every dynamical behaviour can thus be either analytically calculated or obtained using simple numerical simulations. The interesting regime for the KZM, however, is the application to interacting models that cannot be exactly solved, such as the Bose-Hubbard model at hand. Its application to this interacting setting is so far substantially hindered by the lack of systematic ways of adapting and improving it for the particular setting at hand. It is for example, unclear how the precise ramp schedule and its final position can be accounted for. Moreover bounds to the speed of the transition and, as also connected via Lieb-Robinson bounds, to the system size are unknown. While it is often said that evolutions need to be slow enough and correspondingly system sizes large enough, it is not clear what this would mean precisely. Thus, it is not clear in which setting the Bose-Hubbard model has to be probed to produce the Kibble-Zurek predictions. Based on our results, we think it is fair to speculate that the dynamics of quantum phase transitions are far less universal than commonly assumed. They rather seem to pose a intriguing and complicated area of research on quantum many-body dynamics and due to their intrinsic complexity, their future study will have to rely on quantum simulators, much in the spirit of the work presented here.

10.4 SUMMARY: DYNAMICALLY PROBING THE MOTT-SUPERFLUID TRANSITION

In this chapter, we studied the dynamics of the Mott-superfluid phase transition of the Bose-Hubbard model, separating an insulating and a superfluid phase. For this, we relied on an instance of a partially certified analogue quantum simulation and demonstrated the first experimental study of an essentially homogeneous quantum system entering a critical phase in such a setting. The results in 1D could still be efficiently checked numerically. This gives reason to trust the simulator also in higher dimensions. In those 2D and 3D studies, the true power of the experiment emerged and we were able to discuss results that seem completely inaccessible without the simulator. In those results, we uncovered complicated behaviour that could not be captured using any known theory. While the observations were compatible with power-law behaviour as expected from the Kibble-Zurek mechanism, the exponents of those power-laws showed complex behaviour that could not be explained within the realm of this mechanism. Thus, the dynamics of quantum phase transitions on realistic experimental time scales are surely not comprehensively understood. Here again, further connections between static and dynamic properties of Hamiltonian models have to be established. Further efforts in this direction are certainly needed and, given the great difficulty of this problem, will likely be based on analogue quantum simulators.

In the following, we explore the concept of a dynamical quantum simulator further. Specifically, we focus on the read-out that retrieves the result of the simulation. In the study just presented, such a read-out solely focussed on extracting a single parameter, namely the correlation length. Even there, we already saw that this extraction is by no means a trivial task. In general, one would naturally like to maximise the information retrieved from the simulator, rather than just obtaining a single parameter. This task is achieved by *tomography*, which is a reconstruction of the experimental quantum state. We explore this approach in the context of ultra-cold atoms in a continuous optical setup in the next section. This setup has in the past successfully been used to explore issues of equilibration and thermalisation and, due to its continuous nature and involvement of large collections of atoms, is one of the most intriguing challenges for the task of quantum state tomography.

11

QUANTUM FIELD TOMOGRAPHY

The following chapter is based on Ref. [2]. We sincerely thank Adrian Steffens, Tim Langen, Bernhard Rauer, Thomas Schweigler, Robert Hübener, Jörg Schmiedmayer, Carlos A. Riofrío and Jens Eisert for collaboration on this exciting topic.

Quantum simulations have already contributed significantly to our understanding of many-body physics. Given this development, the mindset when it comes to experimental investigations is slowly shifting. In the past, experiments were mostly performed to corroborate or falsify theoretical predictions. The underlying theoretical model was approximately solved and some key quantity, such as a conductance was extracted. This predictions in terms of a single experimentally measurable quantity could then be compared to the actual outcome of an experiment.

The mindset behind quantum simulations is fundamentally different. Here, the experiment is taken as a fully-fledged investigative tool to understand the physical situation at hand. Given the absence of good theoretical descriptions or numerical tools, the information obtained from the experiment plays a very different role, as it no longer is a simple check of a ready-made prediction, but rather a gateway towards understanding new behaviour. This leads to substantially increased expectations when it comes to experimental measurements. In particular, rather than only extracting a single quantity, one aims at a best possible reconstruction of the state, in order not to lose any information provided by the quantum simulator. Due to the large number of degrees of freedom involved in quantum many-body systems, this necessarily relies on a useful ansatz class that captures commonly encountered states well. One promising route is compressed sensing, which reconstructs low rank states well [200, 201]. A different approach relies on tensor-networks [202, 203], which work well as long as entanglement entropies are small, at least in 1D. We follow this mindset, but take it to the level of continuous systems.

Continuous setups have always played an important part in the investigation of ultra-cold atoms. In fact, many physical theories, such as descriptions of electronic behaviour in terms of Luttinger liquids, rely on the absence of a discrete lattice structure. Based on immense progress in recent years, these systems can now be experimentally studied and controlled with unprecedented precision [263–265]. This gives rise to numerous interesting applications. From the viewpoint of this thesis, especially experiments looking into thermalisation of interacting particles [35] and an investigation of Lieb-Robinson bounds [34] should be highlighted and demonstrate that these platforms are capable of significantly contributing to our understanding of quantum many-body systems out of equilibrium.

Mathematically speaking, the continuous setting can be seen as a limiting procedure where the lattice spacing is sent to zero. As anyone who took courses in quantum field theory surely knows, this leads to diverse mathematical difficulties, mostly routed in the fact that, even for finite systems, the Hilbert space is not separable anymore. This requires new ways of thinking of the involved states. While often one follows the algebraic view, where states are merely defined by their action on local operators, we rather focus on a paradigmatic class of conceptually easy states that are still versatile enough to capture quantum many-body systems in and out of equilibrium in many contexts. This will be continuous matrix product states (cMPS), which provide the basis for investigating the read-out of quantum simulations in the continuous context [266].

Continuous matrix-product states

A translational invariant cMPS is described by two matrices $Q, R \in \mathbb{C}^{D^2}$ on the auxiliary system, where the parameter D capturing their size is called the bond dimension. The state is defined as

$$|\psi_{Q,R}\rangle = \mathrm{Tr}_{\mathrm{aux}}\left(\mathcal{P}\, e^{\int_0^L dx\,(Q\otimes\mathbb{1}+R\otimes\Psi^\dagger(x))}\right)|\emptyset\rangle \ ,$$

where $\mathcal{P}$ denotes path ordering with respect to the position x and the trace goes over the auxiliary space on which Q and R are supported.

The general approach of tomography with these states is to reconstruct the matrices capturing the cMPS based on measurement data. We continue by introducing a setup for continuous quantum fields with massive particles that has very successfully been applied to questions of equilibration and thermalisation in the past [35, 265]. For these quantum simulations, we show that cMPS provide an ideal ansatz class to optimise the read-out stage. Based on this, we present the first proof-of-principle application of a quantum field tomography for interacting particles [2].

11.1 ULTRA-COLD BOSONS IN A CONTINUOUS OPTICAL SETUP

The experimental architecture that we focus on in this chapter are ultra-cold bosons that hover in a continuous harmonic trap created by an atom chip [265]. Using evaporative cooling, very low temperatures in the nano-Kelvin regime can be achieved. The cloud is thus, initially, almost in the ground state. Similar to optical lattices, again Feshbach resonances can be used to tune the interaction between the atoms and thus interpolate between free theories and strongly interacting condensed matter systems. As the harmonic trap is large and spans roughly $100\,\mu m$, the system is, to good approximation, translationally invariant in the center of the trap. Therefore, we restrict to this center region, where a fit in terms of a translationally invariant cMPS will be used.

Due to very strong confinement in two directions, the resulting atomic cloud is almost one-dimensional and, in the middle of the trap, described to excellent approximation by a Lieb-Liniger model [267]

$$H = \int_{-L/2}^{L/2} dx \left(\frac{1}{2m}\nabla\Psi^\dagger(x)\nabla\Psi(x) + g_0\Psi^\dagger(x)\Psi^\dagger(x)\Psi(x)\Psi(x)\right) \ .$$

It can be seen as a continuous relative of the Bose-Hubbard model, consisting of a kinetic term and one describing the contact interaction. The model is integrable, in the sense that it can be solved by the Bethe ansatz [268]. Note that, due to the intricate nature of the solution, out of equilibrium questions, such as those of equilibration and thermalisation are hard to answer. This makes it necessary to probe this model in instances of quantum simulations.

In current experiments, preparing out of equilibrium initial states is not a trivial task. In the setup considered here, it is achieved by a sudden split of the condensate along the longitudinal axis. This creates two 1D condensates next to each other [265]. The splitting procedure is a complex 2D process in a quantum field and exactly modelling it is so far out of scope. Nevertheless, the splitting provides a pivotal tool in the creation of out of equilibrium settings. Further, by varying the details of the splitting procedure, a large class of initial states can be prepared [265].

The quantity usually investigated after the splitting is the relative phase between the condensates. It can be probed with comparably simple time of flight techniques and exploiting the fact that each image provides a single shot quantum measurement of the phase [269]. In fact, the possibility to use time of flight imaging is another crucial reason why the splitting procedure of the atomic cloud is usually performed.

Directly after the split, the two condensates are perfectly in phase [35]. Before the time of flight imaging, they are left to evolve up to a time t_{hold}, which we will call hold time. Up to this time scale, the dynamics leads to a relaxation process during which the relative phase decorrelates and eventually reaches the uncorrelated thermal predictions [35]. As is commonly expected in interacting models, the time scales for this process are very short, on the order of milliseconds, and thus much faster than predicted by current bounds on equilibration times scales (see chapter 3). This probe of thermalisation behaviour is particular interesting, as it probes time of flight information, which is intrinsically non-local. Due to the very limited information obtained by the observable, this is still perfectly compatible with equilibration and thermalisation as described in chapter 3 and 4.

In the proof-of-principle application presented here, only phase correlation behaviour was experimentally measured. Since no density information is available, we only reconstruct an effective state for the phase behaviour. The theoretical tools used are, however, general enough to reconstruct the full cMPS as long as enough measurement information is provided [2, 270]. For our reconstruction, no underlying theoretical model is used and it is thus perfectly suited for the context of quantum simulations, where the experiment is used as an investigative tool to explore unknown physical behaviour. The class of cMPS states is best suited for ground states of locally interacting models, or other states that are connected to low spatial entanglement entropies [2]. In this way, it can conceptually be used as an experimental probe for the measurement of entanglement; a prospect that we explore in the final parts of this chapter.

11.2 RECONSTRUCTING PHASE CORRELATIONS

The starting point for our reconstruction is to express the correlation functions in terms of the cMPS matrices. In order to separate phase and density behaviour of the state, we employ a polar decomposition of the field operators

$$\Psi^\dagger(x) = n(x)^{1/2} e^{i\theta_x} \,,$$

where $n(x) = \Psi^\dagger(x)\Psi(x)$ is taken to be the density of one of the two condensates and θ_x is the phase operator at position x. The construction ensures that these effective field operators indeed fulfil the correct commutation relations. The phase correlation functions, which can experimentally be measured, are defined as

$$\begin{aligned} C^{(n)}(x_1,\dots,x_n) &= \operatorname{Re}\left\langle e^{i\left(\theta_{x_1}-\theta_{x_2}+\theta_{x_3}-\cdots+\theta_{x_{n-1}}-\theta_{x_n}\right)}\right\rangle \\ &= \operatorname{Re}\left\langle n(x_1)^{-\frac{1}{2}}\Psi^\dagger(x_1)\Psi(x_2)n(x_2)^{-\frac{1}{2}}\dots\right\rangle \,, \end{aligned}$$

where θ_{x_1} are the phase differences of the two condensates at position x_1 and the angular brackets denote the ensemble average [2]. Since it is sufficient for our tomography procedure, we restrict to even correlations functions which are normal ordered $x_1 \leqslant x_2 \leqslant \cdots \leqslant x_n$. Further, we assume translational invariance in the experimental setup, which is, for the short equilibration time considered here, a reasonable assumption, as we work in the center of the trap [2]. In the cMPS formalism the phase correlation function takes the form

$$C^{(n)}(\tau_1,\dots,\tau_{n-1}) = \sum_{\{k_j\}=1}^{d^2} \rho_{k_1,\dots,k_{n-1}} e^{\lambda_{k_1}\tau_1}\dots e^{\lambda_{k_{n-1}}\tau_{n-1}} \,,$$

with $\tau_k = x_{k+1} - x_k$ being the difference between spatial positions, which are positive due to normal ordering, λ_k are eigenvalues of the transfer operator usually referred to as poles [2] and

$$\rho_{k_1,\ldots,k_{n-1}} = M^{-1}_{1,k_{n-1}} M_{k_{n-1},k_{n-2}} \ldots M^{-1}_{k_2,k_1} M_{k_1,1} \,,$$

where $M = \overline{R}^{\frac{1}{2}} \otimes R^{-\frac{1}{2}}$ in a suitably chosen basis [2, 270].

As only phase information is measured, it is impossible to reconstruct the full cMPS in terms of Q and R matrices. Rather, we will use the experimental data to reconstruct the phase correlation behaviour of the cMPS given in terms of the M matrices and the poles λ_k. We now turn to the details of this reconstruction.

For now, we focus on the experimental data with short hold time after the longitudinal split of $t_{\text{hold}} = 3\,\text{ms}$. A comparison to longer hold times follows later on. In order to obtain the phase correlation behaviour of the cMPS, we have to reconstruct the poles λ_k as well as the M matrix, which is a complex square matrix of size $D \times D$, where D is the bond dimension [2]. This is a task that is feasible for large-scale quantum systems, which highlights the power of cMPS as an ansatz class in this context.

We begin by extracting the poles. For this, it is sufficient to look at two-point correlation functions. This was performed by a straight-forward least-square fit. In a second step, the M-matrix is reconstructed. Using the fitted 2-point correlation function and normalisation conditions, some entries can be fixed a priori [270]. To obtain the other entries, experimentally measured four-point correlation functions are fitted. For this, we use a Nelder-Mead simplex algorithm from the open-source library SciPy [271]. In order to capture the quality of our fit to the correlator, we use the mean relative deviation, defined as

$$\epsilon = \sqrt{\frac{1}{|S|} \sum_{\mathbf{x} \in S} \frac{|C(\mathbf{x}) - C_{\text{rec}}(\mathbf{x})|^2}{|C_{\text{rec}}(\mathbf{x})|^2}} \,,$$

where S denotes the set of normal ordered indices $x_1 \leqslant x_2 \leqslant \cdots \leqslant x_n$. As described in Ref. [2], taking the bond dimension $D = 2$ proved to be sufficient to approximate the four-point correlation function up to a mean relative deviation of 1.4%, which is of the same magnitude as the experimental errors. Thus, we are capable of accurately capturing two- and four-point correlation functions with the cMPS formalism. Naturally, there are many ways of fitting correlation functions and it is, a priori, not at all clear to what extent one has truly gained knowledge of the state. Thus, we are left with the task to certify the reconstruction. It is one of the strong suits of our cMPS method that this is easily possible.

In order to gain trust that the presented method indeed reconstructs the state and can thus function as a tomographic tool, one has to perform steps towards certifying the reconstructing. For this, we use the fitted M-matrix and poles λ_k to predict higher order correlations functions. Here, no fit is performed and the cMPS prediction is compared directly to the experimental values. As presented in Fig. 11.1, these predictions work very well, with a relative mean deviation of 3.2 %. This can be seen as a clear sign that we actually reconstructed the phase behaviour of the state.

To estimate the robustness of the algorithm with respect to experimental noise, a bootstrapping method is used [23]. For this, Gaussian noise is added to the experimentally measured four-point correlations. Subsequently, the reconstruction procedure is implemented and the entry-wise relative standard deviation of the six-point phase correlation functions is compared. For the average over all entries, a deviation of 1.1 % is found, with a maximum relative standard deviation of 2.8 %. Thus, the reconstruction is robust with respect to experimental fluctuations and errors in the measurement procedure.

Having demonstrated clear indications that our tomographic procedure is capable of obtaining the phase behaviour of the quantum field, we now turn to an investigation how our tomographic procedure can be used to approach the thermalisation behaviour of the state.

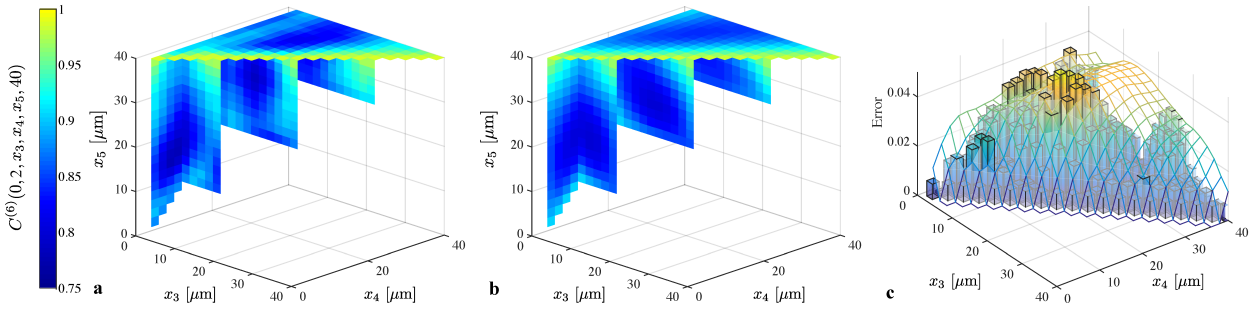

Figure 11.1: *Taken from Ref. [2].* **a** The left plot shows the experimentally obtained six-point correlation function depending on three discretised spatial positions x_3, x_4, x_5 measured in µm. **b** The center plot gives the theoretical prediction, based on the fitted cMPS relying on two- and four-point correlators. **c** On the right, a diagram of the experimental measurement uncertainties is shown (vertical bars) as well as the error in the reconstruction (surface plot) defined as the deviation between the experiment and the tomographic prediction. We see that the cMPS produces the six-point correlators with excellent accuracy.

11.3 INVESTIGATING THERMALISATION

As explained, the experiment begins by splitting a 1D condensate along the longitudinal axis, thus preparing an out of equilibrium state. The resulting condensates are left to evolve freely. As is demonstrated by time of flight measurements, the phase correlations between the condensates equilibrate and can, in a suitable sense, be captured with thermal ensembles for long times [35]. In this section, we evaluate our tomographic results with this thermalisation behaviour in mind. For this, we performed the same procedure of fitting two- and four-point phase correlation functions and using the resulting cMPS to predict six-point correlators for different hold times, during which the condensates can evolve freely. For different times of $t_{\text{hold}} = 3,\ 7,\ 23\,\text{ms}$, we find that our fit quality with a bond dimension $D = 2$ cMPS decreases significantly with relative mean deviations of $\epsilon = 3.2\,\%\,, 10.7\,\%\,, 34.1\,\%$ (see also Fig. 11.2). It is not clear what the origin of this decrease in fit quality is. It can, however, be connected to different aspects of quantum many-body systems out of equilibrium. Previous investigations demonstrated that the experiment can be well-captured within a framework of pure quantum states [35, 265], which allows to apply the ideas and concepts presented in this thesis.

To begin with, as described in chapters 3 and 4, thermalisation behaviour of quantum many-body systems relies on entanglement entropies growing with time, which is necessary to make the pure state compatible with locally looking like a strongly mixed thermal state. With the exception of Anderson insulators, where entanglement entropies saturate quickly and many-body localised model, where entanglement entropies grow only logarithmically, generic interacting models are connected to a linear growth of entanglement entropies [3, 26]. Such a larger entanglement is connected to a larger bond dimension necessary for the cMPS fit, similar to the case of a discrete lattice system and MPS (see section 3.5.1). Therefore, a growth of entanglement entropies over time, as expected from thermalisation behaviour, would be an excellent explanation of our observation that the fit decreases with increasing time. This could potentially be revealed by attempting fits with higher bond dimensions and showing that the state can be reproduced more accurately. Unfortunately, the measurement data used here is not suited to attempt such fits [2]. Still, it seems a promising gateway towards quantifying entanglement in interacting quantum many-body systems, especially as entanglement is notoriously hard to measure experimentally [189, 190].

Another possible reason for the observed decrease in fit quality is connected to Lieb-Robinson bounds (see appendix B). As mentioned, the experiment takes place in a large harmonic trap, where only the central region is observed. For short times, one knows that the effective light cone, as given by Lieb-

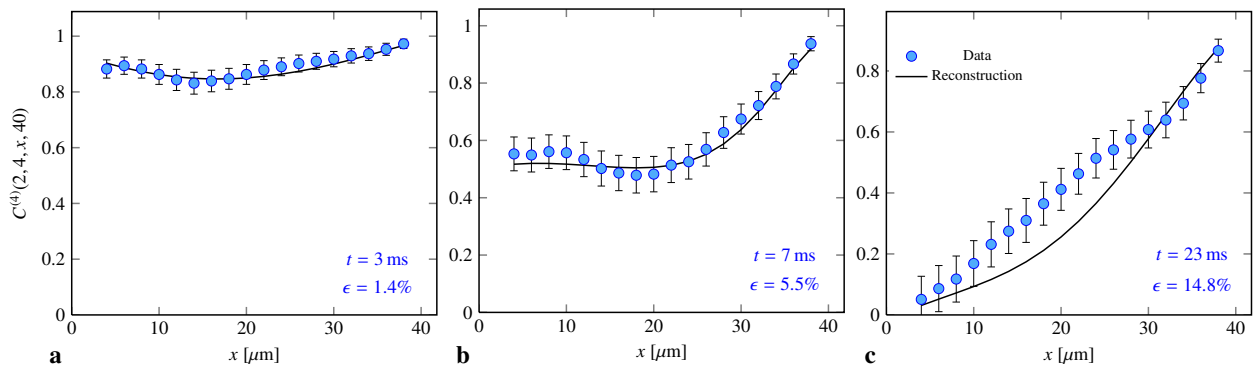

Figure 11.2: *Taken from Ref. [2].* Shown is the four-point phase correlator for a non-trivial cross section where three positions are fixed. Plotted is the experimental data (blue dots) including measurement uncertainties (error bars) as well as the tomographic reconstruction (black line). The plot is presented for different hold times of **a** $t_{hold} = 3\,ms$, **b** $t_{hold} = 7\,ms$ and **c** $t_{hold} = 23\,ms$. As indicated by the relative mean deviation ϵ for the full four-point correlators, the fit quality decreases substantially with equilibration time, which is compatible with out intuition of a growing entanglement entropy with time.

Robinson bounds, only couples the center to a small region around it. Such light-cone like behaviour has also been confirmed experimentally for these platforms [34]. For longer times, however, the light-cone widens and thus includes larger and larger areas of the trap. Thus the harmonic trap should become more and more visible with hold time. Such behaviour can also be seen in the experimentally obtained two-point correlators by observing how much they depend on the position at which they are evaluated [2]. We find for the hold times $t_{hold} = 3\,ms$, $7\,ms$, $23\,ms$ deviations from translational invariance of $0.3 \cdot 10^{-2}$, $5.4 \cdot 10^{-2}$, $8.3 \cdot 10^{-2}$, clearly indicating that for longer hold times, our assumption of translational invariance is considerably less accurate. This is perfectly compatible with the intuition provided by Lieb-Robinson bounds in a trapped model. We now summarise our partial reconstruction of a quantum field in an experiment of ultra-cold atoms in a continuous optical trap.

11.4 SUMMARY: QUANTUM FIELD TOMOGRAPHY

To conclude, in this chapter, we investigated the read-out part of a dynamical quantum simulation. We demonstrated that, in a continuous setup of ultra-cold interacting atoms, continuous matrix product states can be used as an ansatz class for quantum field tomography. We provided the theoretical tools for this task and applied them in a proof-of-principle application on a paradigmatic platform. By using the reconstructed state as a predictive tool, we were further able to gain trust that the reconstructed state indeed captures the experiment well.

Finally, by investigating the observed fit quality, we established connections between the out of equilibrium evolution of the cloud of ultra-cold atoms with important mechanisms of quantum many-body systems out of equilibrium. When pushed out of equilibrium by a transversal split, the system equilibrates and in fact thermalises. Intuitively, such thermalisation behaviour should rely on an entanglement growth that roughly saturates Lieb-Robinson bounds, which would fit well to our observation of a decrease of fit quality in terms of a fixed bond dimension cMPS. Based on this, we provided an outlook how our tomographic procedure could be used as a probe to measure entanglement, which would provide substantial insight into the out of equilibrium behaviour in analogue dynamical quantum simulators.

12

SUMMARY & OUTLOOK

In this thesis, we explored various aspects of interacting quantum many-body systems out of equilibrium. Guided by a quantum information mindset, we were able to approach many long-standing problems on the intersection between quantum mechanics, statistical physics and condensed matter theory. Based on a current review with the involvement of the author of this thesis [3], we introduced and covered a large variety of settings and intriguing questions. In this general framework, the specific results obtained in this thesis were embedded. We will summarise them in the following and present open research questions in the various areas.

We first investigated *equilibration*, where two complementary settings could be identified in which the deviations from equilibrium can be mathematically bounded. Equilibration on average, capturing time averaged distinguishability from static ensembles, applies to very general systems, but deriving realistic equilibration time scales for interacting models seems difficult in this framework. For this task, it seems crucial to identify physical properties, such as transport, that guarantee fast equilibration. After all, there are indeed instances of systems that equilibrate extremely slowly, such as many-body localised models. For understanding the role that concepts like transport play, the second equilibration setting, which is given by free models, will surely prove useful. In the fully Gaussian setting, many processes can be directly calculated. Moreover, as we were able to prove, the evolution of free Hamiltonians that allow for transport will lead to states that are locally indistinguishable from Gaussian states and are thus captured with remarkably few parameters [6]. As this result establishes a connection between transport and the mathematics of equilibration, we hope that it will constitute an important stepping stone in the long-standing task of obtaining realistic equilibration time scales.

From this we moved on and presented different approaches to characterise the equilibrated ensemble. Here, conserved quantities played a crucial role. In case the only conserved quantity that needs to be included in the description is the energy, one obtains a Gibbs state, meaning that the system thermalises. In the realm of this *thermalisation*, it is clearly open what the precise mechanism for the emergence of the Gibbs state is and to what extent it truly results from the eigenstate structure in form of the eigenstate thermalisation hypothesis. For approaching this question, properly understanding the break-down of thermalisation, for example in the context of localising interacting systems, seems to be a promising approach.

In order to explore *localisation*, we carefully introduced the concept of single particle Anderson localisation. We looked at static and dynamical localisation of single electrons and connected it to the localisation of eigenmodes in free models of non-interacting particles. We proceeded to use this eigenmode localisation to derive many-body localisation properties, thus capturing localisation in a general language. Based on this preparatory discussion, we investigated the influence of electronic interactions, resulting in *many-body localisation* (MBL).

Following the various aspects of MBL currently considered in the literature, we gave an in-depth survey of its different facets. Here, both spectral and dynamical readings played a crucial role. In order to unify this picture and move in the direction of comprehensively defining many-body localisation, we proceeded by establishing important links between those dynamic and static characterisations. Specifically, we showed how the existence of a local constant of motion and a non-degenerate spectrum is sufficient to prove that the system allows for information propagation [5]. That is, one can explicitly construct local operators with a support that spreads without limits over time. Using this operator, one can then

devise a protocol that allows two parties to send a classical bit over arbitrary distances. Conversely, our second result showed that a full suppression of propagation on the low energy sector provably implies exponentially clustering correlations for the corresponding eigenstates [4]. This can be seen as an extension of the exponential clustering theorem in the context of localising systems. Using entanglement entropies, our result can be used to show that, in 1D, an efficient tensor network representation for these states can be constructed. While our efforts surely constitute important progress in comprehensively capturing many-body localisation, so far this could not fully resolve the inchoate state of its characterisation. In order to present a unifying definition, surely more such connections are needed and in particular their relation to experimentally measurable quantities like that of particle transport will have to be established.

In the second part of this thesis, we moved to a more experimentally minded framework, in an effort to cope with the fact that numerically simulating quantum systems out of equilibrium is exceedingly hard. Here, *quantum simulators* took the center stage, which are experimental devices that allow to access physical questions that would be completely out of reach without them. We reviewed their general principle, putting focus on a key candidate for such simulations, namely ultra-cold atoms in optical lattices. For this platform, we reviewed the experimental implementation of the Bose-Hubbard model and presented different available measurements that allow to extract the distribution of atoms and probe correlators between them.

We demonstrated the capabilities of ultra-cold atoms in optical lattices by investigating the dynamical signature of *quantum phase transitions*. Similar to our take on MBL, the crucial question here was how static and dynamic properties are interrelated. In particular, we approached the question whether the universal description in terms of power-laws can be used to describe the dynamical crossing of such a transition in an experimentally realistic setting. As an introductory step, we first defined quantum phase transitions and showed how their behaviour can be captured. We then turned towards their dynamical features. With the *Kibble-Zurek mechanism*, we encountered a common description of the crossing of a quantum phase transition.

Based on this introductory discussion of quantum phase transitions, we investigated their dynamics with a platform of ultra-cold atoms in an optical lattice in an instance of a dynamical quantum simulation. In the Bose-Hubbard model, the Mott-superfluid transition was dynamically crossed, thus conducting the first experimental study in such a setting of the dynamics of an essentially homogeneous quantum systems entering a critical phase [1]. In one dimension, we were able to certify the simulation with various numerical tools, which also shows that the experiment, for the time scales investigated, indeed reproduces the dynamical behaviour of a translationally invariant and practically infinite system. Relying on the quantum simulator, also the 2D and 3D quantum phase transitions were probed, which are almost inaccessible using state of the art numerical tools.

For the growth of the correlation length, which is a good indicator for the Mott-superfluid transition, we experimentally observed power-law behaviour as expected from the dynamical universal description in terms of the Kibble-Zurek mechanism, The precise power-law exponents, however, showed a complex behaviour outside of the scope of any known theoretical description. This clearly shows that the connection between static and dynamic features of quantum phase transitions is by no means fully understood and further efforts, most likely building on instances of quantum simulations, will be needed to comprehensively understand those interrelated features.

Quantum simulators certainly have great potential, but in their current implementations also severe limitations. In the context of ultra-cold atoms, in particular, the final read-out of the results will have to improve to exploit their full capabilities. We investigated this task for a continuous platform of ultra-cold atoms, which is one of the hardest instances of the problem. In an effort to maximise the information extracted from this quantum simulator, we provided tools to perform *quantum field tomography*, which effectively reconstructs the experimental quantum field.

Using continuous tensor network states, we were able to reconstruct the phase behaviour of an experimental state in a continuous 1D setup [2]. By predicting higher-order correlation functions, we provided good reason to trust the state reconstruction. By looking at its quality, we were further able to obtain possible signatures of entanglement increase over time, thus connecting this study to the investigation of equilibration and thermalisation in interacting models. We further gave an outlook how such tomography procedures could be used as a means to measure entanglement of ultra-cold atoms, which would greatly improve our current understanding of these systems as analogue quantum simulators. This would surely make them even more powerful and we certainly expect that the open questions in equilibration, thermalisation, many-body localisation and the dynamics of quantum phase transitions will greatly benefit from the application of quantum simulators in the near future.

Naturally, this thesis could only touch upon a small fraction of interesting out of equilibrium behaviour of interacting quantum many-body systems. Most intriguing for future studies will surely be the investigation of problems that lie at the intersection of the two main parts of this thesis. For example, a deeper understanding of many-body localisation as a true quantum phase transition and its characterisation in terms of critical exponents would certainly constitute a fruitful research direction. Further, it would be interesting to see how this transition behaves dynamically and to what extent power-law scaling can be employed to describe the crossing into a localised phase.

Moreover, bosons in random potentials provide an intriguing research area. Due to the unlimited number of particles allowed on local lattice sites, these systems seem ideal candidates to understand the precise role of energy and temperature for the transport behaviour in localised systems and to accurately capture mobility edges in MBL systems. Further, to achieve a clear picture of the similarities and differences of localised systems and spin or Bose glasses would surely be insightful. Here it seems likely that an in-depth debate on the precise classification of transport behaviour in finite systems in the mindset of quantum information theory would be highly useful. In this context, but even more generally, there surely is much more to be learned from an in-depth exchange between condensed matter physics and quantum information theory and we hope that this thesis will serve as an important stepping stone in these endeavours.

PUBLICATIONS OF THE AUTHOR OF THIS THESIS

[1] S. Braun, M. Friesdorf, S. S. Hodgman, M. Schreiber, J. P. Ronzheimer, A. Riera, M. del Rey, I. Bloch, J. Eisert, and U. Schneider. "Emergence of coherence and the dynamics of quantum phase transitions". *Proc. Natl. Acad. Sci.* 112 (2015), p. 3641.

[2] A. Steffens, M. Friesdorf, T. Langen, B. Rauer, T. Schweigler, R. Hübener, J. Schmiedmayer, C. A. Riofrio, and J. Eisert. "Towards experimental quantum field tomography with ultracold atoms". *Nat. Comm.* 6 (2015), p. 7663.

[3] J. Eisert, M. Friesdorf, and C. Gogolin. "Quantum many-body systems out of equilibrium". *Nature Phys.* 11 (2015), p. 124.

[4] M. Friesdorf, A. H. Werner, W. Brown, V. B. Scholz, and J. Eisert. "Many-body localisation implies that eigenvectors are matrix-product states". *Phys. Rev. Lett.* 114 (2015), p. 170505.

[5] M. Friesdorf, A. H. Werner, M. Goihl, J. Eisert, and W. Brown. "Local constants of motion imply transport" (2014). arXiv: 1412.5605.

[6] M. Gluza, C. Krumnow, M. Friesdorf, C. Gogolin, and J. Eisert. *Gaussification and equilibration in free Hamiltonian systems*. In preparation.

BOOKS

[7] R. Abraham and J. E. Marsden. *Foundations of mechanics*. Addison-Wesley, 1987.

[8] F. Schwabl. *Statistical mechanics*. Springer, 2006.

[9] N. Ashcroft and N. Mermin. *Solid state physics*. Philadelphia: Saunders College, 1976.

[10] N. Mott. *Metal-insulator transitions*. Taylor & Francis, 1990.

[11] A. L. Fetter and J. D. Walecka. *Quantum theory of many-particle systems*. Courier Corporation, 2003.

[12] M. E. Peskin and D. V. Schroeder. *An introduction to quantum field theory*. Westview Press, 1995.

[13] J. Gemmer, M. Michel, and G. Mahler. *Quantum thermodynamics: Emergence of thermodynamic behavior within composite quantum systems*. Springer, 2010.

[14] R. Bhatia. *Matrix analysis*. Springer Verlag, 1996.

[15] M. Reed and B. Simon. *Methods of modern mathematical physics*. Vol. 1. Academic Press, 1978.

[16] O. Bratteli and D. W. Robinson. *Operator algebras and quantum statistical mechanics 1*. Springer, 1987.

[17] G. D. Mahan. *Many particle physics*. Plenum Press, 1981.

[18] M. Paris and J. Rehacek. *Quantum state estimation*. Springer, 2004.

[19] S. Sachdev. *Quantum phase transitions*. Cambridge University Press, 1999.

[20] T. Kato. *Perturbation theory for linear operators*. Springer Verlag, 1995.

[21] H. E. Stanley. *Introduction to phase transitions and critical phenomena*. Oxford University Press, 1971.

[22] A. Messiah. *Quantum mechanics*. North-Holland Publishing Company, 1961.

[23] J. Shao. *Mathematical statistics*. Springer, 2003.

[24] J. H. van Lint and R. M. Wilson. *A course in combinatorics*. Cambridge University Press, 1992.

ARTICLES

[25] J. v. Neumann. "Beweis des Ergodensatzes und des H-Theorems in der neuen Mechanik". *Z. Phys.* 57 (1929), p. 30.

[26] A. Polkovnikov, K. Sengupta, A. Silva, and M. Vengalattore. "Non-equilibrium dynamics of closed interacting quantum systems". *Rev. Mod. Phys.* 83 (2011), p. 863.

[27] M. Greiner, O. Mandel, T. Esslinger, T. W. Hänsch, and I. Bloch. "Quantum phase transition from a superfluid to a Mott insulator in a gas of ultracold atoms". *Nature* 415 (2001), p. 39.

[28] S. Braun, J. P. Ronzheimer, M. Schreiber, S. S. Hodgman, T. Rom, I. Bloch, and U. Schneider. "Negative absolute temperature for motional degrees of freedom". *Science* 339 (2013), p. 52.

[29] J. P. Ronzheimer, M. Schreiber, S. Braun, S. S. Hodgman, S. Langer, I. P. McCulloch, F. Heidrich-Meisner, I. Bloch, and U. Schneider. "Expansion dynamics of interacting bosons in homogeneous lattices in one and two dimensions". *Phys. Rev. Lett.* 110 (2013), p. 205301.

[30] U. Schneider, L. Hackermuller, J. P. Ronzheimer, S. Will, S. Braun, T. Best, I. Bloch, E. Demler, S. Mandt, D. Rasch, and A. Rosch. "Fermionic transport and out-of-equilibrium dynamics in a homogeneous Hubbard model with ultracold atoms". *Nature Phys.* 8 (2012), p. 213.

[31] M. Cheneau, P. Barmettler, D. Poletti, M. Endres, P. Schauss, T. Fukuhara, C. Gross, I. Bloch, C. Kollath, and S. Kuhr. "Light-cone-like spreading of correlations in a quantum many-body system." *Nature* 481 (2012), p. 484.

[32] S. Trotzky, Y.-A. Chen, A. Flesch, I. P. McCulloch, U. Schollwöck, J. Eisert, and I. Bloch. "Probing the relaxation towards equilibrium in an isolated strongly correlated one-dimensional Bose gas". *Nature Phys.* 8 (2012), p. 325.

[33] M. Gring, M. Kuhnert, T. Langen, T. Kitagawa, B. Rauer, M. Schreitl, I. Mazets, D. A. Smith, E. Demler, and J. Schmiedmayer. "Relaxation and prethermalization in an isolated quantum system". *Science* 337 (2012), p. 1318.

[34] R. Geiger, T. Langen, I. E. Mazets, and J. Schmiedmayer. "Local relaxation and light-cone-like propagation of correlations in a trapped one-dimensional Bose gas". *New J. Phys.* 16 (2014), p. 053034.

[35] T. Langen, R. Geiger, M. Kuhnert, B. Rauer, and J. Schmiedmayer. "Local emergence of thermal correlations in an isolated quantum many-body system". *Nature Phys.* 9 (2013), p. 640.

[36] P. Jurcevic, B. P. Lanyon, P. Hauke, C. Hempel, P. Zoller, R. Blatt, and C. F. Roos. "Quasiparticle engineering and entanglement propagation in a quantum many-body system". *Nature* 511 (2014), p. 202.

[37] R. Blatt and C. F. Roos. "Quantum simulations with trapped ions". *Nature Phys.* 8 (2012), p. 277.

[38] R. Steinigeweg, A. Khodja, H. Niemeyer, C. Gogolin, and J. Gemmer. "Pushing the limits of the eigenstate thermalization hypothesis towards mesoscopic quantum systems". *Phys. Rev. Lett.* 112 (2014), p. 130403.

[39] S. Langer, F. Heidrich-Meisner, J. Gemmer, I. P. McCulloch, and U. Schollwöck. "Real-time study of diffusive and ballistic transport in spin-$\frac{1}{2}$ chains using the adaptive time-dependent density matrix renormalization group method". *Phys. Rev. B* 79 (2009), p. 214409.

[40] R. Steinigeweg, J. Gemmer, and W. Brenig. "Spin-Current autocorrelations from single pure-state propagation". *Phys. Rev. Lett.* 112 (2014), p. 120601.

[41] U. Schollwöck. "The density-matrix renormalization group in the age of matrix product states". *Ann. Phys.* 326 (2011), p. 96.

[42] C. Gogolin and J. Eisert. "Equilibration, thermalisation, and the emergence of statistical mechanics in closed quantum systems" (2015). arXiv: 1503.07538.

[43] V. Yukalov. "Equilibration and thermalization in finite quantum systems". *Laser Physics Letters* 8 (2011), p. 485.

[44] H. Tasaki. "From quantum dynamics to the canonical distribution: General picture and a rigorous example". *Phys. Rev. Lett.* 80 (1998), p. 1373.

[45] A. Flesch, M. Cramer, I. P. McCulloch, U. Schollwöck, and J. Eisert. "Probing local relaxation of cold atoms in optical superlattices". *Phys. Rev. A* 78 (2008), p. 033608.

[46] D. M. Basko, I. L. Aleiner, and B. L. Altshuler. "Metal-insulator transition in a weakly interacting many-electron system with localized single-particle states". *Ann. Phys.* 321 (2006), p. 1126.

[47] D. M. Basko, I. L. Aleiner, and B. L. Altshuler. "On the problem of many-body localization". In: *Problems of Condensed Matter Physics*. Ed. by A. L. Ivanov and S. G. Tikhodeev. Oxford University Press, 2006. arXiv: cond-mat/0602510.

[48] P. W. Anderson. "Absence of diffusion in certain random lattices". *Phys. Rev.* 109 (1958), p. 1492.

[49] A. Polkovnikov. "Universal adiabatic dynamics in the vicinity of a quantum critical point". *Phys. Rev. B* 72 (2005), p. 161201.

[50] E. J. Torres-Herrera and L. F. Santos. "Local quenches with global effects in interacting quantum systems". *Phys. Rev. E* 89 (2014), p. 062110.

[51] P. Calabrese and J. Cardy. "Time dependence of correlation functions following a quantum quench". *Phys. Rev. Lett.* 96 (2006), p. 136801.

[52] J. Mossel, G. Palacios, and J.-S. Caux. "Geometric quenches in quantum integrable systems". *J. Stat. Mech.* (2010), p. L09001.

[53] V. Alba and F. Heidrich-Meisner. "Entanglement spreading after a geometric quench in quantum spin chains". *Phys. Rev. B* 90 (2014), p. 075144.

[54] A. Eckardt, C. Weiss, and M. Holthaus. "Superfluid-insulator transition in a periodically driven optical lattice". *Phys. Rev. Lett.* 95 (2005), p. 260404.

[55] T. Kitagawa, E. Berg, M. Rudner, and E. Demler. "Topological characterization of periodically driven quantum systems". *Phys. Rev. B* 82 (2010), p. 235114.

[56] C. A. Fuchs and J. van de Graaf. "Cryptographic distinguishability measures for quantum mechanical states" (2009). arXiv: quant-ph/9712042.

[57] W. Matthews, S. Wehner, and A. Winter. "Distinguishability of quantum states under restricted families of measurements with an application to quantum data hiding". *Commun. Math. Phys.* 291 (2009), p. 813.

[58] A. S. L. Malabarba, L. P. Garcia-Pintos, N. Linden, T. C. Farrelly, and A. J. Short. "Quantum systems equilibrate rapidly for most observables". *Phys. Rev. E* 90 (2014), p. 012121.

[59] A. J. Short. "Equilibration of quantum systems and subsystems". *New J. Phys.* 13 (2011), p. 053009.

[60] F. Meinert, M. J. Mark, E. Kirilov, K. Lauber, P. Weinmann, A. J. Daley, and H.-C. Nägerl. "Quantum quench in an atomic one-dimensional Ising chain". *Phys. Rev. Lett.* 111 (2013), p. 053003.

[61] S. Langer, M. Heyl, I. P. McCulloch, and F. Heidrich-Meisner. "Real-time energy dynamics in spin-$\frac{1}{2}$ Heisenberg chains". *Phys. Rev. B* 84 (2011), p. 205115.

[62] I. Bloch, J. Dalibard, and W. Zwerger. "Many-body physics with ultracold gases". *Rev. Mod. Phys.* 80 (2008), p. 885.

[63] M. Endres, M. Cheneau, T. Fukuhara, C. Weitenberg, P. Schauss, C. Gross, L. Mazza, M.-C. Bañuls, L. Pollet, I. Bloch, and S. Kuhr. "Single-site- and single-atom-resolved measurement of correlation functions". *App. Phys. B* 113 (2013), p. 27.

[64] A. Aspuru-Guzik and P. Walther. "Photonic quantum simulators". *Nature Phys.* 8 (2012), p. 285.

[65] S. Bravyi, M. B. Hastings, and F. Verstraete. "Lieb-Robinson bounds and the generation of correlations and topological quantum order". *Phys. Rev. Lett.* 97 (2006), p. 050401.

[66] M. B. Hastings and T. Koma. "Spectral gap and exponential decay of correlations". *Commun. Math. Phys.* 265 (2006), p. 781.

[67] J. Eisert, M. van den Worm, S. R. Manmana, and M. Kastner. "Breakdown of quasilocality in long-range quantum lattice models". *Phys. Rev. Lett.* 111 (2013), p. 260401.

[68] C. Gogolin, M. P. Müller, and J. Eisert. "Absence of thermalization in non-integrable systems". *Phys. Rev. Lett.* 106 (2011), p. 040401.

[69] N. Linden, S. Popescu, A. J. Short, and A. Winter. "Quantum mechanical evolution towards thermal equilibrium". *Phys. Rev. E* 79 (2009), p. 061103.

[70] P. Reimann. "Foundation of statistical mechanics under experimentally realistic conditions". *Phys. Rev. Lett.* 101 (2008), p. 190403.

[71] A. J. Short and T. C. Farrelly. "Quantum equilibration in finite time". *New J. Phys.* 14 (2012), p. 013063.

[72] M. Rigol, V. Dunjko, V. Yurovsky, and M. Olshanii. "Relaxation in a completely integrable many-body quantum system: An ab initio study of the dynamics of the highly excited states of 1D lattice hard-core bosons". *Phys. Rev. Lett.* 98 (2007), p. 050405.

[73] M. Cramer, C. M. Dawson, J. Eisert, and T. J. Osborne. "Exact relaxation in a class of non-equilibrium quantum lattice systems". *Phys. Rev. Lett.* 100 (2008), p. 030602.

[74] J.-S. Caux and F. H. L. Essler. "Time evolution of local observables after quenching to an integrable model". *Phys. Rev. Lett.* 110 (2013), p. 257203.

[75] M. Cramer and J. Eisert. "A quantum central limit theorem for non-equilibrium systems: Exact local relaxation of correlated states". *New J. Phys.* 12 (2010), p. 055020.

[76] M. Schreiber, S. S. Hodgman, P. Bordia, H. P. Lüschen, M. H. Fischer, R. Vosk, E. Altman, U. Schneider, and I. Bloch. "Observation of many-body localization of interacting fermions in a quasi-random optical lattice" (2015). arXiv: 1501.05661.

[77] G. Adesso, S. Ragy, and A. R. Lee. "Continuous variable quantum information: Gaussian states and beyond". *Open Syst. Inf. Dyn.* 21 (2014), p. 1440001.

[78] C. Weedbrook, S. Pirandola, R. Garcia-Patron, N. J. Cerf, T. C. Ralph, J. H. Shapiro, and S. Lloyd. "Gaussian quantum information". *Rev. Mod. Phys.* 84 (2012), p. 621.

[79] S. Bravyi. "Lagrangian representation for fermionic linear optics". *Quantum Inf. and Comp.* 5 (2005), p. 3.

[80] S. Aaronson and A. Arkhipov. "The computational complexity of linear optics" (2011). arXiv: 1011.3245.

[81] C. Gogolin, M. Kliesch, L. Aolita, and J. Eisert. "Boson-Sampling in the light of sample complexity" (2013). arXiv: 1306.3995.

[82] S. Aaronson and A. Arkhipov. "BosonSampling is far from uniform" (2013). arXiv: 1309.7460.

[83] I. Peschel and V. Eisler. "Reduced density matrices and entanglement entropy in free lattice models". *J. Phys. A: Math. Theor.* 42 (2009), p. 504003.

[84] P. Calabrese, F. H. Essler, and M. Fagotti. "Quantum quench in the transverse field Ising chain II: Stationary state properties". *J. Stat. Mech.* (2012), P07022.

[85] M. Fagotti and F. H. L. Essler. "Reduced density matrix after a quantum quench". *Phys. Rev. B* 87 (24 2013), p. 245107.

[86] H. Kim, M. Carmen Banuls, J. Ignacio Cirac, M. B. Hastings, and D. A. Huse. "Slowest local operators in quantum spin chains" (2014). arXiv: 1410.4186.

[87] J. P. Keating, N. Linden, and H. J. Wells. "Spectra and eigenstates of spin chain Hamiltonians". *Commun. Math. Phys.* 338 (2015), p. 1.

[88] D. A. Rabson, B. N. Narozhny, and A. J. Millis. "Crossover from Poisson to Wigner-Dyson level statistics in spin chains with integrability breaking". *Phys. Rev. B* 69 (2004), p. 054403.

[89] J.-S. Caux and J. Mossel. "Remarks on the notion of quantum integrability". *J. Stat. Mech.* (2011), P02023.

[90] J. Watrous. "Quantum computational complexity" (2008). arXiv: 0804.3401.

[91] R. Horodecki, P. Horodecki, M. Horodecki, and K. Horodecki. "Quantum entanglement". *Rev. Mod. Phys.* 81 (2009), p. 865.

[92] M. B. Plenio and S. Virmani. "An introduction to entanglement measures". *Quant. Inf. Comput.* 7 (2007), p. 1.

[93] B. Nachtergaele and R. Sims. "Lieb-Robinson bounds and the exponential clustering theorem". *Commun. Math. Phys.* 265 (2006), p. 119.

[94] B. Nachtergaele and R. Sims. "Locality estimates for quantum spin systems". In: *Selected contributions of the XVth International Congress on Mathematical Physics*. Ed. by V. E. Sidoravicius. Springer, 2009, p. 591.

[95] M. B. Hastings. "An area law for one dimensional quantum systems". *J. Stat. Mech.* (2007), P08024.

[96] I. Arad, A. Kitaev, Z. Landau, and U. Vazirani. "An area law and sub-exponential algorithm for 1D systems" (2013). arXiv: 1301.1162.

[97] E. Hamza, S. Michalakis, B. Nachtergaele, and R. Sims. "Approximating the ground state of gapped quantum spin systems". *J. Math. Phys.* 50 (2009), p. 095213.

[98] J. Eisert, M. Cramer, and M. B. Plenio. "Area laws for the entanglement entropy". *Rev. Mod. Phys.* 82 (2010), p. 277.

[99] N. de Beaudrap, T. J. Osborne, and J. Eisert. "Ground states of unfrustrated spin Hamiltonians satisfy an area law". *New J. Phys.* 12 (2010), p. 095007.

[100] M. Cramer, J. Eisert, M. B. Plenio, and J. Dreißig. "Entanglement-area law for general bosonic harmonic lattice systems". *Phys. Rev. A* 73 (2006), p. 012309.

[101] F. G. Brandao and M. Cramer. "Entanglement area law from specific heat capacity" (2014). arXiv: 1409.5946.

[102] F. G. S. L. Brandao and M. Horodecki. "An area law for entanglement from exponential decay of correlations". *Nature Phys.* 9 (2013), p. 721.

[103] Y. Ge and J. Eisert. "Area laws and efficient descriptions of quantum many-body states" (2014). arXiv: 1411.2995.

[104] D. Perez-Garcia, F. Verstraete, M. Wolf, and J. Cirac. "Matrix product state representations". *Quantum Inf. Comput.* 7 (2007), p. 401.

[105] P. Reimann and M. Kastner. "Equilibration of isolated macroscopic quantum systems". *New J. Phys.* 14 (2012), p. 043020.

[106] S. Goldstein, T. Hara, and H. Tasaki. "Time scales in the approach to equilibrium of macroscopic quantum systems". *Phys. Rev. Lett.* 111 (14 2013), p. 140401.

[107] M. Schiulaz, A. Silva, and M. Mueller. "Dynamics in many-body localized quantum systems without disorder". *Phys. Rev. B* 91 (2015), p. 184202.

[108] N. Y. Yao, C. R. Laumann, J. I. Cirac, M. D. Lukin, and J. E. Moore. "Quasi many-body localization in translation invariant systems" (2014). arXiv: 1410.7407.

[109] T. J. Osborne and N. Linden. "Propagation of quantum information through a spin system". *Phys. Rev. A* 69 (2004), p. 052315.

[110] E. H. Lieb and D. W. Robinson. "The finite group velocity of quantum spin systems". *Commun. Math. Phys.* 28 (1972), p. 251.

[111] T. Barthel and M. Kliesch. "Quasilocality and efficient simulation of Markovian quantum dynamics". *Phys. Rev. Lett.* 108 (2012), p. 230504.

[112] M. Kliesch, C. Gogolin, and J. Eisert. "Lieb-Robinson Bounds and the simulation of time-evolution of local observables in lattice systems". In: *Many-Electron Approaches in Physics, Chemistry and Mathematics*. Ed. by V. Bach and L. Delle Site. Mathematical Physics Studies. Springer, 2014, p. 301.

[113] M. Cramer, A. Serafini, and J. Eisert. "Locality of dynamics in general harmonic quantum systems". In: *Quantum information and many body quantum systems*. Ed. by M. Ericsson and S. Montangero. Publications of the Scuola Normale Superiore, CRM Series, 8, 2008, p. 51.

[114] S. Bachmann, S. Michalakis, B. Nachtergaele, and R. Sims. "Automorphic equivalence within gapped phases of quantum lattice systems". *Commun. Math. Phys.* 309 (2012), p. 835.

[115] S. Michalakis. "Stability of the area law for the entropy of entanglement" (2012). arXiv: 1206.6900.

[116] S. Bravyi, M. B. Hastings, and S. Michalakis. "Topological quantum order: Stability under local perturbations". *J. Math. Phys.* 51 (2010), p. 093512.

[117] S. Michalakis and J. Pytel. "Stability of frustration-free Hamiltonians". *Commun. Math. Phys.* 322 (2013), p. 277.

[118] J. Eisert and D. Gross. "Supersonic quantum communication". *Phys. Rev. Lett.* 102 (2009), p. 240501.

[119] C. Gogolin. "Equilibration and thermalization in quantum systems". PhD thesis. FU Berlin, 2014.

[120] P. Barmettler, D. Poletti, M. Cheneau, and C. Kollath. "Propagation front of correlations in an interacting Bose gas". *Phys. Rev. A* 85 (2012), p. 053625.

[121] H. F. Trotter. "On the product of semi-groups of operators". *Proc. Amer. Math. Soc.* 10 (1959), p. 545.

[122] M. L. Wall and L. D. Carr. "Open source TEBD" (2013). URL: http://physics.mines.edu/downloads/software/tebd%20(2009).

[123] J. Eisert and T. J. Osborne. "General entanglement scaling laws from time evolution". *Phys. Rev. Lett.* 97 (2006), p. 150404.

[124] K. Van Acoleyen, M. Mariën, and F. Verstraete. "Entanglement rates and area laws". *Phys. Rev. Lett.* 111 (2013), p. 170501.

[125] S. Goldstein, J. L. Lebowitz, C. Mastrodonato, R. Tumulka, and N. Zanghi. "Normal typicality and von Neumann's quantum ergodic theorem". *Proc. R. Soc.* 466 (2010), p. 3203.

[126] M. Cramer. "Thermalization under randomized local Hamiltonians". *New J. Phys.* 14 (2012), p. 053051.

[127] S. Goldstein, J. L. Lebowitz, C. Mastrodonato, R. Tumulka, and N. Zanghi. "Approach to thermal equilibrium of macroscopic quantum systems". *Phys. Rev. E* 81 (2010), p. 011109.

[128] R. V. Jensen and R. Shankar. "Statistical behavior in deterministic quantum systems with few degrees of freedom". *Phys. Rev. Lett.* 54 (1985), p. 1879.

[129] M. Srednicki. "Chaos and quantum thermalization". *Phys. Rev. E* 50 (1994), p. 888.

[130] J. M. Deutsch. "Quantum statistical mechanics in a closed system". *Phys. Rev. A* 43 (1991), p. 2046.

[131] M. Rigol, V. Dunjko, and M. Olshanii. "Thermalization and its mechanism for generic isolated quantum systems". *Nature* 452 (2008), p. 854.

[132] W. Beugeling, R. Moessner, and M. Haque. "Finite-size scaling of eigenstate thermalization". *Phys. Rev. E* 89 (4 2014), p. 042112.

[133] A. Khodja, R. Steinigeweg, and J. Gemmer. "Relevance of the eigenstate thermalization hypothesis for thermal relaxation". *Phys. Rev. E* 91 (2015), p. 012120.

[134] G. De Palma, A. Serafini, V. Giovannetti, and M. Cramer. "The necessity of eigenstate thermalization" (2015). arXiv: 1506.07265.

[135] A. Riera, C. Gogolin, and J. Eisert. "Thermalization in nature and on a quantum computer". *Phys. Rev. Lett.* 108 (2012), p. 080402.

[136] M. P. Mueller, E. Adlam, L. Masanes, and N. Wiebe. "Thermalization and canonical typicality in translation-invariant quantum lattice systems" (2013). arXiv: 1312.7420.

[137] F. G. Brandao and M. Cramer. "Equivalence of statistical mechanical ensembles for non-critical quantum systems" (2015). arXiv: 1502.03263.

[138] L. F. Santos, A. Polkovnikov, and M. Rigol. "Entropy of isolated quantum systems after a quench". *Phys. Rev. Lett.* 107 (4 2011), p. 040601.

[139] E. J. Torres-Herrera and L. F. Santos. "Quench dynamics of isolated many-body quantum systems". *Phys. Rev. A* 89 (4 2014), p. 043620.

[140] E. J. Torres-Herrera, D. Kollmar, and L. F. Santos. "Relaxation and thermalization of isolated many-body quantum systems" (2014). arXiv: 1403.6481.

[141] M. Kliesch, C. Gogolin, M. J. Kastoryano, A. Riera, and J. Eisert. "Locality of temperature". *Phys. Rev. X* 4 (2014), p. 031019.

[142] A. Lagendijk, B. van Tiggelen, and D. S. Wiersma. "Fifty years of Anderson localization". *Physics Today* 62 (2009), p. 24.

[143] D. Hundertmark. *A short introduction to Anderson localization*. 2007. URL: http://www.math.uiuc.edu/~dirk/preprints/localization3.pdf.

[144] G. Roati, C. D'Errico, L. Fallani, M. Fattori, C. Fort, M. Zaccanti, G. Modugno, M. Modugno, and M. Inguscio. "Anderson localization of a non-interacting Bose-Einstein condensate". *Nature* 453 (2008), p. 895.

[145] F. Jendrzejewski, A. Bernard, K. Muller, P. Cheinet, V. Josse, M. Piraud, L. Pezze, L. Sanchez-Palencia, A. Aspect, and P. Bouyer. "Three-dimensional localization of ultracold atoms in an optical disordered potential". *Nature Phys.* 8 (2012), p. 398.

[146] J. Billy, V. Josse, Z. Zuo, A. Bernard, B. Hambrecht, P. Lugan, D. Clement, L. Sanchez-Palencia, P. Bouyer, and A. Aspect. "Direct observation of Anderson localization of matter waves in a controlled disorder". *Nature* 453 (2008), p. 891.

[147] W. Kirsch. "An invitation to random Schroedinger operators" (2007). arXiv: 0709.3707.

[148] G. Stolz. "An introduction to the mathematics of Anderson localization". In: *Entropy and the Quantum II*. Vol. 552. Contemp. Math. American Mathematical Society, 2011.

[149] S. S. Kondov, W. R. McGehee, J. J. Zirbel, and B. DeMarco. "Three-dimensional Anderson localization of ultracold matter". *Science* 334 (2011), p. 66.

[150] G. Semeghini, M. Landini, P. Castilho, S. Roy, G. Spagnolli, A. Trenkwalder, M. Fattori, M. Inguscio, and G. Modugno. "Measurement of the mobility edge for 3D Anderson localization". *Nature Phys.* 11 (2015), pp. 554–559.

[151] M. Znidaric, T. Prosen, and P. Prelovsek. "Many-body localization in the Heisenberg XXZ magnet in a random field". *Phys. Rev. B* 77 (2008), p. 064426.

[152] J. H. Bardarson, F. Pollmann, and J. E. Moore. "Unbounded growth of entanglement in models of many-body localization". *Phys. Rev. Lett.* 109 (2012), p. 017202.

[153] A. Pal and D. A. Huse. "The many-body localization transition". *Phys. Rev. B* 82 (2010), p. 174411.

[154] E. Lieb, T. Schultz, and D. Mattis. "Two soluble models of an antiferromagnetic chain". *Ann. Phys.* 16 (1961), p. 407.

[155] J. T. Seeley, M. J. Richard, and P. J. Love. "The Bravyi-Kitaev transformation for quantum computation of electronic structure". *J. Chem. Phys.* 137 (2012), p. 224109.

[156] C. K. Burrell and T. J. Osborne. "Bounds on the speed of information propagation in disordered quantum spin chains". *Phys. Rev. Lett.* 99 (2007), p. 167201.

[157] E. Hamza, R. Sims, and G. Stolz. "Dynamical localization in disordered quantum spin systems". *Commun. Math. Phys.* 315 (2012), p. 215.

[158] L. Pastur and V. Slavin. "Area law scaling for the entropy of disordered quasifree fermions". *Phys. Rev. Lett.* 113 (2014), p. 150404.

[159] H. Abdul-Rahman and G. Stolz. "A uniform area law for the entanglement of eigenstates in the disordered XY chain" (2015). arXiv: 1505.02117.

[160] I. V. Gornyi, A. D. Mirlin, and D. G. Polyakov. "Interacting Electrons in Disordered Wires: Anderson Localization and Low-T Transport". *Phys. Rev. Lett.* 95 (20 2005), p. 206603.

[161] R. Nandkishore and D. A. Huse. "Many body localization and thermalization in quantum statistical mechanics". *Annu. Rev. Condens. Matter Phys.* 6 (2015), p. 15.

[162] M. Serbyn and D. A. Papić Z.and Abanin. "Universal slow growth of entanglement in interacting strongly disordered systems". *Phys. Rev. Lett.* 110 (2013), p. 260601.

[163] D. A. Huse, R. Nandkishore, and V. Oganesyan. "Phenomenology of fully many-body-localized systems". *Phys. Rev. B* 90 (2014), p. 174202.

[164] M. Serbyn, Z. Papić, and D. A. Abanin. "Local conservation laws and the structure of the many-body localized states". *Phys. Rev. Lett.* 111 (2013), p. 127201.

[165] A. Chandran, I. H. Kim, G. Vidal, and D. A. Abanin. "Constructing local integrals of motion in the many-body localized phase". *Phys. Rev. B* 91 (2015), p. 085425.

[166] I. H. Kim, A. Chandran, and D. A. Abanin. "Local integrals of motion and the logarithmic lightcone in many-body localized systems" (2014). arXiv: 1412.3073.

[167] S. Gopalakrishnan, M. Mueller, V. Khemani, M. Knap, E. Demler, and D. A. Huse. "Low-frequency conductivity in many-body localized systems" (2015). arXiv: 1502.07712.

[168] M. B. Hastings. "Quasi-adiabatic continuation for disordered systems: Applications to correlations, Lieb-Schultz-Mattis, and Hall conductance" (2010). arXiv: 1001.5280.

[169] A. Nanduri, H. Kim, and D. A. Huse. "Entanglement spreading in a many-body localized system". *Phys. Rev. B* 90 (2014), p. 064201.

[170] J. Allcock and N. Linden. "Quantum communication beyond the localization length in disordered spin chains". *Phys. Rev. Lett.* 102 (2009), p. 110501.

[171] D. J. Luitz, N. Laflorencie, and F. Alet. "Many-body localization edge in the random-field Heisenberg chain". *Phys. Rev. B* 91 (2015), p. 081103.

[172] V. Kravtsov. "Random matrix theory: Wigner-Dyson statistics and beyond" (2009). arXiv: 0911.0639.

[173] V. Oganesyan and D. A. Huse. "Localization of interacting fermions at high temperature". *Phys. Rev. B* 75 (2007), p. 155111.

[174] B. Bauer and C. Nayak. "Area laws in a many-body localized state and its implications for topological order". *J. Stat. Mech.* (2013), P09005.

[175] S. Bera, H. Schomerus, F. Heidrich-Meisner, and J. H. Bardarson. "Many-body localization characterized from a one-particle perspective" (2015). arXiv: 1503.06147.

[176] J. Goold, S. R. Clark, C. Gogolin, J. Eisert, A. Scardicchio, and A. Silva. "Total correlations of the diagonal ensemble herald the many-body localization transition" (2015). arXiv: 1504.06872.

[177] F. Verstraete and J. I. Cirac. "Matrix product states represent ground states faithfully". *Phys. Rev. B* 73 (2006), p. 094423.

[178] D. A. Huse, R. Nandkishore, V. Oganesyan, A. Pal, and S. L. Sondhi. "Localization-protected quantum order". *Phys. Rev. B* 88 (2013), p. 014206.

[179] J. A. Kjall, J. H. Bardarson, and F. Pollmann. "Many-body localization in a disordered quantum Ising chain". *Phys. Rev. Lett.* 113 (2014), p. 107204.

[180] A. Chandran, J. Carrasquilla, I. H. Kim, D. A. Abanin, and G. Vidal. "Spectral tensor networks for many-body localization" (2014). arXiv: 1410.0687.

[181] J. Z. Imbrie. "On many-body localization for quantum spin chains" (2014). arXiv: 1403.7837.

[182] D. Pekker and B. K. Clark. "Encoding the structure of many-body localization with matrix product operators" (2014). arXiv: 1410.2224.

[183] F. Pollmann, V. Khemani, J. I. Cirac, and S. L. Sondhi. "Efficient variational diagonalization of fully many-body localized Hamiltonians" (2015). arXiv: 1506.07179.

[184] M. Serbyn, M. Knap, S. Gopalakrishnan, Z. Papić, N. Y. Yao, C. R. Laumann, D. A. Abanin, M. D. Lukin, and E. A. Demler. "Interferometric probes of many-body localization". *Phys. Rev. Lett.* 113 (2014), p. 147204.

[185] G. Biroli and J. P. Garrahan. "Perspective: The glass transition" (2013). arXiv: 1303.3542.

[186] I. H. Kim and J. Haah. "Localization from superselection rules in translation invariant systems" (2015). arXiv: 1505.01480.

[187] M. van Horssen, E. Levi, and J. P. Garrahan. "Dynamics of many-body localisation in a translation invariant quantum glass model" (2015). arXiv: 1505.07089.

[188] Z. Papic, E. M. Stoudenmire, and D. A. Abanin. "Is many-body localization possible in the absence of disorder?" (2015). arXiv: 1501.00477.

[189] A. J. Daley, H. Pichler, J. Schachenmayer, and P. Zoller. "Measuring entanglement growth in quench dynamics of bosons in an optical lattice". *Phys. Rev. Lett.* 109 (2012), p. 020505.

[190] M. Cramer, A. Bernard, N. Fabbri, L. Fallani, C. Fort, S. Rosi, F. Caruso, M. Inguscio, and M. Plenio. "Spatial entanglement of bosons in optical lattices". *Nat. Commun.* 4 (2013), p. 3161.

[191] R. Orús. "A practical introduction to tensor networks: Matrix product states and projected entangled pair states". *Ann. Phys.* 349 (2014), p. 117.

[192] R. Feynman. "Simulating physics with computers". *Int. J. Th. Phys.* 21 (1982), p. 467.

[193] J. Ignacio Cirac and P. Zoller. "Goals and opportunities in quantum simulation". *Nature Phys.* 8 (2012), p. 264.

[194] I. Bloch, J. Dalibard, and S. Nascimbene. "Quantum simulations with ultracold quantum gases". *Nature Phys.* 8 (2012), p. 267.

[195] S. Trotzky, L. Pollet, F. Gerbier, U. Schnorrberger, I. Bloch, N. Prokof'ev, B. Svistunov, and M. Troyer. "Suppression of the critical temperature for superfluidity near the Mott transition: Validating a quantum simulator". *Nature Phys.* 6 (2010), p. 998.

[196] B. P. Lanyon, C. Hempel, D. Nigg, M. Müller, R. Gerritsma, F. Zähringer, P. Schindler, J. T. Barreiro, M. Rambach, G. Kirchmair, M. Hennrich, P. Zoller, R. Blatt, and C. F. Roos. "Universal digital quantum simulation with trapped ions". *Science* 334 (2011), p. 57.

[197] P. Schindler, J. T. Barreiro, T. Monz, V. Nebendahl, D. Nigg, M. Chwalla, M. Hennrich, and R. Blatt. "Experimental repetitive quantum error correction". *Science* 332 (2011), p. 1059.

[198] A. Polkovnikov and V. Gritsev. "Breakdown of the adiabatic limit in low dimensional gapless systems". *Nature Phys.* (2008), p. 477.

[199] G. M. D'Ariano, M. G. A. Paris, and M. F. Sacchi. "Quantum tomography". *Adv. Imag. Elec. Phys.* 128 (2003), p. 205.

[200] D. Gross, Y.-K. Liu, S. T. Flammia, S. Becker, and J. Eisert. "Quantum state tomography via compressed sensing". *Phys. Rev. Lett.* 105 (2010), p. 150401.

[201] S. T. Flammia, D. Gross, Y.-K. Liu, and J. Eisert. "Quantum tomography via compressed sensing: Error bounds, sample complexity, and efficient estimators". *New J. Phys.* 14 (2012), p. 095022.

[202] M. Cramer, M. B. Plenio, S. T. Flammia, R. Somma, D. Gross, S. D. Bartlett, O. Landon-Cardinal, D. Poulin, and Y.-K. Liu. "Efficient quantum state tomography". *Nat. Comm.* 1 (2010), p. 149.

[203] T. Baumgratz, D. Gross, M. Cramer, and M. B. Plenio. "Scalable reconstruction of density matrices". *Phys. Rev. Lett.* 111 (2013), p. 020401.

[204] P. Hauke, F. M. Cucchietti, L. Tagliacozzo, I. Deutsch, and M. Lewenstein. "Can one trust quantum simulators?" *Rep. Prog. Phys.* 75 (2012), p. 082401.

[205] L. Aolita, C. Gogolin, M. Kliesch, and J. Eisert. "Reliable quantum certification for photonic quantum technologies" (2014). arXiv: 1407.4817.

[206] D. Jaksch, C. Bruder, J. I. Cirac, C. W. Gardiner, and P. Zoller. "Cold bosonic atoms in optical lattices". *Phys. Rev. Lett.* 81 (1998), p. 3108.

[207] R. Jördens, N. Strohmaier, K. Günter, H. Moritz, and T. Esslinger. "A Mott insulator of fermionic atoms in an optical lattice". *Nature* 455 (2008), p. 204.

[208] U. Schneider, L. Hackermuller, S. Will, T. Best, I. Bloch, T. A. Costi, R. W. Helmes, D. Rasch, and A. Rosch. "Metallic and insulating phases of repulsively interacting fermions in a 3D optical lattice". *Science* 322 (2008), p. 1520.

[209] A. M. Rey. "PhD thesis: Ultracold bosonic atoms in optical lattices" (2004).

[210] C. Chin, R. Grimm, P. Julienne, and E. Tiesinga. "Feshbach resonances in ultracold gases". *Rev. Mod. Phys.* 82 (2010), p. 1225.

[211] E. Toth, A. M. Rey, and P. B. Blakie. "Theory of correlations between ultracold bosons released from an optical lattice". *Phys. Rev. A* 78 (2008), p. 013627.

[212] F. Gerbier, S. Trotzky, S. Fölling, U. Schnorrberger, J. D. Thompson, A. Widera, I. Bloch, L. Pollet, M. Troyer, B. Capogrosso-Sansone, N. V. Prokof'ev, and B. V. Svistunov. "Expansion of a quantum gas released from an optical lattice". *Phys. Rev. Lett.* 101 (2008), p. 155303.

[213] J. Eisert, F. G. Brandao, and K. M. Audenaert. "Quantitative entanglement witnesses". *New J. Phys.* 9 (2007), p. 46.

[214] N. Schuch, F. Verstraete, and J. I. Cirac. "Quantum entanglement theory in the presence of superselection rules". *Phys. Rev. A* 70 (2004), p. 042310.

[215] W. S. Bakr, A. Peng, M. E. Tai, R. Ma, J. Simon, J. I. Gillen, S. Fölling, L. Pollet, and M. Greiner. "Probing the superfluid-to-Mott insulator transition at the single-atom level". *Science* 329 (2010), p. 547.

[216] E. Haller, J. Hudson, A. Kelly, D. A. Cotta, B. Peaudecerf, G. D. Bruce, and S. Kuhr. "Single-atom imaging of fermions in a quantum-gas microscope" (2015). arXiv: 1503.02005.

[217] E. Altman, E. Demler, and M. D. Lukin. "Probing many-body states of ultracold atoms via noise correlations". *Phys. Rev. A* 70 (2004), p. 013603.

[218] S. Fölling, F. Gerbier, A. Widera, O. Mandel, T. Gericke, and I. Bloch. "Spatial quantum noise interferometry in expanding ultracold atom clouds". *Nature* 434 (2005), p. 481.

[219] S. Fölling. "Quantum noise correlation experiments with ultracold atoms" (2014). arXiv: 1403.6842.

[220] S. S. Natu, D. C. McKay, B. DeMarco, and E. J. Mueller. "Evolution of condensate fraction during rapid lattice ramps". *Phys. Rev. A* 85 (2012), p. 061601.

[221] S. Trotzky, Y.-A. Chen, A. Flesch, I. P. McCulloch, U. Schollwöck, J. Eisert, and I. Bloch. "Probing the relaxation towards equilibrium in an isolated strongly correlated one-dimensional Bose gas". *Nature Phys.* 8 (2012), p. 325.

[222] T. W. B. Kibble. "Topology of cosmic domains and strings". *J. Phys. A: Math. Gen.* 9 (1976), p. 1387.

[223] T. W. B. Kibble. "Some implications of a cosmological phase transition". *Phys. Rep.* 67 (1980), p. 183.

[224] W. H. Zurek. "Cosmological experiments in superfluid helium?" *Nature* 317 (1985), p. 505.

[225] W. H. Zurek, U. Dorner, and P. Zoller. "Dynamics of a quantum phase transition". *Phys. Rev. Lett.* 95 (2005), p. 105701.

[226] G. Lamporesi, S. Donadello, S. Serafini, F. Dalfovo, and G. Ferrari. "Spontaneous creation of Kibble-Zurek solitons in a Bose-Einstein condensate". *Nature Phys.* 9 (2013), p. 656.

[227] V. M. H. Ruutu, V. B. Eltsov, A. J. Gill, T. W. B. Kibble, M. Krusius, Y. G. Makhlin, B. Placais, G. E. Volovik, and W. Xu. "Vortex formation in neutron-irradiated superfluid 3 He as an analogue of cosmological defect formation". *Nature* 382 (1996), p. 334.

[228] S. Ulm, J. Roßnagel, G. Jacob, C. Degünther, S. T. Dawkins, U. G. Poschinger, R. Nigmatullin, A. Retzker, M. B. Plenio, F. Schmidt-Kaler, and K. Singer. "Observation of the Kibble-Zurek scaling law for defect formation in ion crystals". *Nat. Comm.* 4 (2013), p. 2290.

[229] K. Pyka, J. Keller, H. L. Partner, R. Nigmatullin, T. Burgermeister, D. M. Meier, K. Kuhlmann, A. Retzker, M. B. Plenio, W. H. Zurek, A. del Campo, and T. Mehlstäubler. "Topological defect formation and spontaneous symmetry breaking in ion Coulomb crystals". *Nat. Comm.* 4 (2013), p. 2291.

[230] L. Cincio, J. Dziarmaga, M. M. Rams, and W. H. Zurek. "Entropy of entanglement and correlations induced by a quench: Dynamics of a quantum phase transition in the quantum Ising model". *Phys. Rev. A* 75 (2007), p. 052321.

[231] J. Dziarmaga, M. Tylutki, and W. H. Zurek. "Dynamics of the Mott insulator to superfluid quantum phase transition in the truncated Wigner approximation". *Phys. Rev. B* 86 (2012), p. 144521.

[232] M. P. A. Fisher, P. B. Weichman, G. Grinstein, and D. S. Fisher. "Boson localization and the superfluid-insulator transition". *Phys. Rev. B* 40 (1989), p. 546.

[233] P. B. Weichman. "Crossover scaling in a dilute bose superfluid near zero temperature". *Phys. Rev. B* 38 (1988), p. 8739.

[234] T. D. Kühner and H. Monien. "Phases of the one-dimensional Bose-Hubbard model". *Phys. Rev. B* 58 (1998), R14741.

[235] A. S. Ferreira and M. A. Continentino. "Mean-field renormalization-group approach to the boson Hubbard model". *Phys. Rev. B* 66 (2002), p. 014525.

[236] F. G. Brandao and A. W. Harrow. "Product-state approximations to quantum ground states". In: *Proceedings of the Forty-fifth Annual ACM Symposium on Theory of Computing*. STOC '13. ACM, 2013, p. 871.

[237] B. Capogrosso-Sansone, S. G. Söyler, N. Prokof'ev, and B. Svistunov. "Monte Carlo study of the two-dimensional Bose-Hubbard model". *Phys. Rev. A* 77 (2008), p. 015602.

[238] J. Carrasquilla, S. R. Manmana, and M. Rigol. "Scaling of the gap, fidelity susceptibility, and Bloch oscillations across the superfluid-to-Mott-insulator transition in the one-dimensional Bose-Hubbard model". *Phys. Rev. A* 87 (2013), p. 043606.

[239] M. P. Kennett. "Out-of-equilibrium dynamics of the Bose-Hubbard model". *ISRN Condensed Matter Physics* (2013), p. 393616.

[240] J. Dziarmaga. "Dynamics of a quantum phase transition and relaxation to a steady state". *Adv. Phys.* 59 (2010), p. 1063.

[241] M. Campostrini, M. Hasenbusch, A. Pelissetto, P. Rossi, and E. Vicari. "Critical behavior of the three-dimensional XY universality class". *Phys. Rev. B* 63 (2001), p. 214503.

[242] J. Avron and A. Elgart. "Adiabatic theorem without a gap condition". *Commun. Math. Phys.* 203 (1999), p. 445.

[243] S. Jansen, M.-B. Ruskai, and R. Seiler. "Bounds for the adiabatic approximation with applications to quantum computation". *J. Math. Phys.* 48 (2007), p. 102111.

[244] J. E. Avron, R. Seiler, and L. G. Yaffe. "Adiabatic theorems and applications to the quantum Hall effect". *Commun. in Math. Phys.* 110 (1987), p. 33.

[245] B. W. Reichardt. "The quantum adiabatic optimization algorithm and local minima". *STOC '04 Proceedings of the thirty-sixth annual ACM symposium on Theory of computing* (2004), p. 502.

[246] T. J. Osborne. "Simulating adiabatic evolution of gapped spin systems". *Phys. Rev. A* 75 (2007), p. 032321.

[247] A. del Campo and W. H. Zurek. "Universality of phase transition dynamics: topological defects from symmetry breaking". *Int. J. Mod. Phys. A* (2014), p. 1430018.

[248] A. Dutta, U. Divakaran, D. Sen, B. K. Chakrabarti, T. F. Rosenbaum, and G. Aeppli. "Quantum phase transitions in transverse field spin models: From statistical physics to quantum information" (2010). arXiv: 1012.0653.

[249] B. Damski and W. H. Zurek. "Adiabatic-impulse approximation for avoided level crossings: From phase-transition dynamics to Landau-Zener evolutions and back again". *Phys. Rev. A* 73 (2006), p. 063405.

[250] A. Chandran, A. Erez, S. S. Gubser, and S. L. Sondhi. "Kibble-Zurek problem: Universality and the scaling limit". *Phys. Rev. B* 86 (2012), p. 064304.

[251] M. Kolodrubetz, B. K. Clark, and D. A. Huse. "Non-equilibrium dynamic critical scaling of the quantum Ising chain". *Phys. Rev. Lett.* 109 (2012), p. 015701.

[252] G. Nikoghosyan, R. Nigmatullin, and M. Plenio. "Universality in the dynamics of second-order phase transitions" (2013). arXiv: 1311.1543.

[253] V. Gritsev and A. Polkovnikov. "Universal dynamics near quantum critical points". In: *Understanding Quantum Phase Transitions*. Ed. by L. D. Carr. Taylor & Francis, 2010.

[254] D. Chen, M. White, C. Borries, and B. DeMarco. "Quantum quench of an atomic Mott insulator". *Phys. Rev. Lett.* 106 (2011), p. 235304.

[255] J. M. Zhang and R. X. Dong. "Exact diagonalization: The Bose–Hubbard model as an example". *Eur. J. Phys* 31 (2010), p. 591.

[256] S. R. Clark and D. Jaksch. "Dynamics of the superfluid to Mott insulator transition in one dimension". *Phys. Rev. A* 70 (2004), p. 043612.

[257] F. M. Cucchietti, B. Damski, J. Dziarmaga, and W. H. Zurek. "Dynamics of the Bose-Hubbard model: transition from Mott insulator to superfluid". *Phys. Rev. A* 75 (2007), p. 023603.

[258] J. Dziarmaga and W. H. Zurek. "Quench in 1D Bose-Hubbard model: Topological defects and excitations from Kosterlitz-Thouless phase transition dynamics". *Sci. Rep.* 4 (2014), p. 5950.

[259] G. Biroli, L. F. Cugliandolo, and A. Sicilia. "Kibble-Zurek mechanism and infinitely slow annealing through critical points". *Phys. Rev. E* 81 (2010), p. 050101.

[260] U. Divakaran, V. Mukherjee, A. Dutta, and D. Sen. "Defect production due to quenching through a multicritical point". *J. Stat. Mech.* (2009), P02007.

[261] E. Canovi, D. Rossini, R. Fazio, and G. E. Santoro. "Adiabatic dynamics in a spin-1 chain with uniaxial single-spin anisotropy". *J. Stat. Mech.* (2009), P03038.

[262] F. Pellegrini, S. Montangero, G. E. Santoro, and R. Fazio. "Adiabatic quenches through an extended quantum critical region". *Phys. Rev. B* 77 (2008), p. 140404.

[263] T. Kinoshita, T. Wenger, and D. S. Weiss. "A quantum Newton's cradle". *Nature* 440 (2006), p. 900.

[264] I. Bouchoule, N. J. Van Druten, and C. I. Westbrook. "Atom chips and one-dimensional Bose gases" (2009). Ed. by J. Reichel and V. Vuletić.

[265] T. Langen, R. Geiger, and J. Schmiedmayer. "Ultracold atoms out of equilibrium". *Annu. Rev. Condens. Matter Phys.* 6 (2015), p. 201.

[266] J. Haegeman, J. I. Cirac, T. J. Osborne, and F. Verstraete. "Calculus of continuous matrix product states". *Phys. Rev. B* 88 (2013), p. 085118.

[267] E. H. Lieb and W. Liniger. "Exact analysis of an interacting bose gas. I. The general solution and the Ground State". *Physical Review* 130 (1963), p. 1605.

[268] J.-S. Caux, P. Calabrese, and N. A. Slavnov. "One-particle dynamical correlations in the one-dimensional Bose gas". *J. Stat. Mech.* (2007), P01008.

[269] D. A. Smith, M. Gring, T. Langen, M. Kuhnert, B. Rauer, R. Geiger, T. Kitagawa, I. Mazets, E. Demler, and J. Schmiedmayer. "Prethermalization revealed by the relaxation dynamics of full distribution functions". *New J. Phys.* 15 (2013), p. 075011.

[270] A. Steffens, C. A. Riofrio, R. Hübener, and J. Eisert. "Quantum field tomography". *New J. Phys.* 16 (2014), p. 123010.

[271] E. Jones, T. Oliphant, P. Peterson, et al. "SciPy: Open source scientific tools for Python" (2001–).

[272] J. Eisert. "Entanglement and tensor network states". *Modeling and Simulation* 3 (2013), p. 520.

[273] A. Milsted, J. Haegeman, and T. J. Osborne. "Matrix product states and variational methods applied to critical quantum field theory". *Phys. Rev. D* 88 (2013), p. 085030.

[274] D. Gross, J. Eisert, N. Schuch, and D. Perez-Garcia. "Measurement-based quantum computation beyond the one-way model". *Phys. Rev. A* 76 (2007), p. 052315.

[275] N. Schuch, M. M. Wolf, F. Verstraete, and J. I. Cirac. "Entropy scaling and simulability by matrix product states". *Phys. Rev. Lett.* 100 (2008), p. 030504.

[276] M. Lubasch, J. Ignacio Cirac, and M.-C. Bañuls. "Unifying projected entangled pair states contractions". *New J. Phys.* 16 (2014), p. 033014.

[277] N. Schuch, D. Perez-Garcia, and I. Cirac. "Classifying quantum phases using matrix product states and projected entangled pair states". *Phys. Rev. B* 84 (2011), p. 165139.

[278] M. B. Şahinoğlu, D. Williamson, N. Bultinck, M. Mariën, J. Haegeman, N. Schuch, and F. Verstraete. "Characterizing topological order with matrix product operators" (2014). arXiv: 1409.2150.

[279] B. Bauer, L. D. Carr, H. Evertz, A. Feiguin, J. Freire, S. Fuchs, L. Gamper, J. Gukelberger, E. Gull, S. Guertler, A. Hehn, R. Igarashi, S. Isakov, D. Koop, P. Ma, P. Mates, H. Matsuo, O. Parcollet, G. Pawlowski, J. Picon, L. Pollet, E. Santos, V. Scarola, U. Schollwoeck, C. Silva, B. Surer, S. Todo, S. Trebst, M. Troyer, M. Wall, P. Werner, and S. Wessel. "The ALPS project release 2.0: Open source software for strongly correlated systems" (2011). arXiv: 1101.2646.

[280] Z. Landau, U. Vazirani, and T. Vidick. "A polynomial-time algorithm for the ground state of 1D gapped local Hamiltonians" (2013). arXiv: 1307.5143.

[281] B. Nachtergaele, Y. Ogata, and R. Sims. "Propagation of correlations in quantum lattice systems". *J. Stat. Phys.* 124 (2006), p. 1.

[282] K. Them. "Towards experimental tests and applications of Lieb-Robinson bounds". *Phys. Rev. A* 89 (2014), p. 022126.

[283] L. Vidmar, S. Langer, I. McCulloch, U. Schneider, U. Schollwöck, and F. Heidrich-Meisner. "Sudden expansion of Mott insulators in one dimension". *Phys. Rev. B* 88 (2013), p. 235117.

[284] N. Schuch, S. K. Harrison, T. J. Osborne, and J. Eisert. "Information propagation for interacting-particle systems". *Phys. Rev. A* 84 (2011), p. 032309.

A

MATRIX-PRODUCT STATES

In this appendix, we briefly review matrix-product states (MPS), which are efficient ways of describing one-dimensional states, making use of the underlying local lattice structure [191, 272]. MPS are applied very successfully to a wide range of fields, from numerical simulations of ground states [41] to the analytic descriptions of quantum field theory [273]. There are several different ways to approach these states. We find it most illustrative to think of an MPS as the result of a truncation procedure of the coefficient tensor of a state. As before, let the state be expressed in terms of its coefficient tensor

$$|\psi\rangle = \sum_{j_1,\cdots,j_L=1}^{d_{spin}} c_{j_1,\cdots,j_L} |j_1,\cdots,j_L\rangle \ .$$

This tensor can now be approximated by performing singular value decompositions over spatial cuts (see Fig. A.1). At each cut, one has the possibility to reduce the amount of information stored by truncating the singular values. Usually, only D many of them are stored at any cut. The sum of the squares of the discarded singular values gives a good measure for the quality of the approximation. In particular, if we move, e.g., from left to right over the chain, the discarded weight is defined as

$$\epsilon_D(|\psi\rangle) = \sum_j \sum_{k>D} s_{j,k}^2 \ ,$$

where $s_{j,k}$ denotes the k-th singular values at a cut j. It is this discarded weight that captures how well the state $|\psi\rangle$ can be written as an MPS with bond dimension D and is directly related to the fidelity between the two states [177]

$$|\langle\psi|MPS_D\rangle| \geqslant 1 - \epsilon_D(|\psi\rangle) \ .$$

This in turn directly gives a bound on the 1-norm distance following [56]

$$\begin{aligned} 1 - |\langle\psi|MPS_D\rangle| \leqslant \| \, |\psi\rangle\langle\psi| - |MPS_D\rangle\langle MPS_D| \, \|_1 \leqslant \sqrt{1 - |\langle\psi|MPS_D\rangle|^2} \\ \Rightarrow \| \, |\psi\rangle\langle\psi| - |MPS_D\rangle\langle MPS_D| \, \|_1 \leqslant \epsilon \ . \end{aligned}$$

Note that the above procedure of simply truncating singular values results in an MPS state that is not normalised. Normalising the state, however only results in a larger fidelity [177].

As is clear from the above construction, any state can be written as an MPS, if one allows the bond dimension to grow exponentially with the system size. One does, however, colloquially speak of a state being an MPS, if it can be approximated up to a fixed 1-norm error by an MPS with a bond dimension that grows only linearly with the system size. Interestingly, for such states, it usually turns out that a bond dimension constant in the system size is sufficient, when one relaxes the error measure and only demands that local observables are well approximated, meaning that only the local 1-norm difference measured by $\|\cdot\|_{1,X}$ for some region X is small [102].

As described above, the success in approximating a state with an MPS is determined by the distribution of singular values over spatial cuts. If one cuts a spin chain into regions X and X^c, the square of these singular values are precisely the eigenvalues of the density matrix reduced to region X or equivalently X^c [41]. The ways these values are distributed can be characterised by looking at the different Renyi entropies

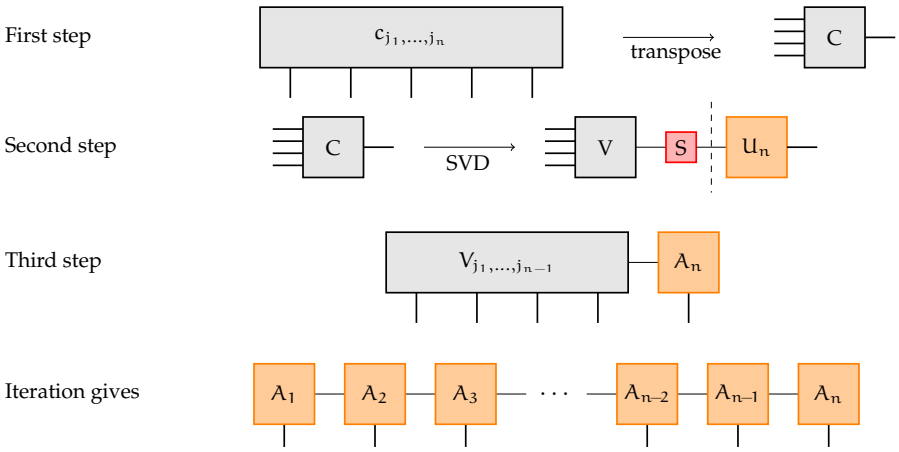

Figure A.1: *We thank Marcel Goihl for providing this figure.* The figure depicts the usual procedure to approximate a general 1D state with an MPS. For this, the coefficient tensor is recast into a product of small matrices. In this figure, the graphic notation from Ref. [274] is used, meaning that open lines are to be interpreted as indices of tensors. If they are joined, it corresponds to the contraction of the corresponding indices. First, one reshapes the coefficient tensor into a matrix using the local structure of the lattice. Then an SVD is performed and the corresponding singular values are truncated down to the bond dimension D. It is in this neglecting of singular values that the approximation error can be controlled. The singular weight is then multiplied to the right. Iteration of this procedure yields the MPS.

of the reduced density matrices [177]. If states are weakly entangled, the singular values have a narrow distribution corresponding to small Renyi entropies and the state can be well captured in terms of an MPS, whereas strongly entangled states have a broad distribution in singular values and require a large bond dimension. Thus, an area-law for a Renyi entropy with $0 \leqslant \alpha < 1$ of a family of states depending on the system size is sufficient to guarantee that the states can be locally approximated by an MPS with a bond-dimension independent of the system size L [177, 275]. Interestingly the von-Neumann entropy itself is not sufficient to provide an error estimate, as the distribution of singular values can be fine-tuned to achieve an arbitrarily large error, even if the state obeys an area-law for the von-Neumann entropy [275].

In higher dimensions, analogues of MPS can be constructed, for example using so-called projected entangled pair states [272]. They are numerically very useful [191, 276] and were used to classify quantum phases [277, 278]. It is, however, not known whether the ground states of gapped local Hamiltonians can be efficiently approximated by a tensor network state in dimensions higher than one. Part of the problem is that it is unknown whether these ground states obey an area law for the Renyi entropies. Interestingly, it was recently pointed out that even the presence of such an area law would not necessarily imply an efficient tensor network description and that large classes of states can be constructed that violate this intuition [103].

One of the most important applications of the tensor network descriptions presented above is that they are the basis for highly efficient numerical descriptions of quantum states [41, 279]. In contrast to exact diagonalisation tools [255], which are typically limited to 10-20 sites, large systems of sometimes more than hundred sites can be considered. Especially when states are expected to have a small amount of entanglement, for example in the search of ground states of gapped local models, this makes them an indispensable tool [41, 280].

B

LIEB-ROBINSON BOUNDS

In this appendix, we give a detailed overview of Lieb-Robinson bounds. The basic principle is to connect the locality of the Hamiltonian with the dynamical evolution of operators in the Heisenberg picture [66, 93, 110, 112]. We provide various formulations of these bounds, present an intuitive outline of the proof and sketch generalisations as well as zero-velocity versions thereof.

We begin by stating several different formulations of such Lieb-Robinson bounds. For this, we consider families of systems with varying size, for example by considering translationally invariant Hamiltonians. The Lieb-Robinson bounds are then required to hold with constants independent of this system size. For the concrete statements, let $B_Y(t)$ be a local operator supported on Y that is time-evolved in the Heisenberg picture and Y_l the enlarged sets of its support Y, as usual. Further, let A_X be a general operator on X, where, as always throughout this thesis, the operators considered are normalised in operator norm. With this, Lieb-Robinson bounds take the following form.

Lieb-Robinson bounds - Different formulations

Definition 17. *(Lieb-Robinson bounds) Let $C, \nu, \mu > 0$ be constants independent of the system size. A Hamiltonian is said to satisfy Lieb-Robinson bounds if one of the following bounds holds.*

***Excitation formulation**:*

$$\|[B_Y(t), e^{igA_X}]\| \leqslant C \min\{|X|, |Y|\} \min(1, g)\, e^{-\mu(d(A_X, B_Y) - \nu t)} ,$$

***Commutator formulation**:*

$$\|[B_Y(t), A_X]\| \leqslant C \min\{|X|, |Y|\}\, e^{-\mu(d(A_X, B_Y) - \nu t)} ,$$

***Reduction formulation**:*

$$\|B_Y(t) - \Gamma_{Y_l}(B_Y(t))\| \leqslant C\,|Y|\, e^{-\mu(l - \nu t)} ,$$

***Truncated Hamiltonian formulation**:*

$$\|B_Y(t) - e^{itH_l} B_Y e^{-itH_l}\| \leqslant C\,|Y|\, e^{-\mu(l - \nu t)} ,$$

with Γ the reduction map introduced in chapter 3.2 and H^l the truncated Hamiltonian including all Hamiltonian terms fully supported on Y_l, which is the set including Y and all sites within distance l of it.

All these bounds share the important feature that time and space are connected linearly with a constant ν that is therefore called the *Lieb-Robinson velocity*. This gives rise to an effective space-time cone, in an analogous way as the speed of light. Outside of this cone, there is an exponential suppression in the distance. Interestingly, this exponential decay is connected to the underlying lattice structure and sending the lattice spacing to zero gives an exact light cone [113].

It is important to note that all these formulations have physical intuition connected to them. The most restricted is the excitation formulation, which can be seen as a statement about signalling between two regions X, Y where a unitary excites the system in X and the effect is measured in Y (see section 3.5.3). The second is a variant thereof, where the restriction of unitarity is dropped. The reduction formulation again is a statement about signalling, but now from the whole complement Y_l^c to a small region Y. The truncated Hamiltonian variant, finally, is the strongest form and implies that information cannot even be transmitted when the Hamiltonian can locally be changed. This discussion immediately establishes some connections between these different bounds. Interestingly, when suitably increasing the corresponding constants, all of these bounds become equivalent.

Lemma 4. *(Connecting Lieb-Robinson bounds) On a finite-dimensional cubic lattice, the different formulations of Lieb-Robinson bounds are all essentially equivalent, in the sense that the can be derived from each other when allowing for slight changes in the corresponding constants.*

The proof of this statement is contained in Refs. [4, 65, 94]. The main appeal of Lieb-Robinson bounds stems from the fact that they can be derived for spin systems from the locality of the Hamiltonian alone. For this, we decompose our Hamiltonians according to the support of the local terms $H = \sum_Z h_Z$, as described in chapter 3.2, which gives the following statement.

Theorem 15 (Lieb-Robinson bounds from locality)**.** *On a cubic lattice of spins, let $H = \sum_Z h_Z$ be a Hamiltonian that is exponentially decaying, in the sense that*

$$\exists\, C', \mu' : \quad \|h_Z\| \leqslant C' e^{-\mu' \mathrm{diam}(Z)} \quad \forall\, Z \subset \Lambda\,,$$

then it fulfils all formulations of Lieb-Robinson bounds for some constants C, ν, μ independent of the system size. The decay constant μ can be chosen arbitrarily close to μ', but has to differ by epsilon $\mu' = \mu + \epsilon$, $\epsilon > 0$.

This statement for exponentially decaying Hamiltonians naturally includes the case of finite range Hamiltonians. For the simplest case of nearest neighbour interactions on a $d_{\mathcal{L}}$-dimensional cubic lattice, the constants in the commutator formulation are given by [111]

$$\begin{aligned} \|[B_Y(t), A_X]\| &\leqslant C \min\{|X|, |Y|\}\, e^{-\mu(d(A_X, B_Y) - \nu t)} \\ C &= 2\,, \\ \mu &= \frac{1}{2}\,, \\ \nu &= 4 d_{\mathcal{L}}\, e \sup_{Z \subset \Lambda} \|h_Z\|\,, \end{aligned}$$

where h_Z are the local nearest neighbour terms, e denotes the euler number and $d_{\mathcal{L}}$ is the lattice dimension. We now turn to the general proof of such bounds in local models and present a high-level argument of the necessary steps.

THREE STEPS OF THE PROOF

Naturally, there are plenty of articles that provide a proof of Lieb-Robinson bounds in different formulations [66, 93, 110, 111] and we have no intention of repeating the argument in all detail. That being said, these proofs are often technical and we think that it might prove useful for some readers to present the argument in an abstract and intuitive form based on Ref. [94]. For this, we pick the commutator formulation, which is the usual basis for the proof. We separate the argument in three main steps. First, the commutator is rewritten in terms of a differential equation, which in turn gives rise to an integral inequality. For this integral, a Picard iteration is performed. This Picard iteration is then the basis for a careful counting argument over all possibles paths connecting the two regions involved in the commutator.

Differential equation

We focus on deriving the commutator formulation. The goal is thus to bound

$$[A_X, B_Y(t)] \,,$$

for some normalised operators A_X, B_Y supported on local and disjoint regions X and Y respectively. In order to stick to the simplest possible setting, we restrict the proof to a nearest neighbour Hamiltonian. In order to obtain the desired bound, we look at the related quantity

$$C_{B_Y}(X,t) = \sup_{A_X \in \mathcal{A}_X} \|[A_X, B_Y(t)\| \,.$$

In order to exploit the locality, we divide the Hamiltonian in two parts

$$H = H_X + H_{\text{rest}} \,,$$

where H_X contains all terms fully supported on X and the other contains the remaining terms. To simplify notation, we introduce the following time evolution operators

$$\begin{aligned} \tau_t(A_X) &= e^{itH} A_X e^{-itH} \,, \\ \tau_t^X(A_X) &= e^{itH_X} A_X e^{-itH_X} \,. \end{aligned}$$

We now introduce a function interpolating between these two evolutions

$$\begin{aligned} f(A_X, B_Y, t) &:= \left[\tau_t\left(\tau_{-t}^X(A_X)\right), B_Y\right] \,, \\ C_{B_Y}(X,t) &= \sup_{A_X \in \mathcal{A}_X} \|f(A_X, B_Y, t)\| \,, \end{aligned}$$

where we used that $\tau_{-t}^X(A_X) \in \mathcal{A}_X$. Differentiating the function f and using the decomposition of the Hamiltonian, we obtain

$$-i\partial_t f(A_X, B_Y, t) = \sum_{Z,\, Z\cap X\neq\emptyset,\, Z\not\subset X} \left[\left[\tau_t(h_Z), \tau_t\left(\tau_{-t}^X(A_X)\right)\right], B_Y\right] \,.$$

Now, this quantity is reordered using the Jacobi identity to recover the original term

$$\begin{aligned} -i\partial_t f(t) &= \sum_{Z,\, Z\cap X\neq\emptyset,\, Z\not\subset X} \left(\left[\tau_t(h_Z), \left[\tau_t\left(\tau_{-t}^X(A_X)\right), B_Y\right]\right] - \left[\tau_t\left(\tau_{-t}^X(A_X)\right), [\tau_t(h_Z), B_Y]\right]\right) \\ &= \sum_{Z,\, Z\cap X\neq\emptyset,\, Z\not\subset X} \left([\tau_t(h_Z), f(t)] - \left[\tau_t\left(\tau_{-t}^X(A_X)\right), [\tau_t(h_Z), B_Y]\right]\right) \,. \end{aligned}$$

The first part of the differential equation corresponds to a unitary evolution and does thus not alter the norm of $f(t)$ [281, 282]. In the other term, one can get rid of the outer commutator by using linearity of the norm and the fact that $\|A_X\| = 1$. With this, also the second term can be related to a single commutator of the type we had at the beginning

$$\left\|\left[\tau_t\left(\tau_{-t}^X(A_X)\right), [\tau_t(h_Z), B_Y]\right]\right\| \leqslant 2\,\|\,[\tau_t(h_Z), B_Y]\,\| \leqslant 2\,\|\tau_t(h_Z)\|\, C_{B_Y}(Z,t) \,.$$

Thus, integrating the above differential inequality yields a bound for the Lieb-Robinson commutator

$$C_{B_Y}(X,t) \leqslant C_{B_Y}(X,0) + 2 \sum_{Z:\, Z\cap X\neq\emptyset,\, Z\not\subset X} \|\tau_t(h_Z)\| \int_0^{|t|} ds\; C_{B_Y}(Z,s) \,.$$

It is worth pointing out that in the sum over Hamiltonian terms, only those are included that connect the region X with its complement. This is a result of introducing the inverse time evolution of H_X at the beginning of the proof; a clever trick that substantially sharpens the resulting Lieb-Robinson bounds at the end [94]. For example, it is immediately clear at this point that Hamiltonian terms that only occupy a single site, such as magnetic field type terms, do not enter the Lieb-Robinson bounds [282].

In the following, we use the above integral inequality as the starting point for a Piccard iteration. This allows us to map the derivation of Lieb-Robinson bounds to a combinatorial problem of connecting different regions with nearest neighbour connections.

Picard Iteration

The Piccard iteration works by reinserting the bound in itself. The first step takes the following form

$$\begin{aligned} C_{B_Y}(X,t) \leqslant & C_{B_Y}(X,0) + 2 \sum_{Z\colon Z\cap X\neq\emptyset,\, Z\not\subset X} \|\tau_t(h_Z)\| C_{B_Y}(Z,0) \\ & + 4 \sum_{Z\colon Z\cap X\neq\emptyset,\, Z\not\subset X} \sum_{Z'\colon Z'\cap Z\neq\emptyset,\, Z'\not\subset Z} \|\tau_t(h_Z)\| \|\tau_t(h_{Z'})\| \int_0^{|t|} ds \int_0^{|s|} ds'\, C_{B_Y}(Z',s') \,. \end{aligned}$$

Iterating this, a large sum appears, where each summand corresponds to a certain way of moving through the lattice [111]. These summands can be constructed as follows. In each step, one picks a Hamiltonian term with the restriction that it has to overlap with the term chosen in the step before. As mentioned earlier, on-site Hamiltonian terms can be discarded in this procedure. In order for such a path to have a non-zero contribution to the Lieb-Robinson commutator, the path has to connect the local support regions of the observables A_X and B_Y. Each path is weighted by the norm of all Hamiltonian terms along its way [111], as well by a $\frac{1}{n!}$ term, where n is the length of the path. The latter term is simply the result of the iterative integration of a constant term. To conclude the argument, we need to count the number of relevant paths or at least provide a reasonable upper bound.

Path counting & Poissonian tails

At this point, we need to count all paths that connect the regions A_X and B_Y and add them with their corresponding weight. To derive Lieb-Robinson bounds, we assume that there is a uniform upper bound on the norm of all local Hamiltonian terms

$$\sup_Z \|h_Z\| \leqslant \kappa \,,$$

where h_Z are the uniquely defined Hamiltonian terms in the local decomposition as used before. In order to get a handle on the number of relevant paths, we use the following simplification. Rather than only counting all paths connecting the relevant regions, we simply count all possible paths of a certain length. In our case of nearest neighbour interactions on a cubic lattice, any Hamiltonian term therefore only connects to few other Hamiltonian terms, the number of which we denote by λ. The starting point for the paths is the support region X of the observable A_X. Since the first step already has to leave the region, they have to involve the boundary ∂X, meaning that there are at most $|\partial X|\lambda$ many starting points. In total, there are only $|\partial X|\lambda^n$ many relevant paths of length n. Assuming initially disjoint observables $[A_X, B_Y(0)] = 0$, we have the following bound [111]

$$C_{B_Y}(X,t) \leqslant |\partial X| \sum_n \frac{(2\lambda\kappa)^n}{n!} \,.$$

This dependence on the boundary ∂X is special to the case of nearest neighbour interactions. For the general case of exponentially decaying Hamiltonians, it has to be replaced by $|X| > |\partial X|$ [94]. With this, we have almost concluded the proof. The last step is based on the insight that to connect two disjoint regions X and Y that are separated by a certain distance $d(X, Y)$, there is a minimum number of Hamiltonian terms that have to be used. Thus, the sum in the above bound does not start at $n = 0$. In the setting of nearest neighbour Hamiltonians, the number of needed terms is precisely given by the distance, which gives

$$C_{B_Y}(X, t) \leqslant |\partial X| \sum_{n \geqslant d(A_X, B_Y)} \frac{(2\lambda\kappa)^n}{n!} .$$

This term is now the tail of a Poissonian distribution. Thus, the proof can be concluded by using a Poissonian tail bound. An important bound here is given by [111]

$$\sum_{n \geqslant d(A_X, B_Y)} \frac{\alpha^n}{n!} \leqslant e^{\alpha e - d(A_X, B_Y)} ,$$

which gives an exponential suppression in the distance $d(A_X, B_Y)$ and concludes the proof of Lieb-Robinson bounds. As recently pointed out, this Poissonian tail bond can be tightened in the case of nearest neighbour terms [282]. This concludes our outline of the proof. We now turn to generalisation of Lieb-Robinson bounds.

GENERALISATIONS

The above proof, despite being presented for nearest neighbour interacting spin-systems on a cubic lattice, can be generalised considerably. In particular, very general lattices are possible, as long as they have a fixed number of nearest neighbours [94, 112]. Moreover, as already mentioned above, it is not necessary that the Hamiltonian has a nearest neighbour interaction structure, but in fact it is sufficient that it is local, in the sense of exponentially decaying interactions.

An interesting debate that considerably gained momentum recently, is to what extent locality of the Hamiltonian is truly needed. In particular, many works started to investigate the dynamical behaviour of models that have interactions decaying according to a power-law [36, 66, 67]. Interestingly, there is a sharp cross-over. For a decay that is stronger than the lattice dimension $d_{\mathcal{L}}$, again an effective light cone emerges. The only difference is that outside of the cone, one no longer finds an exponential decrease, but rather the suppression given by the power-law decay of the Hamiltonian interactions [66, 94]. When the interactions decay even weaker, meaning with a power-law exponent that is equal to the lattice dimension or smaller, the causal structure completely disappears [67].

Given the recent advances in the high-precision control over quantum many-body systems in experiments, it became possible to test Lieb-Robinson bounds also experimentally [31, 34, 36]. Here ion chains, based on charged particles in an electromagnetic trap, due to their long-range Coulomb interactions, even allow to tune the Hamiltonian to achieve a power-law [36]. Complementary, optical lattices based on neutral particles allow for the implementation of nearest neighbour interactions [62]. Interestingly, this allows to test Lieb-Robinson bounds for bosonic particles [31], where the proof presented above breaks down since the creation and annihilation operators are no longer bounded in operator norm.

The search for some form of rigorous Lieb-Robinson bounds in bosonic models is still ongoing. In some experimental settings, the bosonic systems can effectively be described in terms of fermions, such that Lieb-Robinson bounds immediately can be applied [120]. Fully harmonic systems provide another instance of bosonic systems fulfilling a Lieb-Robinson bound [113]. On an intuitive level, for the case of a finite number of particles on each site, it is usually expected that a light-cone like behaviour should hold;

an intuition that was confirmed experimentally [31, 283] and analytically proven for the propagation of a region of bosons on top of an otherwise empty lattice [284]. If, however, the local particle number is not restricted, then supersonic communication is provably possible [118], which clearly shows that generally the light cone like behaviour can be violated for interacting bosons. Thus, it remains open to find natural restrictions on such bosonic systems and see what precise conditions are needed to guarantee the existence of an effective speed of light.

This concludes our discussion of more general versions of Lieb-Robinson bounds. In the following, we turn to localising systems. There, at least in the case of Anderson localisation (chapter 5), tightened versions of Lieb-Robinson bounds are expected to hold, which will be presented in the next section.

ZERO-VELOCITY BOUNDS

In the case of free systems, random onsite potentials can lead to a complete localisation of all eigenmodes of the model. While the mathematical derivation of the systems size scaling is still outstanding, it is expected that this even holds for finite systems with large probability (see chapter 5). In this case, the following zero-velocity Lieb-Robinson can be derived.

Zero velocity Lieb-Robinson bounds

Zero-velocity Lieb-Robinson bounds correspond to the normal ones by setting $v = 0$.

Excitation formulation:

$$\|[B_Y(t), e^{igA_X}]\| \leqslant C \min\{|X|, |Y|\} \min(1, g)\, e^{-\mu d(A_X, B_Y)} ,$$

Commutator formulation:

$$\|[B_Y(t), A_X]\| \leqslant C \min\{|X|, |Y|\}\, e^{-\mu d(A_X, B_Y)} ,$$

Reduction formulation:

$$\|B_Y(t) - \Gamma_{Y_l^c}(B_Y(t))\| \leqslant C|Y|\, e^{-\mu l} ,$$

Truncated Hamiltonian formulation:

$$\|B_Y(t) - e^{itH_l} B_Y e^{-itH_l}\| \leqslant C|Y|\, e^{-\mu l} .$$

While for the $v \neq 0$ case, the bounds are all essentially equivalent, this no longer holds true in the zero-velocity case. Rather they are strictly ordered, meaning that the truncated Hamiltonian formulation is stronger than the reduction formulation, which in turn is stronger than the commutator formulation. Only the excitation and commutator formulation are again essentially equivalent [4].

This concludes our discussion of Lieb-Robinson bounds. We presented different version of them and explained their physical meaning. We proceeded by presenting an abstract outline of the general proof strategy, which gave an intuitive overview of the necessary steps and explained in which way locality of the Hamiltonian is exploited. Finally, we discussed generalisation of such bounds and their sharpened version in the case of Anderson localisation.

C

FERMIONIC GAUSSIFICATION

The following appendix is based on Ref. [6]. We sincerely thank Marek Gluza, Christian Krumno, Christian Gogolin and Jens Eisert for collaborating on this successful project.

In this appendix, we provide the details for the proof of theorem 2. For convenience, we repeat the statement.

Theorem (Gaussification)**.** *Let H be a free fermionic Hamiltonian that has transport and admits Lieb-Robinson bounds. Further, let ρ be an initial state with exponential clustering and fixed particle parity and S be some finite region of consecutive sites. Then for any $\epsilon > 0$, there exists a time interval $[t_{\text{relax}}, t_{\text{rec}}]$, such that*

$$\|\mathrm{Tr}_{S^c}\left(\rho(t) - \rho_G(t)\right)\|_1 \leqslant (2|S|)^{(4+4d_{\mathcal{L}})|S|+1}\epsilon \quad \forall t \in [t_{\text{relax}}, t_{\text{rec}}]\,,$$

where ρ_G is the Gaussian state fixed by the correlation matrix of ρ and t_{relax} is constant in the system size.

Proof. In the following, we provide the proof of the above theorem. We begin by reformulating 1-norm closeness in terms of expectation values of operators

$$\|\mathrm{Tr}_{S^c}\left(\rho(t) - \rho_G(t)\right)\|_1 = \sup_{\substack{A\in\mathcal{A}_S\\ \|A\|=1}} \left|\mathrm{Tr}\left(A\rho(t) - A\rho_G(t)\right)\right|\,.$$

In the next step, we expand the operator in a fermionic operator basis for the subsystem S

$$A = \sum_{m_1,\cdots,m_{2|S|}} a_{m_1,\cdots,m_{2|S|}} \left(r_1(t)\right)^{m_1}\cdots\left(r_{2|S|}(t)\right)^{m_{2|S|}}\,,$$

where r_1 to $r_{2|S|}$ are the fermionic operators on the subsystem. For convenience, we will introduce $\tilde{S} = 2|S|$. Normalisation of an operator $\|A\| = 1$ implies that all of the $2^{\tilde{S}}$ possible coefficients satisfy $|a_{j_1,\cdots,j_{\tilde{S}}}| \leqslant 1$. Thus, the proof of the theorem can be reduced to showing that

$$\left|\mathrm{Tr}\left(r_{s_1}(t)\cdots r_{s_q}(t)\left(\rho - \rho_G\right)\right)\right| \leqslant \epsilon'\,,$$

for some collection of $q \leqslant \tilde{S}$ operators labelled with the indices s_1 to s_p. For this, we expand the time evolution of the fermionic word

$$\left|\sum_{j_1,\cdots,j_q} V_{s_1,j_1}(t)\cdots V_{s_r,j_q}(t)\,\mathrm{Tr}\left(r_{j_1}\cdots r_{j_q}\left(\rho - \rho_G\right)\right)\right|\,,$$

which will be analysed and restricted to the Lieb-Robinson cone in the next step.

Causal cone Based on Lieb-Robinson bounds introduced above, we will separate the lattice $\mathcal{L}$ in two sets: An effective light-cone $\mathcal{C} = \{i \in \mathcal{L}\,|\,\exists j \in S : d(i,j) < (v + 2v_\epsilon)|t|\}$ and its complement $\mathcal{L}\backslash\mathcal{C}$, where v_ϵ will be picked such that the final bound is optimal. In the next step, we will use the bounds to restrict the full dynamics of all fermionic operators to the inside of the effective light cone. As a preparatory step, we need the following basic lemma for dealing with a partial fermionic sum.

Lemma 5 (Partial fermionic unitary)**.** *Let* I *be some subset of the* $2|\mathcal{L}|$ *fermionic lattice indices, labelling creation and annihilation operators and* $V(t)$ *be some unitary rotation on them. Then*

$$\left\| \sum_{j \in I} V_{k,j}(t) r_j \right\| \leqslant 1 \quad \forall\, k\,,$$

where r_j *denotes the usual collection of creation or annihilation operators.*

Proof. The proof can be carried out with straightforward norm estimates and using the normalisation of the two-point correlator γ. We begin with

$$\left\| \sum_{j \in I} V_{k,j} r_j \right\| = \sup_{\substack{|\psi\rangle \\ \||\psi\rangle\|=1}} \langle \psi | \sum_{m \in I} \overline{V}_{k,m} r_m^\dagger \sum_{j \in I} V_{k,j} r_j \, |\psi\rangle = \sum_{m \in I} \sum_{j \in I} \overline{V}_{k,j} V_{k,m} \sup_{\substack{|\psi\rangle \\ \||\psi\rangle\|=1}} \langle \psi | \, r_m^\dagger r_j \, |\psi\rangle \ .$$

We now rewrite this as a matrix multiplication on the index space

$$\left\| \sum_{j \in I} V_{k,j} r_j \right\| \leqslant \sup_{\gamma} \langle k | \, \overline{V} P_I \gamma P_I V \, | k \rangle \ ,$$

where $|k\rangle$ is a vector on the index space, P_I denotes the projector onto the interval I and γ denotes fermionic correlation matrices. Now doing a straightforward norm estimate and using $\|\gamma\| \leqslant 1$, as every fermionic mode cannot support more than one particle, gives

$$\left\| \sum_{j \in I} V_{k,j} r_j \right\| \leqslant \|\overline{V}\| \, \|P_I\| \, \|\gamma\| \, \|P_I\| \, \|V\| \leqslant 1 \ ,$$

which concludes the proof. □

With this, we can approach the suppression outside of the Lieb-Robinson cone.

Lemma 6 (Lieb-Robinson cone)**.** *Let "*$\{j\}$ out LR*" denote the constraint that not all indices are contained inside the Lieb-Robinson cone. We then have*

$$\left\| \sum_{\{j\} \text{ out LR}} V_{s_1,j_1} \cdots V_{s_m,j_m} r_{j_1} \cdots r_{j_m} \right\| \leqslant m \, C'_{LR}(d_{\mathcal{L}}) \, e^{-\mu v_\epsilon |t|} \ ,$$

where C'_{LR} *is a constant connected to summing the exponential tails of the Lieb-Robinson estimate.*

Proof. We begin by splitting the sum according to whether the first index is inside the cone or not

$$\begin{aligned} &\left\| \sum_{\{j\} \text{ out LR}} V_{s_1,j_1} \cdots V_{s_m,j_m} r_{j_1} \cdots r_{j_m} \right\| \qquad \text{(C.0.1)} \\ &= \left\| \sum_{j_1 \notin C} V_{s_1,j_1} r_{j_1} \right\| \left\| \sum_{\{j_2,\cdots,j_L\} \in \mathcal{L}} V_{s_2,j_2} \cdots V_{s_m,j_m} r_{j_2} \cdots r_{j_m} \right\| \\ &+ \left\| \sum_{j_1 \in C} V_{s_1,j_1} r_{j_1} \right\| \left\| \sum_{\{j_2,\cdots,j_L\} \text{ out LR}} V_{s_2,j_2} \cdots V_{s_m,j_m} r_{j_2} \cdots r_{j_m} \right\| \ , \end{aligned}$$

where the other indices are free if j_1 is outside the cone, while at least one other index is outside the cone if j_1 lies in it. We will deal with those two contributions separately. For the first term, where j_1 lies outside of the light cone, we can estimate the second half by one due to normalisation of $c_j(t)$ and for the first half obtain

$$\left\| \sum_{j_1 \notin C} V_{s_1,j_1} r_{j_2} \right\| \leqslant \sum_{j_1 \notin \mathcal{C}} |V_{s_1,j_1}| \leqslant C_{LR} \sum_{l > (v+2v_\epsilon)|t|} \sum_{\substack{m \in \mathcal{L} \\ d(m,s_1)=l}} e^{-\mu(l-v|t|)}$$

$$\leqslant C_{LR} \sum_{l=0}^{L} 2d_{\mathcal{L}} \left(l + (v+2v_\epsilon)|t|\right)^{d_{\mathcal{L}}-1} e^{-\mu(l+2v_\epsilon|t|)} ,$$

where we used that the number of points on a cubic lattice with a fixed distance l to a certain point in our semi-metric is given by $2\,d_{\mathcal{L}}\, l^{d_{\mathcal{L}}-1}$. We now use the following estimate

$$C_{LR} \sum_{l=0}^{L} 2d_{\mathcal{L}} \left(l + (v+2v_\epsilon)|t|\right)^{d_{\mathcal{L}}-1} e^{-\mu l} e^{-\mu v_\epsilon |t|} \leqslant C'_{LR}(d_{\mathcal{L}}) ,$$

where $C'_{LR}(d_{\mathcal{L}})$ is a bounded constant independent of L and t due to the exponential suppression in space and time. This yields

$$\left\| \sum_{j_1 \notin C} V_{s_1,j_1} r_{j_2} \right\| \leqslant C'_{LR}(d_{\mathcal{L}})\, e^{-\mu v_\epsilon |t|} . \tag{C.0.2}$$

With this, we estimated the first term in Eq. (C.0.1). For the second, we notice that the first sum can be bounded by one due to lemma 5. The second term gives the same term as we originally had, but with the order of the fermionic word reduced by one. Thus an iteration gives exactly m error terms of the form in Eq. (C.0.2), which concludes the proof. □

Using the above lemma, we thus can reduce all indices to the inner part of the Lieb-Robinson cone, up to an error

$$\epsilon' \mathrel{+}= \tilde{S} C'_{LR}(d_{\mathcal{L}})\, e^{-\mu v_\epsilon |t|} .$$

Inside this cone, we now introduce a way to keep track of the different index configurations.

Tracking index positions: We proceed by introducing a notion of partitions, which groups the indices j_k and makes them tractable.

Definition 18 (Δ-partitions). *Let $i_1, \ldots, i_n \in \mathcal{L}$. The Δ-partition p associated to these indices is the unique partition $C_1, \ldots, C_l$ of the subindices $1, \ldots, n$ with the following properties:*

- ***i)*** *Each patch C_i is path connected: $\forall a, b \in C_i$ there exists a chain $s_1, \ldots, s_q \in C_i$ with $s_1 = a, s_q = b$ and $d(j_{s_r}, j_{s_{r+1}}) \leqslant \Delta \quad \forall r$.*
- ***ii)*** *All patches are separated by more than Δ:*
  $i \neq j, a \in C_i, b \in C_j \Rightarrow d(j_a, j_b) > \Delta$.

We will use $p_\Delta(\{j_\alpha\}) = p$ to denote that the indices are distributed according to the Δ-partition p and $|p|$ to denote the number of sets in the partition. For concreteness, let us look at a setting of four indices. Here a possible partition could be

$$\{C_1, C_2, C_3\} = \{\{1,3\},\{2\},\{4\}\} ,$$

which would tell us that lattice positions j_1 and j_3 are within distance Δ, while everything else is separated by a distance more than that. We will call a partition even, if it contains only sets with an even number of indices. In general, the sets contained in a partition will be called patches and a patch with $|C_i| = 2$ is referred to as a pair and $|C_i| > 2$ as a cluster. As there are at most $\tilde{S}$ fermionic operators in the fermionic word, the total number of partitions is given by the Bell number $B_{\tilde{S}}$, which can be bounded as $B_{\tilde{S}} \leqslant (\tilde{S})^{\tilde{S}}$ [24]. For each patch of the partition, we will define a corresponding operator given as

$$\hat{C}_r := \hat{C}_r(p, \{j\}, t) := \prod_{s \in C_r} V_{s,j_s}(t) r_{j_s} \ .$$

In the following, we will group the fermionic operators into the patches given by partitions p

$$\mathrm{Tr}\left(r_{s_1}(t) \cdots r_{s_q}(t)(\rho - \rho_G)\right) = \sum_p \mathrm{sign}(p) \sum_{p_\Delta(j_1,\cdots,j_m)=p} \langle \hat{C}_1 \cdots \hat{C}_l \rangle_\rho \ ,$$

where $\mathrm{sign}(p)$ results from a reordering of the fermionic operators into the partitions. The expectation value of these operators can now be decoupled using the exponentially clustering correlations in the initial state.

Decoupling clusters: We proceed by using the fact that the partitions are separated by a length scale Δ. Together with the exponential clustering of the state, we can show that the expectation value can thus be decoupled into a product of expectation values for the individual patches

$$\sum_p \mathrm{sign}(p) \sum_{p_\Delta(j_1,\cdots,j_m)=p} \langle \hat{C}_1 \rangle_\rho \cdots \langle \hat{C}_l \rangle_\rho \ .$$

For this, we rely on the following lemma.

Lemma 7 (Decoupled patches)**.** *Given a Δ-partition into $|p|$ many patches, we have the following bound*

$$\sum_{\substack{j_1,\ldots,j_n \in \mathcal{C} \\ p_\Delta(\{j_\alpha\})=p}} \left| \langle \hat{C}_1 \ldots \hat{C}_{|p|} \rangle_\rho - \langle \hat{C}_1 \rangle_\rho \ldots \langle \hat{C}_{|p|} \rangle_\rho \right| \leqslant \tilde{S} |\mathcal{C}|^{\tilde{S}} C_{\mathrm{clust}} \, e^{-\Delta/\xi} \ ,$$

where $\langle A \rangle_\rho = \mathrm{Tr}(A\rho)$ denotes the expectation value with respect to ρ.

Proof. The decoupling of the clusters works iteratively. We will begin with decoupling the last one

$$\sum_{\substack{j_1,\ldots,j_n \in \mathcal{C} \\ p_\Delta(\{j_\alpha\})=p}} \left| \langle \hat{C}_1 \ldots \hat{C}_{|p|} \rangle_\rho - \langle \hat{C}_1 \ldots \hat{C}_{|p|-1} \rangle_\rho \langle \hat{C}_{|p|} \rangle_\rho \right| .$$

If we expand the clusters back into the original fermionic words, we obtain an involved expression in terms of the evolution matrices V and the fermionic operators c. For simplicity, we will use the trivial bounds $|V_{j,k}| \leqslant 1$ and $\|c\| \leqslant 1$. For each individual fermionic word, we can use the exponential clustering of the initial state, which gives

$$\sum_{\substack{j_1,\ldots,j_n \in \mathcal{C} \\ p_\Delta(\{j_\alpha\})=p}} \left| \langle \hat{C}_1 \ldots \hat{C}_{|p|} \rangle_\rho - \langle \hat{C}_1 \ldots \hat{C}_{|p|-1} \rangle_\rho \langle \hat{C}_{|p|} \rangle_\rho \right| \leqslant \sum_{\substack{j_1,\ldots,j_n \in \mathcal{C} \\ p_\Delta(\{j_\alpha\})=p}} C_{\mathrm{clust}} \, e^{-\Delta/\xi} \leqslant |\mathcal{C}|^{\tilde{S}} C_{\mathrm{clust}} \, e^{-\Delta/\xi} \ ,$$

where we overcounted the contribution of a fixed partition by allowing all indices to freely move over the effective light cone $\mathcal{C}$. This argument can now be iterated for the different patches, yielding

$$\sum_{\substack{j_1,\ldots,j_n \in \mathcal{C} \\ p_\Delta(\{j_\alpha\})=p}} \left| \langle \hat{C}_1 \ldots \hat{C}_{|p|} \rangle_\rho - \langle \hat{C}_1 \rangle_\rho \ldots \langle \hat{C}_{|p|} \rangle_\rho \right| \leqslant \tilde{S} |\mathcal{C}|^{\tilde{S}} C_{\mathrm{clust}} \, e^{-\Delta/\xi} \ ,$$

as there are at most $\tilde{S}$ many patches. This concludes the proof. □

Thus, in this step, we accumulated an approximation error

$$\epsilon' \mathrel{+}= \tilde{S}^{\tilde{S}+1}|\mathcal{C}|^{\tilde{S}} C_{\text{clust}}\, e^{-\Delta/\xi}\,,$$

where we bounded the number of partitions by $\tilde{S}^{\tilde{S}}$. For the Gaussian state, we do not immediately know that it also shows clustering of correlations. Yet, using Wick's theorem, a similar procedure can be carried out, resulting in the following lemma.

Lemma 8 (Decoupling Gaussian patches)**.** *Given a Δ-partition into $|p|$ many patches, we have the following bound*

$$\sum_{\substack{j_1,\dots,j_n\in\mathcal{C}\\ p_\Delta(\{j_\alpha\})=p}} \left| \langle \hat{C}_1\rangle_{\rho_G} \dots \langle \hat{C}_{|p|}\rangle_{\rho_G}] - \langle \hat{C}_1\rangle_{\rho_G} \dots \langle \hat{C}_{|p|}\rangle_{\rho_G} \right| \leqslant \tilde{S}^{\tilde{S}}|\mathcal{C}|^{\tilde{S}} C_{\text{clust}}\, e^{-\Delta/\xi}\,,$$

where $\langle A\rangle_{\rho_G} = \operatorname{Tr}(A\rho_G)$ denotes the expectation value with respect to the Gaussian state ρ_G.

Proof. Here we will show that expectation values of the Gaussian state can be broken down into individual expectation values for the different clusters. For this, we will use that, while we, a priori, do not have exponential clustering for arbitrary operators, the two-point correlation functions have to be equal to those of ρ, by definition of the Gaussian state and thus decay exponentially. Thus, we can use Wick's theorem to break down the correlators into second moments and use exponential clustering on that level. We begin by using the trivial bound $|V_{j,k}| \leqslant 1$ on the evolution matrix, which gives

$$\begin{aligned}
&\left| \sum_{\substack{j_1,\dots,j_n\in\mathcal{C}\\ p_\Delta(\{j_\alpha\})=p}} \langle \hat{C}_1 \dots \hat{C}_q\rangle_{\rho_G} - \langle \hat{C}_1\rangle_{\rho_G} \dots \langle \hat{C}_q\rangle_{\rho_G} \right| \\
&\leqslant \sum_{\substack{j_1,\dots,j_n\in\mathcal{C}\\ p_\Delta(\{j_\alpha\})=p}} \left| \langle a_{j_1}^{(\alpha_1)} \dots a_{j_n}^{(\alpha_n)}\rangle_{\rho_G} - \langle \prod_{i\in p_1} a_{j_i}^{(\alpha_i)}\rangle_{\rho_G} \dots \langle \prod_{i\in p_q} a_{j_i}^{(\alpha_i)}\rangle_{\rho_G} \right|,
\end{aligned}$$

where the triangle inequality was used and any configuration of indices will be bounded individually. Using Wick's theorem we can rewrite the expectation values in both terms as a function of second moments. Here all possible combinations of second moments will appear, which are at most $\tilde{S}! \leqslant \tilde{S}^{\tilde{S}}$ many. Naturally, the first term will contain more such two-point contributions than the second one. The crucial thing to note is that if such a term appears, which is contained in the first, but not in the second term, then this implies that it contains at least one pair of indices with a distance larger than Δ. Using exponential clustering of the two-point correlators, this gives a suppression of $C_{\text{clust}} e^{-\Delta/\xi}$. In total, we thus obtain

$$\left| \sum_{\substack{j_1,\dots,j_n\in\mathcal{C}\\ p_\Delta(\{j_\alpha\})=p}} \langle \hat{C}_1 \dots \hat{C}_q\rangle_{\rho_G} - \langle \hat{C}_1\rangle_{\rho_G} \dots \langle \hat{C}_q\rangle_{\rho_G} \right| \leqslant \tilde{S}^{\tilde{S}}|\mathcal{C}|^{\tilde{S}} C_{\text{clust}}\, e^{-\Delta/\xi}\,,$$

where $|\mathcal{C}|^{\tilde{S}}$ captures the different index configurations and $\tilde{S}^{\tilde{S}}$ all terms appearing in Wick's theorem. □

Thus, decoupling the expectation values of the Gaussian terms yield an approximation error

$$\epsilon' \mathrel{+}= \tilde{S}^{\tilde{S}}|\mathcal{C}|^{\tilde{S}} C_{\text{clust}}\, e^{-\Delta/\xi}\,.$$

Having decoupled the patches, we now separate the terms according to their partition as follows.

A) All even partitions, which have at least one cluster with at least four fermionic operators

B) Only pairs

C) All other partitions, which therefore have a cluster with an odd number of fermionic operators

The terms containing odd partitions immediately have to vanish, as the state has an even particle parity. The quadratic terms in turn are identical for the actual state ρ and its Gaussian counterpart ρ_G, which is fixed by demanding that is has the same second moments. Thus, contributions **B**) and **C**) are bounded with the above error terms, which are exponentially suppressed in Δ, which will be picked later to optimise the bound. The full non-Gaussianity of the initial state is thus contained in contribution **A**), which will be bounded in the following.

Using transport: We now use the transport property of the Hamiltonian (see Def. 5) to show that this non-Gaussian term is dynamically suppressed. This is expressed in the following lemma.

Lemma 9 (Larger clusters)**.** *Let us look at the following sum of Δ-partition of $n \leqslant \tilde{S}$ numbers with only even contributions that contains at least one cluster of size at least four. Then for suitably large t, we have*

$$\sum_{\substack{p \text{ even} \\ \text{with cluster}}} \sum_{\substack{k_1,\cdots,k_n \in \mathcal{C} \\ p_\Delta(\{k_1,\cdots,k_n\})=p}} \left|\langle \hat{C}_1\rangle_\rho \cdots \langle \hat{C}_l\rangle_\rho\right|$$
$$\leqslant \tilde{S}^{(2+2d_\mathcal{L})\tilde{S}+1} 2\, C_{\text{trans}}^4 \left(\Delta^{4d_\mathcal{L}} |\mathcal{C}| t^{-\frac{4d_\mathcal{L}}{3}}\right)\left(1+|\mathcal{C}|^2 C_{\text{clust}}\, e^{-\Delta/\xi}\right) .$$

Proof. We begin by ordering the partitions according to the number of pairs they contain. As the partition contains at least one cluster with at least four indices, we know that there can be at most $(n-4)/2$ pairs in the expansion. We thus have to bound

$$R(t) := \sum_{m=0}^{\lfloor \frac{n}{2}-2\rfloor} \sum_{\substack{p \text{ even} \\ \text{with } m \text{ pairs}}} \left| \sum_{\substack{k_1,\ldots,k_n \in \mathcal{C} \\ p_\Delta(\{k_\alpha\})=p}} \left[\langle \hat{C}_1\rangle_\rho \ldots \langle \hat{C}_{|p|}\rangle_\rho - \langle \hat{C}_1\rangle_{\rho_G} \ldots \langle \hat{C}_{|p|}\rangle_{\rho_G}\right]\right| .$$

In order not to overburden the notation, many dependences are suppressed here, as before. In particular, the precise set of indices s, where the time-evolving fermionic operators are originally supported, is omitted. This should not cause confusion, as all following arguments will be independent of that initial configuration. For the purpose of this proof, the k_s can therefore truly be thought of as free indices, which will be relabeled when needed. In the next step, we order the partitions and move all clusters to the left and all pairs to the right and use that the pairs look identical for the states ρ and its Gaussian counterpart ρ_G

$$R(t) = \sum_{m=0}^{\lfloor \frac{n}{2}-2\rfloor} \sum_{\substack{p \text{ even} \\ \text{with } m \text{ pairs}}} \left| \sum_{\substack{k_1,\ldots,k_n \in \mathcal{C} \\ p_\Delta(\{k_\alpha\})=p}} \left[\langle \hat{C}_1\rangle_\rho \ldots \langle \hat{C}_{|p|-m}\rangle_\rho - \langle \hat{C}_1\rangle_{\rho_G} \ldots \langle \hat{C}_{|p|-m}\rangle_{\rho_G}\right]\langle \hat{C}_{|p|-m+1}\rangle_\rho \ldots \langle \hat{C}_{|p|}\rangle_\rho\right| .$$

Next, we want to decouple the sum of the indices for the cluster and the sum of the indices for the pairs. First, we define p_c as the cluster part of the partition and p_p as the pair part. For concreteness, consider the following example

$$p = \{\{1,2,5,7\},\{3,6\},\{4,8\}\} ,$$
$$p_c = \{\{1,2,5,7\}\} ,$$
$$p_p = \{\{3,6\},\{4,8\}\} .$$

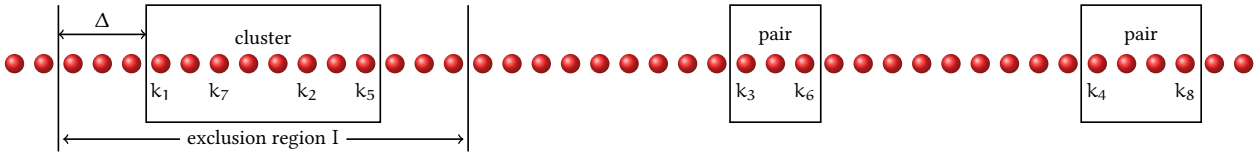

Figure C.1: Example of a partition on the lattice. The indices k_1, k_2, k_5, k_7 form a cluster, while the others form two pairs. The pairs must not be closer than a length $\Delta = 3$ to the cluster, leading to an exclusion region I for the pairs.

Here the partition p implies that indices k_1, k_2, k_5, k_7 are within distance Δ of each other and form a cluster. Correspondingly k_3, k_6 and k_4, k_8 respectively form a pair and all three patches are separated from each other with a distance larger than Δ (see Fig. C.1). As a summation scheme, we first choose the indices of the cluster contributions. The pairs are then still free to be distributed over the lattice except that they have to have a distance larger than Δ to the cluster indices. Thus the cluster indices can be thought of as creating an exclusion region I for the pair indices. Taking the maximum over such exclusion regions, using an operator norm estimate for the cluster contribution and relabelling indices appropriately gives the following bound

$$R(t) = \sum_{m=0}^{\lfloor \frac{n}{2}-2 \rfloor} \sum_{\substack{p \text{ even} \\ \text{with } m \text{ pairs}}} \left(\sum_{\substack{k_1,\dots,k_{|p|-m} \in \mathcal{C} \\ p_\Delta(\{k_\alpha\})=p_c}} 2 \|\hat{C}_1\| \dots \|\hat{C}_{|p|-m}\| \right) \max_{I \subset C} \left| \sum_{\substack{j_1,\dots,j_m \in \mathcal{C}\setminus I \\ p_\Delta(\{j_\alpha\})=p_p}} \langle \hat{C}_{|p|-m+1} \rangle_\rho \dots \langle \hat{C}_{|p|} \rangle_\rho \right| . \tag{C.o.3}$$

The cluster terms can be bounded by using the trivial operator norm estimate $\|r_s\| \leqslant 1$ and the homogeneous suppression of the evolution matrix V. A counting of the possible index configurations gives for each cluster $|\mathcal{C}|$ many positions. Around those positions, the indices can vary on a region that is maximally $(2\tilde{S}\Delta)^{d_\mathcal{L}}$ large. Each contribution is homogeneously suppressed with $C_{\text{trans}} t^{-d_\mathcal{L}/3}$. This gives

$$\begin{aligned} \left(\sum_{\substack{k_1,\dots,k_{|p|-m} \in \mathcal{C} \\ p_\Delta(\{k_\alpha\})=p_c}} 2 \|\hat{C}_1\| \dots \|\hat{C}_{|p|-m}\| \right) &\leqslant 2|\mathcal{C}|^{\frac{n-2m}{4}} \left((2\tilde{S}\Delta)^{d_\mathcal{L}} \right)^{n-2m} \left(C_{\text{trans}} t^{-d_\mathcal{L}/3} \right)^{n-2m} \\ &\leqslant 2(2\tilde{S})^{d_\mathcal{L}\tilde{S}} \left(\Delta^{d_\mathcal{L}} C_{\text{trans}} t^{-d_\mathcal{L}/3} |\mathcal{C}|^{1/4} \right)^{n-2m} \\ &\leqslant 2(2\tilde{S})^{d_\mathcal{L}\tilde{S}} g_{\text{trans}}(t) , \end{aligned}$$

where we defined the following function

$$g_{\text{trans}}(t) := \sum_{m=0}^{\lfloor \frac{\tilde{S}}{2}-2 \rfloor} \left(\Delta^{d_\mathcal{L}} C_{\text{trans}} t^{-d_\mathcal{L}/3} |\mathcal{C}|^{1/4} \right)^{n-2m} .$$

In the relevant regime where the cluster contributions are suppressed, the term in the bracket needs to be smaller than one. This allows to estimate

$$g_{\text{trans}}(t) \leqslant \tilde{S} \left(\Delta^{d_\mathcal{L}} C_{\text{trans}} t^{-d_\mathcal{L}/3} |\mathcal{C}|^{1/4} \right)^4 .$$

To complete the argument, we still need a bound for the second part of the sum in Eq. (C.o.3). For this, we note that rather than looking at the pairs of the partition p, we can also take a maximum over all

possible partition of the corresponding indices into m pairs, which we denote by σ_m. Thus, we define the following function

$$f(m) := \max_{\substack{I \subset C \\ \sigma_m}} \left| \sum_{\substack{j_1,\dots,j_m \in \mathcal{C}\setminus I \\ p_\Delta(\{j_\alpha\})=\sigma_m}} \langle \hat{C}_1 \rangle_\rho \dots \langle \hat{C}_m \rangle_\rho \right| .$$

We thus obtain the bound for the contribution of the clusters in Eq. (C.0.3)

$$\begin{aligned} R(t) &\leqslant \tilde{S}^{\tilde{S}} 2 \left(2\tilde{S}\right)^{d_{\mathcal{L}} \tilde{S}} g_{\text{trans}}(t) \sum_{m=0}^{\lfloor \frac{n}{2}-2 \rfloor} f(m) \\ &=: \beta_S(t) \sum_{m=0}^{\lfloor \frac{n}{2}-2 \rfloor} f(m) , \end{aligned}$$

where $\tilde{S}^{\tilde{S}}$ the sum over the partitions. So what is left to do is to bound the function f. Naturally, if there are no pairs left, the function is trivially one. A single pair corresponding to $f(1)$ can be bounded by relaxing the constraint that the indices form a pair and let them roam free on the full region $\mathcal{C} \setminus I$. The unconstrained problem can be bounded using lemma 5, while exponential clustering can be used to bound the difference of constrained and unconstrained problem, consisting of contributions of terms separated by a distance larger than Δ

$$\begin{aligned} \left| \sum_{\substack{j_{2l-1},j_{2l} \in \mathcal{C}\setminus I \\ d(j_{2l-1},j_{2l}) \leqslant \Delta}} \langle \hat{C}_l \rangle_\rho \right| &\leqslant \left| \sum_{j_{2l-1},j_{2l} \in \mathcal{C}\setminus I} \langle \hat{C}_l \rangle_\rho \right| + \left| \sum_{\substack{j_{2l-1},j_{2l} \in \mathcal{C}\setminus I \\ d(j_{2l-1},j_{2l}) > \Delta}} \langle \hat{C}_l \rangle_\rho \right| \\ &\leqslant 1 + |\mathcal{C}|^2 C_{\text{clust}} e^{-\Delta/\xi} . \end{aligned}$$

The main obstacle for bounding the function f for $m > 1$ is that the partition σ_m ensures that all indices are pairs, which results in a complicated constraint that prohibits that indices occupy closeby lattice regions. To bound the function, we will drop this constraint and show that the difference between the constrained and unconstrained problem can be bounded. This will rely on an recursive argument that eventually recovers the original function $f(m)$, but with a number of pairs m that is reduced by at least two. If we drop the constraint that the pairs must not overlap, the only constraint remaining is that consecutive indices form pairs, meaning that $d(j_{2l-1}, j_{2l}) \leqslant \Delta$. For the product of all unconstrained pairs, this directly gives

$$\left| \sum_{\substack{j_1,\dots,j_{2m} \in \mathcal{C}\setminus I \\ d(j_{2l-1},j_{2l}) \leqslant \Delta}} \langle \hat{C}_1 \rangle_\rho \dots \langle \hat{C}_m \rangle_\rho \right| = \prod_{l=1}^{m} \left| \sum_{\substack{j_{2l-1},j_{2l} \in \mathcal{C}\setminus I \\ d(j_{2l-1},j_{2l}) \leqslant \Delta}} \langle \hat{C}_l \rangle_\rho \right| \leqslant \left[1 + C_{\text{clust}} e^{-\Delta/\xi} |\mathcal{C}|^2\right]^m .$$

This leaves us with controlling the difference between the constrained and unconstrained pairs

$$\epsilon(\sigma_m, I) = \left| \sum_{\substack{j_1,\dots,j_{2m} \in \mathcal{C}\setminus I \\ p_\Delta(\{j_\alpha\})=\sigma_m}} \langle \hat{C}_1 \rangle_\rho \dots \langle \hat{C}_m \rangle_\rho - \sum_{\substack{j_1,\dots,j_{2m} \in \mathcal{C}\setminus I \\ d(j_{2l-1},j_{2l}) \leqslant \Delta}} \langle \hat{C}_1 \rangle_\rho \dots \langle \hat{C}_m \rangle_\rho \right| .$$

In order to get this under control, we will introduce the notion of a refinement of a partition [24]. This gives a partial ordering of partitions where $p > \sigma$ precisely if p can be created by joining sets contained in

σ. The key insight here is that the above difference between constrained and unconstrained pairs precisely amounts to all possible coarsening of the partition σ_m

$$\epsilon(\sigma_m, I) = \left| \sum_{\substack{\sigma \text{ even} \\ \sigma > \sigma_m}} \sum_{\substack{j_1,\dots,j_{2m} \in \mathcal{C}\setminus I \\ p_\Delta(\{j_\alpha\})=\sigma \\ d(j_{2l-1},j_{2l}) \leqslant \Delta}} \langle \hat{C}_1 \rangle_\rho \dots \langle \hat{C}_m \rangle_\rho \right| .$$

This coarsening necessarily leads to pairs that are overlapping. Those will be summarised into numbers $\tilde{C}_l = \prod_r \langle \hat{C}_r \rangle_\rho$ that contain all pairs in that coarsened set. Reordering the sum according to newly created clusters and pairs and including all even partitions q with $w \leqslant m-2$ pairs and at least one cluster yields

$$\epsilon(\sigma_m, I) \leqslant \sum_{w=0}^{m-2} \sum_{\substack{q \text{ even} \\ \text{with } w \text{ pairs}}} \left(\sum_{\substack{j_1,\dots,j_{|q|-w} \in \mathcal{C} \\ q_\Delta(\{j_\alpha\})=q_c \\ d(j_{2l-1},j_{2l}) \leqslant \Delta}} |\tilde{C}_1| \dots |\tilde{C}_{|q|-w}| \right) \max_{I \subset C} \left| \sum_{\substack{k_1,\dots,k_w \in \mathcal{C}\setminus I \\ q_\Delta(\{j_\alpha\})=q_p}} \langle \hat{C}_{|q|-w+1} \rangle_\rho \dots \langle \hat{C}_{|q|} \rangle_\rho \right| .$$

As we only need the homogoneous suppression for those terms, it does not matter whether they are actual clusters or products of pair norms. Thus, we can proceed in the same way as in Eq. (C.0.3). We thus obtain the following recursion formula

$$f(m) \leqslant \beta_S(t) \sum_{l=0}^{m-2} f(l) ,$$

with the final points $f(0) = 1$ and $f(1) = 1 + |\mathcal{C}|^2 C_{\text{clust}} e^{-\Delta/\xi}$ and the relation to the desired bound

$$R(t) \leqslant \beta_S(t) \sum_{l=0}^{\frac{\tilde{S}}{2}-2} f(l) .$$

In each step of the recursion at most $\tilde{S}$ branches can be created, which implies that in total at most $\tilde{S}^{\tilde{S}}$ values appear. As $f(1) > f(0)$ the worst case estimate is all of these branches ending at $f(1) = \left(1 + |\mathcal{C}|^2 C_{\text{clust}} e^{-\Delta/\xi}\right)$. Finally, in the relevant regime, where the above estimate indeed yields a bound, we have $\beta < 1$ and thus $\beta^k < \beta$. Thus, in total we have the bound

$$R(t) \leqslant \tilde{S}^{\tilde{S}} \beta_S(t) \left(1 + |\mathcal{C}|^2 C_{\text{clust}} e^{-\Delta/\xi}\right) .$$

Substituting β, estimating $g_{\text{trans}}(t)$ as described above and using $2 < \tilde{S}$ yields

$$\begin{aligned} R(t) &\leqslant \tilde{S}^{\tilde{S}} \tilde{S}^{|S|} 2\,(2S)^{d_{\mathcal{L}}|S|}\, \tilde{S} \left(\Delta^{d_{\mathcal{L}}} C_{\text{trans}} t^{-d_{\mathcal{L}}/3} |\mathcal{C}|^{1/4}\right)^4 \left(1 + |\mathcal{C}|^2 C_{\text{clust}} e^{-\Delta/\xi}\right) \\ &\leqslant \tilde{S}^{(2+2d_{\mathcal{L}})\tilde{S}+1} 2\, C_{\text{trans}}^4 \left(\Delta^{4d_{\mathcal{L}}} |\mathcal{C}|\, t^{-\frac{4d_{\mathcal{L}}}{3}}\right) \left(1 + |\mathcal{C}|^2 C_{\text{clust}} e^{-\Delta/\xi}\right) . \end{aligned}$$

□

As derived above, the contributions with one cluster give an error term

$$\epsilon' \mathrel{+}= \tilde{S}^{(2+2d_{\mathcal{L}})\tilde{S}+1} 2\, C_{\text{trans}}^4 \Delta^{4d_{\mathcal{L}}} |\mathcal{C}|\, t^{-\frac{4d_{\mathcal{L}}}{3}} \left(1 + |\mathcal{C}|^2 C_{\text{clust}} e^{-\Delta/\xi}\right) .$$

Summarising the different ϵ' created and bounding the $\tilde{S}$ contributions of all terms with $\tilde{S}^{(2+2d_{\mathcal{L}})\tilde{S}+1}$, the proof is concluded by using $|C| = (\nu + \nu_\epsilon) t^{d_{\mathcal{L}}}$ and choosing $\Delta = t^{-d_{\mathcal{L}}/24}$, which in leading order gives a scaling

$$\epsilon \propto t^{-\frac{d_{\mathcal{L}}}{6}} .$$

Thus the non-Gaussianity that can locally be observed is suppressed exponentially in time. In other words, for any fixed error ϵ, we can find a relaxation time t_{relax}, such that the difference to a Gaussian state is bounded by ϵ for all times $t \in [t_{\text{relax}}, t_{\text{rec}}]$. Here, the recurrence time is set by the point where the homogeneous suppression breaks down. □

D

CONSTANTS OF MOTION IMPLY INFORMATION PROPAGATION

The following appendix presents the technical results of Ref. [5]. We sincerely thank Albert H. Werner, Marcel Goihl, Jens Eisert and Winton Brown for the very fruitful collaboration.

In this appendix, we provide a proof for the statement in section 6.2 that the existence of a single constant of motion that is approximately local together with a non-degenerate spectrum is sufficient to prove information propagation. For simplicity and as it can be generalised later on, we begin with the case of an exactly local constant of motion.

Corollary 16 (Information propagation: Strictly local constants)**.** *Let* H *be a Hamiltonian with non-degenerate energies and gaps and* $\mathcal{Z}_X$ *be a strictly local constant of motion supported on* X*, with eigenspaces with dimension larger than* $d_{\min}$*. Then* H *necessarily has transport in the sense that for any finite region* S *containing* X *there exists a local operator* B *initially supported on* X *with* $\|B\| = 1$ *such that* B_t*, on average, has support outside* S

$$\overline{\|B_t - \Gamma_S(B_t)\|} \geqslant 1 - \frac{d^{|S|+|X|/2}}{{d_{\min}}^{1/2}} d^{-N/2} .$$

Proof. We begin by looking at the spectral decomposition of the local constant of motion

$$\mathcal{Z}_X = \sum_{k=1}^{M} \lambda_k P_k ,$$

with exactly local projectors P_k supported on X and M distinct eigenvalues. The goal is then to construct an operator that is block-off-diagonal with respect to the projectors P_k. For this, let $d_{\min}$ be the smallest dimension of the eigenspaces of $\mathcal{Z}_X$, when viewed as a local operator. For the construction, we fix two eigenspaces of $\mathcal{Z}_X$. The larger of the two is then truncated down to the dimension d_{trunc} of the smaller one. Note that the resulting dimension of both spaces is lower bounded by $d_{\min}$. In these subspaces, we further fix some basis labelled by two indices $|k, r\rangle$ where k labels the eigenspaces of $\mathcal{Z}_X$ and r the basis vectors in each of these subspaces. We denote the eigenspaces by $k = 0$ and $k = 1$. The operator A is constructed to be supported on the small region X and taken to be the flip operator between the subspaces

$$B = \sum_{r}^{d_{\text{trunc}}} |k = 0, r\rangle\langle k = 1, r| + |k = 1, r\rangle\langle k = 0, r| .$$

The operator norm of this observable is one and we proceed by constructing an initial state that is an eigenstate of A to eigenvalue 1, but still has large effective dimension. For this, we pick the subspace with smaller dimension and take the equal superposition, denoted by $|\nu\rangle$ of all eigenvectors in this subspace. For this, it is crucial to choose the subspace with smaller dimension, as the truncation in general, is not aligned with the eigenstates of the global Hamiltonian. The number of eigenvectors in the untruncated subspace is lower bounded by $\widetilde{d}_{\min} = d_{\min} d^{N-|X|}$, which is simply the smallest eigenspace dimension of $\mathcal{Z}_X$ when viewed as an operator on the full lattice. The initial state vector is then taken to be

$$|\psi\rangle = \frac{1}{\sqrt{2}}(|\nu\rangle + B|\nu\rangle) .$$

It is straightforward to check that this is indeed an eigenstate of B, since $B^2|\nu\rangle = |\nu\rangle$. What is more, the state vector $|\psi\rangle$ has an effective dimension lower bounded by $\widetilde{d}_{\min}$. Based on this analysis of the constant

of motion, we can directly follow the proof of lemma 2, as presented in section 6.2. Using the construction of the initial state and the observable B described above, we immediately obtain

$$\overline{\|B_t - \Gamma_S(B_t)\|} \geqslant 1 - \frac{d_{sys}}{d_{eff}^{1/2}} ,$$

from the same equilibration results as in section 6.2 (see Eq. (6.2.2)). Inserting the effective dimension described above $d_{eff} \geqslant \widetilde{d}_{min} = d_{min} d^{N-|X|}$ and $d_{sys} = d^{|S|}$ concludes the proof. □

In many localising systems, one does not expect the constants of motion to be strictly local, but only approximately local (see Def. 2) [180]. Using perturbation theory, it follows that this decay is sufficient to obtain local approximations for the eigenprojectors and makes it possible to once again construct an observable A that is transported through the system. This gives rise to the Thm. 10 as stated in section 6.2. For convenience, we repeat the theorem here.

Theorem (Information propagation)**.** *Let H be a Hamiltonian with non-degenerate energies and gaps and $\mathcal{Z}$ be a approximately local constant of motion with decay function g with localisation region X, spectral gap $\gamma > 0$ and eigenspaces with dimension larger than $\widetilde{d}_{min}$. Then H necessarily has information propagation on average in the sense that there exists a local operator B initially supported on $X_l \supset X$ with $\|B\| = 1$ such that B_t, on average, has support outside any finite region S*

$$\overline{\|B_t - \Gamma_S(B_t)\|} \geqslant 1 - 13\frac{g(l)}{\gamma} - \frac{d_s}{2\widetilde{d}_{min}^{1/2}} .$$

Proof. The first step of the proof is to show that the approximate locality of the constant of motion also implies quasi-local eigenprojectors. Let

$$\mathcal{Z} = \sum_{k=1}^{M} \lambda_k P_k$$

and let γ denote the smallest spectral gap. Due to locality, we can express $\mathcal{Z}$ for each fixed l, as

$$\mathcal{Z} = \Gamma_{X_l}(\mathcal{Z}) + V_l ,$$

with a bounded perturbation V_l satisfying

$$\begin{aligned} V_l &= \mathcal{Z} - \Gamma_{X_l}(\mathcal{Z}) , \\ \|V_l\| &< g(l) . \end{aligned}$$

Let P_k^l be the eigenprojectors for the truncated observable. Perturbation theory assures us that the perturbed eigenspaces stay approximately orthogonal (see Thm. VII.3.1 in Ref. [14])

$$\|P_k(\mathbb{1} - P_k^l)\| \leqslant \frac{\|V_l\|}{\gamma} = \frac{g(l)}{\gamma} ,$$

which also implies

$$\|P_k - P_k^l\| \leqslant \frac{2\|V_l\|}{\gamma} = \frac{2g(l)}{\gamma} . \tag{D.0.1}$$

Choosing the distance l large enough such that the function g becomes smaller than $\gamma/2$, we know that the perturbed and unperturbed eigenspaces have the same dimension [14]. This local approximation of the eigenprojectors of the constant of motion are the basis for the construction of the observable B as well as the initial state ρ.

In order to construct the observable, we work with the truncated constant of motion $\Gamma_{X_l}(\mathcal{Z})$, fix two subspaces and construct the same flip operator as in the case of exactly local constants of motion

$$B = \sum_{r}^{d_{\text{trunc}}} |k=0,r\rangle\langle k=1,r| + |k=1,r\rangle\langle k=0,r| \ .$$

Without loss of generality, let $k=0$ be the space with smaller dimension and $k=1$ the one truncated to d_{trunc}. Let $P_1^l|_I$ be the projector on the truncated subspace of P_1^l corresponding to the image of B.

For the initial state, we use the corresponding subspaces, again labelled by $k=0,1$ of the full constant of motion $\mathcal{Z}$. Again we pick the smaller of the two subspaces and define $|\nu\rangle$ to be the equal superposition of all eigenstates within this space. The initial state vector is then

$$|\psi\rangle = \frac{1}{\sqrt{2}}(|\nu\rangle + B|\nu\rangle) \ .$$

By construction, the effective dimension and the equilibration results are the same as in the case of a strictly local constant of motion.

Crucial in the above construction is that we use the truncated constant of motion $\Gamma_{X_l}(\mathcal{Z})$ for the observable B in order to ensure locality, while we use the full object $\mathcal{Z}$ for the initial state in order to achieve a large effective dimension. What remains to be shown is that despite this locality difference in the construction, we still achieve a large expectation value of B with $|\psi\rangle$, but an almost vanishing expectation value with the infinite time average.

As a first step, we show that B is almost block-off-diagonal with respect to the eigenprojectors of the full constant of motion $\mathcal{Z}$. Introducing the identity $\mathbb{1} = P_k^l + Q_k^l$, this takes the following form

$$\|P_k B P_k\| \leqslant \|P_k P_k^l B Q_k^l P_k\| + \|P_k Q_k^l B P_k^l P_k\| \leqslant 2\frac{g(l)}{\gamma} \ .$$

Here we used that B is block-off-diagonal with respect to the truncated constant of motion $\Gamma_{X_l}(\mathcal{Z})$. The same estimate holds for the projectors Q_k.

Using this, bounding the expectation value with the infinite time average is straightforward

$$\begin{aligned} \text{Tr}(B\omega) &= \text{Tr}(BP_0\omega P_0) + \text{Tr}(BQ_0\omega Q_0) \\ &\leqslant \|P_0 B P_0\| + \|Q_0 B Q_0\| \leqslant 4\frac{g(l)}{\gamma} \ . \end{aligned} \tag{D.0.2}$$

We now have to show that the expectation value of B with ρ is large initially

$$\langle\psi|B|\psi\rangle \geqslant \langle\nu|BB|\nu\rangle - \frac{1}{2}|\langle\nu|B|\nu\rangle + \langle\nu|BBB|\nu\rangle| \ .$$

In the following, we show that the first term is almost one, while the other two almost vanish due to the block-off-diagonality. For the first term, we use that $B^2 = P_0^l + P_1^l|_I$, where $P_1^l|_I$ is the projector onto the image of B in P_1^l. Using that $\langle\nu|Q|\nu\rangle$ can only increase if we enlarge the subspace of the projector Q, we obtain

$$\begin{aligned} \langle\nu|BB|\nu\rangle &\geqslant \langle\nu|P_0^l|\nu\rangle - |\langle\nu|Q_0^l|\nu\rangle| \\ &\geqslant \langle\nu|P_0|\nu\rangle - |\langle\nu|Q_0|\nu\rangle| - 4\frac{g(l)}{\gamma} \\ &= 1 - 4\frac{g(l)}{\gamma} \ , \end{aligned}$$

where we used (D.0.1). The second term can be bounded directly using block-off-diagonality

$$|\langle v|B|v\rangle| \leqslant \|P_0 B P_0\| \leqslant 2\frac{g(l)}{\gamma} .$$

The last term, finally can be bounded as follows.

$$\begin{aligned}|\langle v|BBB|v\rangle| &= |\langle v|P_0 B(P_0^l + P_1^l|_I)P_0|v\rangle| \\ &\leqslant \|P_0 B P_0^l\| + \|P_1^l P_0\| \\ &\leqslant \|P_0^l B P_0^l\| + 2\frac{g(l)}{\gamma} + \frac{g(l)}{\gamma} \\ &\leqslant 3\frac{g(l)}{\gamma} .\end{aligned}$$

To summarise, we have

$$\langle\psi|B|\psi\rangle \geqslant 1 - 9\frac{g(l)}{\gamma} . \tag{D.0.3}$$

Putting together the estimates for the expectation value of B with the initial state, the equilibration result and the expectation value of B with the infinite time average, we obtain the desired bound. More precisely, we choose $\rho = |\psi\rangle\langle\psi|$ and proceed as follows

$$\begin{aligned}\overline{\|B_t - \Gamma_S(B_t)\|} &\geqslant \mathrm{Tr}(B\rho) - \overline{|\mathrm{Tr}\left(\Gamma_S\left(B_{t_0}\right)\rho_{-t}\right)|} \\ &\geqslant \mathrm{Tr}(B\rho) - \overline{\|w - \rho_{-t}\|_1} - |\mathrm{Tr}\left(\Gamma_S\left(B_{t_0}\right)w\right)| \\ &\geqslant \mathrm{Tr}(B\rho) - \frac{d_{sys}}{2{d_{eff}}^{1/2}} - |\mathrm{Tr}\left(\Gamma_S\left(B_{t_0}\right)w\right)| .\end{aligned}$$

Inserting the effective dimension $d_{eff} = \widetilde{d}_{min}$ and using Eqs. (D.0.2) and (D.0.3) concludes the proof

$$\begin{aligned}\overline{\|B_t - \Gamma_S(B_t)\|} &\geqslant 1 - 9\frac{g(l)}{\gamma} - \frac{d_s}{2\widetilde{d}_{min}^{1/2}} - 4\frac{g(l)}{\gamma} \\ &\geqslant 1 - 13\frac{g(l)}{\gamma} - \frac{d_s}{2\widetilde{d}_{min}^{1/2}} .\end{aligned}$$

□

ENERGY FILTERING

The following appendix presents the technical basics of Ref. [4]. We sincerely thank Albert H. Werner, Winton Brown, Volkher B. Scholz and Jens Eisert for the very insightful collaboration which resulted in this work.

A important technical tool of this thesis is energy-filtering with respect to a suitable filter function. Energy-filtering of a local observable A supported on X is defined as

$$I_f^H(A) = \int_{-\infty}^{\infty} dt\, f(t)\, A(t)\,.$$

Here $f : \mathbb{R} \to \mathbb{R}^+$ is a so-called filter function, usually taken as a C^∞-function. Here, $A(t) = e^{itH} A e^{-itH}$ refers to time evolution under the full Hamiltonian H, but we later also consider filters with respect to truncated Hamiltonians. Energy-filtering allows to alter the matrix elements of a local observable in the eigenbasis of a Hamiltonian, while still keeping some form of locality [168]. We work with two types of filter functions. Gaussian filter functions in particular provide a good compromise between locality in Fourier space and decay behaviour in real time and hence allow us to pick out narrow energy windows, while still preserving the approximate locality of the observable.

Definition & Lemma 10 (Gaussian filters)**.** *A Gaussian filter is defined as*

$$I_\alpha^H(A) := \sqrt{\frac{\alpha}{\pi}} \int_{-\infty}^{\infty} dt\, e^{-\alpha t^2} A(t)\,,$$

where $\alpha > 0$ defines the sharpness of the filter. The matrix elements in the eigenbasis of the Hamiltonian fulfil

$$\langle r|\, I_\alpha^H(A)\, |s\rangle = \langle r|\, A\, |s\rangle\, e^{-(E_s - E_r)^2/(4\alpha)}\,.$$

For strongly localising systems (see Def. 11), local observables filtered with a Gaussian filter still remain approximately local in the sense that

$$\|I_\alpha^H(A) - I_\alpha^{H_l}(A)\| \leqslant C_{\mathrm{loc}}\, e^{-\mu l}\,,$$

where H_l contains all Hamiltonian supported on the enlarged sets X_l around the support X of A (see chapter 3.2). For systems with a mobility edge (see Def. 12), we have

$$|\langle k|\, [I_f(A), B]\, |k\rangle| \leqslant C_{\mathrm{mob}} e^{-\mu d(A,B)}\,.$$

Proof. The Gaussian suppression of off-diagonal elements readily follows from the definition

$$\begin{aligned}\langle r|\, I_\alpha(A)\, |s\rangle &:= \sqrt{\frac{\alpha}{\pi}} \int dt\, e^{-\alpha t^2}\, \langle r|\, A(t)\, |s\rangle \\ &= \langle r|\, A\, |s\rangle \sqrt{\frac{\alpha}{\pi}} \int dt\, e^{-\alpha t^2} e^{it(E_r - E_s)}\,,\end{aligned}$$

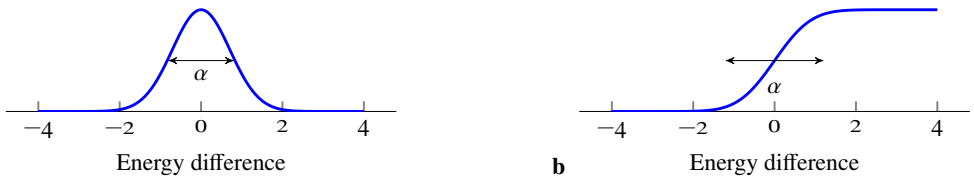

Figure E.1: *Taken from Ref. [4].* Presented is a schematic sketch of the energy filtering under a Gaussian (**a**) and a high-pass (**b**) filter and the role of the sharpness α.

and the fact that the Fourier transform of a Gaussian is again a Gaussian. Assuming strong dynamical localisation, deriving locality is straightforward,

$$\begin{aligned}\|I_\alpha^H(A) - I_\alpha^{H_l}(A)\| &= \left\| \sqrt{\frac{\alpha}{\pi}} \int_{-\infty}^{\infty} dt\, e^{-\alpha t^2} \left(A(t) - e^{itH_l} A e^{-itH_l} \right) \right\| \\ &\leqslant C_{loc}\, e^{-\mu l} ,\end{aligned}$$

where used that the Gaussian filter is normalised. The case with a mobility edge can be shown in the same way. □

Another important filter is the high-pass filter, which blocks large negative energy differences.

Definition & Lemma 11 (High-pass filters)**.** *A high-pass filter is defined by*

$$\Gamma_\alpha(A) := \lim_{\varepsilon \to 0} \frac{i}{2\pi} \int_{-\infty}^{\infty} dt\, \frac{e^{-\alpha t^2}}{t + i\varepsilon} A(t) .$$

Here $\alpha > 0$ describes the sharpness of the filter. The matrix elements can be bounded for any $|E_s - E_r| \geqslant \sigma \geqslant 0$ by

$$\frac{\langle r| \Gamma_\alpha(A) |s\rangle}{\langle r| A |s\rangle} = \begin{cases} \frac{1}{2} e^{-\sigma^2/(4\alpha)} & \text{for } E_r \geqslant E_s \\ 1 - \frac{1}{2} e^{-\sigma^2/(4\alpha)} & \text{for } E_r < E_s \end{cases} .$$

Local observables remain approximately local under a high-pass filter, in the sense that

$$|\langle k| [\Gamma_\alpha(A), B] |k\rangle| \leqslant \frac{e^{-\mu d(A,B)}}{2\pi} \left(4 + \ln \frac{\pi}{4\alpha} \right) .$$

Proof. Calculating the off-diagonal elements of such a high-pass filter relies on the subsequent bound on the error function of a Gaussian random variable proven in Ref. [66], stated here as lemma 12. Making use of the identity proven in Ref. [66]

$$\lim_{\varepsilon \to 0} \frac{i}{2\pi} \int_{-\infty}^{\infty} dt\, \frac{e^{-\alpha t^2} e^{-i\Delta E\, t}}{t + i\varepsilon} = \frac{1}{2\pi} \sqrt{\frac{\pi}{\alpha}} \int_{-\infty}^{0} d\omega\, e^{-(\omega + \Delta E)^2/(4\alpha)} ,$$

the bounds for the matrix elements of $\Gamma_\alpha(A)$ follow from lemma 12. The locality statement can be shown by splitting the integral into three parts [157] and using our assumption of dynamical localisation

$$\begin{aligned}\langle k| [\Gamma_\alpha(A), B] |k\rangle &\leqslant \frac{e^{-\mu d(A,B)}}{2\pi} \times \left(\int_{|t| \leqslant 1} dt\, e^{-\alpha t^2} + \int_{1 \leqslant |t| \leqslant \lambda} dt\, \frac{e^{-\alpha t^2}}{t} + \int_{|t| \geqslant \lambda} dt\, \frac{e^{-\alpha t^2}}{t} \right) \\ &\leqslant \frac{e^{-\mu d(A,B)}}{\pi} \left(1 + \ln \lambda + \frac{1}{2\lambda} \sqrt{\frac{\pi}{\alpha}} \right) .\end{aligned}$$

Here estimating the first term used the $\min(1, t)$ factor included in the definition of a mobility edge (see Def. 12). Choosing

$$\lambda = \frac{\sqrt{\pi}}{2\sqrt{\alpha}}$$

concludes the proof. □

In this lemma, we used the following estimate [66].

Lemma 12 (Hastings-Koma)**.** *Let* $E \in \mathbb{R}$, $\alpha > 0$ *then for all* $\gamma > 0$ *with* $E \leqslant -\gamma$

$$\frac{1}{2\pi}\sqrt{\frac{\pi}{\alpha}} \int_{-\infty}^{0} d\omega \; e^{-\frac{(\omega+E)^2}{4\alpha}} \leqslant \frac{1}{2} e^{-\gamma^2/(4\alpha)}$$

and for all $\gamma > 0$ *with* $E \geqslant \gamma$

$$\left| \frac{1}{2\pi}\sqrt{\frac{\pi}{\alpha}} \int_{-\infty}^{0} d\omega \; e^{-\frac{(\omega+E)^2}{4\alpha}} - 1 \right| \leqslant \frac{1}{2} e^{-\gamma^2/(4\alpha)}.$$

As in the above statements, we refer to the Gaussian and high pass filters of sharpness α as I_α^H and Γ_α^H, respectively. In case the local observable is filtered with the full system Hamiltonian, we often omit the H. It is an interesting insight that the locality structure of a Gaussian filter is independent of its sharpness α for dynamically localising systems, while it still depends on α for a high-pass filter.

F

EIGENSTATE LOCALISATION

The following appendix presents the technical results of Ref. [4]. We sincerely thank Albert H. Werner, Winton Brown, Volkher B. Scholz and Jens Eisert for the very insightful collaboration which resulted in this work.

In this appendix, we provide the proofs for the statements in section 6.4. We begin by proving lemma 3 needed for the proof of theorem 11. For convenience, we restate the lemma.

Lemma (Decoupled energy filtering)**.** *Under the assumption of locally independent gaps, energy-filtering of two observables can be factorised into local energy filters*

$$\left\| I_\alpha^{H_A+H_B}(AB) - I_\alpha^{H_A}(A)\, I_\alpha^{H_B}(B) \right\| \leqslant 2^{4L+1} e^{-\xi^2/(4\alpha)} ,$$

with $\xi = \min\{\eta, \sqrt{2}\tilde{\gamma}\}$*. Here* H_A *and* H_B *are chosen to include all Hamiltonian terms within distance* $d(A,B)/2$ *of the support of* A *and* B *respectively (See Fig. 6.3).*

Proof. To show that instead of applying an energy filter to AB, we can also apply it to the observables individually, we need to use that the eigenvalues of $H_A + H_B$ are disconnected on the two regions and we can thus label them by two different quantum numbers a, b. We hence get

$$\left\| I_\alpha^{H_A+H_B}(AB) - \sum_{a,b} |a,b\rangle\langle a,b|\, AB\, |a,b\rangle\langle a,b| + \sum_{a,b} |a,b\rangle\langle a,b|\, AB\, |a,b\rangle\langle a,b| - I_\alpha^{H_A}(A) I_\alpha^{H_B}(B) \right\| .$$

We will use the triangle inequality and proceed to show that both energy filters give only the diagonal entries up to a small error. Starting with the first term gives the following estimate,

$$\begin{aligned}
&\left\| I_\alpha^{H_A}(A) I_\alpha^{H_B}(B) - \sum_{a,b} |a,b\rangle\langle a,b|\, AB\, |a,b\rangle\langle a,b| \right\| \\
=&\left\| \sum_{a,b} \sum_{a'\neq a, b'\neq b} |a,b\rangle\langle a,b|\, AB\, |a',b'\rangle\langle a',b'| \exp\left(-\frac{(E_a - E_{a'} + E_b - E_{b'})^2}{4\alpha} \right) \right\| \\
=&\sum_{a,b} \sum_{a'\neq a, b'\neq b} \left\| |a,b\rangle\langle a,b|\, AB\, |a',b'\rangle\langle a',b'| \exp\left(-\frac{(E_a - E_{a'} + E_b - E_{b'})^2}{4\alpha} \right) \right\| \\
=&2^{4L}\, e^{-\eta^2/(4\alpha)} ,
\end{aligned}$$

where we assumed locally independent gaps. The second term yields the following estimate,

$$\begin{aligned}
&\left\| I_\alpha^{H_A}(A) I_\alpha^{H_B}(B) - \sum_{a,b} |a,b\rangle\langle a,b|\, AB\, |a,b\rangle\langle a,b| \right\| \\
=&\left\| \sum_{a,b} \sum_{a'\neq a, b'\neq b} |a,b\rangle\langle a,b|\, AB\, |a',b'\rangle\langle a',b'|\, e^{-\frac{(E_a - E_{a'})^2}{4\alpha}} e^{-\frac{(E_b - E_{b'})^2}{4\alpha}} \right\| \\
=&\left\| \sum_{a,b} |a,b\rangle\langle a,b|\, AB \widetilde{D}_{\tilde{\gamma}}^a \widetilde{D}_{\tilde{\gamma}}^b \right\| \leqslant 2^{2L}\, e^{-2\tilde{\gamma}^2/(4\alpha)} .
\end{aligned}$$

Here, $\widetilde{D}^{a}_{\tilde{\gamma}}$ is a diagonal matrix with entries $e^{-(E_a - E'_a)^2/(4\alpha)}$ for $a \neq a'$ and zero otherwise and we assumed locally independent gaps. Adding the two contributions and defining $\xi = \min\{\eta, \sqrt{2}\tilde{\gamma}\}$ concludes the proof. □

We proceed by presenting the proofs for the case of an information mobility edge. In this section, we provide the proof of theorem 12. As a first step, we need the following lemma, which states that each eigenvector only contributes a term that is exponentially suppressed with the distance of the two observables to the correlation function. For this, we need the localisation assumption only for the eigenvector $|k\rangle$ [4].

Lemma 13. *Let A, B be local observables and $|k\rangle$ a weakly localised eigenvector of H, i.e. satisfying*

$$\sup_{t\in[0,\infty)} |\langle k|\,[A(t), B]\,|k\rangle| \leqslant C_{\text{loc}}\, e^{-\mu d(A,B)} .$$

Then the contribution of any eigenvector $|l\rangle, l \neq k$, to the correlation function is exponentially suppressed, in the sense that

$$|\langle k|\,A\,|l\rangle\langle l|\,B\,|k\rangle| \leqslant 2C_{\text{mob}} e^{-\mu d(A,B)} .$$

Proof. The proof of this lemma again uses an energy filter with a Gaussian filter function (see Def. 10) and works with $\langle k|\,B\,|k\rangle = 0$, which can always be achieved by using a shifted observable $\tilde{B} = B - \langle k|\,B\,|k\rangle$. For this proof the filter function is multiplied by a complex factor $e^{it(E_k - E_l)}$ such that its Fourier transform approximately suppresses all transitions except the one from level k to level l. In a mild variant of the above filter function, we define $f : \mathbb{R} \to \mathbb{R}^+$ and the corresponding filter as

$$\begin{aligned} f(t) &:= \sqrt{\frac{\alpha}{\pi}} e^{it(E_k - E_l)} e^{-\alpha t^2} , \\ I_f(A) &:= \int dt\, f(t) A(t) , \\ \langle r|\,I_f(A)\,|s\rangle &= \langle r|\,A\,|s\rangle\, e^{-((E_s - E_r) - (E_l - E_k))^2/(4\alpha)} . \end{aligned}$$

With this energy filter, we can proceed to prove the lemma

$$\begin{aligned} |\langle k|\,A\,|l\rangle\langle l|\,B\,|k\rangle| &= \left| \langle k|\,I_f(A)B\,|k\rangle - \sum_{m\neq l} \langle k|\,A\,|m\rangle\langle m|\,B\,|k\rangle\, e^{-(E_m - E_l)^2/(4\alpha)} \right| \\ &\leqslant |\langle k|\,[I_f(A), B]\,|k\rangle| + |\langle k|\,BI_f(A)\,|k\rangle| + 2^L e^{-\gamma^2/(4\alpha)} \\ &\leqslant C_{\text{mob}} e^{-d(A,B)} + 2^L \left(e^{-\gamma^2/(4\alpha)} + e^{-\zeta^2/(4\alpha)} \right) . \end{aligned}$$

Here, $\gamma > 0$ refers to the smallest gap and $\zeta > 0$ is the smallest degeneracy of the gaps for fixed E_k as defined in the main text and in the last step we used weak dynamical localisation of the eigenvector $|k\rangle$. We can now conclude the proof by choosing α small enough such that

$$2^L \left(e^{-\gamma^2/(4\alpha)} + e^{-\zeta^2/(4\alpha)} \right) \leqslant C_{\text{mob}} e^{-\mu d(A,B)} ,$$

which means that we pick a filter function that is narrow enough in Fourier space. Setting $\xi := \min(\gamma, \zeta)$ it would even be enough to choose

$$\frac{\xi^2}{4} \left(\ln \frac{2^{2L+1}}{C_{\text{mob}}} \right)^{-1} \geqslant \alpha ,$$

independently of $d(A, B)$. □

We now turn to the proof of theorem 12. For convenience, we repeat the theorem here.

Theorem (Clustering of correlations of eigenvectors)**.** *If the Hamiltonian has an information mobility edge at energy* E_{mob} *and it has non-degenerate energies and non-symmetric gaps, then all eigenvectors* $|k\rangle$ *up to that energy* E_{mob} *cluster exponentially, in the sense that for all* $\kappa > 0$

$$\begin{aligned} & |\langle k|AB|k\rangle - \langle k|A|k\rangle\langle k|B|k\rangle| \\ \leqslant & \left(12\pi\Theta(E_k+\kappa)C_{\mathrm{mob}} + \ln\frac{\pi\mu\, d(A,B)\, e^{4+2\pi}}{\kappa^2}\right)\frac{e^{-\mu d(A,B)}}{2\pi}\,, \end{aligned}$$

where $\Theta(E)$ *is the number of eigenstates up to energy* E *and* κ *can be chosen arbitrarily to optimise the bound.*

Proof. The proof runs along and builds upon the lines of thought of both Ref. [66] and of [157], and generalises both. The basic idea is again to start from the correlation function and to transform it into an expression depending on the commutator. For this, we fix a constant $\kappa > 0$ and define

$$P = \sum_{E_l \leqslant E_k+\kappa} |l\rangle\langle l|$$

to be the projector onto the subspace of energies smaller than $E_k + \kappa$ and write $P^\perp$ for $\mathbb{1} - P$. Decomposing the identity with respect to P and $P^\perp$ and using a high-pass filter Γ_α for a suitable $\alpha > 0$ (see Def. 11), we separate the correlator into terms

$$\begin{aligned} \langle k|AB|k\rangle &= \langle k|(A-\Gamma_\alpha(A))PB|k\rangle \\ &+ \langle k|(A-\Gamma_\alpha(A))P^\perp B|k\rangle \\ &+ \langle k|BP\Gamma_\alpha(A)|k\rangle + \langle k|BP^\perp\Gamma_\alpha(A)|k\rangle \\ &+ \langle k|[\Gamma_\alpha(A),B]|k\rangle\ . \end{aligned}$$

Lets consider the first term on the right-hand side of Eq. (F.0.2) that contains P and expand the projector in the eigenbasis of H, which gives

$$\begin{aligned} |\langle k|(A-\Gamma_\alpha(A))PB|k\rangle| &\leqslant \sum_{E_l\leqslant E_k+\kappa} |\langle k|(A-\Gamma_\alpha(A))|l\rangle\langle l|B|k\rangle| \\ &\leqslant 2\sum_{E_l\leqslant E_k+\kappa} |\langle k|A|l\rangle\langle l|B|k\rangle|\,. \end{aligned}$$

Here, we used that all matrix elements decrease under a high-pass filter (see lemma 11) for all $\alpha > 0$. As before, we set $\langle k|B|k\rangle = 0$ w.l.o.g. and then proceed by bounding all the terms in the sum individually. Using lemma 13 yields

$$|\langle k|(A-\Gamma_\alpha(A))PB|k\rangle| \leqslant 4\,\Theta(E_k+\kappa)C_{\mathrm{mob}}e^{-\mu d(A,B)}\,,$$

where $\Theta(E_k+\kappa)$ simply is the number of eigenvectors contained in P. The other term in Eq. (F.0.2) containing P can be bounded analogously, yielding

$$|\langle k|BP\Gamma_\alpha(A)|k\rangle| \leqslant 2\,\Theta(E_k+\kappa)C_{\mathrm{mob}}e^{-\mu d(A,B)}\,.$$

The terms containing $P^\perp$ in Eq. (F.0.2) are bounded using the explicit form of the matrix elements of a high-pass filter (see lemma 11), which delivers

$$\langle k|BP^\perp\Gamma_\alpha(A)|k\rangle \leqslant \sum_{E_l>E_k+\kappa} \langle k|B|m\rangle\langle m|DA|k\rangle\ ,$$

where D is a diagonal matrix whose entries are bounded by $e^{-\kappa^2/(4\alpha)}/2$. A simple norm estimate concludes the estimation of this term

$$\langle k| BP^{\perp}\Gamma_{\alpha}(A)|k\rangle \leqslant \|D\| \leqslant \frac{e^{-\kappa^2/(4\alpha)}}{2} .$$

The other term containing $P^{\perp}$ can be estimated in the same way

$$\langle k| (A-\Gamma_{\alpha}(A))P^{\perp}\Gamma_{\alpha}(A)|k\rangle \leqslant \frac{e^{-\kappa^2/(4\alpha)}}{2} .$$

The commutator term in Eq. (F.0.2) is bounded by using locality of a high-pass filter (see lemma 11). We are still free to choose a value for α in the high-pass filter. Taking

$$\alpha = \frac{\kappa^2}{4\mu d(A,B)}$$

gives

$$\langle k| [\Gamma_{\alpha}(A), B]|k\rangle \leqslant \left(12\pi\Theta(E_k+\kappa)C_{\mathrm{mob}} + 2\pi + 4 + \ln\frac{\pi\mu d(A,B)}{\kappa^2}\right)\frac{e^{-\mu d(A,B)}}{2\pi} .$$

This concludes the proof. □

We now provide the proof of corollary 13. It follows from the above results that in the case of 1D systems, the corresponding eigenstates satisfy an area law for a suitable entanglement entropy, which in turn implies that they can be well approximated by a matrix-product state of a low bond dimension. We bound the bond dimension by using theorem 1 from Ref. [102]. For convenience, we repeat the corollary here.

Corollary (Area laws and matrix-product states)**.** *An eigenvector* $|k\rangle$ *of a localising Hamiltonian can be approximated by an MPS with fidelity* $|\langle k|\mathrm{MPS}_D\rangle| \geqslant 1-\epsilon$*, where the bond dimension* D *for a sufficiently large system is given as follows.*

a *If the Hamiltonian shows strong dynamical localisation and has non-degenerate energies and locally independent gaps, then the statement holds for all eigenvectors* $|k\rangle$ *and, for some constant* $C > 0$*, the approximation has a bond dimension*

$$D = C\,(L/\epsilon)^{\frac{16}{\mu \log_2 e}} .$$

b *If the Hamiltonian has an information mobility edge at energy* E_{mob}*, and has non-degenerate energies and non-symmetric gaps, then the statement holds for all eigenvectors below this energy* E_{mob} *and the bond dimension is given by*

$$D = \mathrm{poly}\left(\Theta(E_k+\kappa), L\right) ,$$

for any fixed κ *which enters in the precise form of the polynomial.*

Proof. As a first step of the proof, we reformulate our clustering of correlation results (see Thm. 12) in terms of a correlation length according to Ref. [102]. For this, we need a decay of the correlator of the form $2^{-d(A,B)/\xi}\ \forall d(A,B) > l_0$ and start by rewriting our bound as

$$\begin{aligned} |\langle k|AB|k\rangle - \langle k|A|k\rangle\langle k|B|k\rangle| &\leqslant Ce^{-\mu d(A,B)} \\ &= C2^{-\mu \log_2 e\, d(A,B)} . \end{aligned} \tag{F.0.6}$$

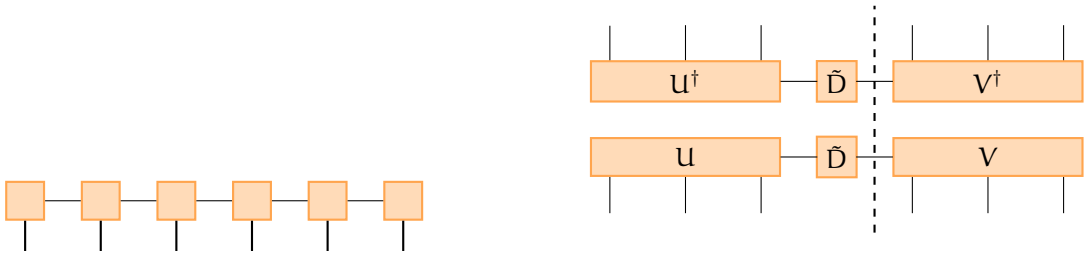

Figure F.1: *Taken from Ref. [4].* MPS description of an eigenstate $|E_k\rangle\langle E_k|$. Theorem 1 in Ref. [102] allows to bound the bond dimension across cuts by providing an upper bound to the smooth max entropy. The reduced state of the suitably normalised matrix product state is $\rho = U\tilde{D}^2U^\dagger$.

Next we split the decaying term and use one part to get rid of the constant prefactor C and the other to preserve an exponential decay with a correlation length $\xi := 2/(\mu \log_2 e)$. This yields

$$|\langle k|AB|k\rangle - \langle k|A|k\rangle\langle k|B|k\rangle| \leqslant 2^{-d(A,B)/\xi} \quad \forall\, d(A,B) \geqslant l_0 \,,$$

where $l_0 = \xi/(\log_2 C)$. Following Ref. [102], we use the exponential clustering to obtain a description of the eigenvector $|k\rangle$ in terms of MPS (see also Fig. F.1). This is based on the so called smooth max entropy. For this quantity, rather than evaluating the entropy for the state itself, an optimisation over some δ-ball in state space is performed [57]

$$H_{\max}^{\delta}(\rho_X) := \min_{\tilde{\rho}_X \in \mathcal{B}_\circ(\rho_X)} \log_2(\operatorname{rank}(\tilde{\rho}_X)) \,,$$

with

$$B_\delta(\rho_X) := \{\tilde{\rho}_X : \frac{1}{2}\|\rho_X - \tilde{\rho}_X\|_1 < \delta\}$$

being a ball of density matrices around ρ_X (see appendix A of Ref. [102] for details). According to theorem 1 in Ref. [102], we can obtain an upper bound for the smooth max entropy for any bipartite cut, as long as the system size L is larger than $C_{\text{cut}} l_0/\xi$ with a constant $C_{\text{cut}} > 0$. Picking the approximation parameter in the smooth max entropy to be $\delta(l) = 2^{-l/(8\xi)}$, then Ref. [102] provides a bound of the form

$$H_{\max}^{\delta(l)} \leqslant c' l_0 \xi^{c\xi} + l \,, \tag{F.o.7}$$

for all $l \geqslant 8\xi$ with constants $c, c' > 0$. In the following, we make corollary 3 in Ref. [102] explicit, by deriving concrete bounds on the bond dimension of the matrix-product state chosen to approximate $|k\rangle$. Naturally, the first step for this is to express $|k\rangle$ as a matrix-product state vector with, a priori, exponentially large bond dimension (see Fig. F.1). For simplicity, we restrict the proof here to a linear system with open boundary conditions, but it can equivalently be reformulated for a periodic system on a ring [102]. The bond dimension of the matrix-product state is bounded by truncating at each cut explicitly. For this, we start at one end of the chain and look at each cut separately. In each step, we apply a singular value decomposition (see also Fig. F.1). Since we are truncating spectral values in each step, the positive operators are no longer normalised to unit trace and are states only up to normalisation. This results in a reduction on the left side of the cut of $\rho = U\tilde{D}^2U^\dagger$, with U being unitary and $\tilde{D}$ diagonal. The goal is now to truncate the diagonal matrix $\tilde{D}$ to a fixed bond dimension D while creating only a small discarded weight [41]. Following lemma 14 in appendix B of Ref. [102], for any $\nu > 0$, we can choose the bond dimension as

$$D = 2^{H_{\max}^{\nu}(\rho)} \,,$$

and create a discarded weight

$$\sum_{D+1}^{2^L} \lambda_k \leqslant 3\nu \,,$$

where λ_k are the eigenvalues of ρ or equivalently of $\tilde{D}^2$. Each time we create discarded weight, the fidelity with our original pure quantum state potentially is reduced by the discarded weight [177], upper bounded by 3ν. The truncation results in a subnormalised state. Renormalising, however, only increases the fidelity, allowing us to obtain a normalised MPS approximation. Thus, in total, the fidelity of our MPS approximation with bond dimension $D = 2^{H^{\nu}_{\max}(\rho)}$ is bounded by

$$|\langle\psi|\mathrm{MPS}_D\rangle| \leqslant 1 - L3\nu \,,$$

where L is the size of the linear 1D system. For a fixed global error $\epsilon > 0$, we therefore obtain an allowed local error

$$\nu = \frac{\epsilon}{3L} \,.$$

We now fix ν to take the role of $\delta(l)$ in (F.o.7). Plugging this bound into Eq. (F.o.7) and using $\delta(l) = 2^{-l/(8\xi)}$, we obtain

$$H^{\frac{\epsilon}{3L}}_{\max} \leqslant c' l_0 \xi^{c\xi} + 8\xi \log_2 \frac{3L}{\epsilon} \,,$$

and thus obtain an approximation with

$$D = 2^{c' l_0 \xi^{c\xi}} \left(\frac{3L}{\epsilon}\right)^{8\xi} \,.$$

Coming back to our original clustering assumption in Eq. (F.o.6), this yields

$$D = C^{c' \xi^{c\xi+1}} \left(\frac{3L}{\epsilon}\right)^{8\xi} \,,$$

with $\xi = 2/(\mu \log_2 e)$. Thus, we finally have a polynomial scaling in the constant $C > 0$ as well as the in the system size and in the inverse error of the approximation $1/\epsilon$. The rest of the proof follows directly by inserting the constants from theorem 12. □

G

EXPERIMENTALLY CROSSING THE MOTT-SUPERFLUID TRANSITION

The following chapter is based on Ref. [1]. We sincerely thank Simon Braun, Sean S. Hodgman, Michael Schreiber, Jens P. Ronzheimer, Arnau Riera, Marco del Rey, Immanuel Bloch, Jens Eisert, and Ulrich Schneider for the successful collaboration.

In this appendix, we present the details of the experimental study discussed in chapter 10. We begin with the extraction of the correlation length from the experimental data.

Extraction of the correlation length

In this section, we describe the read-out of our quantum simulation, namely the extraction of the correlation length. First, it is first important to note that, as described in section 8.3.1, this information is directly contained in the time of flight image

$$\langle \Psi^\dagger(r,t)\Psi(r,t)\rangle = |\hat{w}_0(k)|^2 \sum_{\mu,\nu} e^{ik(r_\mu - r_\nu) - i\frac{m(r_\mu^2+r_\nu^2)}{2\hbar t}} \langle b_\mu^\dagger b_\nu\rangle \,,$$

where the left hand side is the particle distribution that is measured and $|\hat{w}_0(k)|^2$ is the Fourier transform of the Wannier function that can easily be calculated (see section 8.2.1). In order to define a correlation length, an exponential decay has to be assumed. Taking the local densities $\langle n_{j,k}\rangle$ into account, we use a fit

$$\langle b_j^\dagger b_k\rangle \approx \sqrt{\langle n_j\rangle}\sqrt{\langle n_k\rangle} e^{-d(j,k)/\xi} \,, \tag{G.0.1}$$

where ξ is the correlation length.

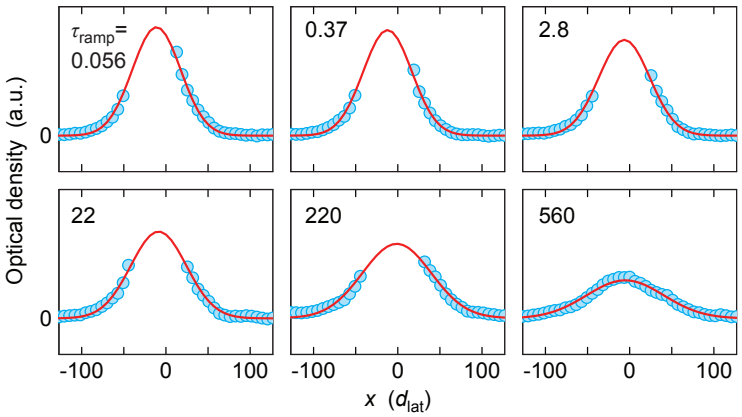

Figure G.1: *Taken from Ref. [1].* Shown are the experimentally obtained density profiles (blue dots) and fits in terms of a Gaussian (red lines) for different total ramp durations τ_{ramp}. Positions x are measured in the natural lattice distance d_{lat} of the system, while the density is presented in arbitrary units, as only the relative shape is of interest.

The experimental study described here was carried out in a 3D trap. Thus all extracted correlations are always averaged over the imaging direction, which leads to a 2D image (see Fig. 10.1). A small central cross section along the x axis of these image is taken and averaged over. The resulting 1D profile can then be fitted according to Eq. (G.0.1). We approach this extraction of the averaged density by experimentally

taking images of the density profile (see Fig. G.1). Due to a saturation of the camera in the center of the cloud, only the tails could be experimentally measured. This required a fit to access the full profile, which was performed using a Gaussian function, which fits the experimentally observed tails nicely. Using the fitted experimental density profile, we obtain

$$\langle n_k \rangle = e^{-r_k^2/(4R^2)} ,$$

where r_k is the position corresponding to index k and R is the fitted cloud radius. With this, Eq. G.0.1 can be used to extract the correlation length from time of flight images in a robust fashion. We now turn to a discussion of the influence of the trap for the dynamical crossing of the Mott-superfluid transition.

Influence of the trap

Without the trap, the system size hardly matters (see Fig. 10.3), but starts to play a crucial role in trapped models (see Fig. G.2). For the 1D experiments discussed here, the 3D cloud of atoms is decoupled into 1D tubes. Due to the elliptical shape of the harmonic trap, these 1D tubes all contain different particle numbers, while they are all confined in the same trap profile [1, 32]. Thus, the experimental images are an average over these configurations. As demonstrated in Fig. G.2, these different particle numbers give different correlation length behaviour. For each particle number, the correlation length starts to decrease at some point and the experimental decrease is the result of the average over the different 1D tubes.

In order to obtain an intuitive understanding for the decrease of the correlation length fitted in terms of a real exponentially decaying function, let us analyse the trapped system in more depth. The first physical intuition one connects with a trapped model is the inhomogeneous density profile. One might expect that the change of the correlation length connects to the redistribution of atoms within the trap. This turns out not to be true. As demonstrated in Fig G.2, the density profile is hardly changed on the time scales investigated here. Thus, the effect of the trap is more subtle than a simple redistribution of particles.

By looking at the full correlation function within the trap (see Fig. G.3), we notice that the correlator is only real for short evolution times. For longer times, the imaginary part starts to grow. In a system with mirror symmetry and translational invariance, this can never take place as

$$\begin{aligned}\overline{\langle a_k^\dagger a_l \rangle} &= \langle a_l^\dagger a_k \rangle = \langle a_0^\dagger a_{k-l} \rangle \\ &= \langle a_0^\dagger a_{l-k} \rangle = \langle a_k^\dagger a_l \rangle ,\end{aligned}$$

which means that the trap is needed to cause an imaginary part. What is more, since the Hamiltonian including the trap is real, all static thermal states are completely real, leading to a vanishing imaginary part of the correlator, independent of the presence of a trap. Thus, the imaginary part of the correlator is a clear signature of the out of equilibrium dynamics caused by the trap. This directly gives us an underlying reason, why the correlation length decreases for long ramp times. More and more of the correlations become imaginary, which is simply not included in our fit in terms of a real exponential decay. A further investigation of these out of equilibrium signatures of correlation dynamics in trapped systems would surely constitute interesting research for the near future, but is not immediately connected to the dynamics of quantum phase transitions discussed here.

While we are having a closer look at the correlation behaviour, it is instructive to also look at the real part in more detail (see Fig. G.3). The ramp starts in the ground state, which is expected to have an exponential decay of correlations [62]. For longer ramps, this exponential fit does not work as well. Still, it seems the only obvious way to define a correlation length without in-depth knowledge of the actual functional behaviour of the correlator.

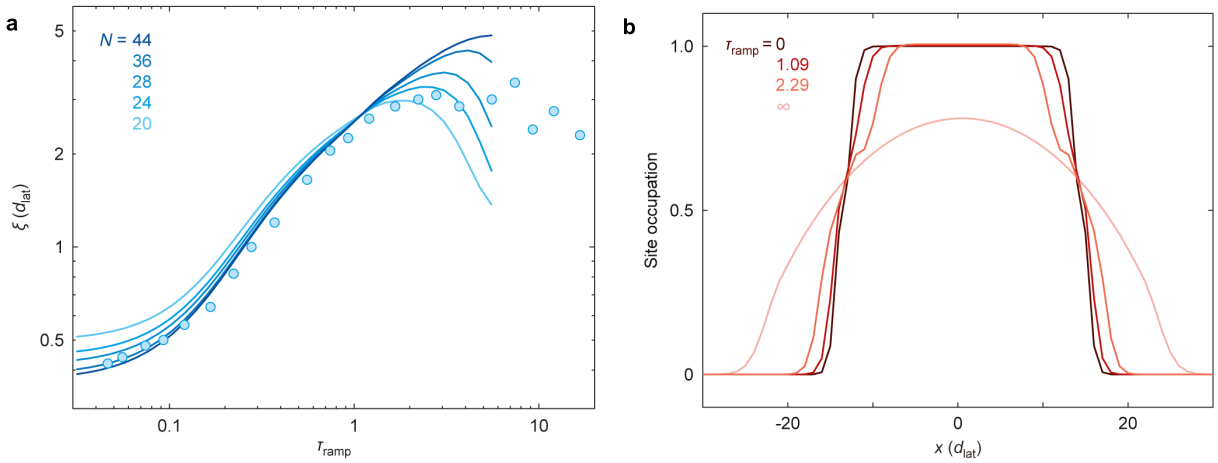

Figure G.2: *Taken from Ref. [1].* **a** Plotted is the behaviour of the correlation length ξ for different particles numbers N in the same harmonic trap. The experimentally observed data (blue dots) are necessary an average over the 1D tubes with different particle numbers. The numerical simulation of those systems using t-DMRG (blue lines) shows a strong dependence on this particle number. This explains the decrease of the experimentally observed correlation length for long ramp times in the trapped system. **b** Shown is the density profile given by the site occupation corresponding to the number of particles on a site, as calculated with t-DMRG depending on the lattice position x. For the different ramp times τ_{ramp}, we find that this profile hardly changes and is significantly different from the profile of a superfluid corresponding to an infinitely slow evolution. This demonstrates that the influence of the trap in our setup is not a redistribution of particles.

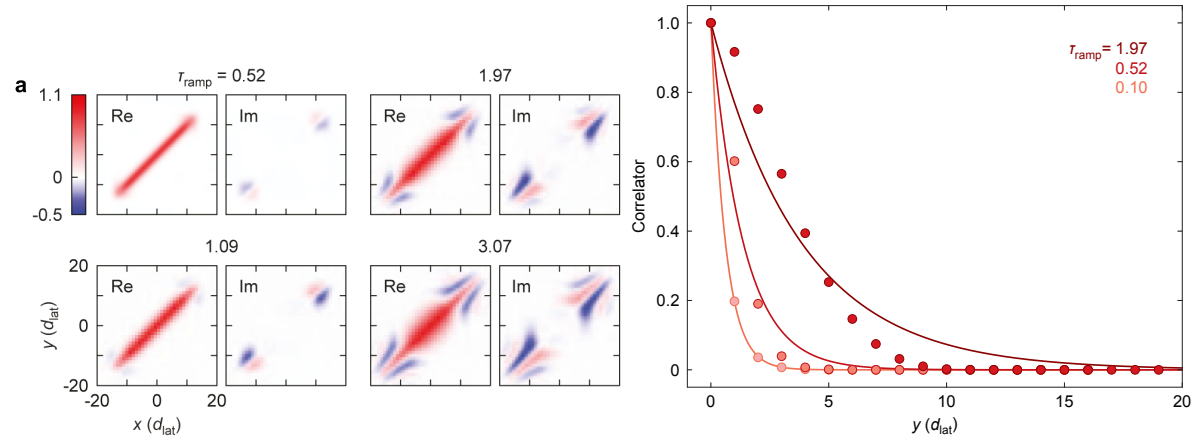

Figure G.3: *Taken from Ref. [1].* **a** These plots show the t-DMRG calculation for the correlator in the trapped model, separated into real and imaginary part for different ramp times τ_{ramp}. The non-zero imaginary part is a signature of the out of equilibrium dynamics caused by the trap. **b** Presented is the real part of those correlator as dots. The lines show the best exponential fit, demonstrating that the exponential decaying function fits well, but becomes less accurate for longer ramp times.

ACKNOWLEDGEMENTS

In my private life, I have been blessed with the most ingenious and compassionate people imaginable. They surely know that I am eternally grateful.

Concerning my life as a scientist, my gratitude belongs to my supervisor Jens Eisert, who, without a doubt, is the father of my academic carrier. I am forever thankful for the opportunities he gave me and the fun and productive years that ensued.

I also would like to thank all other fascinating scientists I had the pleasure to work with, in numerous collaborations, during conferences and in within the Q-Mio group in Berlin. They have shown me how much fun and joy academic discussions can bring and the results presented in this thesis only exist because of these inspiring scientific exchanges.

Many people have also been a tremendous help in writing this thesis. I would like to particularly thank Albert Werner, Henrik Wilming, Martin Kliesch, Nicolas Tech, Jonas Hörsch and Felix Stete for invaluable feedback on various chapters.

Impressively, many people discussed this thesis chapter by chapter with me in weekly sessions. For this, my heartfelt gratitude goes out to Christian Krumnow, Dominik Hangleiter, Jaqueline Lekscha, Ingo Roth, Rodrigo Gallego, Sybille Rosset, Aniruddha Bapat, Janina Gertis and Carlos Riofrío.

Finally, I had the pleasure to work with the master students Marcel Goihl and Marek Gluza. Joining them on their path to becoming scientists and discussing our projects and countless parts of this thesis was simply fantastic. It is with great delight that I consider the intriguing questions that thesis had to leave open and think of these aspiring scientists one day tackling them.

SUMMARY OF RESULTS

This thesis investigates quantum-many body systems out of equilibrium in a variety of physically relevant and intriguing settings. It provides an overview of the recent developments in this field and based on the author's recent review [3] illuminates many interesting connections and summarises open questions.

In this general framework, the various results of the author are embedded. While they often rely on advanced mathematics, great care is taken to present them in an intuitive way and most technical material is discussed separately in appendices. In the context of equilibration, work created as part of this thesis [6] is able to capture the Gaussification of correlated initial states for a large class of free models. This allows to significantly extend equilibration results of free models, which are of crucial importance, as they provide reasonable relaxation time scales and immediately connect to our physical intuition in terms of ballistic spreading.

Building on two surprising connections between static and dynamic features of Hamiltonians, which in general are hard to obtain, the results of this thesis further greatly contribute to the recent debate on the true nature of quantum many-body localisation. For those interacting models, we derive the localised structure of eigenstates from a dynamical suppression of information propagation on the low-energy sector [4]. Further, we show how a non-degenerate spectrum, indicating the presence of interactions, and the existence of an approximately local constant of motion are sufficient to show information propagation, if arbitrary energies are allowed [5].

In the context of quantum phase transitions, we continue such connections between static and dynamic features. We specifically investigate the Mott-superfluid transition of the Bose-Hubbard model and ask to what extent it has a universal dynamical signature. In a joint experimental, numerical and analytical effort, complex behaviour of these dynamics is uncovered, thus challenging the common believe that the Kibble-Zurek mechanism is sufficient to fully capture such transitions [1].

We embed such experimental investigation in the recent debate on quantum simulators, which give the exciting perspective of solving notoriously and even provably hard problems efficiently in the laboratory. For such devices, we argue that the final read-out of the results is an important out-standing problem to be solved. We approach this issue in the case of a continuous quantum field, in which the notion of reconstructing the quantum state is even conceptually unclear. Based on tensor network methods, we demonstrate that in an experiment of ultra-cold atoms in a continuous setup, states can nevertheless efficiently be obtained [2].

Thus, this thesis constitutes not only an important review of the field of quantum many-body systems out of equilibrium, but, using advanced mathematical and numerical tools, has significantly contributed to our understanding of various important out-standing questions in interacting many-body systems.

GERMAN SUMMARY OF RESULTS

In dieser Doktorarbeit werden Quantenvielteilchensysteme außerhalb des Equilibriums in verschiedenem physikalischen Kontext untersucht. Aufbauend auf einem Übersichtsartikel [3] zu diesem Feld, an dem der Autor dieser Arbeit beteiligt war, werden wichtige Entwicklungen dargestellt, wesentliche Querverbindungen gezogen und offene Fragen präsentiert. In diesen Rahmen sind die analytischen und numerischen Arbeiten des Autors eingebettet. Trotz ihrer teils tiefgehend mathematischen Natur wurde großer Wert darauf gelegt, diese auf intuitive Weise zu präsentieren. Technische Details werden daher separat in Anhängen diskutiert.

Im Bereich der Equilibrierung gelang es zu zeigen, dass korrelierte Anfangszustände durch die Entwicklung unter freien fermionischen Modellen lokal gegen einen Gaußschen Zustand streben [6]. Damit können Gaußsche Equilibrierungsergebnisse verallgemeinert werden, woraus sich wichtige Intuition für den wechselwirkenden Fall ableiten lässt.

Aufbauend auf zwei unerwarteten Verbindungen zwischen statischen und dynamischen Eigenschaften von Hamiltonoperatoren, welche im Allgemeinen schwer zu etablieren sind, trägt diese Arbeit signifikant zur Debatte bei, wie Vielteilchenlokalisierung zu fassen ist. Es wird gezeigt, dass Lokalisierungseigenschaften von Eigenzuständen aus einer dynamischen Lokalisierung unterhalb einer Energieschranke hergeleitet werden können [4]. Darüber hinaus wird hergeleitet, dass die Anwesenheit einer lokalen Erhaltungsgröße zusammen mit einem nichtentarteten Spektrum ausreicht, um dynamische Ausbreitung von Information zu garantieren [5].

Im Bereich der Quantenphasenübergänge wird der Zusammenhang von dynamischen und statischen Eigenschaften wechselwirkender Modelle tiefergehend untersucht. In einer vereinten experimentellen, analytischen und numerischen Arbeit wird die Dynamik des Phasenübergangs des Bose-Hubbard Modells analysiert. Hierbei tritt komplexes Verhalten zu Tage, das bisher weder durch den Kibble-Zurek Mechanismus, noch durch andere Theorien erklärt werden kann [1]. Diese experimentelle Untersuchung wird in den weiter gefassten Rahmen von Quantensimulatoren eingebettet. Solche Simulatoren zeigen eine Perspektive auf, harte quantenmechanische Probleme im Labor effizient zu lösen. Der finale Schritt einer solchen Quantensimulation ist die Rekonstruktion der Simulationsergebnisse. Wir untersuchen diesen für ultrakalte Atome in einer kontinuierlichen Falle. Ausgehend von Tensornetzwerkmethoden zeigen wir, dass (trotz der Schwierigkeiten kontinuierlicher Architekturen) effiziente Quantenfeldtomographie durchgeführt werden kann und wir demonstrieren diese darüber hinaus auch direkt experimentell [2].

Zusammenfassend gibt diese Arbeit nicht nur einen umfassenden Überblick über Quantenvielteilchensysteme außerhalb des Gleichgewichts, sondern nutzt darüber hinaus elaborierte mathematische Methoden und numerische Simulationen, um unser Verständnis von Vielteilchensystemen signifikant zu erweitern.

DECLARATION OF ORIGINALITY

Hiermit bestätige ich, dass ich die vorliegende Arbeit selbstständig und nur mit Hilfe der angegebenen Hilfsmittel angefertigt habe. Alle Stellen der Arbeit, die wörtlich oder sinngemäß aus Veröffentlichungen oder aus anderweitigen fremden Quellen entnommen wurden, sind als solche kenntlich gemacht. Ich habe die Arbeit noch nicht in einem früheren Promotionsverfahren eingereicht.

Mathis Friesdorf

CURRICULUM VITAE

Der Lebenslauf ist in der Online-Version aus Gründen des Datenschutzes nicht enthalten.